ELECTROCHEMISTRY AND PHOTOPHYSICOCHEMICAL STUDIES OF TITANIUM, TANTALUM AND VANADIUM PHTHALOCYANINES IN THE PRESENCE OF NANOMATERIALS

A thesis submitted in fulfilment of the requirements for the degree of

DOCTOR OF PHILOSOPHY

OF

RHODES UNIVERSITY

By

VONGANI PORTIA CHAUKE

May 2011

DEDICATION

To my parents Mr Joel Masidi Chauke

and Mrs Thabitha Makaela Chauke

ACKNOWLEDGEMENTS

I would like to give thanks to God for without him this would not have been possible.

To my supervisor Professor Tebello Nyokong, thank you for your guidance, support, patience and sharing your knowledge with me. It has been great working under your supervision; you are with no doubt a phenomenal woman. Thank you for the opportunities you created for me to go and broaden my knowledge and research skills in England and Paris.

Many thanks to Professor M. Cook, Dr. F Beudiou and their research groups for their help and support during my stay there.

Dr. E Antunes, thank you for your support, encouragement, novel ideas and your contributions to this work. Dr. Y. Asrlanoglu and Dr. F. Matemadombo, I truly appreciate your help and contributions to this work. Many thanks to Dr. W. J. U. Chidawanyika and Miss S. D'Douza for your help with AFM and contributions to this work. Thanks to Mr. Marvin for your help with the TEM images.

To the chemistry department, it has been absolutely fantastic being part of you since 2000 and something! I appreciate all the tea moments, ideas and laughter we shared. Miss G. Cobus, thank you for everything.

To my family away from home, S22, you guys are absolutely incredible, you are the BEST. Thank you for all the good times, the crazy moments, idea sharing and support.

Many thanks to Mr. Rene and Mrs Biddy Schalker, for your kindness, support and for giving me a home in Grahamstown. Thank you.

To all my true friends, "*Friends are siblings God forgot to give us*", Miss Nolwazi 'dr. Ice-cream' Nombona, Anthonia 'Afgan' Folake Afolaya, Basani M. Nkuna, Miss Nomampondo 'Penny' Penelope Magwa and Mr. Samson Mielie 'Sammy' Khene, thank you so much for your continuous support, the crazy moments,

encouragement, listening to my 'gobbledygook' lol and your love! You guys have re-defined friendship for me, you are the best.

To my special friend Dr. Cecil C. Z. Mutambanengwe, thank you for your patience, support and everything; your invaluable support and friendship kept me sane and is truly appreciated. You are trully special Kiri!

To my family: my parents Mr. Joel M. And Mrs Thabitha M. Chauke, you are the BEST and are my everything! Thank you for your continuous support, believing in me, your love and prayers. A special thanks to the rest of my family, my aunts, Dinah E. Sombhane, Miss. Mkateko Sindy D.D Sombhane and her family, my cousin sister Miss Kholofelo 'Kholo-mankholos' Hlungwani, my uncle Mr Themba. R Sombhane and his family, Mrs Tsakani. Matukane and her family, Dr. Nkhensani. Chauke and her family, Ms. Florance Chauke, Mrs J. Chauke and her family, my granies Mr. D.N. and Mrs E. Chauke, Mrs. M. M Sombhane and Mrs. Rendani Mabaso and her family for your prayers, love and support. I am grateful to you all for your love and support that kept me going throughout the duration of this PhD.

To NRF and DST/MINTEK thank you for their financial support.

"I can no other answer make, but, thanks, and thanks".
- William Shakespeare

ABSTRACT

The syntheses of tetra- and octa-substituted phthalocyanine complexes of titanium (IV) oxide vanadium (IV) oxide and tantalum (V) hydroxide and their electrochemical characterisation are presented in this work. The structures and purity of these complexes were confirmed by NMR, infrared and mass spectroscopies and elemental analysis. They show good solubility in most common solvents especially non-viscous solvents such as dichloromethane and chloroform. The cyclic voltammograms (CV) showed reversible to quasi reversible behavior for all the reduction couples and the oxidation peaks were irreversible. Spectroelectrochemistry of the complexes confirmed metal and ring redox processes for TaPc and TiPc derivatives and ring based processes only for VPc complexes. The synthesis of gold nanoparticles and their conjugation with the new phthalocyanines was carried out. Similarly, single walled carbon nanotubes were conjugated to selected tantalum complexes and the characterization of all the nanomaterials and their conjugates using different techniques that include TEM, XRD and AFM is also presented in this work.

The photophysical and photochemical properties and photocatalytic oxidation of cyclohexene properties of the newly synthesised in the presence of gold nanoparticles were investigated. The compounds were stable, well within the stability range for phthalocyanines. The singlet oxygen quantum yield values increased drastically in the presence of gold nanoparticles. The photocatalytic products obtained from the reaction were cyclohexene oxide, 2-cyclohexen-1-ol, 2-cyclohexene-1-one and 1,4-cyclohexanediol. The percentage conversion values,

yields and selectivity values improved significantly in the presence of AuNPs. Singlet oxygen was determined to be the main agent involved in the photocatalytic oxidation of cyclohexene.

The electrocatalytic oxidation of bisphenol A and *p*-nitrophenol was carried out using nickel tetraamino phthalocyanine and all the newly synthesised metallophthalocyanine in the presence of gold nanoparticles and single walled carbon nanotubes. The charge transfer behaviour of AuNPs was enhanced in the presence of TaPc, TiPc and VPc complexes. The presence of single walled carbon nanotubes further improved electron transfer and minimised electrode passivation.

CONTENTS

LIST OF SYMBOLS

$^1O_2(^3\Sigma_g)$	- Ground state molecular oxygen
$^1O_2(\Delta_g)$	- Excited singlet oxygen
A	- Absorbance
D	- Diffusion coefficient
E	- Potential
$E_{1/2}$	- Half-wave potential
E_p	- Peak potential
E_{pa}	- Anodic peak potential
E_{pc}	- Cathodic peak potential
I	- Light intensity
	- Current
I_{abs}	- Amount of light absorbed by sensitizer
I_{abs}	- Intensity of light absorbed
I_p	- Peak current
I_{pa}	-Anodic current
I_{pc}	- Cathodic current
n	- Number of electrons transferred
Q	- Electrical charge (C)
R	- Universal gas constant
S_0	- Ground singlet state

S_1 - Excited singlet state

T - Transmittance

T_1 - First excited triplet state

T_2 - Second excited triplet state

V - Volume

α - Non-peripheral position

β - Peripheral position

Γ - Surface coverage or concentration

ΔA - Change in absorbance

ΔE - Difference in peak potentials

ε_S - Singlet state molar extinction

ε_T - Triplet state molar extinction

ν - Scan rate

τ_T - Triplet lifetime

Φ_Δ - Singlet oxygen quantum yield

Φ_P - Photodegradation quantum yield

Φ_T - Triplet quantum yield

LIST OF ABBREVIATIONS

^{1}H-NMR	- Proton nuclear magnetic resonance
Ac_2O	- Acetic anhydride
AFM	-Atomic force microscopy
AuNPs	-Gold nanoparticles
BPA	-Bisphenol A
C	- Concentration
CT	- Charge transfer
CV	- Cyclic voltammetry
	- Cyclic voltammogram
DABCO	- 1,4-Diazobicyclo-octane
DBN	-1,5-Dizabicyclo[4.3.0]non-5-en
DBU	-1,8-Diazabicyclo[5.4.0]undec-7-ene
DCM	- Dichloromethane
DMF	- Dimethylformamide
DMSO	- Dimethylsulfoxide
DNA	- deoxyribonucleic acid
DPBF	- 1,3-Diphenylisobenzenefuran
EDC	-Endocrine distrupting chemical
EIS	-Electrochemical impedance spectroscopy

F - Fluorescence

GCE - Glassy carbon electrode

H_2Pc - Metal-free phthalocyanine

HOMO - Highest occupied molecular orbital

HPLC - High performance liquid chromatography

IC - Internal conversion

IR - Infrared

ISC - Intersystem crossing

LMCT - ligand to metal charge transfer

LUMO - lowest unoccupied molecular orbital

MLCT - Metal to ligand charge transfer

2-ME -2-Mercaptoethanol

MPc - Metallophthalocyanine

NIR - Near infred

NiTAPc -Nickel tetra amino phthalocyanine

NLO -Nonlinearoptics

NO -Nitric oxide

ODS - optical data storage

OL - Optical limiting

OTTLE - Optically transparent thin-layer electrodes

P - Phosphorescence

Pc - Phthalocyanine

PDT - Photodynamic therapy

Ps - Photosensitization

PNP -*p*-Nitrophenol

SPR - Surface Plasmon Resonance

SWCNTs -Single-walled carbon nanotubes

TaPc -Tantalum phthalocyanine

$TBABF_4$ - Tetrabutylammonium tetrafluoroborate

TBAP - Tetrabutylammonium perchlorate

TOABr - Tetraoctylammonium bromide

TEM -Transmission electron microscopy

THF - tetrahydrofuran

TiPc -Titanium phthalocyanine

TLC - thin layer chromatography

TX - Triton X-100

UV/Vis - ultraviolet/visible

VPc -Vanadium phthalocyanine

VR - Vibrational relaxation

XRD -X-Ray diffraction

LIST OF FIGURES

LIST OF SCHEMES

LIST OF TABLES

1. Introduction

The aim of this work is to synthesise thio-substituted metallophthalocyanines (MPc) for application in photo- and electro-catalysis in the absence and presence of nanomaterials. The interest in nanomaterials is increasing owing to their remarkable properties, therefore, gold nanoparticles and single walled carbon nanotubes (SWCNTs) will be synthesised and conjugated with MPcs through simple processes of self assembly for AuNPs and adsorption for SWCNTs. These processes are made possible because of the strong affinity of gold for sulphur and by π-π interactions for SWCNTs and MPcs. The SWCNTs will be non-covalently conjugated to selected synthesised TaPc complexes with the aim of enhancing catalysis, minimising electrode surface poisoning and improving electrode regeneration. A general synthetic approach for MPcs and nanomaterials, conjugation and characterisation is discussed in this chapter.

1.1. Discovery, structure and applications of phthalocyanines.

In 1907, Braun and Tcherniac accidentally discovered a mysterious blue compound, later characterised as a metal-free phthalocyanine (H_2Pc). It was a by-product in the synthesis of *o*-cyanobenzamide from phthalamide [1, 2]. Twenty years later, Diesbach and van der Weid discovered more phthalocyanine derivatives from the synthesis of *o*-dibromobenzene and cuprous cyanide [3]. It was only later that the structure of H_2Pc was elucidated by Linstead and co-workers [4-7], with the structure being confirmed by Robertson and co-workers using X-Ray diffraction

analysis [8-10]. The term 'phthalocyanine' was used by Linstead, he related 'phthalo' to its various phthalic acid precursor derivatives and 'cyanine' (a Greek term) for the colour blue.

Phthalocyanines (Pcs) are a class of flexible compounds which have a planar 18-π electron heterocyclic aromatic system derived from naturally occurring porphyrins such as porhine (**1**), Fig. 1.1. Substituting four nitrogen on the *meso*-CH bridges in complex **1** gives a porphyrazine (**2**), Fig. 1.1, and a phthalocyanine (**3**) is formed from the fusion of four benzene rings on the pyrrole β-positions. Pcs are formally known as tetrabenzo – tetraazaporphyrins (TBTAP) [4-7, 11].

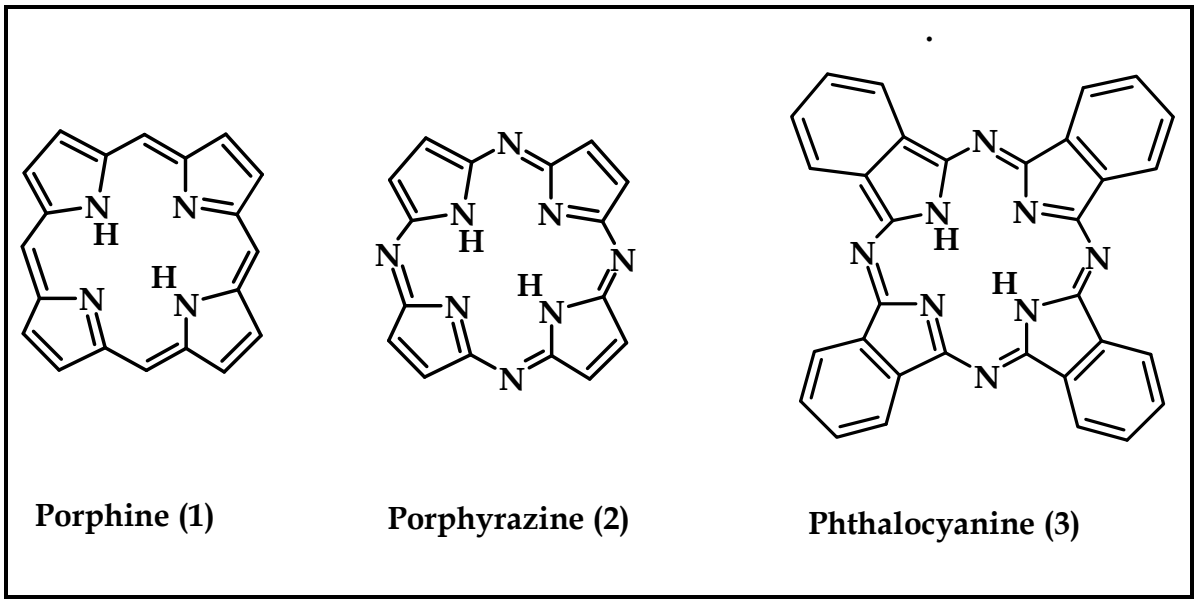

Figure 1.1: Molecular structures of porphyrin – like molecules.

The pyrrole nitrogen atoms form a cavity into which metal ions can be incorporated [12]. More than 70 metal ions can and have been inserted into the phthalocyanine cavity by a coordinate-covalent bond between the nitrogen atoms and metal ions to yield metallophthalocyanines (MPcs, **4**), Fig. 1.2.

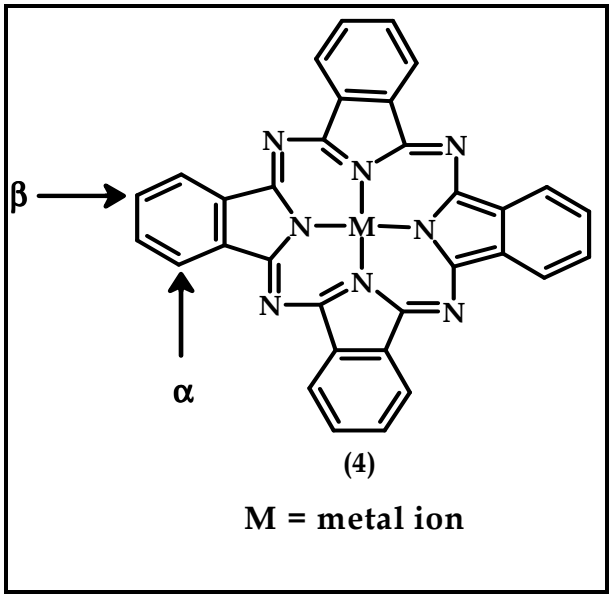

Figure 1.2: The structure of metallophthalocyanines (MPcs)

The geometry of MPcs is determined by the size of metal ion in the Pc cavity. An un-metallated Pc (H_2Pc) (**3**) has a square planar geometry with a D_{2h} symmetry. If the planarity of the MPc complex is maintained following metal ion insertion into the Pc cavity, the symmetry increases from D_{2h} to D_{4h}. The increased symmetry results from the reduction in the allowed electronic transition of the complex. The diagonal distance between nitrogen atoms in the Pc cavity is ~ 396 pm [12, 13] and may limit larger metal ions such as Ta^{5+} [14], Ti^{4+} [15] and V^{4+} [16] from fitting perfectly into the cavity of the Pc. This distorts and reduces the geometry and symmetry of the macrocycle to C_{4v}. For example OTiPc has a C_{4v} symmetry [15] and Cl_2TiPc has a D_{3h} symmetry [17].

In cases where a larger metal ion is coordinated to the phthalocyanine ring, the ion sits on top of the ring and is located between 0.1 and 1.8 Å from the plane defined by the four isoindole nitrogen atoms [18]. This results in an angle (⌀) of less than 180^o

between the plane of the isoindoline unit and the nitrogen atom – metal ion (N-M) bond {Fig. 1.3(b)} compared to Fig. 1.3(a) where the angle is 180°. Such a bonding situation introduces conformational stress into the phthalocyanine ring, particularly for the sp^2 isoindoline nitrogen atoms.

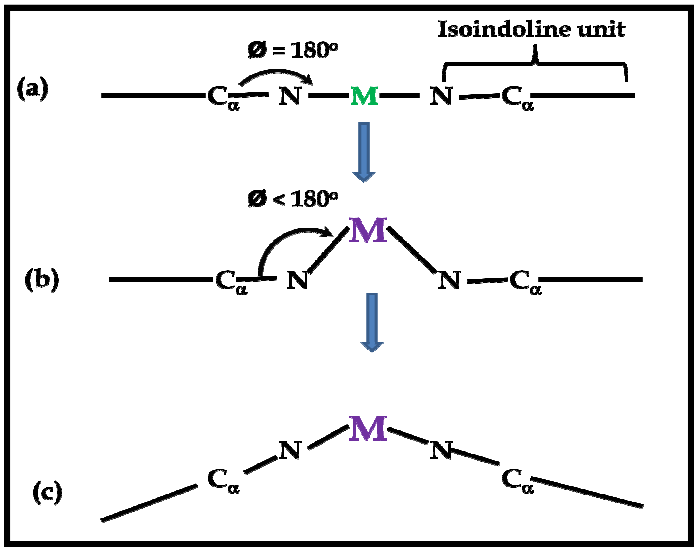

Figure 1.3: Model structures of (a) a complex with a small metal ion and (b, c) a complex with a larger central metal ion during (b) and after rearrangement.

In response to the stress, the phthalocyanine ring restuctures the isoindoline units rotating them around axis via their C_α atoms {Fig. 1.3(c)}, thereby re-storing the 180° angle between the isoindoline unit and the N-M bond. After rearrangement, the molecule maintains a concave shape {Fig. 1.3(c)} [18].

The metal out of plane distances as defined by the four isoindole nitrogen atoms and the out of plane distances. Metal ions distances in this work vary from 0.575 to 1.234 Å [14-16]. These values are rough estimates from work that has been done by a number of researchers [14-16] where they looked at different MPcs with different substituents and axial ligands but the same metal centres. From the structure of vanadium phthalocyanines (OVPc) studied in 1980, Ziolo *et al*. [16] found that

vanadium was positioned 0.575 Å above the plane. In 1982 Hiller *et al.* [15] published the two structures of TiOPc and in both structures titanium was positioned 0.70 and 0.71 Å above the plane. The structure of TaF_3Pc was elucidated by Schweiger *et al.* [14] in 1997 where they found that tantalum was positioned at a staggering distance of 1.234 Å above the plane [14]. In this work, phthalocyanines with large metal ions that include tantalum, titanium and vanadium will be synthesised

MPcs are widely used in a number of applications in the scientific and medicinal fields. This is owed to their notable properties that include flexibility, chemical, physical and thermal stabilities. Traditionally, Pcs are used as dyes and pigments for jeans, inks in pens, ink – jet printing and paints for plastics [12]. They find many applications in light driven processes such as photocatalysis [12, 19-22], photoredox reactions [12] and photovoltaic cells [23]. Recently, a lot of attention has been directed to applications in material science [24-28], in these areas Pcs have been used as liquid crystals [29-31], Langmuir-Blodgett films [32-35], in electrophotographic applications [36-38], optical data storage [39-41], in fuel cells [42], electrochemical sensors [43-45] and in nonlinear optics (NLO) [46-48]. Pcs have also attracted a lot of attention in medical applications, in particular photodynamic therapy (PDT); a cancer treatment that uses photosensitizers (Pcs or porphyrins) laser light and oxygen [1, 49-51].

The interest in this work is to further explore MPcs containing large central metals for application in photo- and electro- catalysis.

1.2. The syntheses of phthalocyanines

Synthesis of phthalocyanines is achieved via the cyclotetramerisation of phthalic acid derivatives that contain nitrogen functional groups. Some of the classical precursors include phthalonitriles and diiminoisoindolines. The aim of this work is to synthesise tetra- and octa-substituted metallophthalocyanines with sulphur bearing substituents.

1.2.1. Unsubstituted phthalocyanines

Unsubstituted phthalocyanines are achieved through a one step condensation reaction which involves precursors commonly derived from phthalic acid (**5**) and its derivatives. Some of the phthalic acid derivatives include o-cyanobenzamide (**6**), phthalimide (**7**), phthalic anhydride (**8**), o-dibromobenzene (**9**), diiminoisoindoline (**10**) and phthalonitrile (**11**), **Scheme 1.1.**

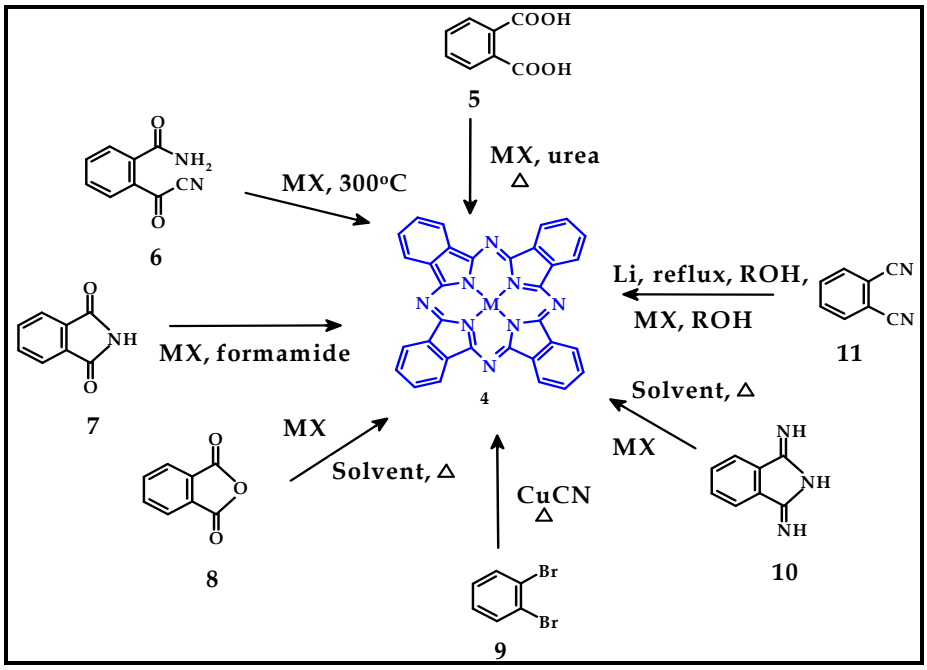

Scheme 1.1: Various synthetic routes for MPcs from common starting material, where MX = metal salt.

Generally, phthalonitriles can be reacted under various reaction conditions to give either metallated (**4**) or metal free phthalocyanines (**3**). Reacting phthalonitriles (**11**) with a strong base such as 1,8-diazobicyclo[5.4.0]undec-7-ene (DBU) or 1,5-dizabicyclo[4.3.0]non-5-en (DBN) in alcohols affords metal free phthalocyanines (**3**). This approach generally gives very high yields and is the simplest approach. Metal free phthalocyanines (**3**) are guaranteed to form in high yields when a phthalonitrile (**11**) is treated with labile metals such as lithium or sodium in *n*-pentanol or other alcohols. This affords disodium or dilithium phthalocyanines that can easily be demetallated by treatment with concentrated H_2SO_4 or glacial acetic acid [5, 52, 53]. Alternatively, phthalonitriles (**11**) can be converted into 1,3-diiminoisoindoline (**10**) in the presence of ammonia gas at room temperature in methanol solution [54]. The advantage of using 1,3-diiminoisoindoline (**10**) is that cyclization is achieved without difficulty. When 1,3-diiminoisoindoline (**10**) is refluxed in the presence of a hydrogen donor such as succinonitrile or boiling tetralin, a metal free phthalocyanine is produced [5, 52].

A phthalonitrile (**11**), 1,3-diiminoisoindoline (**9**) or o-cyanobenzamide (**6**) and an appropriate metal salt may also be used to achieve specific metallated phthalocyanines. Metal-free phthalocyanines (**3**) can also be used as precursors for MPcs by refluxing them with the suitable metal salt in high boiling solvents such quinoline or dimethylformamide [55]. This method however is suitable for metal ions with small radii that can easily be accommodated into the Pc cavity [55]. For large scale production of phthalocyanines, phthalic anhydride (**8**) is often used. This

method if favoured for its cost effectiveness and simplicity [56, 57], however the purity of the products is less than when phthalonitriles are employed.

1.2.2. Substituted phthalocyanines

Poor solubility in most common solvents is synonymous with unsubstituted phthalocyanines. This is derived from the extreme hydrophobicity of the aromatic core and planarity of the phthalocyanine which causes the molecules to stack up on each other resulting in highly stable crystal structures with high molecular lattice energies. The insolubility of Pcs is a major advantage in their use as dyes and pigments as this guarantees strong attachments to material and resistance against heat, light and chemicals to avoid fading. However, most applications require solubility in most common organic solvents and water, therefore in an effort improve solubility, substituents can be introduced on the phthalocyanine ring either on the peripheral (β) or non-peripheral (α) positions, (Fig. 1.2). These facilitate solvation since they increase the distance between the stacked molecules [58,59].

Substitution of phthalocyanines can be achieved by two basic methods. The first entails the direct substitution onto a preexisting phthalocyanine and a classic example of this is the sulphonation of phthalocyanines [60]. The second method (discussed in detail in the sections below) involves the condensation of substituted precursors and it results in far cleaner reactions. This method will be employed for the synthesis of MPcs in this work.

1.2.2.1. Tetra-substituted phthalocyanines

Introducing substituents on one of the α or β positions of the Pc ring results in tetrasubstituted Pc with improved **solubility** as well as altered electronic properties. The condensation of a mono substituted phthalonitrile at either the α (**12, 13**) or β position (**15, 16**) (**Scheme 1.2**) affords a mixture of positional tetra-substituted phthalocyanines (isomers). For α substituted, the symmetry of isomers is C_{4h}, D_{2h}, C_{2v} and C_s with a statictical mixture of 12.5 %, 12.5 %, 25 % and 50 %, in that order [61, 62].

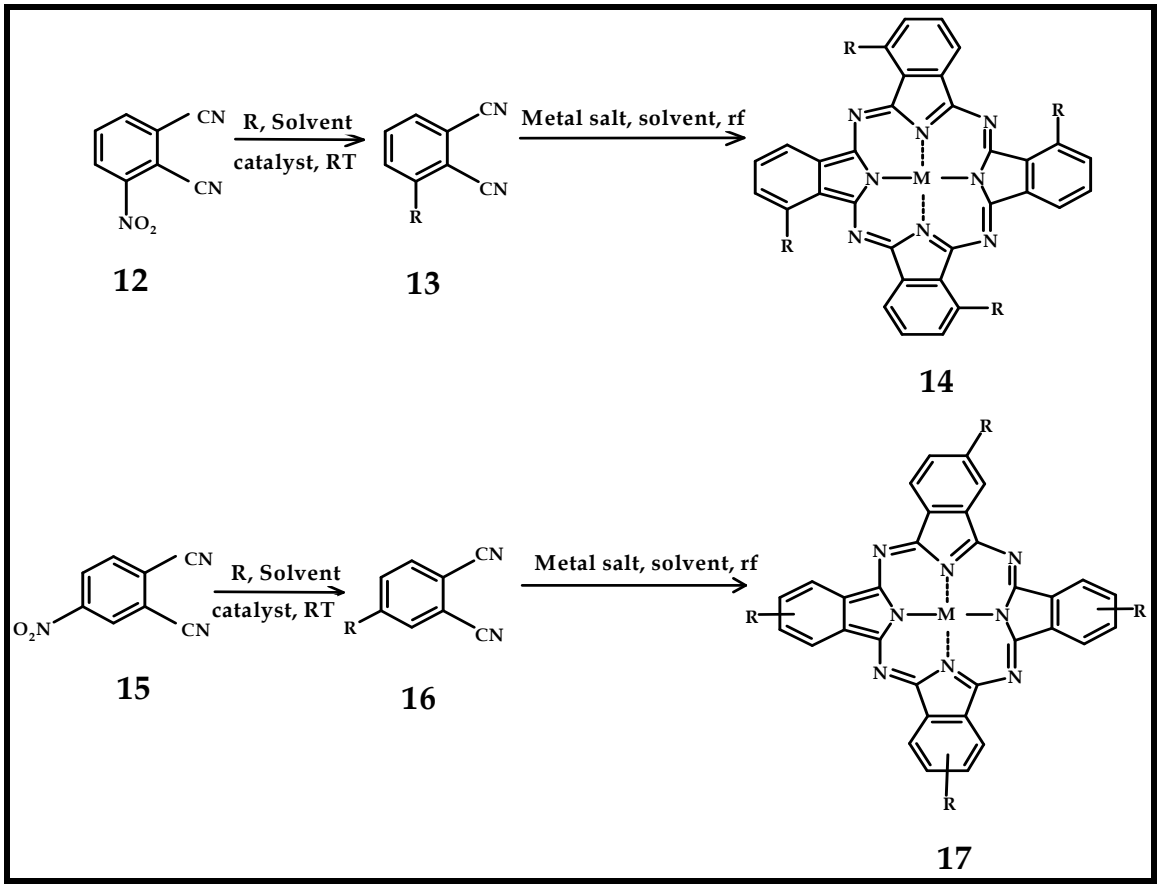

Scheme 1.2: Synthesis of tetrasubstituted MPcs from monosubstituted phthalonitriles at the non-peripheral (α) (12, 13) and peripheral (β) (15, 16) positions, rf = reflux.

The separation of these isomers is theoretically possible due to their different geometries, but it has only been accomplished for very specific phthalocyanine using a specially designed high performance liquid chromatography (HPLC) column [59, 63]. Generally the best results of separation are enriched isomeric fractions even in cases where there is specialised equipment [63]. State-of-the-art fields such as nonlinear optics require distinct molecular geometries. On the other hand, an isomeric mixture is often suitable for many applications thus the tedious process of separating the reaction mixture for individual isomers was not part of this work.

1.2.2.2. Octasubstituted peripherally and non-peripherally phthalocyanines

The major advantage of preparing octasubstituted phthalocyanines is that isomerically pure products are obtained which are easier to purify than tetrasubstituted phthalocyanines. The synthesis entails the cyclotetramerisation of 4,5-disubstituted phthalonitriles (**18**), **Scheme 1.3**, to achieve peripherally octasubstituted phthalocyanines (**19**).

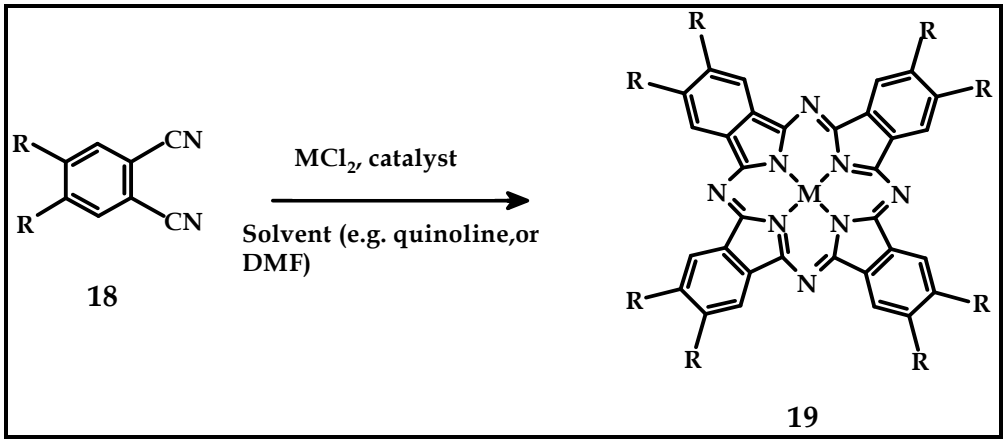

Scheme 1.3: Synthesis of octasubstituted MPc from disubstituted phthalonitrile (18).

In this work only alkylthio (RS) non-peripherally octasubstituted phthalocyanines will be synthesised, hence a more detailed explanation is given for the non-peripherally substituted derivatives.

The method employed for the synthesis of non-peripherally octasubstituted phthalocyanines was developed by Cook's group [64]. It involves the use of dicyanohydroquinone (**20**) as the starting material. This is followed by the formation of a triflate (**21**) that is a result of reacting 2,6-dicyanohydroquinone (**20**) with *p*-toluenesulfonyl chloride and potassium carbonate (a base) in acetone as depicted in **Scheme 1.4**. Nucleophilic aromatic substitution of the alkylthio group occurs in the presence of a base (K_2CO_3) to afford an alkylthio substituted phthalonitrile (**22**). The phthalonitrile (**22**) is then refluxed in 1-pentanol in the presence of a metal salt and DBU, which is essential in the cyclisation to form the MPc (**23**).

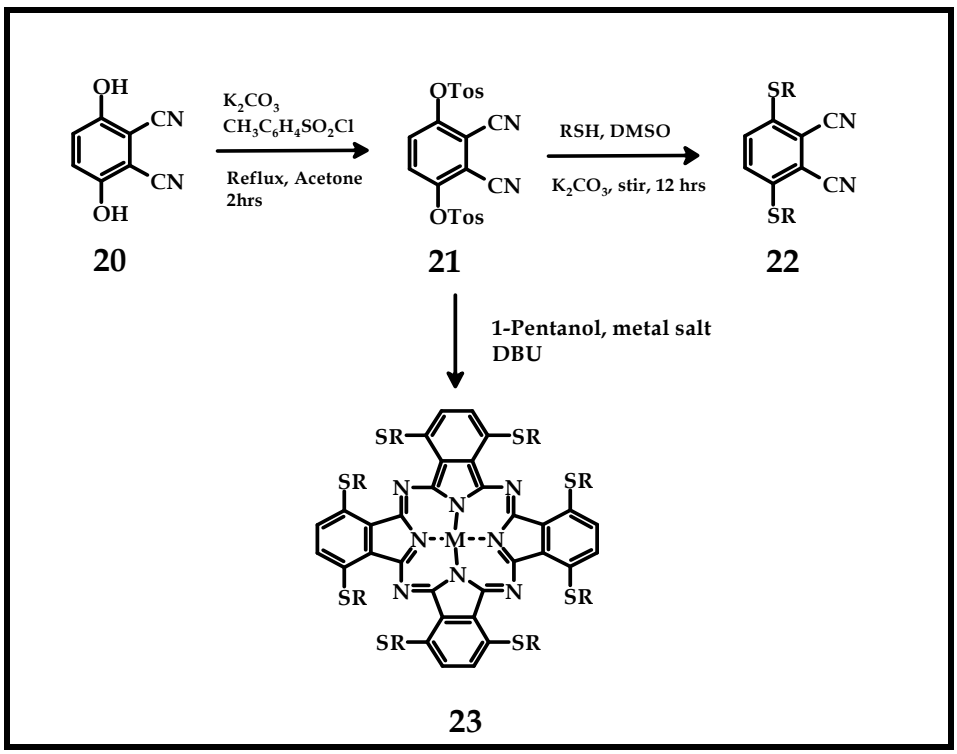

Scheme 1.4: Synthesis of non-peripherally substituted alkylthio MPc.

1.2.2.3. Survey of the synthesis of TaPc, TiPc and VPc complexes

This work focuses on the synthesis of thio substituted titanium, tantalum and vanadium phthalocyanines and a selected number of known thio substituted Pcs are listed and compared in Table 1.1 [65 – 72]. The TiPc complexes are relatively known compared to the TaPc and VPc as shown in Table 1.1, particularly the tetra substituted TiPc complexes. The scarcity of TaPc complexes arises from the difficulties in synthesis caused by the large size of tantalum metal which makes cyclisation difficult. Cl_3TaPc [65] and tetra sulphonated tantalum phthalocyanine {TaPc$(SO)_3$} [66] have been reported. Thio substituted VPc complexes are similarly not well known and Table 1.1 lists a selection of known VPc complexes and they include octylpenta thio [67] and tetra-ortho-[(4-*t-butyl*) thiophenoxy) [68] and ortho-octadecylthiol [68] substituted VPcs. For this reason, there is a need to synthesise more thio substituted TiPc, TaPc and VPc complexes.

As Table 1.1 shows, TaPc complexes are not too eminent in the history of phthalocyanines therefore the syntheses of tetra and octasubstituted TaPc complexes with thio substituents will be carried out in this work. The complexes that will be synthesised are shown in Fig. 1.4 and 1.5. Similarly tetra substituted TiPc and VPc complexes will be synthesised (Fig. 1.4). Alkythio (1-pentane thiol and 1-octanethiol) and 2-mercaptopyridine were the desired substitutents for reasons that include improving solubility, lowering oxidation potentials in order to improve electrocatalytic oxidation and increasing triplet state yields hence increasing singlet oxygen yields required in photocatalysis.

Table 1.1: A list of selected known TiPc, TaPc and VPc complexes containing alkylthio, alkylthio substituents on the peripheral and non-peripheral positions.

MPcs	**Q band absorption(nm)**	**Solvent**	**References**
β-OTiPc(SPh)$_4$	714	DCM	[70]
α-OTiPc(SPh)$_4$	747	DCM	[70]
β-OTiPc(SCH$_2$Ph)$_4$	714	DCM	[70]
α-OTiPc(SCH$_2$Ph)$_4$	746	DCM	[70]
β-OTi(SC$_6$H$_{13}$)$_4$	720	CHCl$_3$	[71]
α-OTiPc(SC$_5$H$_{11}$)$_8$	808	DCM	[72]
β-OTiPc(SC$_6$H$_{13}$)$_8$	739	CHCl$_3$	[71]
β-OTiPc(SC$_2$H$_4$N(CH$_3$)$_2$)$_4$	723	CHCl$_3$	[69]
β-XTiPc(SC$_2$H$_4$N(CH$_3$)$_2$)$_4$	720	CHCl$_3$	[69]
β-OTiPc(SC$_2$H$_4$N(CH$_3$)$_2$)$_8$	739	CHCl$_3$	[69]
β-OTiPc(SC$_2$H$_4$N(CH$_3$)$_2$)$_8$	729	CHCl$_3$	[69]
Cl$_3$TaPc	697	CHCl$_3$	[65]
Cl$_3$TaPc(SO$_3$)$_4$	696	DMSO	[66]
α-OVPc(SC$_5$H$_{11}$)$_8$	850	DCM	[67]
OVPc(-ortho-SPh-*4t-butyl*)$_4$	748	DCM	[68]
OVPc(ortho-SC$_{10}$H$_{11}$)$_4$	745	DCM	[68]

Ph = phenyl, X = catechol

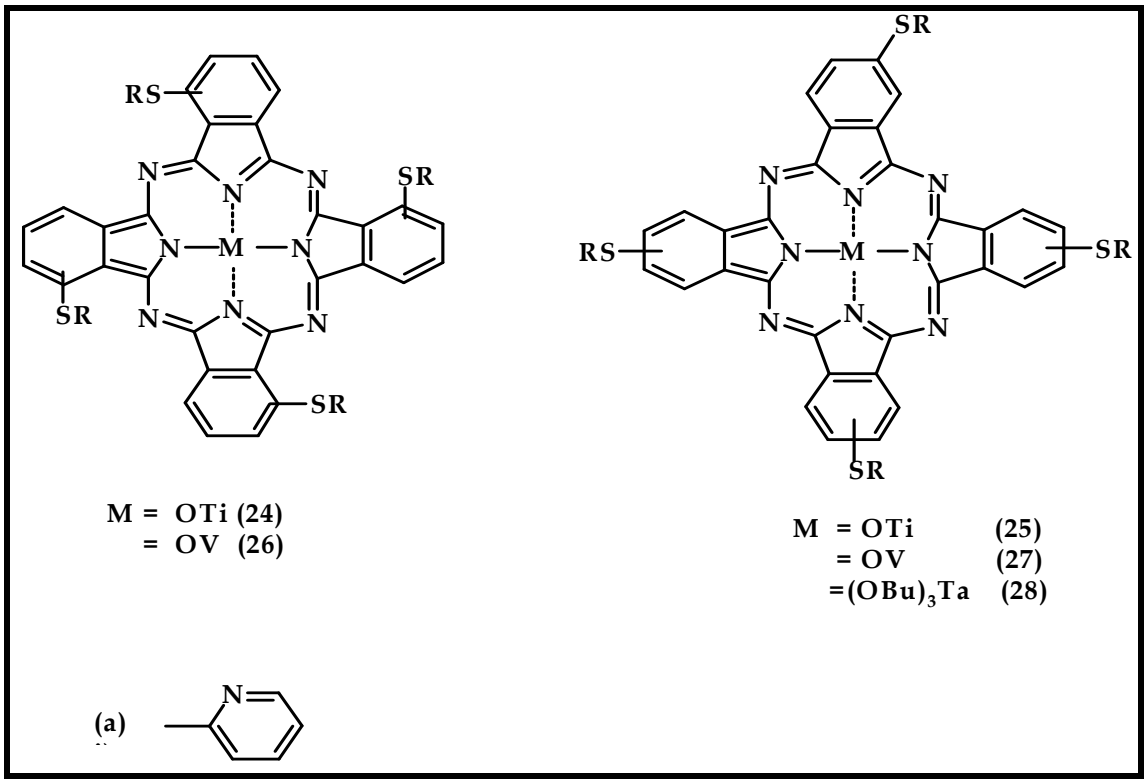

Figure 1.4: Structures of tetrasubstituted TiPc, TaPc and VPc complexes synthesised in this work.

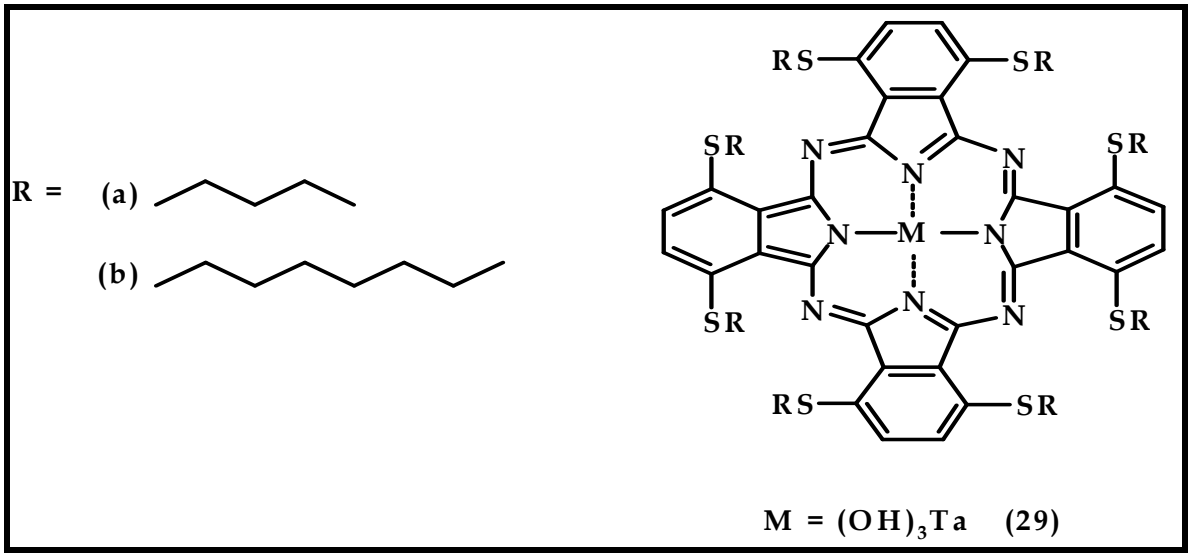

Figure 1.5: Structures of octasubstituted TaPc complexes synthesised in this work.

Nickel tetra amino phthalocyanine (NiTAPc, **30**) which is not new will also be employed in this work

1.3. Electronic absorption spectra for phthalocyanines

Metallophthalocyanines (MPcs) are characterized by two major absorption bands in the visible region of the spectrum (~ 670 nm), namely the Q band and a weaker absorption called the B band [73], Fig. 1.6.

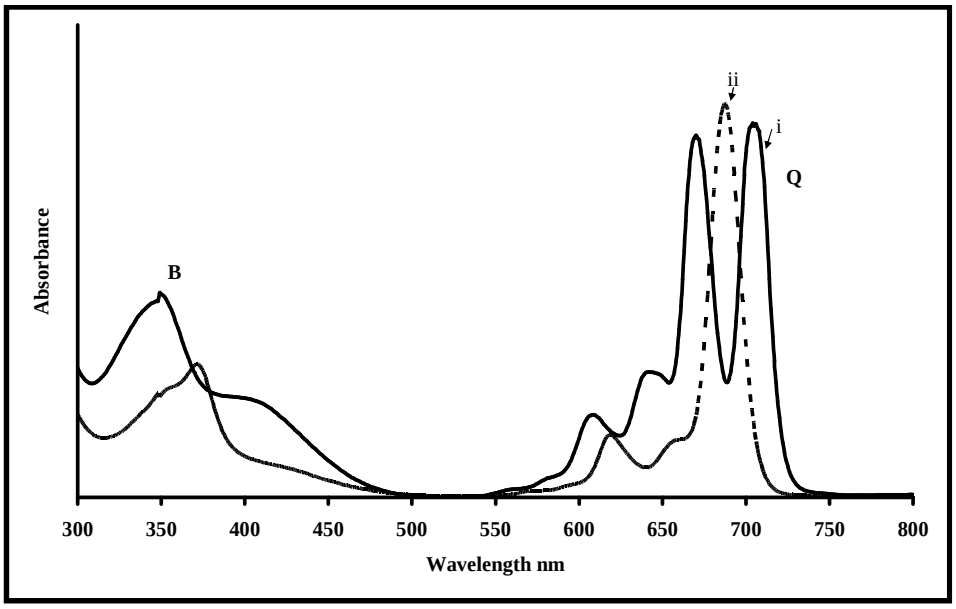

Figure 1.6: Ground state electronic absorption of an (i) unmetallated phthalocyanine and (ii) metallated phthalocyanine.

The assignment of the Q and B bands are based on the four-orbital model (Fig. 1.7), proposed by Gouterman's group [73-75]. The Q band arises from π - π^* transitions from a_{1u} the highest occupied molecular orbitals (HOMO) of the MPc ring to the lowest unoccupied molecular orbitals (LUMO), e_g^*. The symmetry of an unmetallated Pc, H_2Pc, is reduced due to the two protons in the cavity and this results in the splitting of the Q band (Fig.1.6), caused by the e_g orbital losing degeneracy.

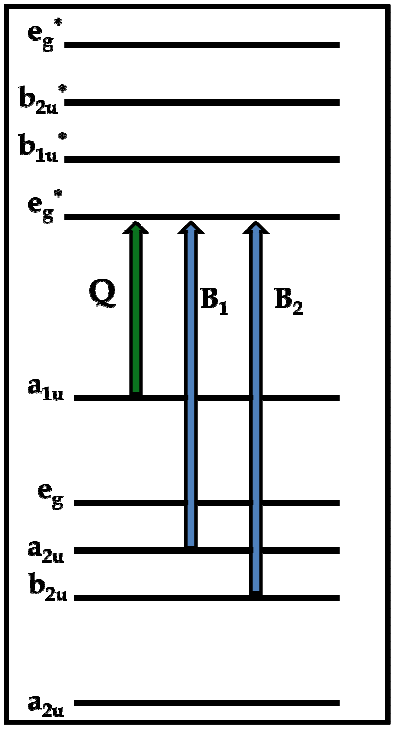

Figure 1.7: Electronic transitions in phthalocyanines showing the origin of the Q and B absorption bands.

Other characteristic bands of MPcs namely the N, L and C bands are found at higher energies (below 300 nm) in the ground state electronic absorption spectra. They are primarily due to π - π^* transitions [13].

The Q band wavelength is influenced by the position of substituents on the Pc ring as well as the nature of the substituents (electron donating or withdrawing groups). Substituting at the non-peripheral (α) position shows a greater shift to the red region than peripheral (β) substitution [76]. This is as a result of more destabilisation of the HOMO when substitution is at the α position compared to β position. Electron donating substituents such as alkoxy, alkylthio or alky(phenyl)thio groups tend to shift the spectrum to the red region [77, 78]. This is due to the destabilisation of the

HOMO such that the HOMO - LUMO gap is reduced and thus lower energies are observed [79]. Electron withdrawing groups such as nitro or sulphonyl groups, tend to shift the Q band to the blue region [77]. The nature of the central metal as well as their oxidation state can shift the position of the Q band. A red shift is typically observed with increase in size of the central metal and its oxidation state [67, 72, 80].

Listed in Table 1.1 are the of UV/Vis data (Q band positions) for a selected number of TiPc, VPc and TaPc complexes. Noticeably, the α substituted MPc complexes show a significant red shift in the Q band position compared to β substituted MPc complexes. Also, to note is the typical red-shiftness of octa substituted complexes.

1.4. Photophysics and photochemistry

The physical and chemical changes that are induced by the action of light absorption are represented as studies of photophysics and photochemistry, respectively. The photochemical studies of the TiPc and TaPc complexes (Fig. 1.4 and 1.5) which are quantified by singlet oxygen and photodegradation quantum yields; will be carried out in this work. Similarly, photophysical studies will be carried as well, where triplet quantum yields and triplet lifetimes will be determined. Phototransformation of cyclohexene using these complexes will be perfomed and all these studies will also be carried out in the presence of gold nanoparticles.

When a molecule on the ground state ($\mathbf{S_0}$) absorbs light, it gets excited to the unoccupied orbitals of higher energy states, $\mathbf{S_1}$, as shown by the Jablonski diagram in Fig. 1.8. In solution, excited molecules are short lived due to collisions and thus

undergo vibrational relaxation (**VR**) to the first level of S_1 state. From the **S_1** state the excited molecules can either loose energy by emitting light (fluorescence, **F**) or by releasing heat to the surroundings through internal conversion (**IC**). Some excited molecules may undergo intersystem crossing (**ISC**) into the triplet excited state (**T_1**), where the energy rich molecules (if long lived) transfer energy to other molecules through photosensitization (**PS**) or the molecules may emit light (phosphorescence, **P**) and therefore return to their ground state (**S_0**) [81].

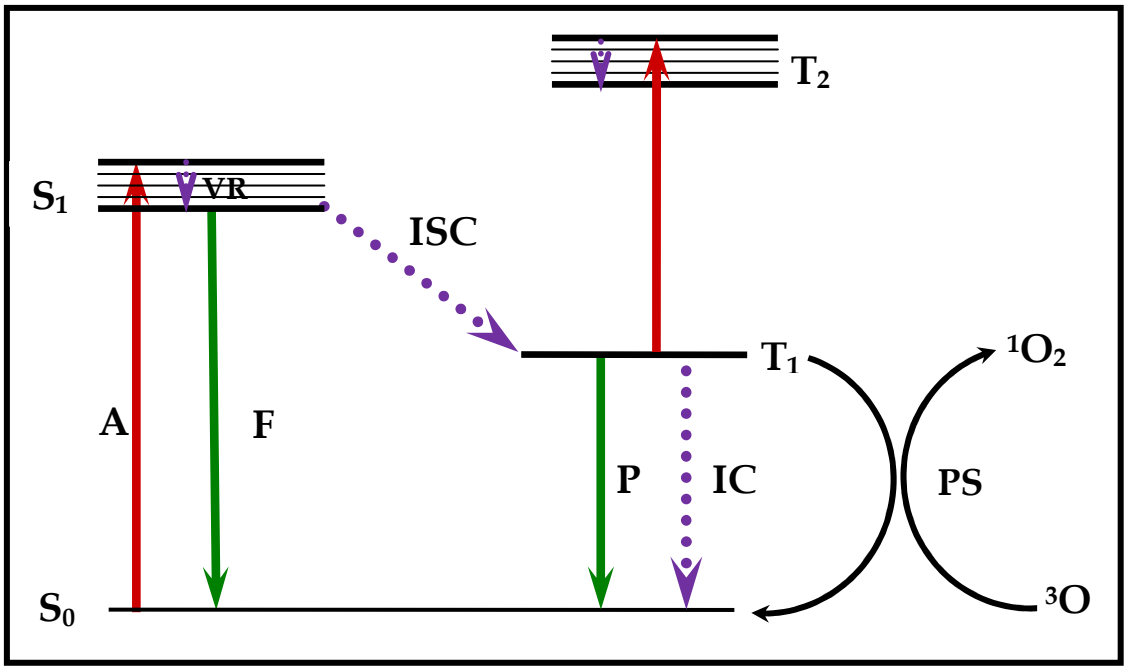

Figure 1.8: A customized Jablonski diagram showing transitions between the excited and ground states, where A = Absorption; VR = Vibrational relaxation, IC = Internal conversion, ISC = Intersystem crossing; F = Fluorescence; P = Phosphorescence; PS = photosensitization.

1.4.1. Photophysical processes: triplet quantum yield (Φ_T) and lifetimes (τ_T).

The triplet state parameters, the triplet lifetimes (τ_T) and triplet quantum yields (Φ_T), were determined using a technique called laser flash photolysis where

the change in absorbance in the triplet state (T_1 – T_2), which is directly related to the triplet quantum yield [82], is determined.

The triplet quantum yield (Φ_T) is determined by the triplet absorption comparative method [82] using zinc phthalocyanine (ZnPc) as a standard, Equation 1.1.

$$\Phi_T = \Phi_T^{Std} \cdot \frac{\Delta A_T . \varepsilon_T^{Std}}{\Delta A_T^{Std} . \varepsilon_T} \qquad (1.1)$$

where ΔA_T and ΔA_T^{Std} are the changes in the triplet state absorbance of the sample and the standard, respectively. ε_T and ε_T^{Std} are triplet state molar extinction coefficients for the sample and the standard, respectively. Φ_T^{Std} is the triplet quantum yield for the standard, ZnPc. ε_T and ε_T^{Std} were determined from the molar extinction coefficients of their respective ground singlet state (ε_S and ε_T^{Std}), the changes in absorbances of the ground singlet states (ΔA_S and ΔA_S^{Std}) and changes in the triplet state absorptions, (ΔA_T and ΔA_T^{Std}) according to Equations 1.2 and 1.3:

$$\varepsilon_T = \varepsilon_S \frac{\Delta A_T}{\Delta A_S} \qquad (1.2)$$

$$\varepsilon_T^{Std} = \varepsilon_S^{Std} \frac{\Delta A_T^{Std}}{\Delta A_S^{Std}} \qquad (1.3)$$

The lifetimes of the triplet state, τ_T, are determined by fitting data obtained from the laser flash photolysis into OriginPro 7.5 software, for example.

MPcs with high quantum yields ($\Phi_T > 0.40$) and long triplet lifetimes ($\tau_T > 1$ μs) are considered efficient as photosensitisers. The Φ_T values are influenced by several

factors which include the nature of the MPc complex and solvent used. Heavy atoms or substituents bearing heavy atoms such as halogens encourage ISC thus resulting in high Φ_T values. In addition, phthalocyanines with diamagnetic metals such as Ga [83], In [84] or Al [85] have larger Φ_T values and longer triplet lifetimes than paramagnetic ones such as Cu [86]

1.4.2. Photochemical processes

Photochemical parameters of interest to this work are singlet oxygen (Φ_Δ) and photodegradation (Φ_P) quantum yields. These parameters are essential for photocatalysis.

1.4.2.1. Singlet oxygen quantum yield (Φ_Δ)

Singlet oxygen ($^1O_2$, $^1\Delta_g$) is generated when oxygen in its triplet state ($^3O_2$) interacts with a sensitizer (MPc) in a process called photosensitization, (**Scheme 1.5**, Equations 1.4 - 1.6; see also Fig. 1.8), where the excited $^3MPc^*$ transfers its energy to molecular oxygen ($^3O_2$) to produce the highly reactive and potent singlet oxygen via a mechanism called Type II.

MPc + *hv*	⟶	$^1MPc^*$	⟶ $^3MPc^*$	(1.4)
$^3MPc^* + {}^3O_2$	⟶	$^1O_2\,(^1\Delta_g)$ + MPc		(1.5)
$^1O_2(^1\Delta_g)$ + MPc	⟶	Oxidation Products		(1.6)

Scheme 1.5: Type II mechanism, where *hv* = light energy.

It has been observed that following photosensitization, molecular oxygen returns to its ground state and in an event where there is sufficient molecular oxygen, singlet

oxygen is produced several times from the same MPc concentration. Eventually, singlet oxygen will react with the MPc resulting in degradation of the MPc. Photosensitisation can also take place through Type I mechanism (**Scheme 1.6,** Equations 1.7 – 1.12) which involves the production of radical ions following the interaction of an $^3MPc^*$ with molecular oxygen in its ground state to forms superoxides and hydroperoxyl radicals.

$^3MPc* + O_2 \rightarrow MPc^{+\bullet} + O_2^{-\bullet}$	(1.7)
$^3MPc* + Subs \rightarrow MPc^{-\bullet} + Subs^{+\bullet}$	(1.8)
$MPc^{-\bullet} + O_2 \rightarrow MPc + O_2^{-\bullet}$	(1.9)
$O_2^{-\bullet} + H_2O \rightarrow OH^- + HO_2^{\bullet}$	(1.10)
$HO_2^{\bullet} + HO_2^{\bullet} \rightarrow H_2O_2 + O_2$	(1.11)
$H_2O_2 + O_2^{-\bullet} \rightarrow OH^{\bullet} + OH^- + O_2$	(1.12)

Scheme 1.6: Type I mechanism.

Singlet oxygen may be determined using two methods: (i) using chemical quenchers (ii) or using luminescence at 1270 nm [87]. In this work a chemical quencher 1,3-diphenylisobenzofuran (DPBF) was used; it is commonly used as a quencher in organic solvents. Other examples of quenchers include tetrasodium anthracene-9,10-bis-methylmalonate (ADMA), thiols, carotene, ascorbate and histidine [87, 88].

The reaction of singlet oxygen with DPBF yields endoperoxides as shown in **Scheme 1.7.**

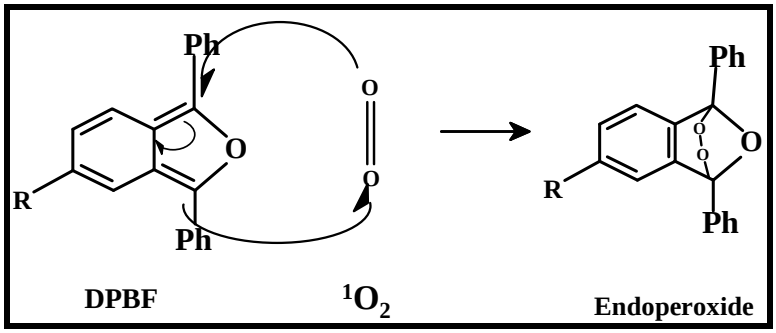

Scheme 1.7: [4+2] cycloaddition of DPBF by singlet oxygen.

After singlet oxygen is generated, it is trapped by a singlet oxygen quencher DPBF (**Scheme 1.7)**. The disappearance of the quencher is directly related to the production of singlet oxygen and this is monitored spectroscopically.

To quantify the singlet oxygen generation, quantum yields (Φ_Δ) of singlet oxygen will be determined. In 1905, Einstein postulated that one molecule was associated with one quantum [89], and emphasised the importance of photochemical reactions in relation to Einstein' postulation. Consequently, the Photochemical Equivalent Stark-Einstein law was invented and it states that 'each molecule that takes part in a photochemical reaction absorbs one quantum of light' or briefly 'one molecule one quantum'. Therefore the quantum yield in this regard is = {Number of reacting molecules]/[Number of photons absorbed} [89].

Singlet oxygen quantum yield values may be determined using the relative method [90 - 92], with ZnPc as reference and DPBF as chemical quencher, using Equation 1.13:

$$\Phi_\Delta = \Phi_\Delta^{Std} \cdot \frac{R_{DPBF} I_{abs}^{Std}}{R_{DPBF}^{Std} I_{abs}} \qquad (1.13)$$

where Φ_{Δ}^{Std} is the singlet oxygen quantum yield for the standard, e.g. ZnPc. R_{DPBF} and R_{DPBF}^{Std} are the DPBF photodegradation rates in the presence of a sensitizer under investigation and the standard respectively. I_{abs} and I_{abs}^{Std} are the rates of light absorption by the sensitizer and standard, respectively. The singlet oxygen quantum yield values should, to a certain extent, correspond to the triplet quantum yield values. The latter has to be greater than the former and the higher the population and the longer the lifetime in the triplet state, the more likely the chances of getting notable singlet oxygen quantum yields.

1.4.2.2. Photodegradation quantum yield (Φ_P)

Photodegradation is a photochemical process that involves the degradation of the conjugated chromophore of the phthalocyanine into smaller molecular fragments. This process is initiated and driven by singlet oxygen in the presence of light to afford the photo-oxidation products, phthalamide, as suggested by Schnurpfeil *et al.* [92], **Scheme 1.8**.

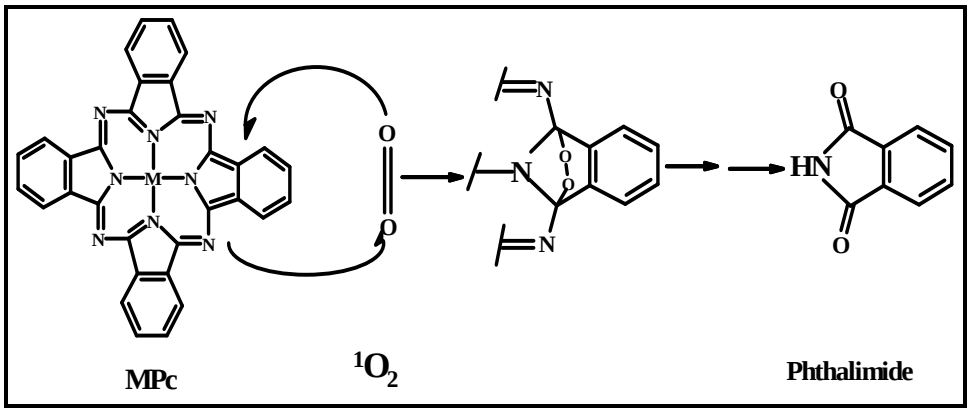

Scheme 1.8: [4+2] cycloaddition reaction of MPc with singlet oxygen

The mechanism suggests that singlet oxygen reacts with tetra-azaporphyrin derivatives in a Diel-Alder [4+2]-cycloaddition, with the phthalocyanine acting as a diene and the singlet oxygen as the dienophile.

There are several factors that can influence the process of photodegradation. It has been reported [93, 94] that electron donating substituents on the phthalocyanine ring encourage rapid degradation due to the ease of oxidation brought by the presence of these substituents. Electron-withdrawing substituents, on the other hand have a tendency to stabilise the phthalocyanine ring, making oxidation difficult to occur.

Solvents also influence photodegradation processes; it has been observed that solvents such as chloroform and dichloromethane (DCM) encourage photodegradation due to radicals formed from C-Cl bond cleavage assisting in the photodegradation process. In aqueous media, photodegradation rates are low, presumably due to aggregation, given that the generation of singlet oxygen in aggregates is very low [95, 96].

Photodegradation quantum yield, Φ_P, indicates the number of molecules degraded per quantum of light absorbed, this can be used to determine the stability of a phthalocyanine when exposed to light. Pc photodegradation is identified by the decrease in absorbance of the Q band of the phthalocyanine under investigation, without the formation of new peaks in the visible region.

To determine photodegradation quantum yield Equation 1.14 [92] will be employed:

$$\Phi_P = \frac{(C_0 - C_t)VN_A}{I_{abs}St} \qquad (1.14)$$

where C_o and C_t (mol dm^{-3}) are the MPc (under investigation) concentrations before and after irradiation, respectively; V is the reaction volume; S, the irradiated cell area (2.0 cm^2); t, the irradiation time (s); N_A, the Avogadro's number and I_{abs}, the overlap integral of the radiation source intensity and the absorption of the Pc (the action spectrum) in the region of the interference filter transmittance.

Photostability of MPc complexes is important for photocatalysis (photosensitization). The photostability of the MPc complexes depends mainly on the type of radiation, MPcs are more stable in visible light compared to UV irradiation [1]. To mimic what would happen on a large scale photocatalytic setup, photodegradation experiments will be performed under the sun for selected MPcs, and for more controlled experiments, irradiations will be performed under white light (400 to 900 nm) and at the Q band region.

1.4.3. Survey of the photophysics and photochemistry of selected TiPc and TaPc complexes

Listed in Table 1.2 are the photochemical and photophysical parameters for known alkoxythio substituted TiPc complexes and unsubstituted TiPc and TaPc complexes. Generally, all the substituted TiPc complexes showed good values of Φ_T and τ_T. The Φ_T values were above 0.40 except for the unsubstituted TiPc complex. The unsubstituted TaPc similarly showed good results. The photochemical parameters, i.e. Φ_Δ and Φ_P values were well within the expected range for good photosensitisers [1] except the stability of these complexes was in the 10^{-4} range, hence relatively unstable compared to the 'usual' 10^{-5} range.

Table 1.2: Photochemical and photophysical parameters of known TiPc and TaPc complexes.

MPc	Φ_T (DMSO)	τ_T (μs) (DMSO)	Φ_Δ (DCM)	Φ_P (DCM)	Reference
Cl_3TaPc	0.62	280	-	-	[65]
OTiPc	0.31	660	-	-	[65]
$OTi(SPh)_4$	0.82	150	0.86	4.8×10^{-4}	[20]
α-$OTi(SPh)_4$	0.38	150	0.69	5.3×10^{-4}	[20]
$OTi(SCH_2Ph)_4$	0.70	200	0.77	4.5×10^{-4}	[20]
α-$OTi(SCH_2Ph)_4$	0.50	150	0.64	5.0×10^{-4}	[20]

DMSO = dimethylsufoxide, DMF = dimethylformamide, DCM = dichlormethane.

The aim of this work is to determine the photochemical and photophysical parameters of the synthesised TiPc and TaPc complexes (Fig. 1.4 and 1.5) and their gold nanoparticles conjugates. The aim is to utilise these complexes for the phototransformation of cyclohexene, briefly discussed below.

1.4.4. Photocatalytic oxidation of cyclohexene

Petroleum companies produce tons of alkanes and alkenes as by products [97]. Since there is increasing need to conserve natural resources, it is essential that such products be re-used in other industrial processes instead of being disposed. Alkanes and alkenes can be partially oxidized to fine chemicals such as alcohols, ketones and aldehydes [98]. Phthalocyanines have been extensively used as enzyme-like catalysts for the degradation of pollutants such as chlorinated phenols [99 - 101] and sulfonated compounds [102 - 104], however, their use as photocatalysts has received

less attention hence their exploration in this work. Photocatalytic oxidation is more favourable than chemical methods (suing oxidants) since selectivity may be achieved more readily [105].

Photocatalytic oxidation may take place through Type II mechanism as shown in **Scheme 1.5**, where the energy rich MPc interacts with ground state molecular oxygen to produce singlet oxygen which is involved in the process of phototransformation. Type I mechanism in some cases has been reportedly [20] involved in the photooxidation of alkanes and alkenes, however Type II dominates.

The photochemical oxidation of alkenes using porphyrins has received more attention than when phthalocyanines [106] are used. The major difficulty of using porphyrins is their weak photostability relative to phthalocyanines, the former decompose easily, especially in oxidative media [107]. Alkene photo-oxidation using phthalocyanines has been reported before [19, 105].

No work has been reported on the photocatalytic oxidation of cyclohexene using TaPc, TiPc or VPc complexes and their gold nanoparticles conjugates. Listed in Table 1.3 are selected MPcs that have been employed in the phototransformation of cyclohexene.

Table 1.3: Cyclohexene phototransformation yields by selected MPcs

MPc	**Solvent**	**% Yield**	**Reference**
PdPcS	DMF/H_2O	19.59	[108]
AlPcS	DMF/H_2O	10.62	[108]
ZnPcS	DMF/H_2O	6.64	[108]
ZnPc	DMF/CH_2Cl_2	6.6	[19]

S = $S0_3$

Xue *et al* [108] employed palladium, aluminium and zinc phthalocyanine sulfonate to selectively photooxidize cyclohexene. The yields were 19.59, 10.62 and 6.64 %, respectively. It is very interesting to note the increasing percentage yield values with increase in the central metal size. The percentage yield values for the unsubstituted ZnPc was the same as the sulfonated ZnPc.

The aim of this work is to use sythesised TaPc and TiPc complexes (Fig. 1.4 and 1.5) and their conjugates with gold nanoparticles for the oxidation of cyclohexene. VPc complexes were not studied due to their paramagnetic nature that quenches the triplet state. Photocatalytic oxidation will take place under white light irradiation and Q band irradiation to assess the effect of different light exposures on these experiments.

1.5. Electrochemistry of phthalocyanines

Solution electrochemistry of MPcs is characterised by redox processes pertaining to metal centres or the phthalocyanine ring. MPcs have their own unique

redox properties, hence the solution chemistry of the synthesised TaPc, TiPc and VPc complexes will be carried out.

The dianion nature (i.e. Pc^{-2}) of phthalocyanines allows for their reduction or oxidation. A Pc ring can undergo up to two oxidation processes, that is, Pc^{1-}/Pc^{2-} and Pc^{0}/Pc^{1-}. This occurs by the removal of electrons from the a_{1u} orbital (HOMO) as shown in Fig. 1.9. Reduction is achieved as successive additions of electrons as follows: $Pc^{-2} \rightarrow Pc^{-3} \rightarrow Pc^{-4} \rightarrow Pc^{-5}$ and Pc^{-6} [109] where the e_g (LUMO) orbital is filled up, Fig. 1.9, each species characterised by distinct spectra.

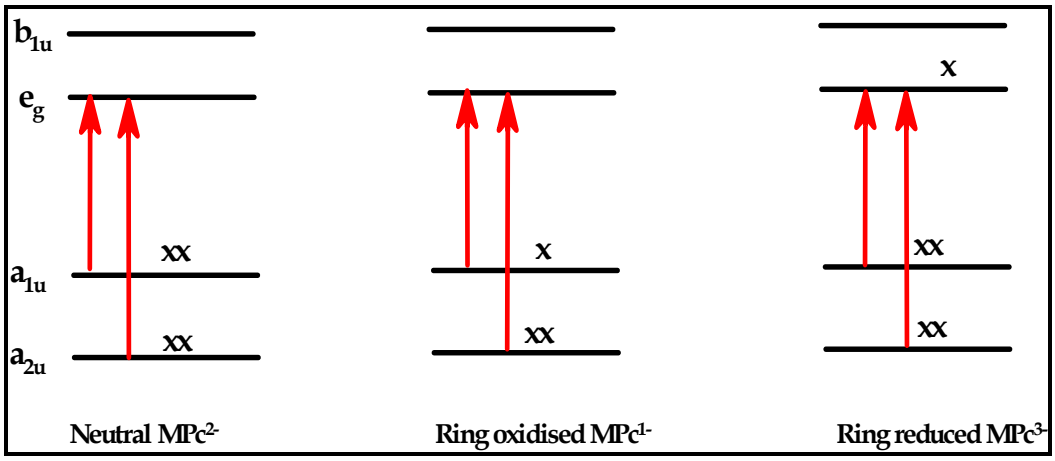

Figure 1.9: Energy levels depicting transitions in leading to oxidation and reduction of a Pc ring, x = electron.

This kind of redox activity is common in H_2Pcs and phthalocyanines with metals that are not redox active, i.e., they do not have d-orbitals between the HOMO and LUMO gap of the Pc, Fig. 1.10a. Oxidation and reduction of MPcs with redox active metals may take place on the ring or at the metal. Their metal orbitals lie between the HOMO and LUMO of the Pc, Fig 1.10b.

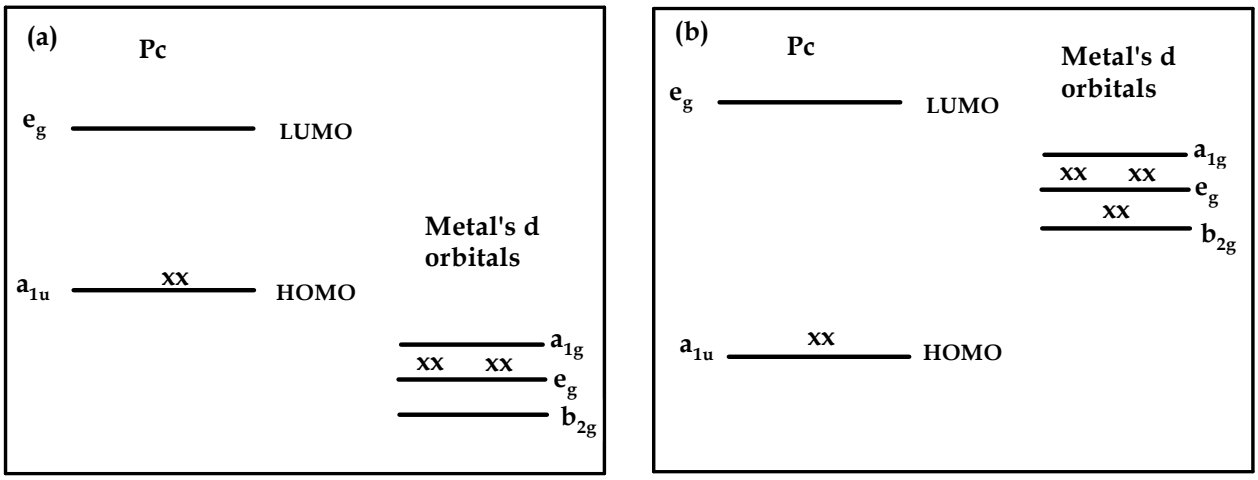

Figure 1.10: A modified energy level diagram for an MPc where the metal d orbitals are (a) not between the HOMO and LUMO of the Pc and (b) between the HOMO and LUMO, x = electron.

Several factors that can influence the redox properties of phthalocyanines in solution include the nature of substituents on the ring, the type of solvent used, nature and oxidation state of the central metal as well as the nature of the axial ligand [109]. Electron donating substituents increase the electron density making MPcs easier to oxidise whereas electron-withdrawing substituents decrease electron density thus making oxidation more difficult and reduction easier.

The newly synthesised TiPc, TaPc and VPc complexes will be characterised using cyclic voltammetry and the observed redox processes will be confirmed by spectroelectrochemistry which combines electrochemical and spectroscopic techniques to observe electrogenerated products [110-112]. For spectroelectrochemistry optically transparent thin layer electrodes (OTTLE) are often employed.

1.5.1. Survey of the electrochemical properties of TiPc, TaPc and VPc complexes

1.5.1.1. Electrochemistry of TiPc complexes

The electrochemistry of thio-substituted titanium phthalocyanines is not very well known. The few reported OTiPc are shown in Table 1.4 [70, 72, 113, 114]. Their electrochemical characteristics are rather unique. One step two electron processes have been reported [70, 113]. Most TiPc derivatives do not show oxidation processes and the range of TiPc complexes with low oxidation potentials (important for electrocatlytic oxidation) has to be increased, hence this study.

Table 1.4: Electrochemical data of TiPc complexes with thio substituents in dimethyl formamide (DMF) using tetrabutyl ammonium tetrafluoroborate ($TBABF_4$). Half-wave potentials ($E_{1/2}$) as V vs. Ag|AgCl on glassy carbon electrode (GCE).

Complex	$Ti^{II}Pc^{2-}/Ti^{II}Pc^{3-}$	$Ti^{III}Pc^{2-}/Ti^{II}Pc^{2-}$	$Ti^{IV}Pc^{2-}/Ti^{III}Pc^{2-}$	Oxidation processes	References
α-OTiPc$(SC_6H_{13})_8$	-	-1.09	-0.73	0.54, 0.36, 0.95	[72]
α-OTiPc$(SPh)_4$	-1.33	-0.46	-0.07	No oxidation	[70]
β-OTiPc$(SPh)_4$	-1.20	-0.37	-0.07	No oxidation	[70]
α- OTiPc$(SCH_2)_4$	-1.30	-0.40	-0.09	No oxidation	[70]
β-OTiPc$(SCH_2)_4$	-1.28	-0.42	-0.09	No oxidation	[70]
β-OTiPc$(SPh)_8$	-1.22	-0.38	-0.05	No oxidation	[114]
α-OTiTAPc	~ -1.3	-0.84	-0.45	0.75, 0.91	[114]

1.5.1.2. Electrochemistry of TaPc complexes

Tau and Nyokong reported unsubstituted Cl_3TaPc [65] which only showed reduction processes. This was expected as Ta has a high oxidation state thus makes oxidation difficult to take place. Reduction processes were observed at -0.31 V ($Ta^{V}Pc^{-2}/Ta^{IV}Pc^{-2}$), -0.48 V ($Ta^{IV}Pc^{-2}/Ta^{IV}Pc^{-3}$) and -0.98 V ($Ta^{IV}Pc^{-2}/Ta^{I}Pc^{-4}$) vs. Ag|AgCl, a multiple electron process was observed for the last process. Apart from this report, there is no information in literature on the electrochemistry of TaPc derivatives. This study reports on substituted TaPc derivatives. The aim is to reduce oxidation potentials hence increasing the chances of observing oxidation. The ease of oxidation will enhance their electrocatalytic properties.

1.5.1.3. Electrochemistry of VPc complexes

The electrochemical characterisation of vanadium phthalocyanines has been reported [67, 115, 116]. However, their scarcity and interesting properties have prompted new derivatives. Table 1.5 shows redox assignments of selected VPc. The study carried out by Kadish and co-workers [115] using aryloxy and alkoxy tetrasubstituted phthalocyanines showed three reduction couples and two oxidation couples which were all due to ring based processes. Sogabe and co-workers [116] studied VPc complexes with electron withdrawing groups (flouro) and observed three reduction couples and only one oxidation couple. The reason for the one oxidation couple could be due to the electron withdrawing groups which make oxidation difficult.

Table 1.5: Electrochemical data of OVPc complexes in DMF containing tetrabutylammonium perchlorate (TBAP). Half-wave potentials ($E_{1/2}$) as V vs. Ag|AgCl.

Complex	$V^{IV}Pc^{4-}/V^{IV}Pc^{5-}$	$V^{IV}Pc^{3-}/V^{IV}Pc^{4-}$	$V^{IV}Pc^{2-}/V^{IV}Pc^{3-}$	$V^{IV}Pc^{1-}/V^{IV}P2^{5-}$	$V^{IV}Pc^{0-}/V^{IV}Pc^{1-}$	References
α-$OVPc(SC_6H_{13})_8$	-1.14	-0.89	-0.54	0.68	1.02	[67]
$OVPc[OC_6H_3(t\text{-}Bu)_2]_4$	-1.94	-1.97	-0.51	0.94	1.34	[115]
$OVPc(OC_8H_{17})_4$	-2.07	-1.12	-0.62	0.76	1.21	[115]
$OVPc(Bu)_4$		-1.08	-0.58	0.94		[115]
$OVPcF_{16}Pc$	-1.41	-0.62	-0.29	1.34		[116]

Thus the range of VPc complexes suitable for electrocatalysis is extended in this study. The aim of this work is to characterise TiPc, TaPc and VPc complexes using the electrochemical methods.

1.5.2. Electrocatalysis

Electrocatalysis is defined as the enhancement of electrode kinetics by material through minimising overpotential. Many electrode reactions occur at high overpotentials because of unfavourable kinetics [117-120]. To make such electrochemical reactions useful and cost effective, it is important and necessary to find an electrocatalyst that will lower overpotentials and speed up reaction rates. The purpose of an electrocatalyst is to lower activation potentials and increase sensivity. There are two types of electrocatalysis: heterogeneous and homogeneous. Heterogeneous electrocatalysis will be employed thus it will be briefly discussed.

Heterogeneous electrocatalytic processes involve the immobilization of transition metal complexes, such as the TaPc, VPc or TiPc complexes employed in this work, on the electrode surface [119]. The catalytic process involves three steps as shown in Fig. 1.11. The initial process involves the transfer of substrate from the bulk solution to the electrode surface or within the double layer followed by the exchange of electrons between the electrode and the substrate and finally the removal of the products from the electrode surface, which may involve desorption [120].

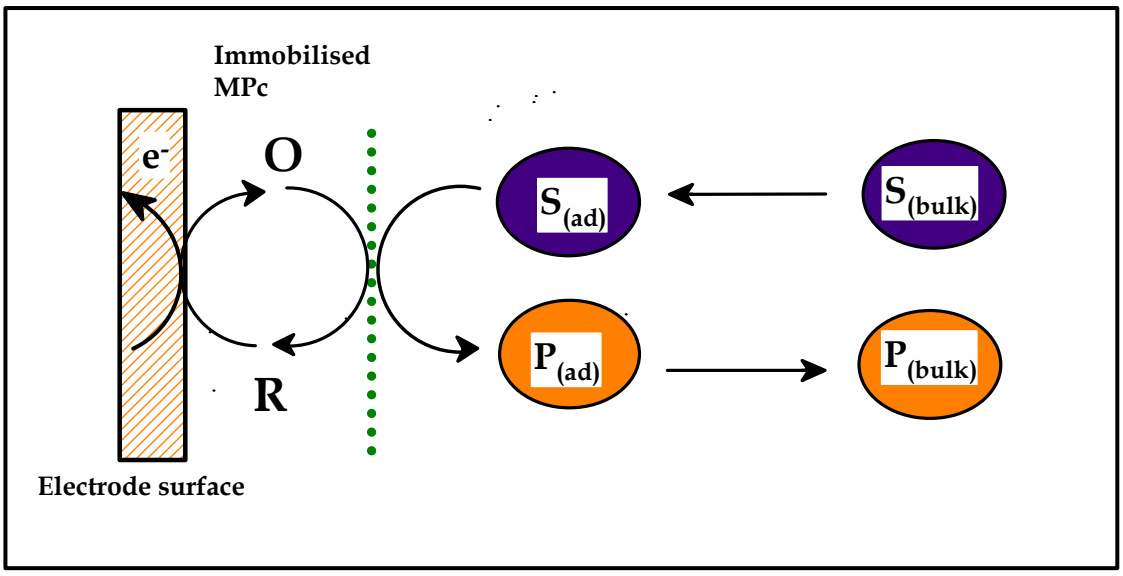

Figure 1.11: Schematic representation of heterogeneous electrocatalysis where S is the substrate and P is the product.

This work involves immobilising MPcs on a gold electrode surface to minimise overpotentials observed on bare electrodes [121, 122] for the catalysis of phenolic type compounds.

MPcs have been confirmed as good electrocatalysts for a number of analytes [123, 124]. Their extraordinary catalytic nature is owed to their electron rich structure and their good thermal and chemical stability. Generally, electrocatalysis has been

observed at potentials close to the central metal or the ring potentials [124]. Electrocatalysis by MPcs usually starts with the metal or Pc ring reduction or oxidation. This is followed by a chemical reaction with an analyte to form a product and finally the regeneration of the catalyst. Equations 1.15 to 1.18 illustrate the action of electrocatalysis for reduction, where A denotes the analyte and P the product.

$$M^{V}Pc^{2-} + e^{-} \rightarrow M^{IV}Pc^{2-} \quad (1.15)$$

$$M^{IV}Pc^{2-} + A \rightarrow M^{V}Pc^{2-} + P \quad (1.16)$$

OR

$$M^{V}Pc^{2-} + e^{-} \rightarrow M^{IV}Pc^{3-} \quad (1.17)$$

$$M^{IV}Pc^{3-} + A \rightarrow M^{V}Pc^{2-} + P \quad (1.18)$$

There are several ways of immobilising an electrocatalyst on electrode surfaces and some methods include drop dry [125] and electropolymerisation [114, 126]. These two methods will be employed in this work and are discussed below:

- ***Electropolymerisation:***

This method involves the formation of a stable electro-conducting polymer on an electrode surface. The process involves repetitive cyclic voltammetry of a monomer that has substituents bearing groups (e.g. N or S) that can easily be oxidised or reduced. Cyclic voltammetry is used for the formation of polymers on electrode surfaces such that the potential window for the experiment is within the oxidation or

reduction potential of the polymerisable moiety of the monomer. In this work, nickel tetramino Pc (NiTAPc) was employed where the electropolymerisable group was the NH_2. The advantages of this method are: reproducibility and polymer thickness control.

- ***Drop- dry:***

This method is by far the easiest way to achieve a film on the electrode surface. A drop of a saturated solution containing the catalyst is placed onto the electrode surface and solvent is allowed to dry off. Considerable electrocatalysis takes place even though the uniformity, stability and reproducibility of films using this method are not too good.

1.5.3. Characterisation of modified electrode surfaces

Modified electrodes are characterised in order to confirm the existence of a film. Characterisation techniques that were used in this work include cyclic voltammetry and electrochemical impedence spectroscopy (EIS).

1.5.3.1. Cyclic voltammetry and surface coverage

The surface coverage values are calculated for the adsorbed complexes by first determining the effective area of the electrode (a gold electrode will be used) using a redox probe system, $[Fe(CN)_6]^{3-/4-}$, and applying the Randles–Sevcik {Equation (1.19)} for a reversible process [127, 128]:

$$I_{pa} = (2.69 \times 10^5) n^{3/2} D^{1/2} v^{1/2} A C_o \qquad (1.19)$$

where D and C_o are the diffusion coefficient and bulk concentration of the redox probe, respectively. n is the number of electrons transferred (n = 1), v is the scan rate and A is the effective surface area.

The surface coverage values of modified electrodes were estimated by integrating the charge under the observed redox peak, using equation (1.20).

$$\Gamma_{polyMTAPc} = \frac{Q}{nFA} \qquad (1.20)$$

where Q (C) is the charge under the observed redox peak, n (=1) is the number of electrons transferred, A is the real surface area of the electrode (calculated from equation 1.19) and F is Faraday's constant (95485 C mol^{-1}).

1.5.3.2. Electrochemical impedance spectroscopy

Electrochemical impedance spectroscopy (EIS) is a technique used to evaluate the electrochemical behaviour of electrode surfaces and/or electrolyte material [129] processes. External parameters that affect the conductivity of an electrochemical system [129] can be determined using this technique.

EIS makes use of a three electrode set up where electrical voltage or current is applied to the electrode. The resulting response is monitored and/or recorded. The overall electronic response is due to microscopic process that take place throughout the cell. The spectroscopic processes that occur include transport of electrons through the electronic conductor and movement of charged particles towards an

electrode through a concentration gradient. The flow rate of the charged particles depends on the ohmic resistance of the electrode, the type of electrolyte used as well as the reaction rates at the electrode-electrolyte interfaces [129].

Experimentally obtained impedance data for a given electrode-material system may be analysed by using electrical equivalent circuits. These circuits (RC circuits) consist of simple elements such as resistance (R) and capacitance (C) which are connected to model the electrochemical processes [129, 130]. The resistance in an equivalent circuit represents the electrical conductivity of the electrolyte (bulk resistance) and the capacitance (double-layer capacitance) caused by the charge which is in excess at the electrode-electrolyte interface. The most commonly used equivalent circuit in EIS is the Ershler-Randles circuit [129], which contains the electrolyte resistance (R_E), charge transfer resistance (R_{CT}) and the double layer capacitance (C_d). Randles equivalent circuit also takes into account the fact that the reaction rate might be controlled by the transport phenomenon of electroactive species [129], by having an extra component called Warburg impedance (Z_W). This component is connected in series with the charge transfer resistance.

Impedance data is graphically represented as a Nyquist plot where the imaginary part (-Z'', y axis) is plotted versus the real part (Z', x-axis) of impedance is shown in Fig. 1.12.

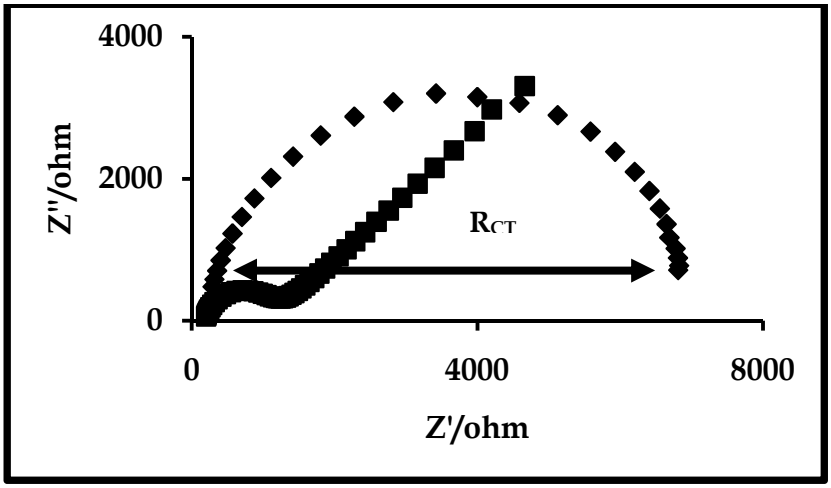

Figure 1.12: Nyquist plot for the electrochemical system

In this work, EIS will be used to calculate R_{CT}, R_E and C_d. R_{CT} values are influenced by nature of the electrode surface [130] and this gives a better understanding on the electrocatalytic nature of different films.

1.6. Analytes studied in this work

1.6.1. Bisphenol A (BPA)

Bisphenol A shown in Fig. 1.13 is primarily used to make polycarbonate plastic and epoxy resins, which are widely used for a number of applications such as in the manufacturing of baby feeding bottles, food containers, dental sealants and epoxy food can lining [131].

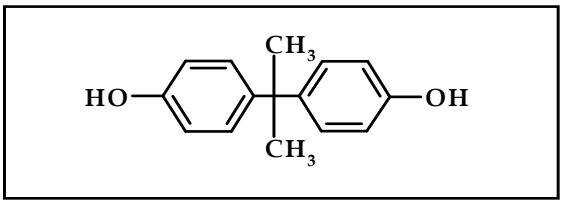

Figure 1.13: Structure of bisphenol A.

BPA is one of the highest volume chemicals produced worldwide [132]. The global BPA capacity in 2003 was 2.2 million metric tones (~ 6.4 billion pounds) with a 6 – 10 % growth in demand expected per year. It has be proven in both *in vivo* and *in vitro* experiments that BPA acts as an endocrine disrupting chemical (EDC) [133]. The use of BPA to manufacture daily needed items has prompted speculations about the possible harmful effects to humans and animals when exposed to BPA. There is extensive evidence that proves that BPA acts as estrogen mimics. The consequences of this are associated with human diseases which include ovarian dysfunction or endometrial hyperplasia and recurrent miscarriages [133, 134]. These dire consequences of high levels BPA have thus motivated the development of sensors for detection of BPA at very low concentrations. Various sensitive methods that include high performance liquid chromatography (HPLC) [135], mass spectrometry [136] and electrochemical methods [137, 138] have been employed to detect BPA. The latter method is preferred because there is no need for extensive separation and preparation before use.

Several electrochemical studies have been carried out to detect BPA using different electrodes modified with different material including MPcs as shown in Table 1.6 [137 – 141]. Also listed in Table 1.6 are the limits of detection values for BPA by different electrodes modified with various materials.

Table 1.6: Detection limit values of BPA using different electrode surfaces.

Sensor	**Detection limit (μM)**	**References**
CoPc-CPE	0.01	[137]
Tyr-SF-MWCNT-CoPc/GCE	0.03	[138]
Tyr-MWCNTs paste electrode	1	[139]
Tyr-SWCNT paste electrode	0.02	[139]
Tyr-CPE	0.15	[140]
CPE	0.0075	[141]

CoPc = cobalt phthalocyanine, GCE = glassy carbon electrode, CPE = carbon paste electrode, MWCNT = multi-walled carbon nanotubes, SWCNT = single-walled carbon nanotubes, Tyr = tyrosinase, Tyr-SF = tyrosinase silk fibroin

These values were all determined electrochemically. It is quite surprising to note that incorporation of tyrosinase on MWCNTs in the presence of CoPc and silk fibroin resulted in less favourable detection limits on CoPc - carbon paste electrode (CoPc-CPE). CPE electrode alone was the most sensitive. The problem of electrode passivation and improving detection limits still persist.

The aim of this work is to modify gold electrode surface with the synthesised TiPc, TaPc, VPc and NiTAPc complexes and use the chemically modified electrodes to detect BPA. To enhance catalysis, gold nanoparticles will be conjugated with MPc complexes that have sulphur bearing substituents. To improve passivation, TaPc that showed the best catalytic sensitivity towards BPA will be adsorbed on single walled carbon nanotubes.

Polymers of different thickness will be formed on gold surfaces using NiTAPc through the processes of polymerisation. To improve catalysis, these polymers will be converted to 'O-Ni-O' bridges.

The transformation of NiPc polymers into 'O-Ni-O' were reported by Agboola and co-workers [142, 143] where they observed excellent and improved catalysis after polymer transformation. They studied the effects of film thickness toward the electrooxidation of chlorophenols and nitrite where the expectations were high for thicker films. This was proven otherwise and they deduced that it is the outer layer of the film that is catalytic.

1.6.2. *p*-Nitrophenol (PNP)

PNP was detected only with NiTAPc polymer films for comparison with BPA. Nitrophenols have been extensively used as raw materials for the production of pesticides, insecticides, herbicides [144], explosives and a variety of synthetic compounds such as dyes [145]. *p*-Nitrophenol (PNP), Fig. 1.14, is one of the typical biorefactory organic compounds and is considered one of the 114 priority toxic pollutant by the US Environmental Protection Agency [146]. *p*-Nitrophenol can damage the liver, kidneys, central nervous system to mention but a few [146].

The increasing contents of this pollutant in the environment have caused many health problems as well as waste water treatment problems.

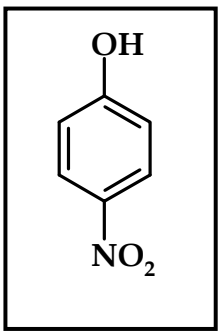

Figure 1.14: Strucuture of *p*-nitrophenol.

Rezzano and co-workers [147] reported the oxidation of PNP with a nickel-protoporphyrin IX dimethyl ester (NiPPIX) polymer that was immobilised on a glassy carbon electrode (GCE) and they observed an oxidation potential of PNP at 1.04 V which was at higher potential than what Obirai and co-workers [148] observed at a potential of ~ 0.78 V where they used polymerised and transformed nickel tetra-4-(pyrrol-1-ly)phenoxyphthalocyanine (*poly*-NiTPhPyPc) to Ni(OH)TPhPyPc polymer on a GCE.

1.7. Nanomaterials

Nanomaterials can be defined as objects which are at least one dimension, with sizes that range between 1 and 100 nm [149]. They have attracted a lot of attention in recent years due to their extraordinary characteristic size. Their chemical and physical properties depend on their shape and size [150]. They find many applications in catalysis, imaging, optics and many others.

Part of the focus of this work will be the synthesis of gold nanoparticles, their conjugation with MPcs, characterisation of both the synthesised nanoparticles and

their conjugates with MPcs, and finally their application in photo- and electrocatalyses. In addition, single walled nanoparticles will be utilised in electrocatalysis to mainly improve passivation by oxidation products and to improve sensitivity values.

1.7.1. Gold nanoparticles (AuNPs)

1.7.1.1. History, properties and applications

Gold nanoparticles are important materials in nanotechnology and have been most studied [150]. Historically, solutions of AuNPs have existed since the 5th century BC. Ancient belief is that these particles had healing powers [151]. In Roman times, gold and silver colloids were used to colour glass with different intense colours such as yellow, red or mauve.

As a relatively inert metal, gold is stable in a number of harsh conditions, however solutions containing I^- or CN^- can dissolve AuNPs [151]. In addition, gold can form bonds with sulphur [152]. Other than thiols, AuNPs have been successfully conjugated to alchilamine and phenylphosphines [153].

The electrochemical properties of nanometals are size dependant where the catalytic properties of AuNPs are believed to originate from their quantum scale [154] and the large surface-to-volume ratio [155]. Also, AuNPs act as electron antennas; thus enhance electron transfer in redox reactions.

One of the well known physical properties of metal nanoparticles is their ability to absorb visible light due to the surface plasmon resonance (SPR) effect [156, 157]. The SPR effect is the collective oscillation of conduction electrons ($6S^1$ for Au) in the nanoparticles, which resonates with the electromagnetic field of the incident light [156, 157]. The position of surface plasmon absorption for spherical AuNPs with a diameter range of 2 and 100 nm is at ~ 520 nm [158]. AuNPs also exhibit considerable ultraviolet absorption [158, 159], this is useful for photocatalysis because it implies that the full solar spectrum can be used for driving photo-initiated reactions on a large scale. Other applications of AuNPs that utilise the SPR effect include imaging, sensing, medicine, photonics and optics [160, 161]. AuNPs have also been used for charge storage and conductivity [162] in memory storage devises [163,164] and molecular switches [165].

1.7.1.2. Synthesis of gold nanoparticles

The synthesis of gold nanoparticles or metal nanoparticles can be achieved by physical or chemical methods. Chemical method will be used in this thesis hence will be discussed.

The common chemical methods for the synthesis of AuNPs are based on the reduction of a metal salt for example $AuCl_3$ in solution to afford nanoparticle colloids [166]. The two popular methods (the Turkevich and Brust and Shiffrin methods) involve the reduction of Au+ ions and the chemisorptions or physisorption of ligands on the surface of the nanoparticle to avoid their coagulation and precipitation.

The Turkevich method [167] is well known for obtaining aqueous solutions of gold nanoparticles that can easily be functionalised. This method involves the reduction of $HAuCL_4$ in a boiling solution of sodium citrate [168]. The citrate molecules act as both reducing and stabilising agents for AuNPs.

The Brust and Shiffrin two phase method [169] is mostly used for thiol stabilised gold nanoparticles that are soluble in organic solvents. A gold metal salt (e.g. $AuCl_3$) is dissolved in water and reacted with tetraoctylammonium bromide (TOABr) in toluene which acts as a phase transfer agent. The toluene/water solution is then mixed thoroughly with a solution of a reducing agent ($NaBH_4$) in the presence of an alkanethiol. These particles are called monolayer protected clusters [170] and they have demonstrated versatility because the thiol monolayer acts an efficient stabiliser that ensures chemical modification.

1.7.1.3. Metallophthalocyanine – gold nanoparticle (MPc-AuNPs) conjugates

Since MPcs and AuNPs have remarkable catalytic properties, combining these two entities to further enhance both photo- and electrocatalysis is worth exploring. The synthesised MPcs will be attached to TOABr-AuNPs to form MPc-AuNPs conjugates. The photochemical and photophysical parameters of the conjugates will be carried out to determine their stability under light exposure and their efficiency as photosensitisers. This will be used in the phototransformation of cyclohexene as well as electrochemical detectors for BPA.

The photochemical and photophysical properties of the newly synthesised TaPc and TiPc complexes (Figure 1.4 and 1.5) and their gold nanoparticles conjugates have not

been studied. The photochemical and photophysical properties VPc complexes were not studied due to paramagnetic nature of vanadium. Cook and co-workers [171] have reported the generation of singlet oxygen through a 1,4,8,11,15,18-hexahexyl-22-methyl-25(11-mercaptoudecyl) phthalocyaninato zinc (HMMZnPc). They conjugated the HMMZnPc with TOABr–AuNPs to form HMMZnPc-AuNPc and determined the singlet oxygen quantum yield (Φ_Δ) values for both the HMMZnPc and HMMZnPc-AuNPc. They also observed a drastic increase of Φ_Δ from 0.45 to 0.65 on conjugation.

In electrochemistry, Pal and Ganesan [172] incorporated zinc phthalocyanines and silver/gold nanoparticles in mesoporous molecular sieves MCM-41 for use as electrode modifiers for the reduction of O_2. They compared the different components individually and found that ZnPc-MCM-41-AuNPs/AgNPs composite showed the best electrocatalytic response.

1.7.2. Single walled carbon nanotubes (SWCNT)

The history of single walled carbon nanotubes dates back to the early 90s where they were independently reported in Nature [173, 174] although Oberlin and co-workers [175] observed a similar structure in 1976. SWCNTs will be conjugated with TaPc complexes for application in the electrocatalytic detection of BPA with the aim of enhancing sensitivity, minimising passivation and improving electrode recovery after catalysis. TaPc complexes were employed since they showed the best electrocatalytic behaviour.

1.7.2.1. Properties and applications of SWCNTs

SWCNTs are one dimensional nanometer scale carbon structures [176]. The structure of SWCNTs can be conceptualised by wrapping a one-atom-thick layer of a graphene sheet, i.e., an interlinked hexagonal lattice of carbon atoms into a seamless cylinder [177], Fig. 1.15. The diameter of most SWCNTs is almost 1 nm with a length that can be many thousand times longer. The interest in these nanomaterials lies in their remarkable mechanical, electrical and optoelectronic properties [178].

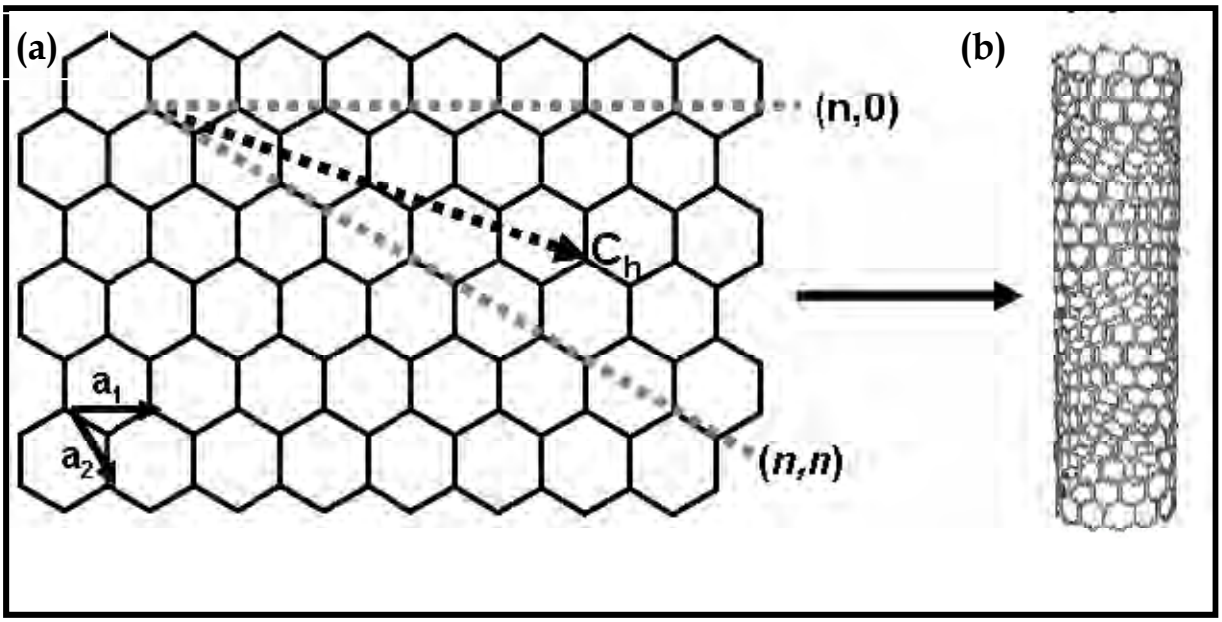

Figure 1.15: Schematic representation of SWCNTs (a) graphene sheet like structure and (b) seamless cylinder like structure.

These nanomaterials show improved features compared to classical materials such as organic polymers and some semiconductors. In addition, the graphitic surface of SWCNTs is chemically robust which guarantees stability for long term use [177]. High electrical conductivity, thermal stability and high surface areas [179, 180] are SWCNTs properties that have found their applications in many areas such as in

electronics, optoelectronics, sensing, fillers in new generation polymer composites, therapeutics and diagnostics [180 - 182].

1.7.2.2. Chemical functionalisation of SWCNTs

The high polarizability of SWCNTs and their smooth surface results in strong van der Waals interaction between the sheets which results in insolubility of these materials. Their structure is such that it allows for functionalisation at the end of the tubes as well as the surfaces of the tubes. This enables solubility and chemical compatibility with other molecules. There are two main ways of modifying or functionalising SWCNTs: (i) by covalently attaching desired molecules (ii) or by non-covalent attachment, i.e. adsorption. In this project adsorption was employed and will therefore be discussed briefly.

Non-covalent modification is as a result of intermolecular bonding which preserve the π conjugated structure backbone of the nanotubes and thus their instrinsic electronic and catalytic properties [183 -185]. This functionalisation is best achieved by planar molecules (e.g. MPcs) that are capable of adsorbing onto the carbon nanotube surface via π-π interactions [186, 187].

The non-covalent linking of SWCNTs with MPcs has been studied extensively. A few examples include a study by Geraldo and *et al*. [188] where the electrocatalytic oxidation of hydrazine was improved by non-covalently linked CoPc on SWCNTs. Similary, Silva and *et al.* [189] functionalised SWCNTs with CoPc and tetrasulfonated NiPc (NiTSPc) by simple adsorption for the electrocatalytic oxidation of 2-mercaptoethanol (2-ME) and nitric oxide (NO). The electrodes showed high

stability under hydrodynamic conditions and the modified electrodes enhanced electron transfer for the electrocatalytic oxidation of 2-ME and NO.

1.7.2.3. Characterisation techniques for nanoparticles

The initial point for characterizing metal nanomaterials is ideally 'seeing' them under of microscopes such as transmission electron microscopy (TEM). TEM is a microscopy technique that produces images from the interaction of electrons with the specimen. Other than visualizing, TEM offers accurate measurement of particle size and size distribution [190, 191]. Fig. 1.16 is an example of a TEM image which shows dispersed AuNPs.

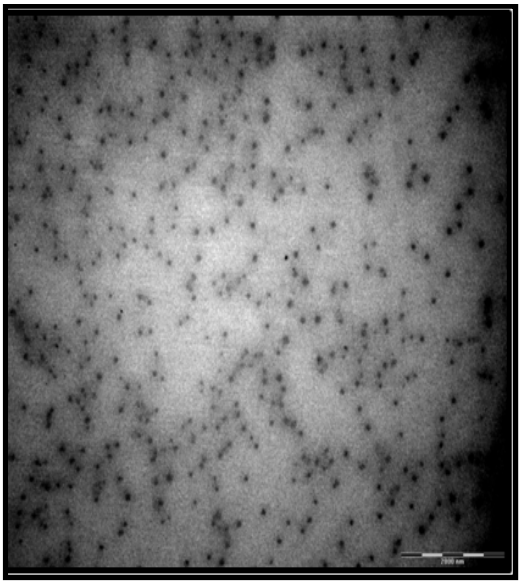

Figure 1.16: A TEM image of AuNPs [Not published].

In addition to TEM, atomic force microscopy (AFM) will be used to characterise the AuNPs. AFM is a very high resolution type of scanning probe microscopy [192]. An example of an AFM image of AuNPs is shown in Fig. 1.17

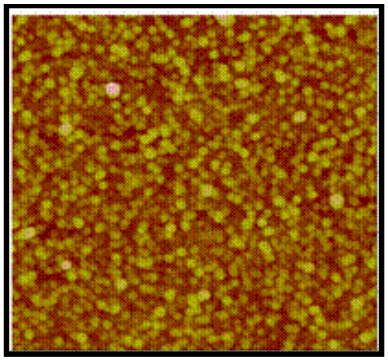

Figure 1.17: an example of AMF image [193]

X-Ray diffraction (XRD) will also be employed to determine the sizes of the nanometals [194]. This technique will be employed to determine the size of the nanoparticles using the Debye-Scherrer Equation 1.21 [194]:

$$d(A) = \frac{k\lambda}{\beta Cos\theta} \qquad (1.21)$$

where k is an empirical constant equal to 0.9, λ is the wavelength of the X-ray source, (1.5405 Å), β is the full width at half maximum of the diffraction peak, and θ is the angular position of the peak.

1.8. Summary of aims

Studies that involve nanomaterials (AuNPs and SWCNTs) and MPcs are on the increase due to the notable properties of these materials. The key step in this research is to synthesise new MPcs and conjugate them to nanomaterials (AuNPcs and SWCNTs) and utilise the conjugates as photo- and electrocatalysts. The critical

step in improving photocatalytic processes is to develop new catalysts that will allow use of the most abundant, cheap and green energy source of light energy, sunlight, i.e. to develop a catalyst that will exhibit absorption throughout the spectrum of light (~ 280 to 3000 nm). MPcs are known for their strong absorption in the visible region (~ 670 – 720 nm) of the spectrum with newer MPcs absorbing in the near infrared regions (750 – 810 nm). AuNPs also absorb visible light and ultraviolet light considerably. Combining MPcs and AuNPs for light driven reactions is logical, worth studying and will be applied in the photocatalytic transformation of cyclohexene. To mimic large scale reactions, photocatalytic reactions will be exposed to white light, and controlled filtered light (at the Q band of an MPc).

MPcs and nanomaterials (AuNPs and SWCNTs) are very well known for their flexibility and hence applications in many fields. In this work, MPcs, AuNPs and SWCNTs will be employed in the electrocatalytic oxidation of BPA. BPA is used to make plastics that are used daily, such as microwave plastics, storage containers and soft drink bottles. The aim is to develop a sensor that will detect BPA commonly used in plastics such as microwave plastic, using minimal energy at very low concentrations with minimised electrode passivation (which is almost inevitable with phenolic type analytes such BPA). If these are successful, proudly it can be said that a potential simple, cheap and very effective sensor has been developed.

In short, the aims are:

- To synthesise TiPc, TaPc and VPc complexes (Figs. 1.4 and 1.5)

- Synthesise TOABr-AuNPs and conjugate them to synthesised MPcs to form MPc-AuNPc conjugates.
- Study the photophysics and photochemistry of TiPc and TaPc and MPc-AuNPc complexes and use them for the phototransformation of cyclohexene
- To electrochemically detect BPA with the synthesised MPc and MPc-AuNPs. Selected TaPc complexes will adsorbed onto SWCNTs and will be used as electrocatalysts for BPA detection.
- To immobilise nickel tetra amino phthalocyanine (NiTAPc) through polymerisation for use in BPA detection.

Chapter 2: Experimental

2. Experimental

This chapter consists of the materials (chemical reagents used for synthesis, photophysiochemistry and electrochemistry), equipment and experimental procedures used in this project.

2.1 Materials

Synthesis reagents

1-Pentanethiol, 1-octanethiol, 1,8-diazabicyclo{5.4.0}-undec-7-ene (DBU), potassium carbonate, 2,3-dicyanohydroquinone (**20**), *p*-toluenesulfonyl chloride, sodium borohydride ($NaBH_4$), tetraoctylammonium bromide (TOABr), gold (III) chloride and titanium (IV) butoxide, tantalum (V) butoxide, vanadium tetrachloride, were purchased from Sigma-Aldrich. Column chromatography was performed on silica gel 60 (0.04 – 0.063 mm), preparative thin layer chromatography was performed on silica gel 60 P F_{254} and size-exclusion column (bio-beads).

Photophysics and photochemistry reagents

Zinc(II)phthalocyanine (ZnPc), 1,3-diphenylisobenzofuran (DPBF), cyclohexene, cyclohexene oxide, 2-cyclohexene-1-ol, cyclohexene-1-one, 1,4-cyclohexanediol and 1,4-diazobicyclo-octane (DABCO) were purchased from Sigma Aldrich.

Electrochemistry reagents

Ammonium ferrous sulphate, tetrabutylammonium tetrafluoroborate ($TBABF_4$), KH_2PO_4 , Na_2HPO_4, NaOH, 4-nitrophenol, bisphenol A, and single

walled carbon nanotubes (SWCNT) (0.7 – 1.2 nm diameter and 2 – 20 μm length) were purchased from Sigma Aldrich. Ultra pure water was obtained from a Milli-Q Water System (Millipore Corp, Bedford, MA, USA).

Solvents

Toluene, Acetone, acetonitrile, dimethylsulphoxide (DMSO), deuterated chloroform ($CDCl_3$), tetrahydrofuran (THF), toluene, chloroform ($CHCl_3$), 1-chloronaphthalene, dichloromethane (DCM), 1-pentanol, ethanol, methanol, dimethylsufoxide (DMSO) and dimethylformamide (DMF) were purchased from Merck.

2.2. General equipment

- Ground state electronic absorption spectra were performed on a Varian Cary 500 UV-Vis-NIR spectrophotometer or Shimadzu UV - 2550 spectrophotometer.
- Infra-red spectra (KBr pellets) were recorded on Perkin Elmer Spectrum 2000 FT-IR Spectrometer.
- ^1H nuclear magnetic resonance signals were obtained from a Bruker EMX 400 NMR spectrometer; all solutions were dissolved in deuterated solvents.
- Elemental analysis was performed at Rhodes University using a Vario Elementor EL111 series.
- Maldi-TOF mass spectrometry was carried out at Rhodes University using a Bruker Smartbeam TOF/TOF Mass spectrometer. The instrument was

operated in positive ion mode using an m/z range of 400 – 3000. The voltage of the ion sources were set at 19 and 16.7 kV for ion sources 1 and 2 respectively, while the lens was set at 8.50 kV. The reflector 1 and 2 voltages were set at 21 and 9.7 kV respectively. The spectra were acquired using dithranol as the MALDI matrix, using a 354 nm N_2 laser at Rhodes University or an ABI Voyager DE-STR Maldi TOF instrument at the University of Stellenbosch.

- Transmission electron microscope (TEM) images were obtained using a JEOL JEM 1210 transmission electron microscope at 100 kV accelerating voltage.
- Atomic force microscopy (AFM) images were recorded in the non-contact mode in air with a CP-11 Scanning Probe Microscope from Veeco Instruments (Carl Zeiss, South Africa) at a scan rate of 1 Hz. The images were obtained using a spring constant range of 20 – 80 N/m, and resonant frequency range of 217 – 276 Hz and samples for AFM were prepared drying the samples on a glass slide for ~ 24 hours or spin coating.
- X-ray powder diffraction patterns were recorded on a Bruker D8, Discover equipped with a proportional counter, using Cu-Kα radiation (λ = 1.5405 Å, nickel filter). Data were collected in the range from $2\theta = 5^o$ to 60^o, scanning at 1^o min^{-1} with a filter time-constant of 2.5 s per step and a slit width of 6.0 mm.
- Cyclic (CV), chronoamperometry, chronocoulometry and square wave (SWV) voltammetry experiments were performed using Autolab potentiostat PGSTAT 302 (Eco Chemie, Utretch, The Netherlands) driven by the General Purpose Electrochemical System data processing software (GPES, software

version 4.9, Eco Chemie), using a conventional three-electrode system. Faradaic impedance measurements were performed with Autolab FRA equipment using a 10 mV rms sinusoidal modulation.

- Spectroelectrochemical data was recorded using an optically transparent thin-layer electrochemical (OTTLE) cell which was connected to a Bioanalytical System (BAS) CV 27 voltammograph.
- The products for the phototransformation of cyclohexene were analyzed using an Agilent HP 5890 gas chromatograph (GC), fitted with a flame ionization detector (FID), using a DB-5MS column (0.25 m length, 0.2 mm internal diameter, 0.25 μm film thickness). The GC parameters were as follows: the initial oven temperature was at 50 ^{o}C, maximum oven temperature was 280 ^{o}C, equilibration time was 0.15 min, initial ramp rate was 10 ^{o}C/min at 180^{o}C for 2 min, the second was 10 ^{o}C/min at 280^{o}C for 2 min and total run time was 27 min.

2.3. Methods

2.3.1. Photophysical, photochemical and photocatalytic oxidation of cyclohexene

Triplet absorption and decay kinetics were recorded on a laser flash photolysis system. The excitation pulses were produced by a Nd: YAG laser (Quanta-Ray, 1.5 J / 9 ns) pumped tunable dye laser (Lambda Physic FL 3002, Pyridin 1 dye in methanol) for TiPc complexes (**24** and **25**). The analyzing beam source was derived from a Thermo Oriel xenon arc lamp, and a photomultiplier tube

(PMT) was used as detector. Signals were recorded with a Tektronix TDS 3032C two-channel digital real-time oscilloscope and the kinetics curves were averaged over 256 laser pulse. Triplet lifetimes were determined by exponential fitting of the kinetic curves using OriginPro 7.5 software. For TaPc complexes (**28**, **29a** and **29b**) a NT342B series tunable laser system that consists of nanosecond optical parametric oscillator and Q-switched pump laser (with a pump wavelength of 355 nm and a pulse duration of 4 – 6 ns) in a single housing was used. It has a maximum pump energy of 135 mJ.

General Electric Quartz line lamp (300 W) was employed for the determination of photodegradation (Φ_P) and singlet oxygen quantum yields (Φ_Δ), and for the phototransformation of cycloxehene. A 600 nm glass cut off filter (Schott) and a water filter were used to filter off ultraviolet and infrared radiations respectively. An interference filter (Intor, 740 nm for complexes **24**, **25** and **28** or 750 nm for complexes **29a** and **29b** with a band width of 40 nm) was additionally placed in the light path before the sample, hence ensuring excitation at the Q band only (700 to 780 nm or 710 to 790 nm, respectively), Fig. 2.1(a). Experiments were also performed where white light (from quartz line lamp) or sunlight was employed. The wavelength range for unfiltered light is ~ 400 nm to near infrared region {Fig. 2.1(b)}; hence it does not include the B band of phthalocyanines, but covers a wider absorption region. The unfiltered light will be referred to as white light in this work. Light intensities were measured with a POWER MAX 5100 (Molelectron detector incorporated) power meter

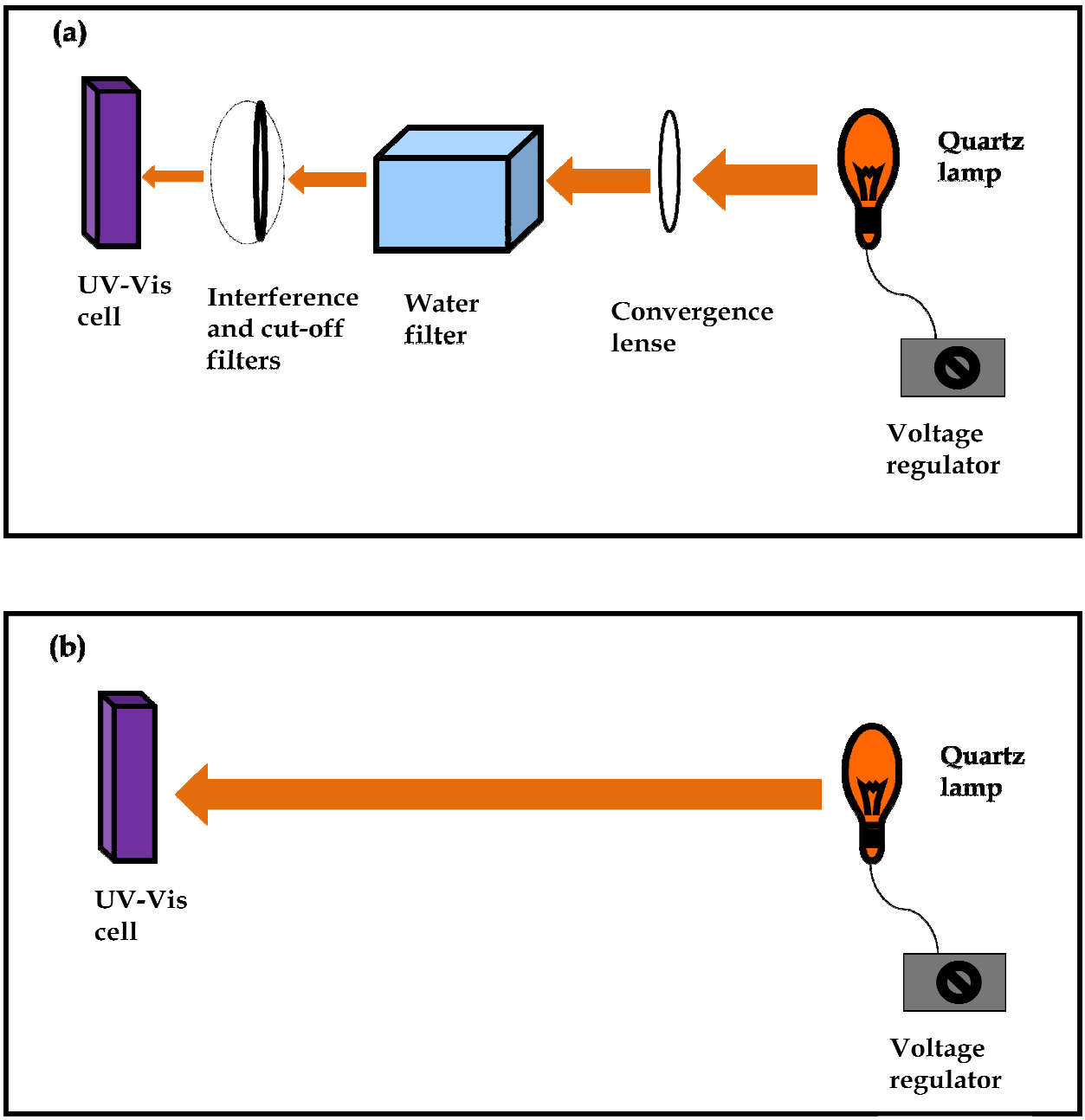

Figure 2.1: Photo-irradiation set-up for (a) filtered and (b) unfiltered light irradiation.

Singlet oxygen quantum yields of the synthesised MPcs and MPc-AuNPc conjugates were determined by monitoring the absorbance decay of DPBF at ~ 415 nm in toluene. To avoid chain reactions induced by DPBF in the presence of singlet oxygen [92], the concentration of DPBF was lowered to ~ 3 x 10^{-5} mol dm^{-3}. Solutions of sensitizer (absorbance = 0.2 at the irradiation wavelength) containing DPBF were

prepared in the dark and irradiated in the Q band region using the setup described above. The light intensity for singlet oxygen studies was 5 x 10^{15} photons s^{-1} cm^{-2} for filtered light (Q band irradiation). The light intensity for the white light was 2 x 10^{16} photons $s^{-1}cm^{-2}$. Photodegradation quantum yields were carried in a similar way but in the absence of a singlet oxygen quencher (DPBF) where the decrease of Q band absorption with time was monitored spectroscopically. Similarly, the photocatalytic oxidation of cyclohexene was carried out using the set up described in Fig. 2.1(a). At different time intervals of the reaction, samples of reaction were injected into the GC to analyse the product formation. The light intensity for Q band and white light irradiation was 14 x 10^{16} photons s^{-1} cm^{-2}.

2.3.2. Electrochemical methods

For the electrochemical characterisation of the newly synthesised MPcs, a glassy carbon electrode (GCE, 3.0 mm diameter) was used as the working electrode. Silver-silver chloride (Ag|AgCl) and platinum wire were used as pseudo-reference and counter electrodes respectively. Electrochemical characterisation experiments were performed in freshly distilled DMF or DCM containing $TBABF_4$ as the supporting electrolyte. Prior to scans, the working electrode was polished with alumina paste on a Buehler felt pad followed washing with de-ionised water.

Electrode modification was achieved by electropolymerisation and drop-dry methods on a gold electrode (1.6 mm diameter). Electropolymerisation was achieved by repetitive cycling of NiTAPc in DMF at 0.1 Vs^{-1} with $TBABF_4$ as the supporting electrolyte to form poly-NiTAPc. The polymers were transformed to 'O-Ni-O'

bridges by cycling in 0.1 mol L^{-1} solution of NaOH. For the drop-dry method, a drop of the complex of interest {AuNPc or MPc-AuNPs in toluene or DCM:acetone, respectively; SWCNT in $CHCl_3$ or TaPc-SWCNT suspended in $CHCl_3$ following sonication} was placed on the electrode surface and left to dry for ~10 min in the oven. This allowed for adsorption of the complexes onto the electrode surface. The removal of the excess catalyst was accomplished by rinsing the electrode in toluene or DCM (for AuNPs and their conjugates) or $CHCl_3$ (for SWCNT or their conjugates) followed by acetone before use.

Electrocatalytic experiments were all performed in de-aerated solutions; this was achieved by bubbling argon prior experiments and the argon atmosphere was maintained throughout the experiments. pH 7 and 12 phosphate buffer solutions were prepared from KH_2PO_4 and Na_2HPO_4, and NaOH was used to adjust the pH. A stock solution of 1 x 10^{-3} mol L^{-1} bisphenol A (BPA) was prepared in a mixture of deionised water/acetonitrile (60:30 v/v). This solvent mixture was employed due to the lack of solubility of BPA in water alone. For practical BPA applications, samples were obtained from a local food market in Grahamstown. Three types of plastic products were used; microwave plastic from meat package, baby feeding bottle and a soft drink bottle. Both plastic products were washed thoroughly with water and soap to remove blood stains and animal fat. The plastic products were then placed in a big bowl, separately, and exposed to high microwave power for 10 minutes [137]. This was repeated three times on different days. The BPA concentrations were determined using the standard addition method.

2.4. Synthesis

NiTAPc is well known and was synthesised according to literature [195]; it is not reported further in this work.

2.4.1. Synthesis of tetra substituted phthalocyanines using monosubstituted phthalonitriles, (Scheme 3.1) [196, 197]

*3-(2-Mercaptopyrine) phthalonitrile (**13**).*

Under a blanket of nitrogen, 2-mercaptopyridine (4.66 g, 42 mmol) and 3-nitrophthalonitrile (**12**) (7.27 g, 42 mmol) were dissolved in DMF (60 mL) and stirred at room temperature for about 15 minutes. Finely ground K_2CO_3 (15 g, 108 mmol) was then added portion-wise over a period of 4 hours and the reaction was left to stir for an additional 14 hours at room temperature. The mixture was added to 100 mL of water and stirred for 30 minutes. The resulting precipitate was filtered off, washed thoroughly with water, dried and recrystallised in ethanol. Yield 6.47 g (64 %). IR [(KBr) ν_{max}/cm^{-1}]: 3065 (Ar-CH), 2230 (C≡N), 1580 (C=C). ^{1}H-NMR ($CDCl_3$): δ, ppm 8.42 (1H, d, Ar-H), 7.92 (1H, d, Ar-H), 7.77 (1H, d, Ar-H), 7.70 (1H, t, Ar-H), 7.65 (1H, t, Ar-H), 7.36 (1H, d, Ar-H), 7.18 (1H, t, Ar-H).

*4-(2-Mercaptopyrine) phthalonitrile (**16**).*

The synthetic outline for **16** was as described for **13** except 4-nitrophthalonitrile (**15**) was employed instead of **12**. The quantities for the reagents employed were: 2-mercaptopyridine (2.33 g, 21 mmol), 4-nitrophthalonitrile (**15**) (3.63 g, 21 mmol) and DMF (30 mL). Yield: 5.43 g (55 %). IR [(KBr) ν_{max}/cm^{-1}]: 3095-3021 (Ar-CH), 2230 (C≡N), 1574 (C=C). ^{1}H-NMR ($CDCl_3$): δ, ppm 8.55 (1H, d, Ar-H),

7.87 (1H, d, Ar-H), 7.77 (1H, d, Ar-H), 7.74-7.69 (2H, t, Ar-H), 7.42 (1H, t, Ar-H), 7.27 (1H, t, Ar-H).

*1,(4) – (2-Mercaptopyridine) pthalocyaninato titanium (IV) oxide (**24**).*

Under a stream of nitrogen, a mixture of titanium butoxide (0.25 g, 1.5 mmol), 3-(2-mercaptopyridine)phthalonitrile (**13**, 0.5 g, 2.1 mmol), DBU (1.66 mL, 12 mmol) and 1-pentanol (10 mL) was stirred at 160 ^{o}C for 5 hours. After cooling, methanol was added to the solution. The resulting precipitate was filtered and washed twice with methanol. Column chromatography over silica was done using $CHCl_3$ as eluent. Yield: 0.17g (38 %). UV/Vis (toluene): λ_{max} (nm) (log ε) 335 (4.45) 642(4.10) 720(5.12). IR (KBr): ν_{max}/cm^{-1}; 3058 (Ar-H), 1558 (C=C), 1523, 1452, 1345, 1201, 1109, 1093 (C-S-C), 898 (Ti=O). ^{1}H-NMR ($CDCl_3$): δ, ppm: 8.90-9.35 (m, 5H, Pc-H), 8.45-8.89 (m, 7H, Pc-H), 7.75-8.25 (m, 8H, Pyridyl-H), 7.43-7.68 (m, 8H, Pyridyl-H), Calc. for $C_{52}H_{28}N_{12}S_4OTi$: C 61.64; H 2.78; N 16.59 %; Found: C 61.07, H 2.90, N 15.78. MALDI-TOF MS *m/z*: Calcd.: 1013 amu. Found: $[M-H]^+$ 1012 amu.

*2,(3) – (2-Mercaptopyridine) pthalocyaninato titanium (IV) oxide (**25**).*

The synthesis of **25** was as outlined for **24** except **16** was employed instead of **13**. The amounts of reagents employed were: **16** (0.25 g, 1.05 mmol), titanium butoxide (0.66 g, 5.26 mmol), DBU (1.66 mL, 12 mmol) and 1-pentanol (10 mL). Yield: 0.18 g (31%). UV/Vis (toluene): λ_{max} (nm) (log ε) 335 (5.17) 635(4.80) 701(5.58). IR (KBr): ν_{max}/cm^{-1}; 3063 (Ar-H), 1560 (C=C), 1523, 1452, 1345, 1201, 1109, 1095 (C-S-C), 900 (Ti=O). ^{1}H-NMR ($CDCl_3$): δ, ppm: 8.50-9.25 (m, 8H, Pc-H), 7.75-8.49 (m, 4H, Pc-H), 6.75-7.40 (m, 16H, Pyridyl-H), Calc. for $C_{52}H_{28}N_{12}S_4OTi$: C 60.61; H 2.74; N 16.29

%; Found: C 62.09, H 3.01, N 15.96 %. MALDI-TOF MS *m/z*: Calcd: 1013 amu. Found: $[M-H]^+$ 10.12 amu.

*1,(4) – (2-Mercaptopyridine) pthalocyaninato vanadium (IV) oxide (**26**).*

The synthesis of **26** was as outlined for **24**, except vanadium tetrachloride instead of titanium butoxide was employed. The amounts of reagents employed were: **13** (0.25 g, 1.05 mmol), vanadium (IV) tetrachloride (0.66g, 3.42 mmol), DBU (1.66 mL, 12 mmol) and 1-pentanol (10 mL). Yield: 0.37g (63.6%). UV/Vis (Toluene): λ_{max} (nm) (log ε) 335 (4.17) 649(4.13) 730(5.79). IR (KBr): ν_{max}/cm^{-1}; 3063 (Ar-H), 1560 (C=C), 1523, 1452, 1345, 1201, 1307, 1285, 1201, 1109, 1095 (C-S-C), 930 (V=O). ^{1}H-NMR ($CDCl_3$): δ, ppm: 8.45-9.30 (m, 8H, Pc-H), 7.70-8.45 (m, 4H, Pc-H), 6.70-7.30 (m, 16H, Pyridyl-H), Calc. for $C_{52}H_{28}N_{12}S_4OV.H_2O$: C 60.44; H 2.73; N 16.25 %; Found: C 60.73, H 3.04, N 15.40 %. MALDI-TOF MS *m/z*: Calcd: 1016 amu.: 1016 amu. Found: $[M-4H]^+$ 1012 amu.

*2,(3) – (2-Mercaptopyridine) pthalocyaninato vanadium (IV) oxide (**27**).*

The synthesis of **27** was as outlined for **24** except **16** instead of **12**, and vanadium (IV) tetrachloride instead of titanium butoxide were employed. The amounts of reagents employed were: **16** (0.25 g, 1.05 mmol), vanadium (IV) tetrachloride (0.66g, 3.42 mmol), DBU (1.66 mL, 12 mmol) and 1-pentanol (10 mL). Yield: 0.28g (47 %). UV/Vis (toluene): λ_{max} (nm) (log ε) 337 (4.42) 631(4.91) 705(5.84). IR (KBr): ν_{max}/cm^{-1}; 3063 (Ar-H), 1560 (C=C), 1523, 1452, 1345, 1201, 1307, 1285, 1201, 1109, 1095 (C-S-C), 932 (V=O). ^{1}H-NMR ($CDCl_3$): δ, ppm: 8.45-9.30 (m, 8H, Pc-H), 7.70-8.45 (m, 4H, Pc-H), 6.70-7.30 (m, 16H, Pyridyl-H), Calc. for $C_{52}H_{28}N_{12}S_4OV$: C

61.46; H 2.77; N 16.54 %; Found: C 62.14, H 2.97, N 15.40 %. MALDI-TOF MS *m/z*: Calcd: 1016 amu.: 1016 amu. Found: $[M-4H]^+$ 1012 amu.

*2,(3) – (2-Mercaptopyridine) pthalocyaninato tantalum (IV) butoxide (**28**).*

The synthesis of **28** was as outlined for **24** except **16** instead of **12**, and tantalum butoxide (V) instead of titanium butoxide were used. The amounts of reagents employed were: **16** (0.25 g, 1.05 mmol), tantalum (IV) butoxide (0.66 g, 1.21 mmol), DBU (1.66 mL, 12 mmol) and 1-pentanol (10 mL). Yield: 0.25g (42 %). UV/Vis (Toluene): λ_{max} (nm) (log ε) 335 (4.59) 620(4.15) 688(5.74), 710 (5.79). IR (KBr): ν_{max}/cm^{-1}; 3063 (Ar-H), 1560 (C=C), 1523, 1452, 1345, 1201, 1307, 1285, 1201, 1109, 1095 (C-S-C), 910, (Ta-O). ^{1}H-NMR ($CDCl_3$): δ, ppm: 8.32-9.33 (m, 8H, Pc-H), 7.71-8.50 (m, 4H, Pc-H), 6.70-7.30 (m, 16H, Pyridyl-H), Calc. for $C_{52}H_{31}N_{12}S_4O_3Ta$: C 52.16; H 2.61; N 14.04 %; Found: C 53.09, H 3.04, N 14.04 %. MALDI-TOF MS *m/z*: Calcd: 1197 amu. Found: [M-Ta] 965 amu.

2.4.2. Synthesis of octasubstituted metallophthalocyanes using disubstituted phthalonitriles (Scheme 3.2) [198, 199]

*3,6-Bis(4′-methylphenylsulfonyloxy) phthalonitrile (**21**).*

p-Toluenesulfonyl chloride (10.32 g, 27 mmol) was added to a mixture of 2,3-dicyanohydroquinone (**20**) (4.04 g, 12.5 mmol) and potassium carbonate (13.8 g, 50 mmol) in acetone (15 ml). The mixture was refluxed for 2 hours. Thin layer chromatography (TLC) was performed to determine the consumption of 2,3-dicyanohydroquinone. The mixture was cooled to room temperature, poured to water (40 ml) and stirred for 1 hour in water. The light brown product was filtered

and oven dried to give **21**. Yield: 9.51g (79 %) IR [(KBr) v_{max}/cm^{-1}]: 3432, 3239, 3085, 2243, 2226 (CN), 1504, 1449, 1315, 1279, 1204, 1174, 1142, 1021, 1004, 979, 934, 847, 749, 694, 638, 614.

*3,6-Di(pentylthio)-4,5-dicyanobenzene (**22a**).*

1-Pentanethiol (2.39 g, 22.9 mmol) was dissolved in DMSO under a nitrogen atmosphere and 3,6-bis(4'-methylphenylsulfonyloxy) phthalonitrile (**21**) (4.30 g, 9.18 mmol) was added. The mixture was stirred for 15 minutes and finely ground anhydrous potassium carbonate (5.07 g, 36.7 mmol) was added in portions for 2 hours while stirring. The mixture was stirred under a nitrogen atmosphere for a further 12 hours. Water was added and the aqueous phase extracted using chloroform (3 x 50 ml). The extracts were further treated with 5 % sodium carbonate solution (2 x 250 ml). The solution was further treated with water (2 x 250 ml) and the solvent was evaporated off using a rotavapor. The product (**22a**) was recrystallised from ethanol. Yield: 2.19g (71.7 %). IR [(KBr)v_{max}/cm^{-1}]: 3084, 2951, 2930, 2864, 2378(S-C), 2225(C≡N), 1444, 1283, 1202, 1181, 1173, 1145, 877, 847, 827, 725, 547, 447. ^{1}H-NMR($CDCl_3$):δ, ppm 7.49 (2-H,s,Ar-H), 2.99-3.02 (4-H,t, $-CH_2$), 1.63-1.71 (4-H,m, $-CH_2$), 1.37-1.46 (4-H,m, $-CH_2$), 1.28-1.36 (4-H, m,$-CH_2$), 0.88-0.91 (6-H, t,$-CH_3$).

*3,6-Di(octylthio)-4,5-dicyanobenzene (**22b**).*

Synthesis and purification of **22b** were similar to that of compound **22a**, except 1-octanethiol was used instead of 1-pentane thiol. The amounts of reagents employed were: 1-octanethiol (2.39 g, 16.3 mmol), 3,6-bis(4'-

methylphenylsulfonyloxy) phthalonitrile (**21**) (4.30 g, 9.18 mmol), ground anhydrous potassium carbonate (5.07 g, 36.7 mmol). Yield: 1.79 g, (58.1 %). IR [(KBr)ν_{max}/cm^{-1}]: 2920, 2850, 2388(S-C), 2225(C≡N), 2023, 1637, 1466, 1422, 1204, 1143, 1032. ^{1}H-NMR($CDCl_3$):δ, ppm 7.40 (2-H,s,Ar-H), 2.98-3.10 (4-H,t, -CH_2), 1.62-1.75 (4-H,m, -CH_2), 1.61 – 1.50 (4-H-broad m, -CH_2), 1.40-1.52 (4-H,m, -CH_2), 1.21-1.38 (18-H, m,-$CH_2CH_2CH_3$).

*1,4,8,11,15,18,22,25-Octapentylthiophthalocyaninato tantalum(V) butoxide (**29a**).*

3,6-Dipentylthiophthalonitrile (**22a**) (0.8 g, 1.20 mmol) in 1-pentanol (7.0 ml) was refluxed under a nitrogen atmosphere and tantalum (V) butoxide (0.138 g, 0.34 mmol) was added. After the addition of DBU (0.30 ml, 0.86 mmol), the reaction was continued for 6 hours. The mixture was cooled and column chromatography over silica was done with $CHCl_3$ as eluent. Yield: 0.25g (42 %). UV/Vis (DCM): λ_{max} (nm) (log ε) 276(6.36) 348(5.62) 722(5.44) 814 (5.81). IR [(KBr) ν_{max}/cm^{-1}]: 3290 (OH), 2922, 2852, 2350, 1561, 1459, 1361, 1310, 1279, 1156, 109, 932, 908(Ta-O), 750 (C-S-C). ^{1}H NMR (400MHz, $CDCl_3$): δ, ppm 7.65 (8H, s, Ar-H), 3.20 (16H, broad s, S-CH_2), 1.89 (16H, quintuplet, CH_2), 1.61 (16H, quintuplet, CH_2), 1.50 (16H, sextuplet, CH_2), 1.0 (24H, t, CH_3). *Anal. Cal*. $C_{72}H_{99}N_8S_8O_3Ta$: C, 55.36, H, 6.38, N, 7.17 %. Found: C, 55.45, H, 7.21, N, 7.92 %. MALDI-TOF MS *m/z*: Calcd: 1561.52 amu. Found: (M-Ta) 1330 amu.

*1,4,8,11,15,18,22,25-Octaoctylthiophthalocyaninato tantalum(V) butoxide (**29b**).*

Synthesis and purification of **29b** were similar to that of compound **29a,** except **22b** was employed instead of **22a**. The amounts of reagents employed were:

3,6-dioctylthiophthalonitrile (**22b**) (0.81 g, 1.20 mmol, 1-pentanol (~8 ml), tantalum (V) butoxide (0.139 g, 0.34 mmol), DBU (0.30 ml, 0.86 mmol). Yield 0.31 (48 %). UV/Vis (DCM): λ_{max} (nm) (log ε) 416(3.82) 662(4.00) 609(3.73) 717 (4.41), 814 (5.76). IR [(KBr) ν_{max}/cm^{-1}]: 3419 (OH), 2955, 2920, 2850, 2538, 2400, 1637, 1563, 1432, 1368, 1312, 1281, 1223, 1181, 1142, 1091, 1031, 910, (Ta-O), 867, 787, 751 (C-S-C), 720. ^{1}H NMR (400MHz, $CDCl_3$): δ, ppm 7.51 (8H, s, Ar-H), 3.2 (16H, broad s, S-CH_2), 1.90 (32H, quintuplet, CH_2), 1.79 (32H, quintuplet, CH_2), 1.05 (56H, sextuplet, $CH_2CH_2CH_3$). *Anal. Cal*. $C_{96}H_{147}N_8S_8O_3Ta$: C, 60.72, H, 7.80, N, 5.90. Found: C, 60.92, H, 8.41, N, 6.42 %. MALDI-TOF MS *m/z*: Calcd: 1898.16 amu. Found: (M-Ta) 1666.5 amu.

2.5. Synthesis of nanomaterials.

Synthesis of gold nanoparticles (AuNPs) and MPc-AuNPs conjugates

The synthesis of gold nanoparticles (using phase transfer agent TOABr as a protecting ligand) was achieved following the method described by Brust *et al.* [169] and Kotiaho *et al*. [200] with slight modifications. Briefly gold (III) chloride trihydrate solution (25 mmol L^{-1}, 4 mL) was vigorously stirred with a solution of TOABr (85 mmol L^{-1}, 6 mL) in toluene until all the gold chloride was transferred to the organic phase, as judged by the change of colour from orange to red [169, 200]. An aqueous solution of a reducing agent $NaBH_4$ (3.6×10^{-2} mol L^{-1}) was then added drop-wise over a period of 10 minutes. The mixture was then stirred vigorously for 30 minutes. The organic phase was separated and washed with water.

Solid complexes of conjugates of the newly synthesised MPcs (Figs. 1.4 and 1.5) with AuNPs were synthesized by mixing the two and allowing time (~28 – 30 hours) for the MPcs to react with the gold nanoparticles. The solvent (toluene) was then evaporated. The uncoordinated MPcs derivatives were removed in a size-exclusion column (bio-beads).

The purification of SWCNT

The SWCNT were purified by following methods described previously in literature [201] with modification as follows: SWCNT (150 mg) were momentarily suspended in a mixture of concentrated HNO_3:H_2SO_4 (1:3) and stirred at 70^{o}C for 2 hours. They were subsequently washed with water and dried in the oven overnight at 70 ^{o}C. The **28**-SWCNT and **29a**-SWCNT conjugates were formed by mixing complexes **28** or **29a** (3.5 mg) and SWCNT (1.0 mg) in $CHCl_3$ (1.5 mL) and stirred for ~ 12 h. Adsorption of TaPc derivatives onto SWCNT is expected due to ππ interactions between the two. TaPc complexes were chosen since they showed better electrocatalytic behaviour.

Results and discussion

Chapter 3:

Synthesis and spectroscopic characterisation

Chapter 4:

Photophysical, photochemical and photocalytic properties

Chapter 5:

Electrochemical characterisation

Chapter 6:

Electrocatalysis

List of publications

The results presented in this thesis have been published in journals listed below:

1. Remarkable sensitivity for detection of bisphenol A on a gold electrode modified with nickel tetraamino phthalocyanine containing Ni-O-Ni bridges, **Vongani Chauke**, Fungisai Matemadombo and Tebello Nyokong, *J. Haz. Mat.,* 178 (2010) 180.
2. Synthesis and electrochemical characterization of new tantalum (V) alkythio phthalocyanines, Vongani Chauke and Tebello Nyokong, *Inorg. Chim. Acta*, 363 (2010) 3662.
3. The electrochemical behavior of gold nanoparticle-tantalum (V) phthalocyanine composites: applications towards the electroanalysis of bisphenol A., **Vongani P. Chauke**, Wadzanai Chidawanyika and Tebello Nyokong, *Electroanal*., 23 (2011) 487.
4. Photocatalytic behaviour of tantalum (V) phthalocyanines in the presence of gold nanoparticles towards the oxidation of cyclohexene, **Vongani P. Chauke**, Edith Antunes, Wadzanai Chidawanyika, Tebello Nyokong, *J. Mol. Catal. A:Chem.,* 335 (2011) 121.
5. Synthesis and photophysical behaviour of tantalum and titanium phthalocyanines in the presence of gold nanoparticles: Photocatalysis towards the oxidation of cyclohexene, **Vongani P. Chauke**, Yasin Arslanoglu, Tebello Nyokong, (2011) *J. Photochem. Photobiol. A:Chem*, 221 (2011) 38.
6. Electrochemical behavior of phthalocyanines containing high oxidation state central metals: titanium (IV), vanadium (IV), tantalum (V), **Vongani P. Chauke**, Yasin Arslanoglu and Tebello Nyokong, *Polyhedron* 30(2011) 2132.
7. Conjugates of tantalum phthalocyanines with gold nanoparticles or single walled carbon nanotubes: characterization and improved stability towards bisphenol A

electrocatalysis, **Vongani P. Chauke**, Edith Antunes and Tebello Nyokong, *J. Electroanal. Chem.* (2011) *in press*.

3.1 Synthesis and spectroscopic characterisation of phthalocyanines.

3.1.1. Tetrasubstituted metallophthalocyanines (Scheme 3.1.)

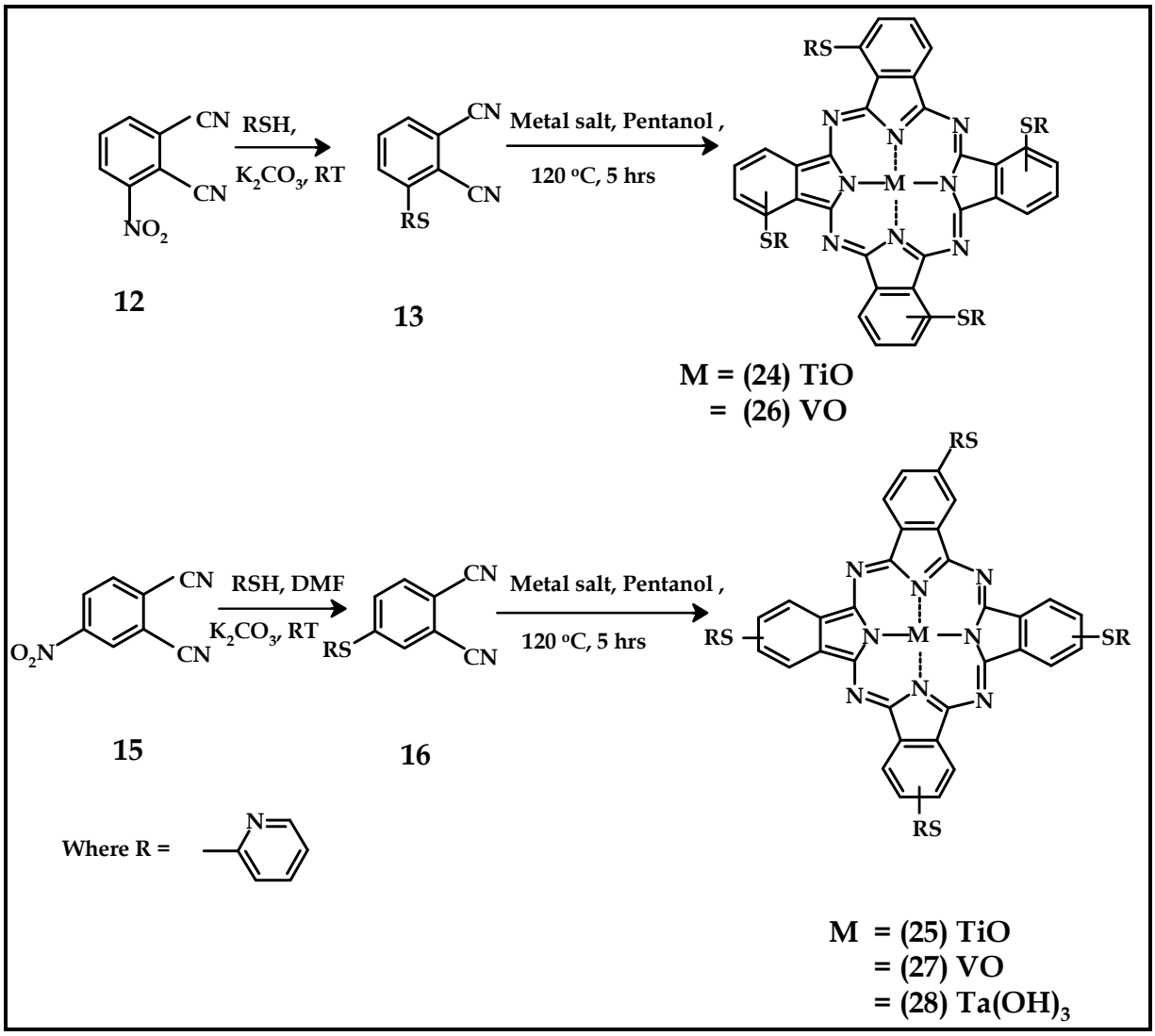

Scheme 3.1: Synthesis of titanium, vanadium and tantalum (M = $Ti^{IV}O$, OV^{IV}, $(OH)_3Ta^{V}$) non peripherally substituted phthalocyanine.

Scheme 3.1 gives the synthetic pathways for TiPc (**24** and **25**), VPc (**26** and **27**) and TaPc (**28**) complexes discussed in this work. Complexes **13** and **16** were treated with corresponding metal salts: titanium (IV) butoxide, anhydrous tantalum (V) butoxide or vanadium (IV) chloride in the presence of DBU as the catalyst to afford

TiPc (**24** and **25**), VPc (**26** and **27**) and TaPc (**28**) complexes (**Scheme 3.1**). Titanium, vanadium and tantalum are large metals that do not to fit perfectly in a phthalocyanine core centre. Column and preparative thin layer chromatography with silica gel were employed to obtain the pure products from the reaction mixtures. The synthesised complexes (**24 – 28**) are soluble in organic solvents such as dichloromethane, chloroform chloronaphthalene, dimethylformamide (DMF) and dimethylsulfoxide (DMSO). The new compounds were characterized by UV-Vis, IR and NMR spectroscopies, and elemental analysis. The analyses are consistent with the predicted structures as shown in the experimental section, with the percent carbon values differing from the calculated values by less than ~1 %. The disappearance of characteristic C≡N stretches in IR spectra confirmed the formation of the newly synthesised MPcs. Furthermore, the presence of the typical Ti=O stretches at ~ 898 cm^{-1}, V=O at ~ 930 cm^{-1} and Ta-O at ~ 910 cm^{-1} was confirmation that the TiPc, VPc and TaPc complexes, respectively, were formed. The new complexes were found to be pure by ^{1}H NMR with all the substituents and ring protons observed in their respective regions. The metal salts employed for synthesis of the MPc complexes were titanium butoxide, tantalum butoxide and vanadium tetrachloride, however the axial ligands obtained are oxo and hydroxide as a result of the purification process and the MPcs are more stable with these axial ligands. The ground state electronic absorption spectra of the synthesized complexes are shown in Fig. 3.1. Complexes **24** and **26** {with substituents on the α (non-peripheral) position show quite broad UV/Vis and red-shifted spectra, Fig. 3.1(a) and (b) curves (ii), relative to the corresponding complexes (**25** and **27**) that are β- (non-peripheral)

substituted. This red shifting is typical for MPc with substituents on the α positions and is explained by linear combinations of atomic orbitals (LCAO) coefficients at the α positions of the HOMO being greater than those at the β positions. This results in the destabilisation of the HOMO level, this way reducing the energy level (ΔE) between the HOMO and LUMO thus causing a red shift [202, 203].

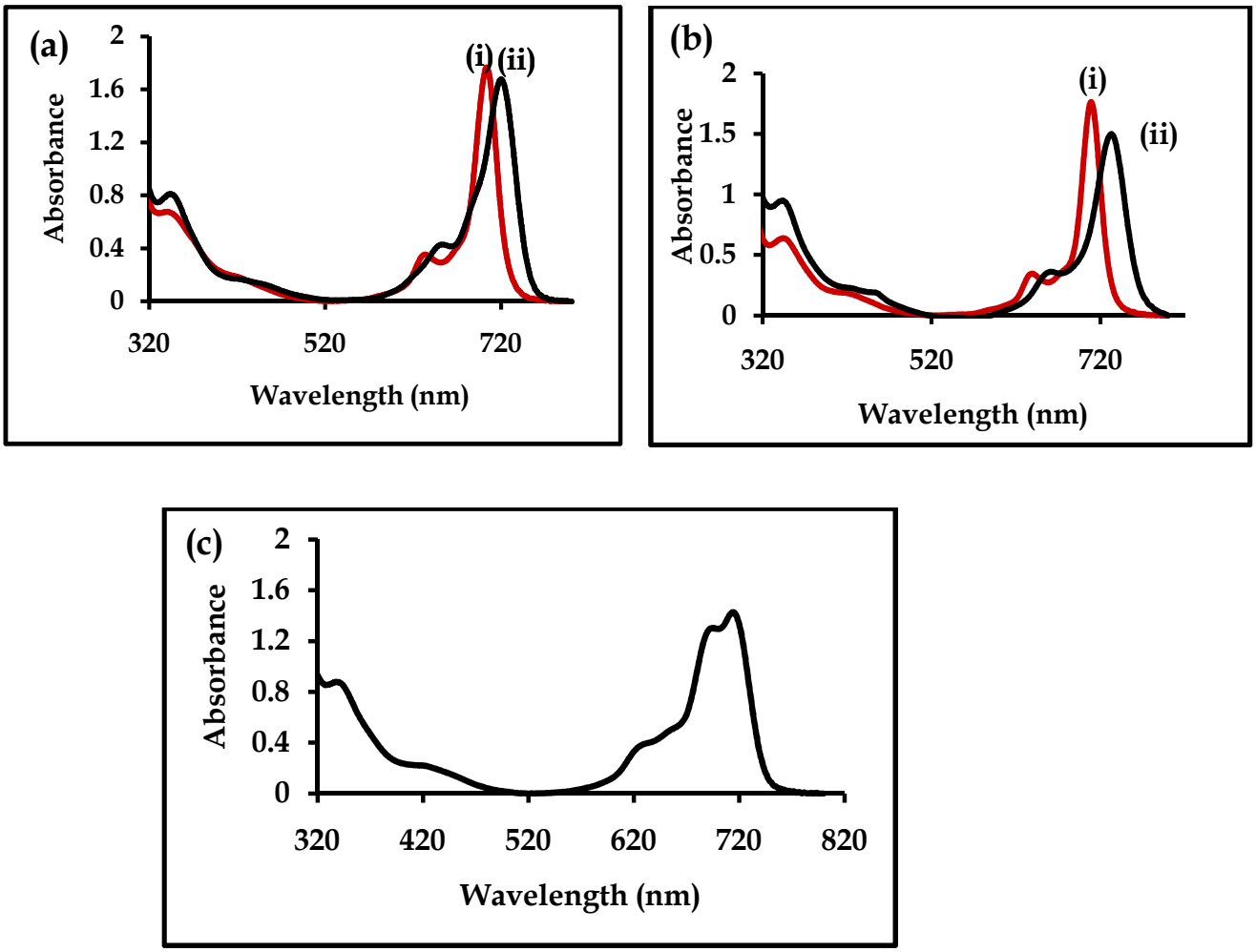

Figure: 3.1: Ground state electronic absorption spectra of complexes (a) 25 (i) and 24; (b) 27 (i) and 26 (ii); and (c) 28 in toluene. Concentration ~ 1.8 x 10^{-5} mol L^{-1}.

Table 3.1 summerises the Q band positions of the newly synthesised tetra-susbtituted MPcs (**24 – 28)** in toluene.

Table 3.1: UV-Visible spectra (Q bands only) of MPc derivatives (24 - 28) in toluene.

MPc	Q band (nm)
24	730
25	720
26	705
27	701
28	688, 710

The broadening in the spectra of **24** and **25** could be a result of aggregation or loss of symmetry due to the presence of bulky groups at the non-peripheral positions. Aggregation at the concentrations of ~ 1.8 x 10^{-5} mol L^{-1}, Fig.3.1 (a) and (b), was ruled out since Beer's law was obeyed for concentrations ranging from 2.85 x 10^{-6} to 1.34 x 10^{-5} mol L^{-3}. Besides, aggregation is expected to be more evident for peripheral compared to non-peripheral substitution. Furthermore demetallation was ruled out by the addition of zinc acetate and refluxing in the presence of the complex in 1-pentanol. Thus the most likely reason for the broadening is the loss of symmetry. It has been reported that deformation of the Pc ring occurs when methoxyphenyl substituents are located at non-peripheral positions [204]. The loss of symmetry is more pronounced for TaPc derivative (**28**) as judged by the split Q band, Fig. 3.1(c), Table 3.1, even though this complex is substituted at peripheral positions. This is due to the large size of the Ta central metal which lies more out of the plane of the ring when compared to the other central metals because of its size.

3.1.2. Octasubstituted metallophthalocyanines (Scheme 3.2).

Scheme 3.2 gives the synthesis pathways for the octasubstituted TaPc (**29a** and **29b**) complexes synthesised in this work. 3,6-Bis(4'-methylphenylsulfonyloxy) phthalonitrile (**21**), was used to prepare 3,6-disubstituted phthalonitrile derivatives (**22a** and **22b**), through base-catalysed nucleophilic aromatic displacement. The reactions were carried out in DMSO at room temperature and gave yields of 71.7 % for **22a** and 58.1 % for **22b**. The syntheses of TaPc complexes (**29a** and **29b**) were achieved by treatment of substituted 3,6-dicyanobenzenes **22a** and **22b** with anhydrous tantalum (V) butoxide in 1-pentanol in the presence of DBU (**Scheme 3.2**). DBU acts as a nucleophilic base which allows the reaction to proceed under mild conditions while preventing the formation of side products typical of reactions that use strong bases [205].

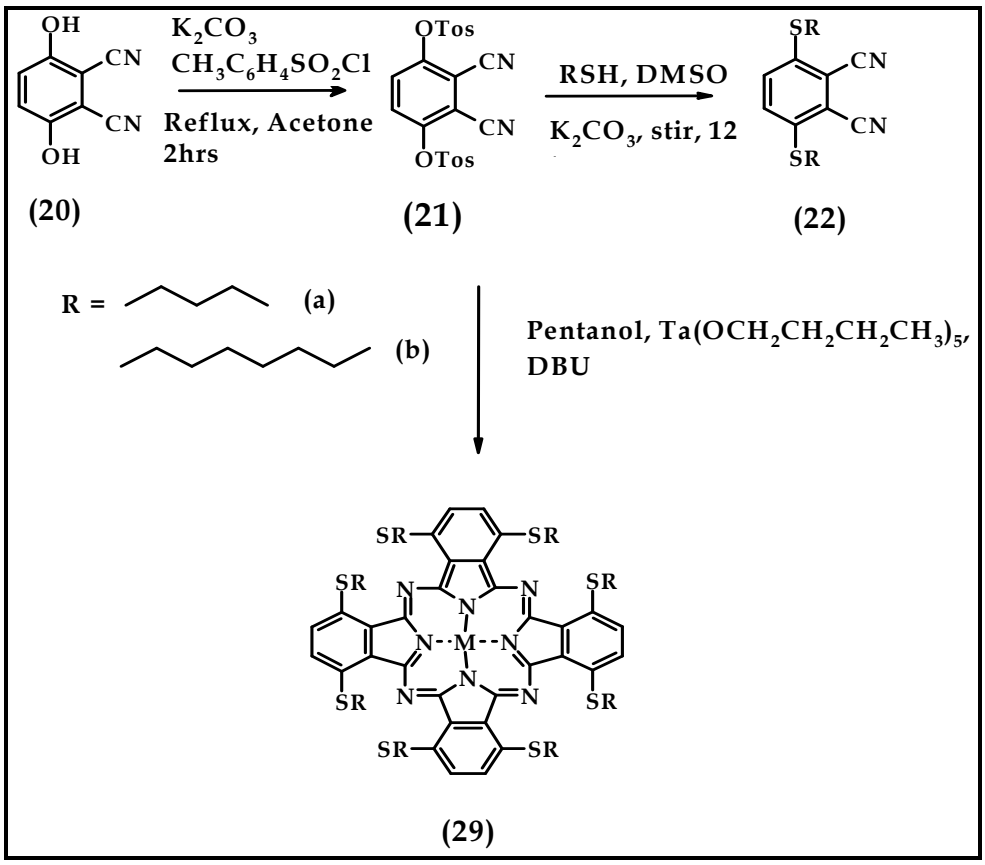

Scheme 3.2: Synthesis of tantalum [M = $(OH)_3Ta^V$ for 29a and 29b] non peripherally substituted phthalocyanine.

Column and preparative thin layer chromatography with silica gel were employed to obtain the pure products from the reaction mixtures. The synthesised complexes (**29a** and **29b**) show good solubility in organic solvents such as dichloromethane, chloroform and chloronaphthalene; and were characterized by UV-Vis, IR, mass and NMR spectroscopies. The analyses are consistent with the predicted structures as shown in the experimental section. After conversion into TaPc complexes, the characteristic C≡N stretch at 2225 cm^{-1} of 1,2-dicyanobenzenes **22a** and **22b** disappeared, indicative of metallophthalocyanine formation. The formation of $(OH)_3$TaPc (containing OH instead of butoxy groups) could be a result of the

purification process. The presence OH was proved by infrared spectroscopy and C-S-C vibrations were observed at ~ 750 cm^{-1} [206].

The substituted TaPc derivatives were found to be pure by ^{1}H NMR with all the substituents and ring protons observed in their respective regions, Fig. 3.2. This figure shows a clean ^{1}H NMR spectrum confirming the purity of the complex. The pentylthio substituted complex **29a** showed the resonances belonging to ring protons as a singlet at 7.65 ppm. Similarly, the octylthio substituted complex **29b** showed the resonances belonging to ring protons as a singlet at 7.51 ppm.

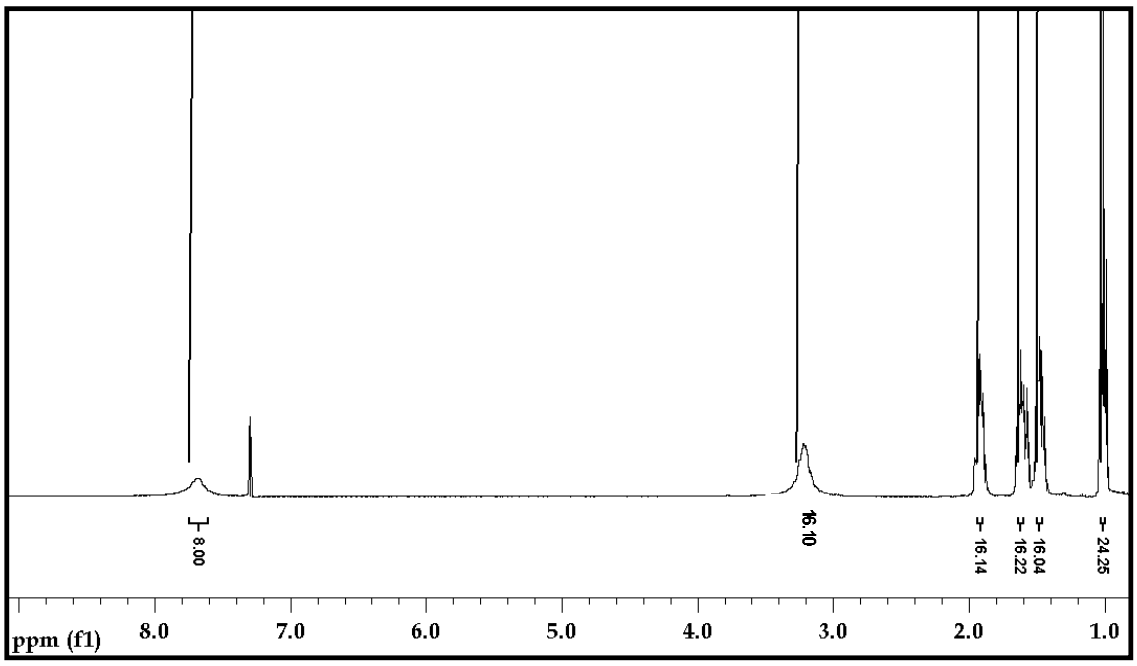

Figure 3.2: ^{1}H-NMR spectrum of complex 29a

Mass spectral studies confirmed the loss of Ta since as already stated Ta is a large metal and it does not fit properly into the cavity of a phthalocyanine core. Ta ion is vulnerable to displacement if exposed to harsh conditions such as during ionisation in mass spectrometry hence the observed mass. However elemental analyses unequivocally confirmed the formation of the complexes.

The ground state electronic absorption spectra of complexes **29a** and **29b** show sharp Q bands {Figs. 3.3(a) and (b)}, typical of unaggregated MPc complexes. Beer's law was obeyed for concentrations ranging from 1.85 x 10^{-7} to 2.28 x 10^{-5} mol dm^{-3}. The Q bands were observed at 808 and 812 nm in DCM for **29a** and **29b**, respectively, Table 3.2.

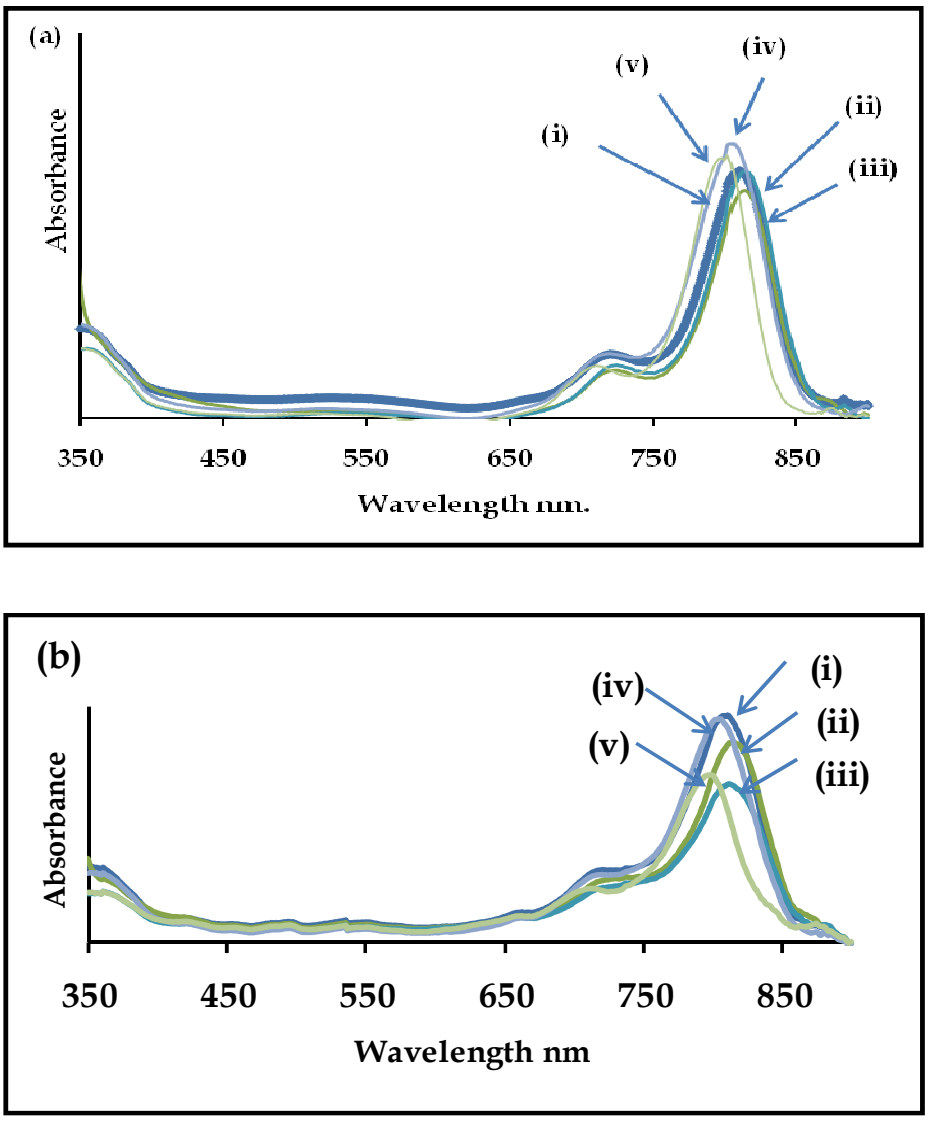

Figure 3.3: Ground state electronic absorption spectra of TaPc complexes 29a (a) and 29b (b) in (i) $CHCl_3$, (ii) chloronaphthalene, (iii) DCM, (iv) THF, (v) toluene. ~ concentrations = 1 x 10^{-5} M

The Q bands were relatively red-shifted when compared to the tetrasubstituted TaPc (**28**), and the rest of the tetrasubstituted MPcs in this work (**24** - **28**). Similarly, in toluene, the octasubstituted TaPcs (**29a** and **29b**) were more red shifted than the tetrasubstituted TaPc complex (**28**).

Table 3.2. UV-Visible spectra of TaPc MPc derivatives in various solvents.

Complex	**Solvent**	**Q band (nm)**
29a	Toluene	795
	THF	804
	DCM	808
	1-CNP	810
	$CHCl_3$	809
29b	Toluene	794
	THF	800
	DCM	812
	1-CNP	815
	$CHCl_3$	809

This is typical of MPcs with substituents on the non-peripheral position and also characteristic of MPc containing sulfur substituents, more so the number and nature of substituents has increased from four to eight. In terms of solvent, the Q band is more red shifted in chlorinated solvents: $CHCl_3$, 1-CNP and DCM, Table 3.2. It has been reported before that there is more red shifting in chlorinated solvents [207]. The reported [208, 209] trend based on the solvents' refractive index is not observed in Table 3.2.

3.2. Characterisation of AuNPs and SWCNTs – MPc conjugates

Gold nanoparticles show a strong absorption in the visible range due to surface plasmon resonance (SPR) [156]. The absorption peak is dependent on various factors such as particle size and shape [156, 157], dielectric constant of the surrounding solvent and inter-particle size [156, 157, 210]. The size dependence of absorption spectra has been reported before and has been confirmed by both theoretical and experimental studies [156,157,211]. The UV-Vis absorption spectrum of the gold nanoparticles employed in this work, Fig. 3.4, shows an absorption peak at 520 nm and this is consistent with the reported SPR peak for gold nanoparticles [211].

After the formation of the MPc-AuNPs conjugates, spectral changes of the TaPc derivatives were observed. For examples, the Q band for complex **29a** alone was observed at 805 nm, Fig. 3.4(iii), and at 794 nm in the presence of AuNPs, Fig. 3.4(ii), in DCM:acetone solvent mixture, showing a blue shifting. The solvent mixture was employed to ensure that both AuNPs and TaPc dissolve. The blue shifting is a result of the increase in the gap between the highest occupied molecular orbital (HOMO) and the lowest unoccupied molecular orbital (LUMO) in phthalocyanines, normally observed in the presence of electron withdrawing groups. The blue shift suggests π-deficiency of the TaPc complexes in the presence of AuNPs.

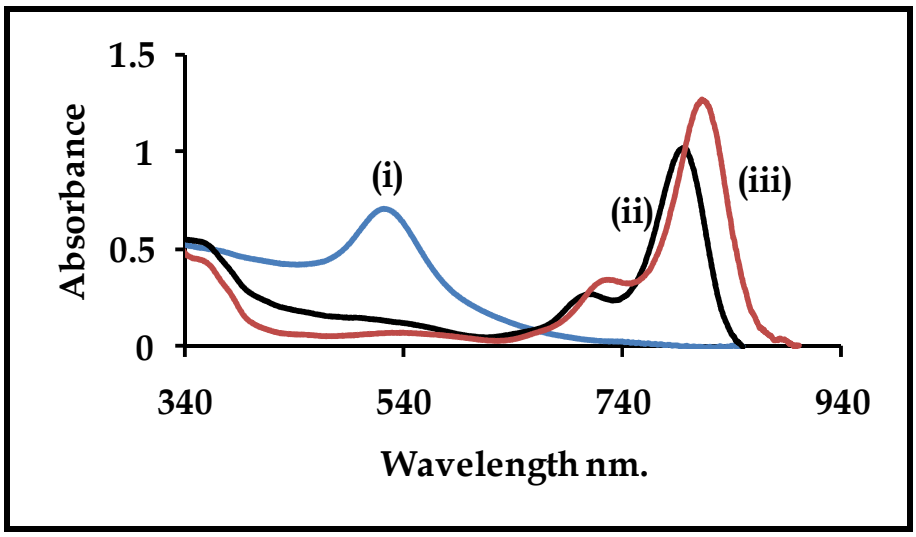

Figure 3.4: UV-Vis absorption spectra of gold nanoparticles (i) AuNPs alone, (ii) 29a-AuNPs, and (iii) 29a alone in DCM:acetone. Size of AuNPs is 20 nm.

Fig. 3.5(a) shows the TEM images of AuNPs {Fig. 3.5(a)} and **25**-AuNPs {Fig.3.5(b)}. Fig. 3.5(a) illustrates the distribution and spherical nature of the gold nanoparticles employed in this work. Upon conjugation with the complex **25**, Fig 3.5(b), the gold nanoparticles appear to be 'surrounded' by MPc illustrated by the dark spots. The AuNPs were stabilized by TOABr; it is possible for the stabilizer to be replaced by the alkylthio groups of TaPc derivatives to form a bond, or that the TaPc derivatives are just adsorbed onto the AuNPs.

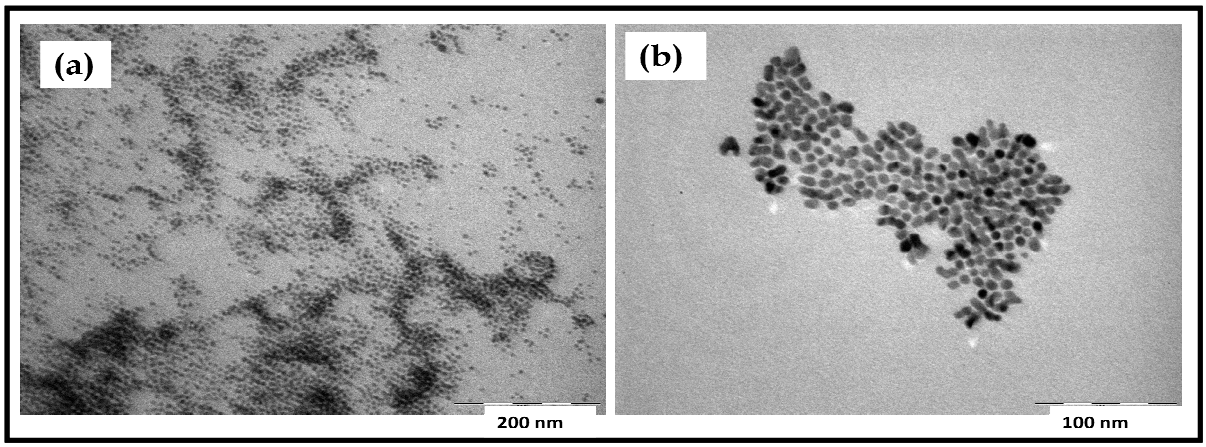

Figure 3.5: TEM images of (a) AuNPs in water and (b) AuNPs modified with complex 25.

Fig. 3.6 shows the XRD pattern for the AuNPs employed in this work, with the peaks observed at 2θ values of 27.41° 31.65°, 38.17°, 45.40° and 56.38°. The average size for the AuNPs was then worked out to be 10 nm (first batch, used for electrocatalysis) and 20 nm (second batch, used for photocatalysis), using the peak that fits the structure database reflection for gold using Equation 1.21.

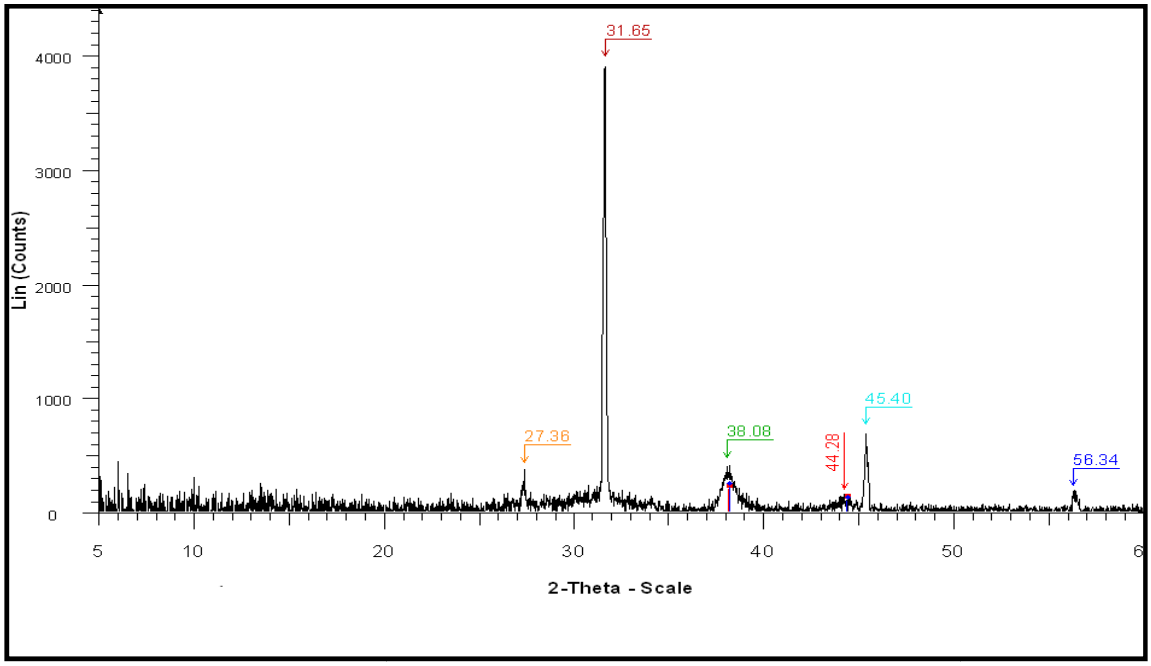

Figure 3.6: X-ray diffractogram of AuNPs.

Atomic force microscopy data, (Fig. 3.7) provided the information about the morphology of AuNPs on a cross section of the glass surface coating from toluene in the absence and presence of the TaPc derivatives. The average roughness (Ra) value of 0.628 nm was obtained for AuNPs alone and the value decreased to 0.0927 nm for AuNP-MPc conjugates. The decrease may be due to aggregation in the presence of TaPc derivatives. The histogram in Fig. 3.7(c), shows populations of AuNPs with size distributions from 20 nm and below in the section analysed, to occur more frequently.

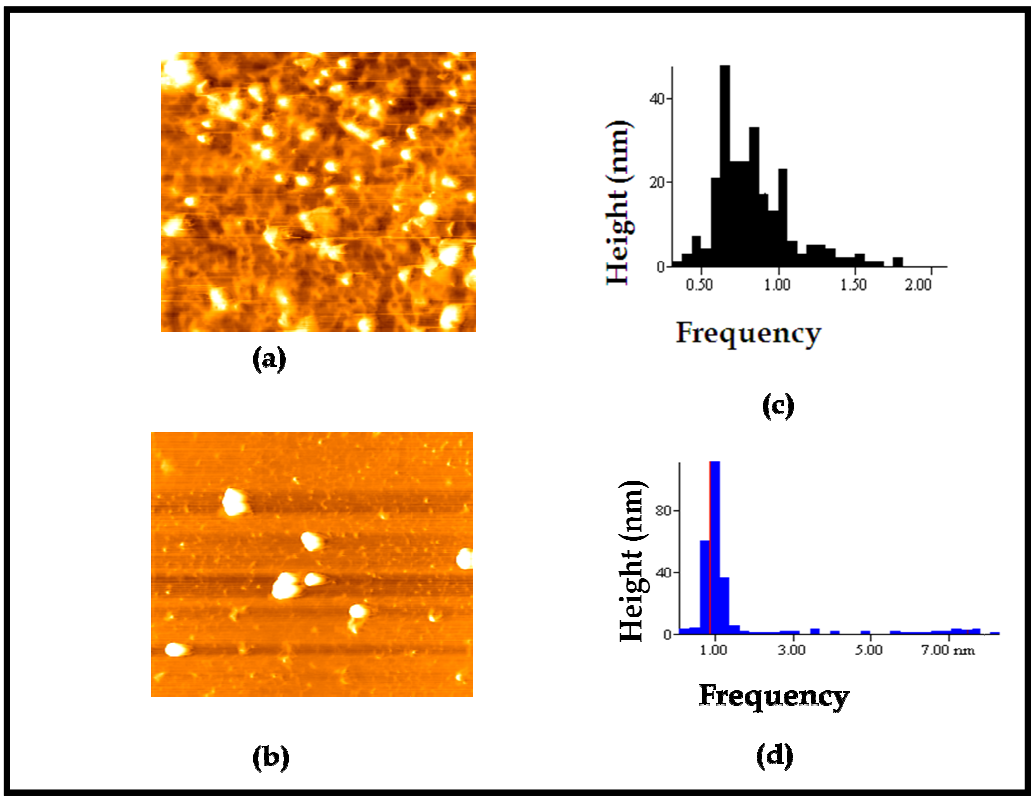

Figure 3.7: AFM images of AuNPs in the absence (a) and presence (b) of complex 29a deposited on a glass surface from toluene. The corresponding histograms are shown in (c) and (d).

In Fig. 3.7(d) for AuNPs in the presence of complex **29a** there is a domination by the larger sizes, with size distribution of up to 114 nm, showing increased aggregation. This indicates that modification of AuNPs with the newly

synthesised complexeses was successful to some extent. The rough estimates of the AuNPs sizes from the AFM histograms {Fig. 3.7 (c)} and region analysis were 20 nm and after conjugation with TaPc, the size increased to ~ 40 nm {Fig. 3.7 (d)}.

The purified SWCNT and MPc-SWCNT conjugates were characterised and visualised using TEM. Fig. 3.8(a) shows the SWCNT alone with rod-like shapes and closely packed together. Fig. 3.8(b) shows the interaction of SWCNT with complex **28**. The spaces between rod-like SWCNTs seem to be decreased due to the presence of complex **28** on the SWCNTs.

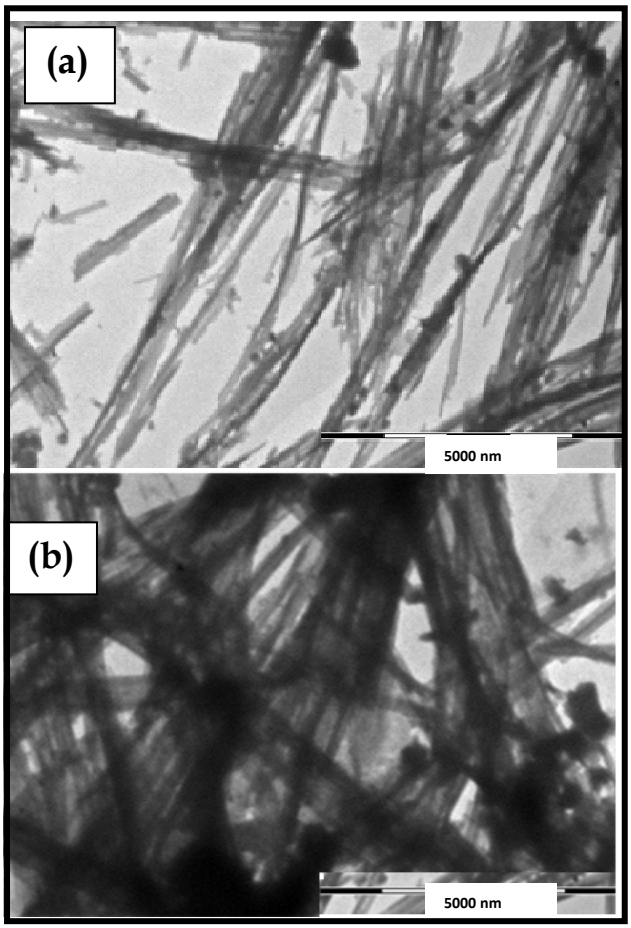

Figure 3.8: TEM images of (a) SWCNT in toluene (b) SWCNT modified with complex 28.

4. Photochemical, photophysical and photocatalytic properties.

These studies were not performed for VPc complexes (**26** and **27**) due to the paramagnetic nature of vanadium which shortens the triplet state. The size of AuNPs used for these studies was 20 nm.

4.1. Photophysical parameters: triplet quantum yields (Φ_T) and lifetimes (τ_T)

Triplet quantum yield (Φ_T) is a measure of the fraction of light absorbing molecules that undergo intersystem crossing to the meta-stable triplet excited state. The competence of phthalocyanines as photocatalysts or photosensitisers depends on their high triplet quantum yields and lifetimes since they can transfer energy to ground state oxygen to produce singlet oxygen. A typical triplet decay curve for complex **24** is shown in Fig.4.1, where the triplet state population decreases with increase in time.

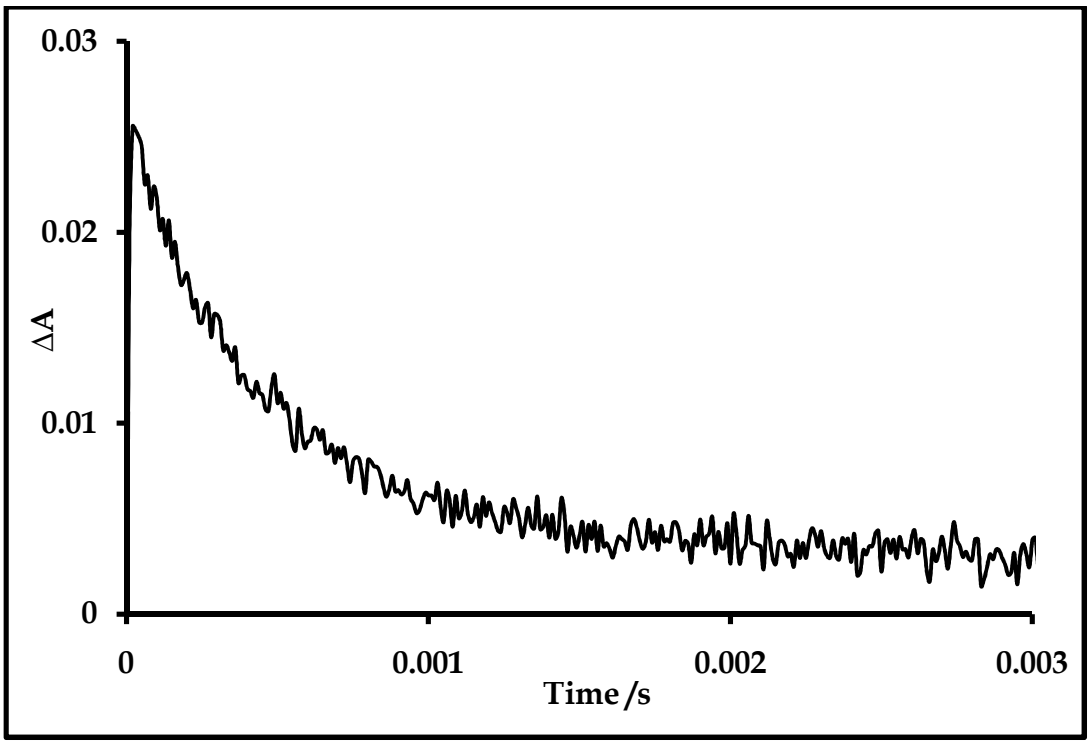

Figure 4.1: Triplet decay curve for 24 in toluene, excitation wavelength = 720 nm.

Table 4.1 gives the triplet quantum yield (Φ_T) values and triplet lifetimes (τ_T) for the substituted TiPc and TaPc complexes. Φ_T values were higher for complexes **24** and **25** (0.67 and 0.62, respectively) complexes compared to the TaPc complex (**28**) with a value of 0.28. The low value of Φ_T for TaPc (**28**) could be a result of low symmetry discussed above. It has been reported that loss of symmetry leads to efficient radiationless deactivation of the lowest excited states of free-base porphyrins [212], this could be the case for TaPc (**28**) resulting in low Φ_T value. However, complexes **29a** and **29b** also showed good Φ_T values of 0.56 and 0.47, repectively. AuNPs improved the triplet quantum yields for **24**, **25, 29a** and **29b** through enhanced spin-orbit coupling due to heavy atom effect [213], Table 4.1.

Table 4.1. Triplet quantum yield values (Φ_T) and lifetimes (τ_T) for complexes 24 – 29 and their AuNPs conjugates in toluene.

MPc	**Φ_T**	**τ_T (μs)**
24	0.67	79
25	0.62	82
28	0.28	49
29a	0.56	71
29b	0.47	98
24-AuNPs	0.70	34
25-AuNPs	0.74	27
28-AuNps	0.26	20
29a-AuNPs	0.74	42
29b-AuNPs	0.93	18

The presence of the bromide atoms on TOABr (the AuNPs protecting ligand) also increase intersystem crossing due to heavy atom effect [212]. The increase in Φ_T

value was not observed for complex **28**. The triplet lifetimes were shorter in the presence of AuNPs, this corresponds to the increased quantum yield values.

4.2. Photochemical parameters

4.2.1. Singlet oxygen quantum yields (Φ_Δ).

Singlet oxygen quantum yields are an evaluation of a phthalocyanine's ability to produce singlet oxygen. The latter plays a significant role in photocatalytic oxidation reactions [92]. Singlet oxygen quantum yield (Φ_Δ) values (Table 4.2) were determined using DPBF as the singlet oxygen quencher in toluene, where the phthalocyanines were irradiated with light in the Q band region. Following light irradiation, DPBF decay was monitored spectrophotometrically at ~ 410 nm as shown in Fig. 4.2 where the rate of DPBF decay is directly proportional to the singlet oxygen production by the photosensitizer.

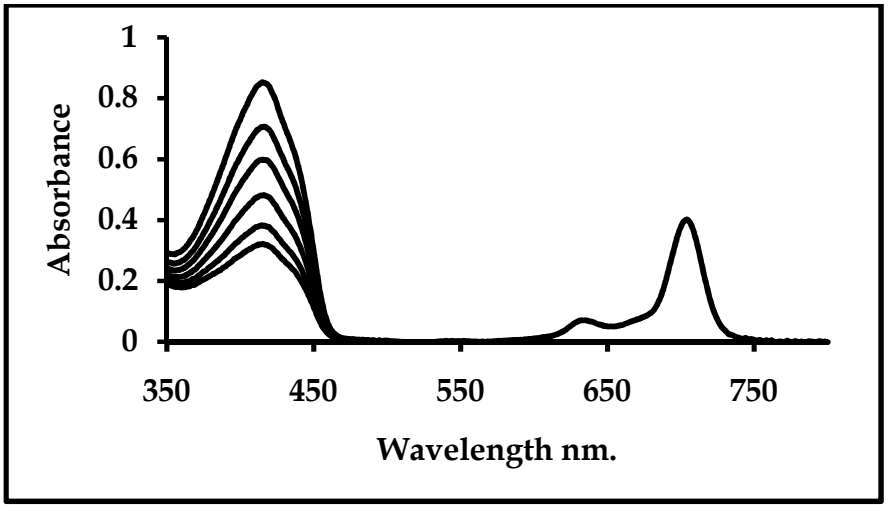

Figure 4.2: Photodegradation of DPBF in the presence of complex 24 in toluene.

The complexes showed relatively good singlet quantum yield values that ranged from 0.36 to 0.63, with the TaPc complexes **28**, **29a** and **29b** exhibiting the

lowest values of 0.41, 0.47, and 0.36, due to their relatively low triplet quantum yield values compared to the TiPc complexes. The Φ_Δ value for complex **28** was unusually larger than its Φ_T. On introducing AuNPs to the TiPc and TaPc complexes, a drastic increase of the Φ_Δ values for the TiPc (**24** and **25**) and TaPc (**29a** and **29b**) complexes was observed, Table 4.2., except for complex **28** where there was a surprising decrease in the singlet oxygen quantum yield.

Table 4.2: singlet oxygen quantum yields of TaPc and TiPc complexes and their AuNPs conjugates.

MPc	**Φ_Δ in toluene**	**Φ_Δ in toluene (MPc-AuNPs)**
24	0.63	0.72
25	0.54	0.67
28	0.41	0.23
29a	0.47	0.75
29b	0.36	0.88

The AuNPs promote a higher production of singlet oxygen due to enhanced triplet excited state yield of the sensitizer. Improved singlet oxygen generation by metal nanoparticles has been observed and reported by Zhang *et al.* [214]. Silver nanoparticles were employed by Zhang *et al.*[214], and the photosensitizer was described as being 'sandwiched' between the silver nanoparticle island films enabling more singlet oxygen production due to enhanced triplet excited yield of the sensitizer. Their concept may be related to this study where gold nanoparticles are employed instead of silver nanoparticles. In addition, it is possible that the presence of the bromide atoms on the TOABr (the AuNPs protecting ligand) increases the

energy transfer to the triplet state of TiPc and TaPc complexes in the presence of AuNP, through heavy atom effect [171], with the exception of complex **28**, hence larger Φ_Δ values .

4.2.2. Photodegradation quantum yields (Φ_P).

The process of phthalocyanine photodegradation is initiated and driven by singlet oxygen in the presence of light [92]. The stability of MPcs is important for light driven processes such as PDT and photocatalysis, the latter was explored in this work. For this reason, MPcs were irradiated at the Q band where the light was filtered such that only the Q band was exposed. To mimic large scale experiments where sunlight is utilised, white light was also employed and the rate of degradation was monitored for selected TaPc complexes (**29a** and **29b**) that showed the highest stability under Q band irradiation.

4.2.2.1. Q band irradiation

The photodegradation stabilities were determined in toluene by monitoring the spectra of the complexes with time, during photolysis, Fig. 4.3 (a) and (b).

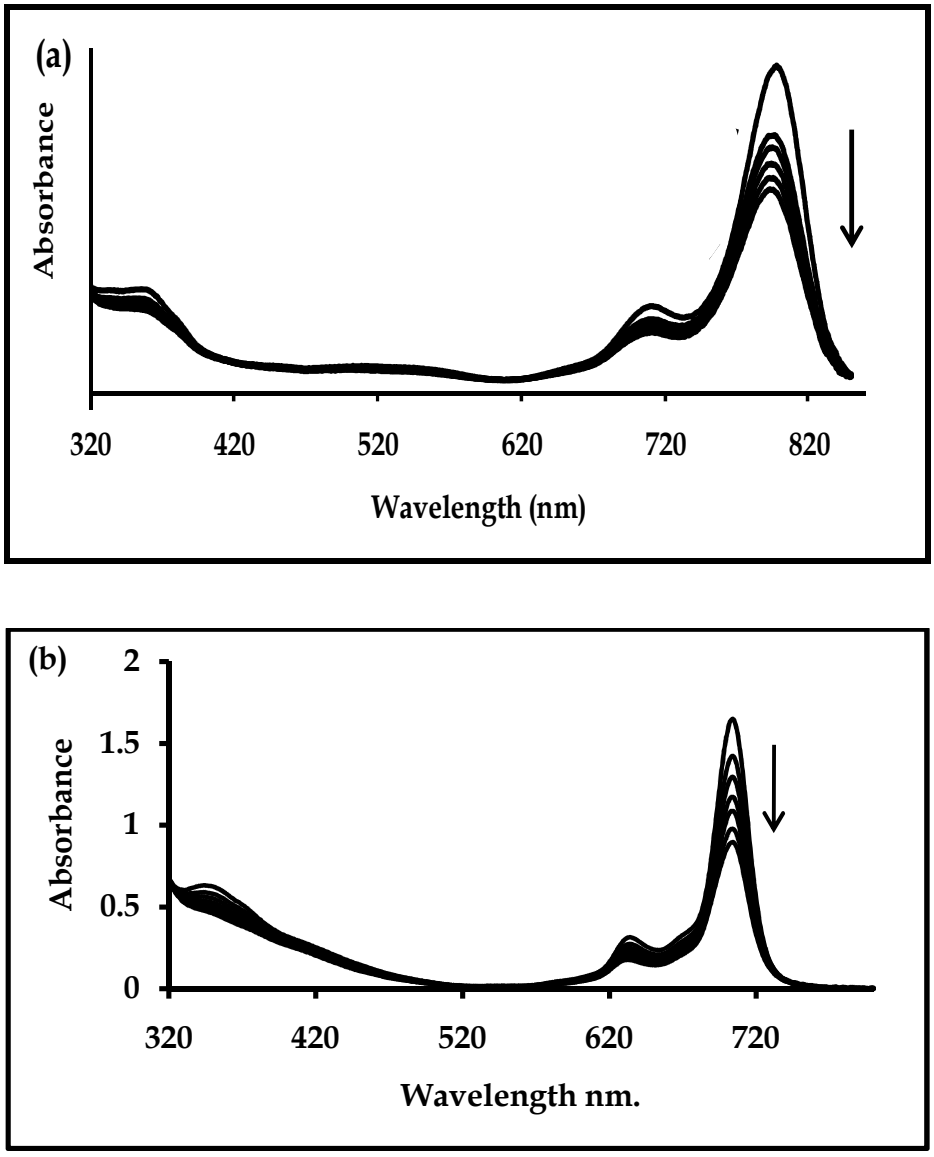

Figure 4.3: Photodegradation spectra of complex (a) 29a and (b) 24 in toluene. [29a] ~ 3.02 x 10^{-5} mol L^{-1} and [24] ~2.20 x 10^{-5} mol L^{-1}.

The MPc complexes are degraded by singlet oxygen generated by them according to Scheme 1.8, hence the magnitude of singlet oxygen quantum yield is directly related to the photodegradation quantum yield. Other factors that can influence Φ_P include the nature of the solvent and the substitutents on the phthalocyanine ring. Equation 1.14 was employed to calculate the photodegradation quantum yield values. In general the TaPc complexes, Table 4.3 were very stable even in the presence of

AuNPs. Typical values for unstable phthalocyanines are of the order of 10^{-3} [213]. There was no clear trend regarding Φ_P values in the presence of AuNPs.

The photodegradation of TaPc derivatives followed first order kinetics with the plots of $\ln(C_0/C)$ (where C and C_0 are absorbances measured for the Q band of the MPc complex at time t and t_0, respectively) versus time in seconds, shown in Fig. 4.4 (i and ii). The slopes of the plots gave the effective reaction rate constants, k. Table 4.3 shows large rate constants for degradation of complexes **29a** and **29b** which are octa-substituted with alkylthio substituents, while the k values were lower for the rest of the complexes which are tetra-substituted with arylthio groups. In the presence of AuNPs, the rate constants increased for arlythio tetra-substituted complexes, but decreased for **29a** and **29b**.

Table 4.3. Photodegradation quantum yields under Q band irradiation and rate constants for all TiPc and TaPc complexes in the absence and presence of AuNPs in toluene.

MPc	Φ_P	k (s^{-1})
24	2.29×10^{-5}	2.76×10^{-5}
25	5.66×10^{-5}	2.14×10^{-5}
28	5.20×10^{-6}	5.12×10^{-6}
29a	2.07×10^{-6}	7.16×10^{-5}
29b	1.45×10^{-6}	7.35×10^{-5}
24-AuNPs	3.73×10^{-5}	3.03×10^{-5}
25-AuNPs	2.18×10^{-5}	3.57×10^{-5}
28-AuNPs	1.80×10^{-6}	6.54×10^{-5}
29a-AuNPs	2.45×10^{-6}	6.04×10^{-5}
29b-AuNPs	1.02×10^{-6}	4.75×10^{-5}

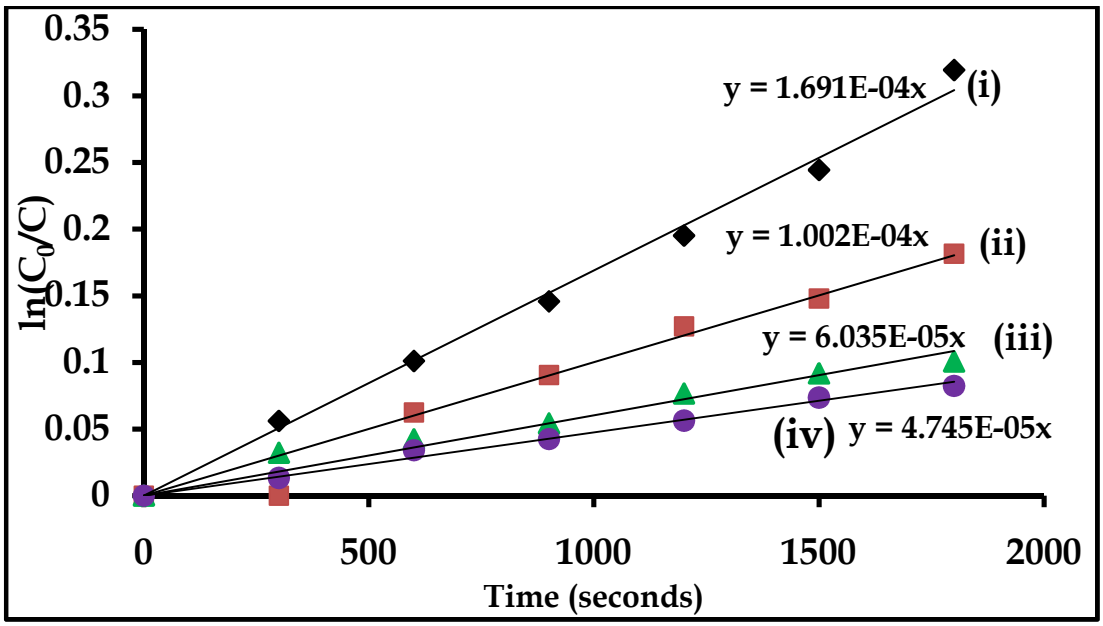

Figure 4.4: A plot of $\ln(C_0/C)$ vs. time for conjugates under white irradiation: 29b-AuNPs (i) and 29a-AuNPs (ii) and under Q band irradiation: 29a-AuNPs (iii) and 29b-AuNPs (iv). Solvent = toluene.

4.2.2.2. White light irradiation

The photostability of the TaPc complexes (**29a** and **29b**) also depends mainly on the type of radiation. These complexes (**29a** and **29b**) were chosen since they showed more stablility under Q band irradiation (Table 4.3). In general, MPc complexes are more stable in visible light compared to UV irradiation [215]. Irradiation using white light will include the Q band, but it is more extended than the Q band irradiation (which ranges from 710 to 790 nm for the TaPc derivatives under discussion). The selected TaPc complexes (**29a**) were completely degraded by exposure to sunlight (for 8 h), Fig. 4.5, whose main intensity is at ~ 550 nm. In order to study the degradation of the complexes under more controlled conditions, white light was employed from a tungsten lamp (400 to 900 nm), to photodegrade the complexes in the presence and absence of AuNPs.

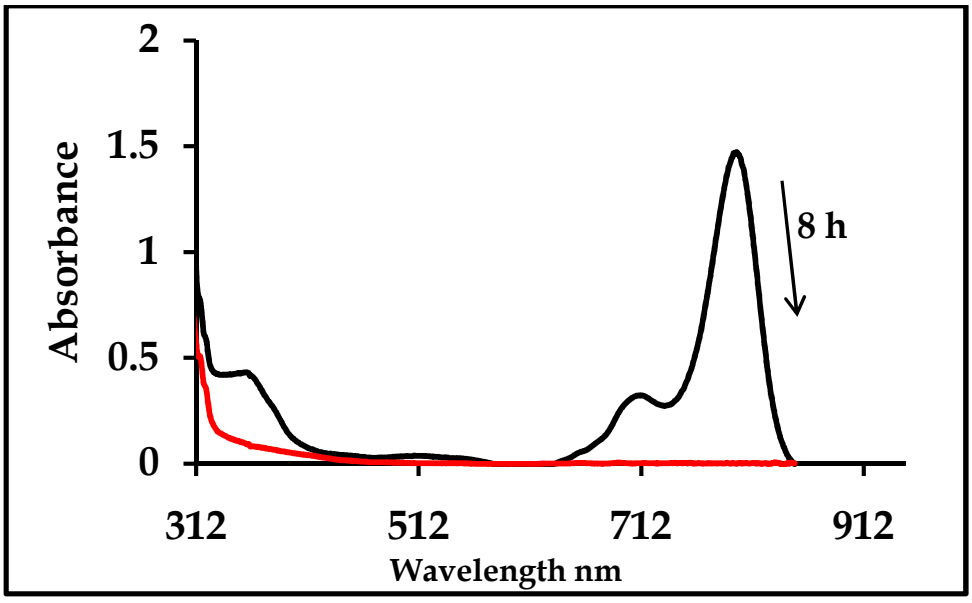

Figure 4.5: Photodegradation spectra of complex 29a in toluene by direct sunlight. Concentration ~ 3.10 x 10-5 mol L-1. Irradiation period ~ 8 hours.

At the wavelength of the tungsten lamp, it is not expected that the excitation will be at the B band of the phthalocyanine molecule; however, there will be a larger wavelength range as opposed to the excitation of the Q band only. Thus singlet oxygen by Type II mechanis (**Scheme 1.5**) is expected to be the dominant route for degradation under white light from the tungsten lamp. Photolysis induced by UV irradiation of the MPc derivatives has been shown to follow first-order kinetics [216]. Plots of ln (C_0/C) versus time in Fig. 4.4 (i and ii), gave the rate constants for white light photolysis as listed in Table 4.4. The rate constants are larger for the white light since a larger range of wavelengths is employed. It is also possible with white light that heat is involved in the degradation process since near infrared light is involved. The Φ_P values (Table 4.4) are surprisingly larger for white light compared to Q band irradiation only for **29b-**AuNP and **29a**, Tables 4.3 and 4.4.

Table 4.4: Photodegradation quantum yields under white light irradiation and rate constants in the presence and absence of AuNPs in toluene.

MPc	**Φ_P**	**k (s^{-1})**
29a	2.27 x 10^{-6}	1.80 x 10^{-4}
29b	1.17 x 10^{-6}	1.15 x 10^{-4}
29a-AuNPs	2.36 x 10^{-6}	1.00 x 10^{-4}
29b-AuNPs	1.59 x 10^{-6}	1.70 x 10^{-4}

In order to check if singlet oxygen is involved during photodegradation in white light, photobleaching experiments were performed in the presence of diazabicyclooctane (DABCO); a singlet oxygen scavenger. The photobleaching rate

constant was calculated to be 8.71 x 10^{-6} s^{-1}. This rate was slower than the rates listed in Table 4.3, confirming a significant singlet oxygen involvement in the mechanism. Thus, it is possible that both singlet oxygen and radicals are involved in the photobleaching mechanism.

4.3 Photocatalytic oxidation of cyclohexene

Photocatalytic oxidation reactions were carried out under filtered light, i.e. Q band irradiation and white light irraditation. For the latter, only TaPc complexes (**29a** and **29b**) and their AuNPs conjugates were selected due to their high stability compared to the tetrasubstituted TiPc (**24** and **25**) and TaPc (**28**) complexes. The possible oxidation products for cyclohexene have been reported before [19, 108], they include cyclohexene oxide, cyclohexenol, cyclohexenone and cyclohexanediol. The products obtained in this work were confirmed by the spiking of the photocatalysed samples with the respective standards. Control experiments were performed where cyclohexene was photooxidized in the absence of MPcs and MPc-AuNPs conjugates. The results for the control experiments showed negligible formation of the products. Similarly, in the absence of light but in the presence of TaPc derivatives (with or without AuNPs), no products were formed.

The main products obtained (and confirmed by spiking) are: cyclohexene oxide, 2-cyclohexen-1-ol, 2-cyclohexene-1-one and 1,4-cyclohexanediol. These are obtained as main products both by Q band and white light irradiations.

4.3.1. Percentage conversion values for cyclohexene.

Table 4.5 shows the percentage conversion of cyclohexene using TiPc and TaPc complexes and their AuNPs conjugates as photocatalysts under Q band irradiation and white light (for the latter, only complexes **29a** and **29b** and their AuNPs conjugates).

The percentage conversion values were generally higher for the MPc-AuNPs with **24**-AuNPs and **25**-AuNPs conjugates (39.1 and 37.6 %, respectively) having the highest percentage conversion values, compared to all the free complexes. This is associated with their increased singlet oxygen quantum yields compared to the MPcs complexes alone. The percentage conversion variations are shown in Fig. 4.6 for 180 minutes irradiation , for tetrasubstituted complexes, **24**, **25** and **28**. The first 30 minutes show a drastic increase in the percentage conversion for the TiPc and TaPc complexes (**24**, **25** and **28**) and their AuNPs conjugates. This is followed by a slow conversion process until the reaction was stopped at 180 minutes.

Table 4.5: Percentage conversion of cyclohexene by the listed complexes and AuNPs conjugates in toluene. Photolysis time = 180 min.

MPc	Q band irradiation	White light
	% Conversion[a]	% Conversion[a]
24	27.4	-
25	19.7	-
28	13.8	-
29a	24.2	48.1
29b	18.0	45.2
24-AuNP	39.1	-
25-AuNP	37.6	-
28-AuNPs	11.9	-
29a-AuNPs	35.4	92.3
29b-AuNPs	30.4	90.0

(a) $\%\text{conversion} = \frac{(1 - \text{cylohexene}_{\text{initial}}) - (1 - \text{cyclohexene}_{\text{remaining}})}{(1 - \text{cyclohexene}_{\text{initial}})} \times 100$

In the presence of a singlet oxygen scavenger, DABCO [Fig. 4.6 (vii)], the percentage conversion of complex **24** was very minute (1.97 %) relative to **24** (and the other complexes in this study) in the absence of DABCO. The low percentage conversion values in the presence of DABCO suggest that singlet oxygen is the most active species in the photo-transformation of cyclohexene. On the other hand, the slight conversion of cyclohexene in the presence of DABCO implies that it is not only singlet oxygen that is involved; there is a likelihood of involvement of other reactive oxygen species.

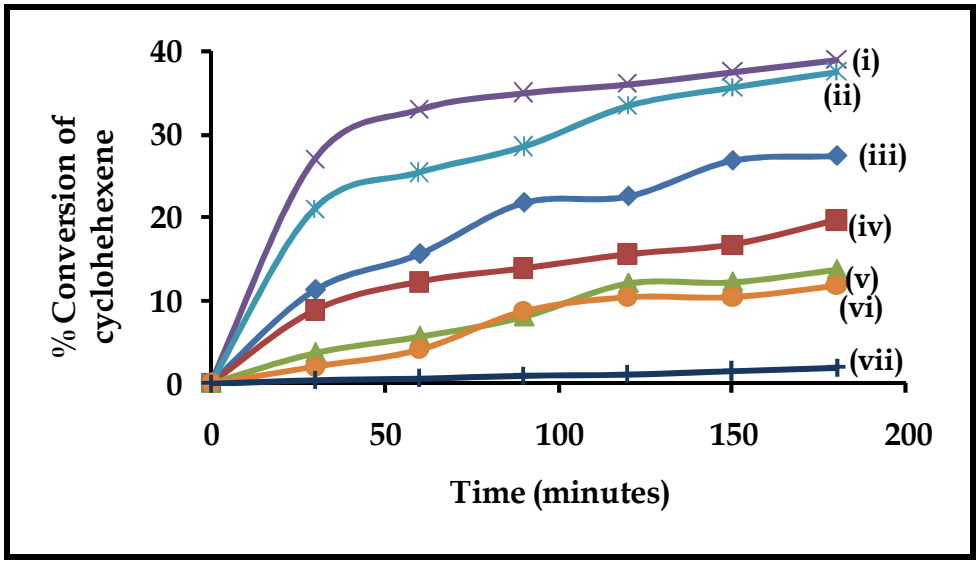

Figure 4.6: Plots of percentage conversion plots of cyclohexene over a period of 180 minutes for tetrasubstituted TiPc and TaPc complexes, where (i) is 24-AuNPs, (ii) 25-AuNPs, (iii) 24, (iv) 25, (v) 28, (vi) 28-AuNPs and (vii) 24 in the presence of DABCO in toluene. [24] = 3.1 x 10^{-5} mol L^{-1} or [25] = 4.30 x 10^{-5} mol L^{-1}, or [28] = 4.82 x 10^{-5} mol L^{-1}, [cyclohexene] = 4.06 x 10^{-2}. DABCO = 0.0029 g/mL. Irradiation was at the Q band.

Fig. 4.7 shows the variation of the percentage conversion over a period of 180 minutes for octasubstituted TaPc complexes (**29a** and **29b**). There is a fast increase in percentage conversion until ~ 50 min, after that there is slow or no increase. Complexes **29a**-AuNPs and **29b**-AuNPs gave the highest conversions at all times compared to complexes **29a** and **29b** in the absence of AuNPs. The reaction was also carried out in the presence of DABCO, Fig 4.7(v), it was added until there was no change in the GC trace of cyclohexene. The percentage conversion for complex **29a** after 180 minutes in the presence of DABCO was ~ 3.5 % - this is small compared to complexes **29a** and **29b** and their conjugates in the absence of DABCO. The low percentage conversion in the presence of DABCO again illustrates that singlet oxygen is the main agent involved in the photocatalytic oxidation of cyclohexene.

However, the fact that there is a slight conversion of cyclohexene in the presence of DABCO suggests that it is not only singlet oxygen that is involved; there is a possibility of involvement of other reactive oxygen species. To prove that other radicals were involved, photolysis of cyclohexene in the presence of benzoquinone (free radical scavenger) was carried out. A decrease of the conversion of less than 1% was observed illustrating that free radicals were involved.

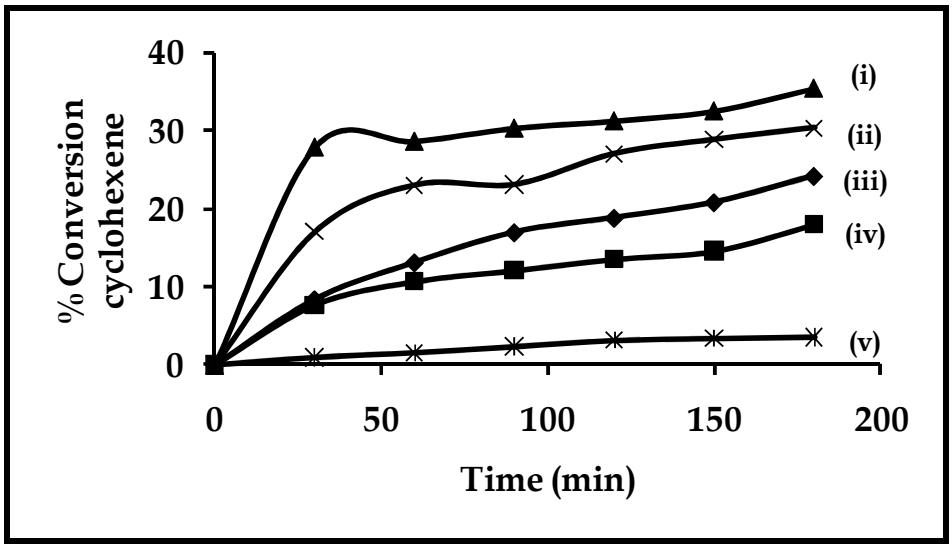

Figure 4.7: Plots of percentage conversion plots of cyclohexene over a period of 180 minutes for octasubstituted TaPc complexes, where (i) is 29a-AuNPs, (ii) 29b-AuNPs, (iii) 29a, (iv) 29b and (v) 29a in the presence of DABCO in toluene. Using Q band irradiation; [29a] = 2.80 x 10^{-5} mol L^{-1} or [29b] = = 5.60 x 10^{-5} mol L^{-1}, [cyclohexene] = 4.06 x 10^{-2}. DABCO = 0.0029 g/mL. Irradiation was at the Q band.

The percentage conversion values for catalytic reactions exposed to white light were high, Table 4.5. The values were 48.1 %, 45.2 %, 92.3 % and 90.0 % for **29a**, **29b**, **29a**-AuNPs and **29b**-AuNPs, respectively.

4.3.2. Fate of the catalyst

The percentage conversion values were notably higher for white light compared to Q band irradiation, however the complexes underwent considerable bleaching during catalysis {Fig. 4.8(a)} in the photocatalytic experiments involving white light. Less bleaching was observed on irradiation at the Q band, Fig. 4.8(b). In the presence of AuNPs using white light (or Q band irradiation), the degradation of the TaPc derivatives was similar to that observed in Figs. 4.8(a) or 4.8(b), respectively. The alkyl substituents on the TaPc complexes are electron-donating and are prone to oxidative attack due to the increased electron density. Furthermore, the complexes conjugated with the AuNPs are prone to degradation as a result of increased singlet oxygen.

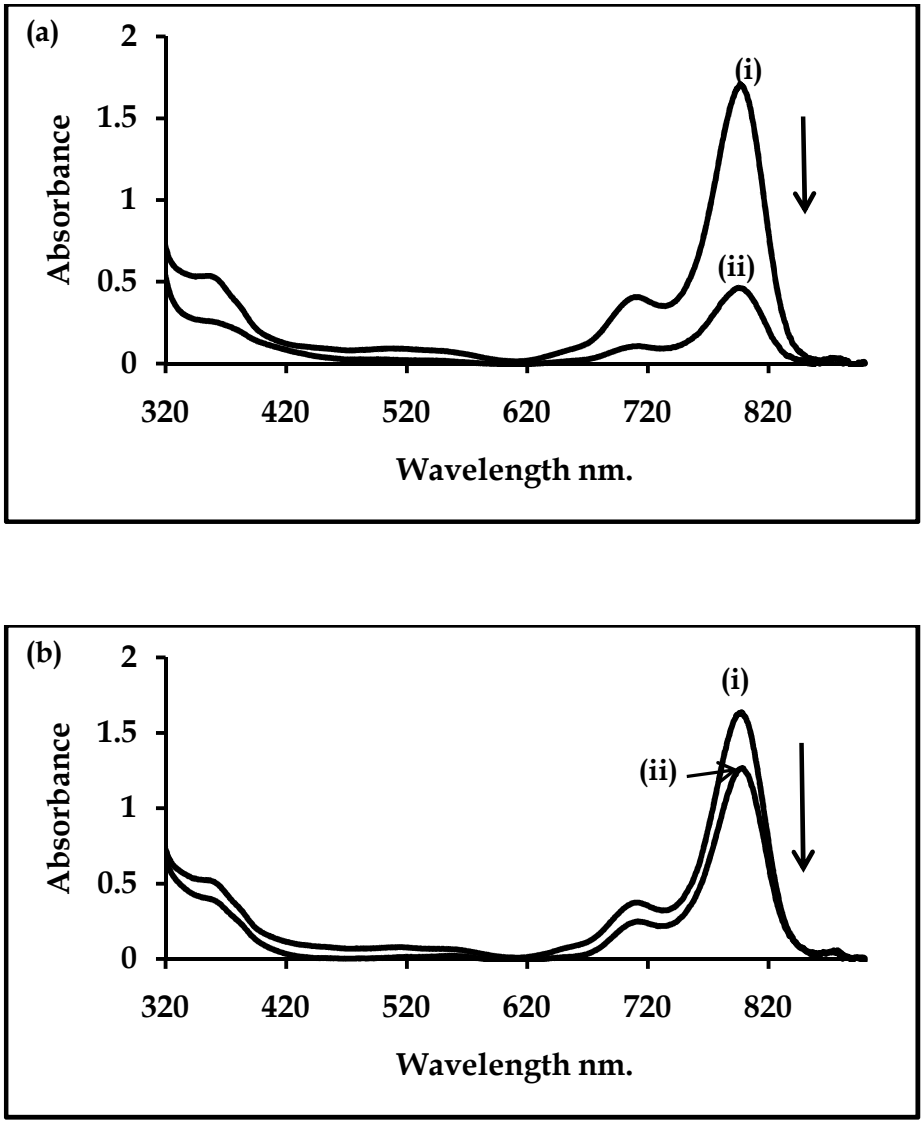

Figure 4.8: Spectral changes observed for complex 29a during the photocatalytic transformation of cyclohexene under (a) white light irradiation and (b) Q band irradiation. Irradiation over 180 min. (i) before and (ii) after photolysis

However, in the presence of DABCO, Fig. 4.9 (ii), photobleaching of the MPc complexes was minimal, compared to that without DABCO {Fig. 4.9 (iii)} showing the involvement of singlet oxygen in the photocatalytic oxidation.

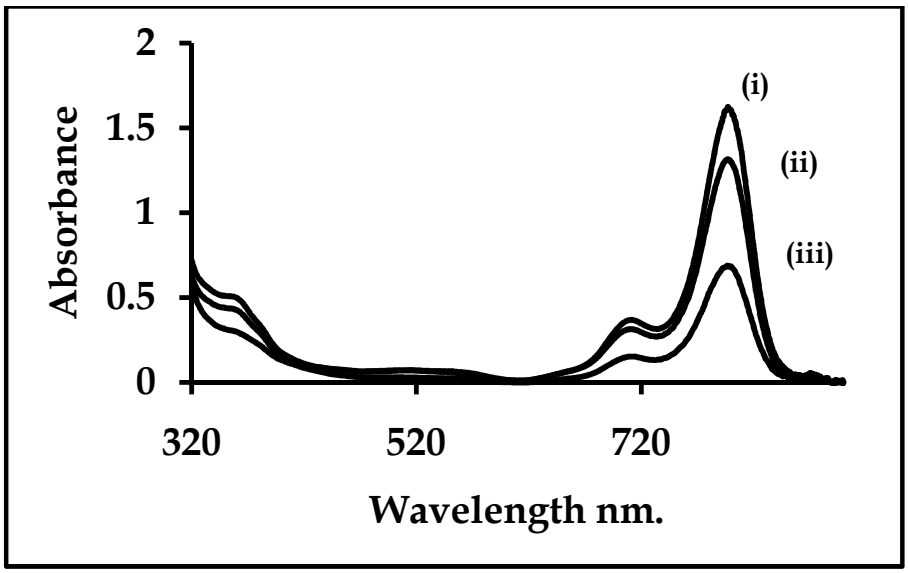

Figure 4.9: Electronic absorption spectra for 29b (i) before photoirradiation, (ii) after 180 minutes in the presence of DABCO and (iii) after 180 minutes in the absence of DABCO [29b] = 5.6 x 10^{-5} mol L^{-1}. [DABCO] = 0.0029 g/mL. Q band irradiation. Solvent = toluene.

Photobleaching was also experienced during catalysis by the rest of the phthalocyanines employed for cyclohexene photooxidation Figs. 4.10(a) – (d). The TaPc complex (**28**), Fig 4.10(a) alone and in the presence of AuNPs did not experience extreme photobleaching (due to small Φ_Δ values) compared to complexes **24** and **25** and their AuNPs conjugates and the other TaPc complexes (**29a** and **29b**). Complex **24**, Fig. 4.10(b), did not experience drastic (~ 50 %) bleaching compared to its corresponding AuNP conjugate (**24**-AuNPs) as can be seen in Fig. 4.10(c). Complex **24**-AuNPs was decreased by up to ~ 72 % from the original absorbance. This supplements and further reiterates the involvement of singlet oxygen in the photo-transformation of cyclohexene and the photodegradation of MPcs as singlet oxygen quatum yield values were increased on introducing AuNPs for all complexes except **28**. Similarly, complex **25**-AuNPs, Fig. 4.10(d), showed drastic photobleaching of up to ~ 80 %. In the presence of DABCO (figure not shown) photobleaching of the

MPc complexes was minimal again illustrating the involvement of singlet oxygen in the photo-oxidation reactions.

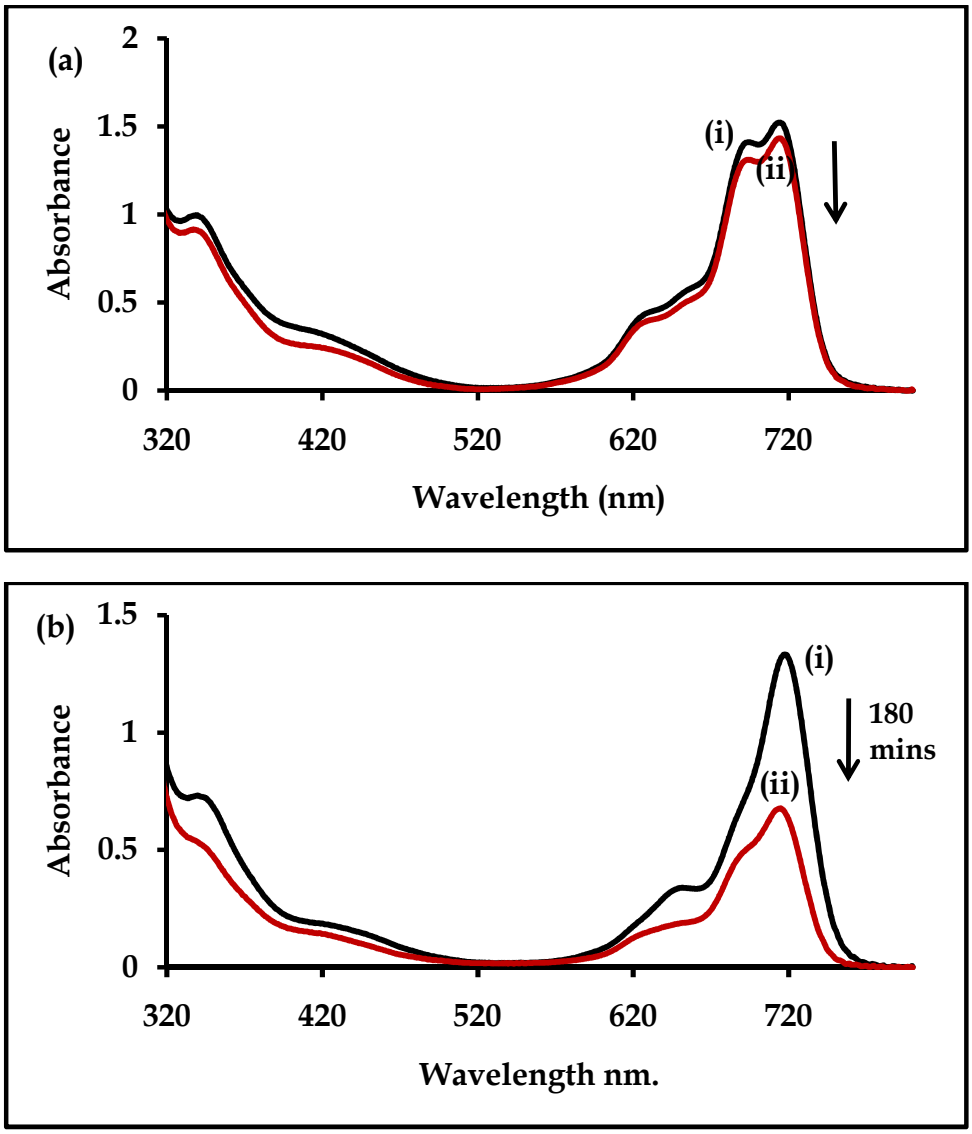

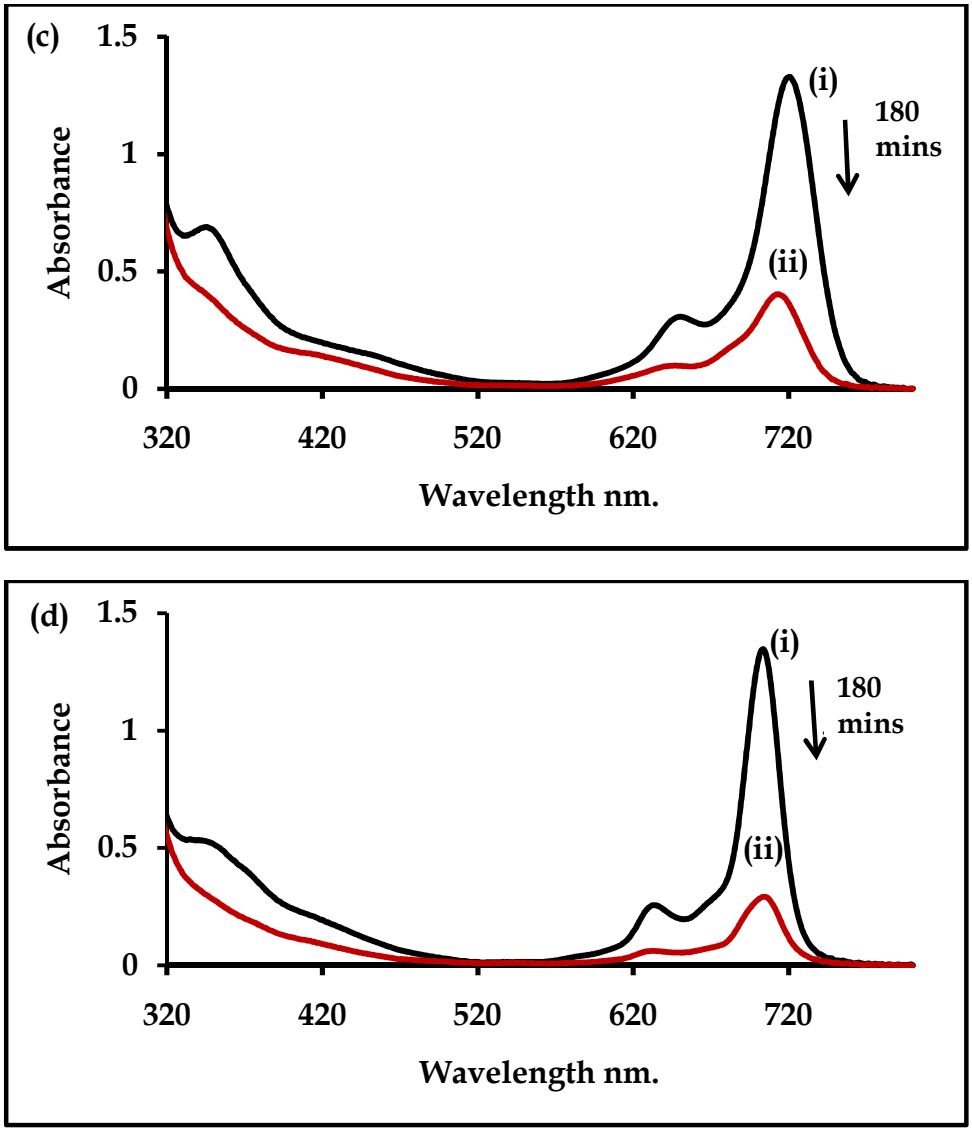

Figure 4.10: Spectral changes observed for complex (a) 28, (b) 24, (c) 24-AuNPs and (d) 25-AuNPs during the photocatalytic transformation of cyclohexene. Irradiation over 180 min at the Q band. (i) before and (ii) after photolysis.

4.3.3. Product yields

4.3.3.1. Octasubstituted TaPc derivatives

Table 4.6 shows the product yields obtained for TaPc derivatives that were exposed to both white light and filtered light, (Q band irradiation) in the abscence and presence AuNPs after 180 minutes of irradiation.

Table 4.6: Percentage selectivity values for cyclohexene photocatalytic products. Photolysis time = 180 min

MPc	Product	Q band irradiation	White light	Product yields under Q band irradiation (%)[b]
		% Selectivity[a]	% Selectivity[a]	
29a	**Cyclohexene oxide**	17.9	27.8	6.3
	2-Cyclohexen-1-ol	35.1	40.5	9.15
	2-Cyclohexene-1-one	26.2	38.0	8.6
	1,2-Cyclohexanediol	40.8	86.0	21.2
29b	**Cyclohexene oxide**	27.3	30.2	6.8
	2-Cyclohexen-1-ol	38.3	39.9	9.1
	2-Cyclohexene-1-one	35.1	52.2	11.8
	1,2-Cyclohexanediol	33.4	60.3	13.7
29a-AuNP	**Cyclohexene oxide**	46.0	50.8	11.5
	2-Cyclohexen-1-ol	20.4	29.8	6.7
	2-Cyclohexene-1-one	23.0	37.7	8.6
	1,2-Cyclohexanediol	30.1	34.0	7.7
29b-AuNP	**Cyclohexene oxide**	38.1	42.4	9.7
	2-Cyclohexen-1-ol	29.1	30.3	7.0
	2-Cyclohexene-1-one	27.3	77.3	17.5
	1,2-Cyclohexanediol	26.7	30.6	6.9

[a] $\% \text{ selectivity} = \text{epoxide}_{\text{obtained}} / [(1 - \text{cyclohexene}_{\text{initial}}) - (1 - \text{cyclohexene}_{\text{final}})]$

[b] based on the substrate cyclohexene.

The yields for the main products ranged from 6.3 to 21.2 %, values which are higher than reported in literature [108], where the values of the similar products (cyclohexenone, cyclohexenol, cyclohexane diol, cyclohexene hydroperoxide and cyclohexene oxide) ranged from 0.02 to 4.4 % using ZnPc as a photocatalyst. Cyclohexene oxide has been reported as one of the minor products by Sehlotho and Nyokong [19] using ZnPc as a photocatalyst. In this work cyclohexene oxide is a major product in the presence of **29a**-AuNP.

4.3.3.2. Tetrasubstituted TiPc andTaPc derivatives

The product yields of complexes **24**, **25** and their AuNPs conjugates are listed in Table 4.7. The product yield values were somewhat notable; they were however generally smaller than yields for TaPc complexes containing long alkyl chains (**29a** and **29b,** Table 4.6) but were higher than reported in literature [19, 108]. The product yields ranged from 1.7 to 13.1 %. The main product for **25** and **25**-AuNP with the largest Φ_Δ values is cyclohexene oxide. While for **28** and **28**-AuNP, with very low Φ_Δ values, the main product is cyclohexenediol. This suggests that the amount of singlet oxygen present, determines the yield of the products formed.

Table 4.7: Percentage selectivity values for cyclohexene photocatalytic products. Photolysis time = 180 min at the Q band.

MPc	Product	% Selectivity[a]	Product yields (%)[b]
24	Cyclohexene oxide 2-Cyclohexen-1-ol 2-Cyclohexene-1-one 1,2-Cyclohexanediol	28.4 22.9 17.0 4.3	5.7 6.6 5.1 1.7
25	Cyclohexene oxide 2-Cyclohexen-1-ol 2-Cyclohexene-1-one 1,2-Cyclohexanediol	32.4 24.4 26.2 2.8	6.8 9.1 11.8 13.7
28	Cyclohexene oxide 2-Cyclohexen-1-ol 2-Cyclohexene-1-one 1,2-Cyclohexanediol	12.3 11.6 9.7 24.5	5.8 5.9 5.6 9.6
24-AuNP	Cyclohexene oxide 2-Cyclohexen-1-ol 2-Cyclohexene-1-one 1,2-Cyclohexanediol	40.3 26.3 26.8 7.2	12.3 6.9 7.1 2.6
25-AuNP	Cyclohexene oxide 2-Cyclohexen-1-ol 2-Cyclohexene-1-one 1,2-Cyclohexanediol	36.9 28.9 29.1 8.6	7.3 5.6 13.1 2.3
28-AuNP	Cyclohexene oxide 2-Cyclohexen-1-ol 2-Cyclohexene-1-one 1,2-Cyclohexanediol	12.9 8.6 7.2 17.6	4.2 3.1 3.3 9.6

[a] $\%\ \text{selectivity} = \text{epoxide}_{\text{obtained}} / [(1 - \text{cyclohexene}_{\text{initial}}) - (1 - \text{cyclohexene}_{\text{final}})]$

[b] **based on the substrate cyclohexene.**

4.3.4. Percentage selectivity

4.3.4.1. Octasubstituted TaPc complexes (29a and 29b)

Table 4.6 also shows percentage selectivity for the main products formed during the photocatalytic oxidation of cyclohexene under Q band and white light irradiations. Generally percentage selectivity values increased under white light experiments; however photobleaching of the MPc was a major drawback as discussed above. Alcohol is one of the desired products derived from oxidation of alkenes in the petrochemical industry. The percentage selectivity values for cyclohexenol (35.1 and 38.3 %, for complexes **29a** and **29b**, respectively) under Q band irradiation, are higher than those reported for the photochemical oxidation of cyclohexene using sulfonated MPc (M = Pd, Al and Zn) [108], where percentage selectivity values ranged from 1.6 to 34.9% in the solvents: dimethylformamide:H_2O, dioxane:H_2O and acetonitrile. Figs. 4.11 and 4.12 show the percentage selectivity values variations over a period of 180 minutes for complexes **29a** and **29a**-AuNPs, respectively at the Q band irradiation.

The transformation of cyclohexene, as shown in Figs. 4.11 and 4.12, was marked by a sweeping increase in selectivity of products of products for the first 30 minutes, followed by slowing down until photolysis was stopped at 180 minutes.

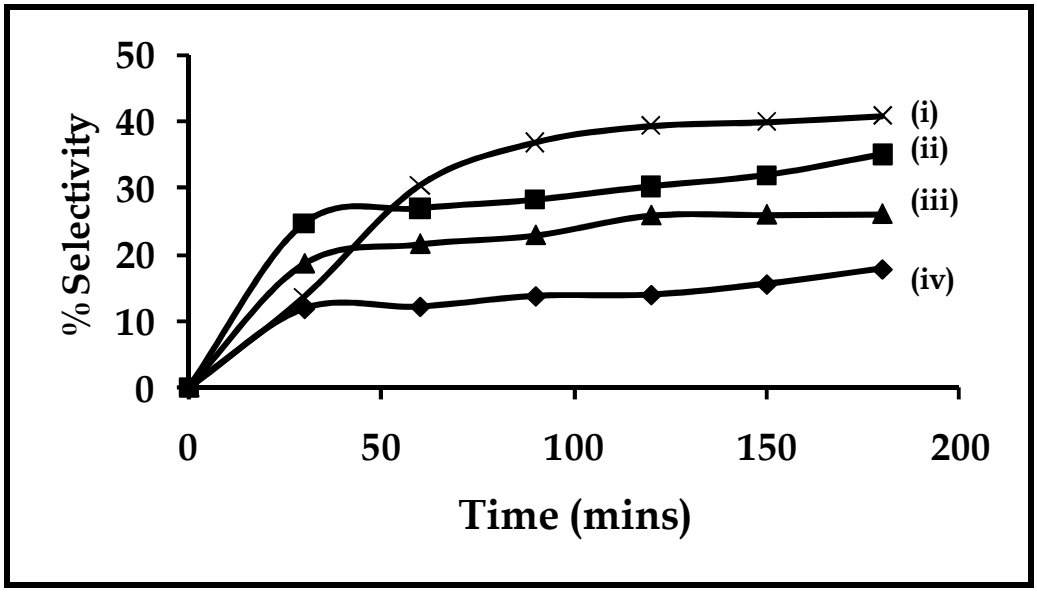

Figure 4.11: Percentage selectivity plots of cyclohexene products in toluene using complex 29a where (i) is 1,2 – cyclohexanedione, (ii) 2-cyclohexen-1-ol, (iii) 2-cyclohenene-1-one and (iv) cyclohexene oxide. [29a] = 2.80 x 10^{-5} mol L^{-1}. Irradiation was at the Q band.

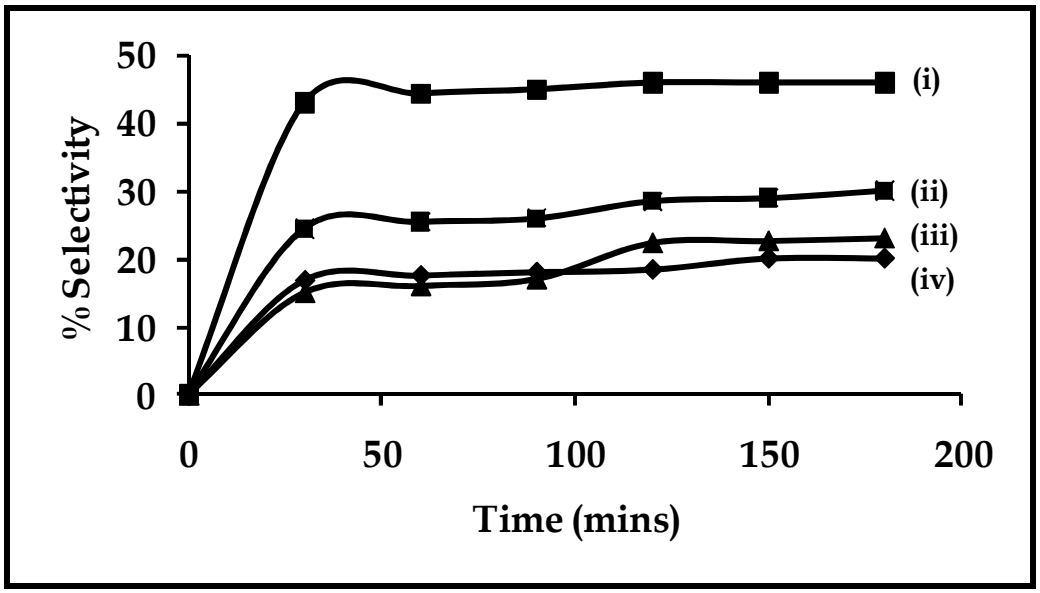

Figure 4.12: Percentage selectivity plots of cyclohexene products in toluene using complex 29a-AuNPs where (i) is cyclohexene oxide, (ii) 2-cyclohexen-1-ol, (iii) 2-cyclohenene-1-one and (iv) 1,2-cyclohexanedione. Irradiation was at the Q band.

4.3.4.2. Tetrasubstituted TiPc and TaPc complexes (25, 26 and **28)**

The highest percentage selectivity value in Table 4.7 is for cyclohexene oxide for complexes **24** and **25** and their corresponding AuNPs conjugates. The percentage selectivity values increased from 28.4 and 32.4 % for **24** and **25**, respectively, to 40.3 and 36.9 % for **24**-AuNPs and **25**-AuNPs, respectively. The highest selectivity for complex **28** was for 1,2-cyclohexanediol. The values were 24.5 % for **28** and 17.6 % for **28**-AuNP, again showing a decrease for complex **28** as opposed to an increase for all MPc-AuNPs. As already mentioned, the percentage selectivity values for cyclohexenol were also impressive for complexes **24** and **25**. Alcohol is one of the desired products derived from oxidation of alkenes in the petrochemical industry. The values for cyclohexenol were 22.9 % and 24.4 %, for complexes **24** and **26**, respectively and for complex **28** a low value of 11.6 % was obtained. Fig. 4.13 shows the percentage selectivity values over a period of 180 minutes for complexes **25**, **25**-AuNPs and **28**, respectively. The cyclohexene photo-transformation products, as shown in Figs. 4.13 was marked by a drastic increase in percentage selectivity for the first 30 minutes, followed by slowing down until photolysis was stopped at 180 minutes. For complex **24**, at 90 minutes, a drastic increase of 1,2 cyclohexanediol followed by its low production until 180 minutes was observed. The same was observed for complex **25**-AuNPs where 1,2-cyclohexanediol increased sharply after 120 minutes.

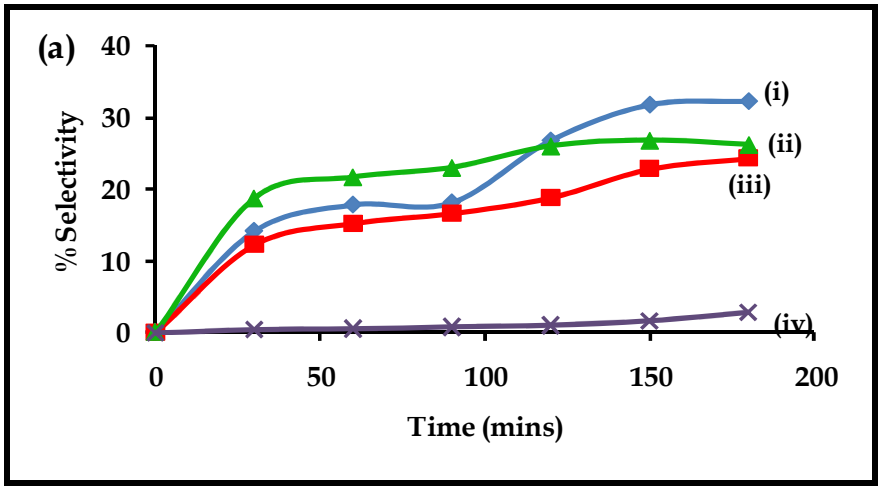

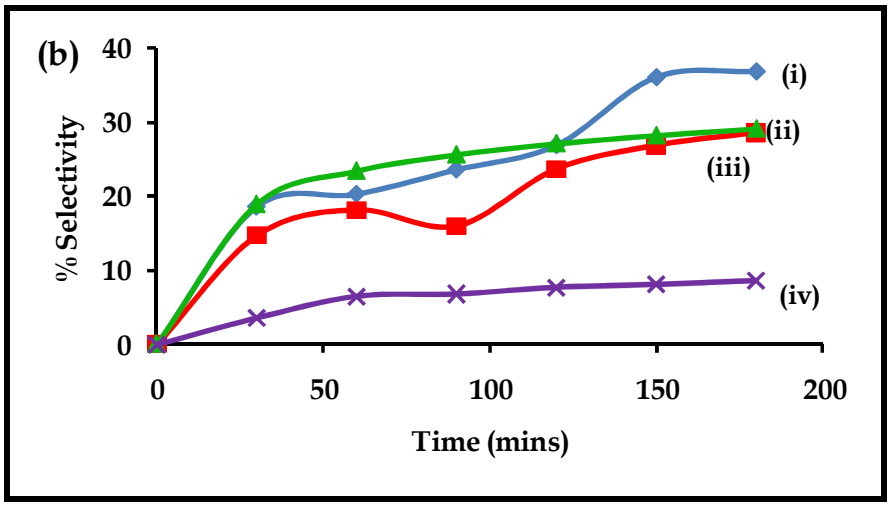

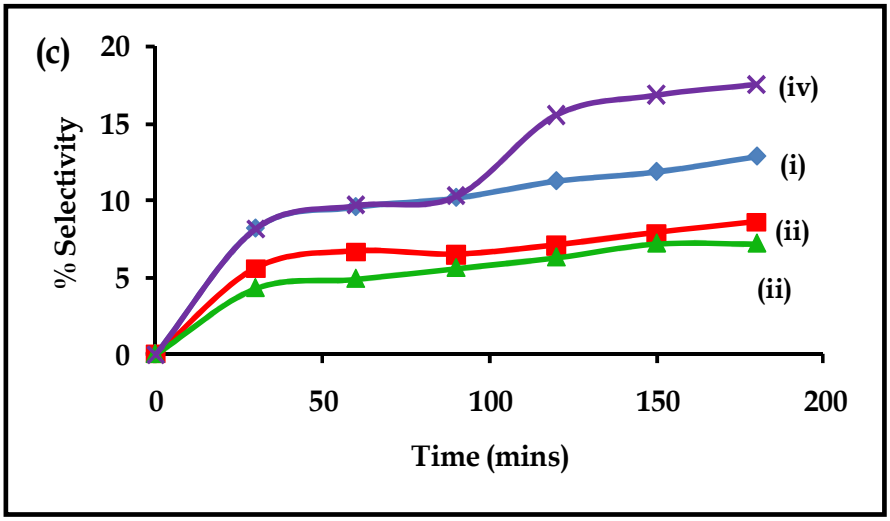

Figure 4.13: Percentage selectivity plots of cyclohexene products in toluene using complex (a) 24, (b) 25- AuNPs and (c) 28-AuNPs; where (i) is 1,2 – cyclohexanediol, (ii) 2-cyclohexen-1-ol, (iii) 2-cyclohenene-1-one and (iv) cyclohexene oxide. [24] = 4.30 x 10^{-5} mol L^{-1}. [25] = 4.30 x 10^{-5} mol L^{-1}. [28] = 4.82 x 10^{-5} mol L^{-1}. Irradiation was at the Q band.

In literature, two major pathways are suggested for the sensitisation reactions by phthalocyanines. One is the energy transfer from an electronically excited complex to ground state molecular oxygen that subsequently yields singlet oxygen (**Scheme 1.5**). Another is the electron transfer from the excited complex to ground state molecular oxygen or reacting substrates thereby generating radicals such as superoxide radicals, Type I mechanism. As stated above, the percentage conversion of cyclohexene was slowed down in the presence of DABCO, Figs. 4.6 and 4.7, implying that singlet oxygen played a major role in photocatalytic oxidation. The mechanism proposed in this work is shown in **Scheme 4.1** and is similar to that proposed by Sehlotho *et al.* [19]. Several reports [217 - 220] have shown that zwitterions, biradicals, endo-peroxides, peroxiranes are formed when ethylene interacts with singlet oxygen, hence the proposed mechanism in **Scheme 4.1**.

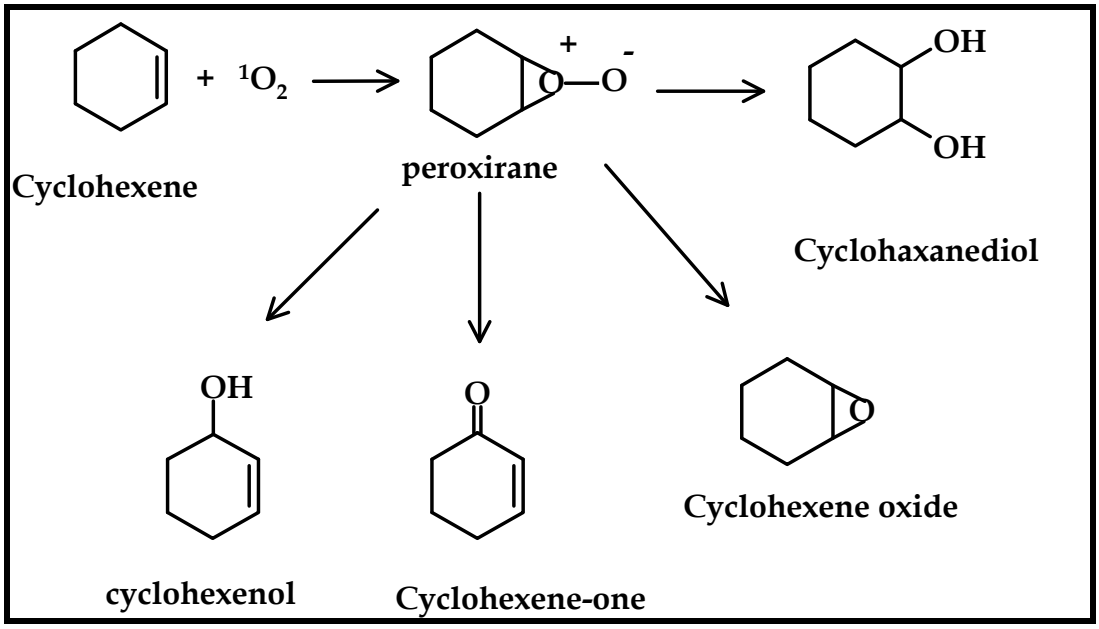

Scheme 4.1: Proposed mechanism for the formation of the photooxidation products.

4.4. Conclusion

The stability of the newly synthesised MPcs complexes and MPc-AuNPs has been studied. The complexes were more stable under Q band irradiation. The singlet oxygen production was improved significantly by the presence of AuNPs and this was attributed to the good triplet quantum yields. Photocatalytic oxidation of cyclohexene was carried out successfully. The percentage conversion of cyclohexene was improved by the presence of gold nanoparticles. Percentage selectivity values were generally improved when compared to literature values; however photobleaching was experienced during the photocatalytic conversion of cyclohexene. The percentage yields for products were improved significantly compared to literature.

Chapter 5: Electrochemical characterisation

In this chapter the electrochemical characterisation of the newly synthesised MPc complexes (Figs. 1.4 and 1.5 and **Schemes 3.1** and **3.2**) are discussed. These experiments were performed on a glassy carbon electrode (GCE) in order to compare with the reported data on phthalocyanines. GCE was chosen due to its wide range usable potential.

5.1. Titanium phthalocyanines.

Cyclic (CV) and square wave (SWV) voltammograms for complexes (**24** to **25**) are shown in Figs. 5.1 and 5.2. Fig. 5.1(a) and (b) show the SWV and CV for complex **24**. The CV shows two reduction processes labelled **II** and **III** and a split irreversible oxidation process labelled **I** at half-wave ($E_{1/2}$) potentials of -0.46, -0.85 and 0.78V (E_p) vs Ag|AgCl, respectively, Table 5.1. The anodic to cathodic current ratio (I_{pa}/I_{pc}) was near unity for the two reduction couples. The couples were reversible with cathodic and anodic peak separations (ΔE) of 84 and 97 mV for couples **II** and **III**, respectively (when compared to ferrocene standard with ΔE = 70 mV)). Couple **I** was assigned to ring oxidation, proven by spectroelectrochemistry below. The split nature of couple **I** could be due to aggregation at the concentrations used for cyclic voltammetry [221]. The pyridine groups encourage oxidation due to their electron donating nature hence oxidation is observed in **24,** while oxidation was not observed for α-OTiPc$(SPh)_4$ and β-OTiPc$(SPh)_4$ [70], Table 5.1. This makes the pyridine ligand to be useful for applications which require ease of oxidation as is the case in electrocatalytic oxidations.

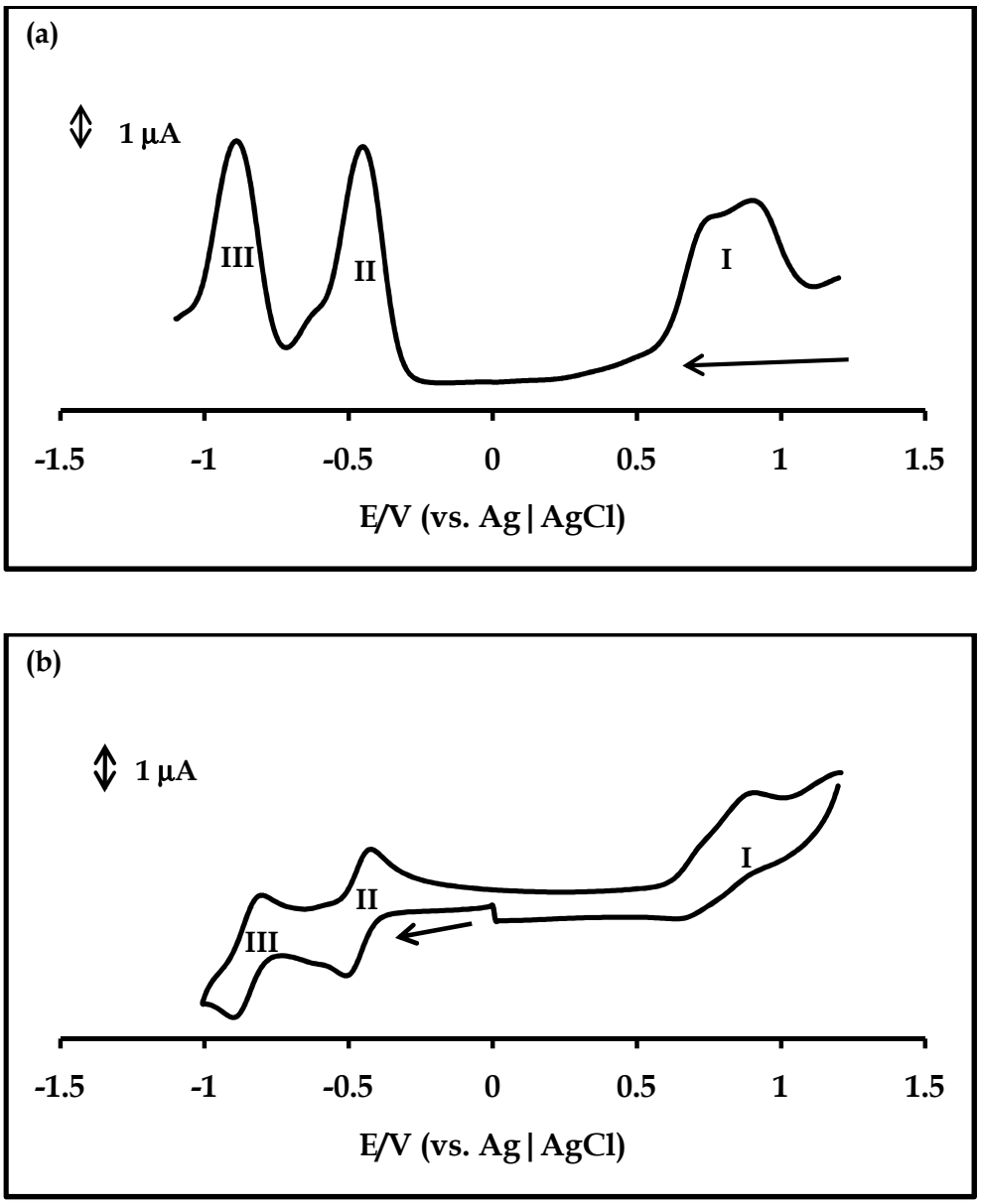

Figure 5.1: Square wave (a) and cyclic (b) voltammograms for complex 24 in DMF containing 0.1 M $TBABF_4$. Scan rate = 100 mV/s.

Similarly, the corresponding TiPc complex (**25**), Fig. 5.2, with susbtituents in the peripheral positions exhibits two reduction processes (**II** and **III**) and one oxidation process labelled **I**. These were observed at half-wave ($E_{1/2}$) potentials of -0.40, -0.74 and 0.75 V (E_p) vs Ag|AgCl for processes **II**, **III** and **I**, respectively, Fig. 5.2 and Table 5.1. Reduction couples **II** and **III** were quasi reversible in that ΔE was 112 mV

for both. For all the reduction couples for the TiPc derivatives, plots of peak currents (i_p) versus the square root of scan rate ($v^{1/2}$) were linear suggesting that the processes were diffusion controlled.

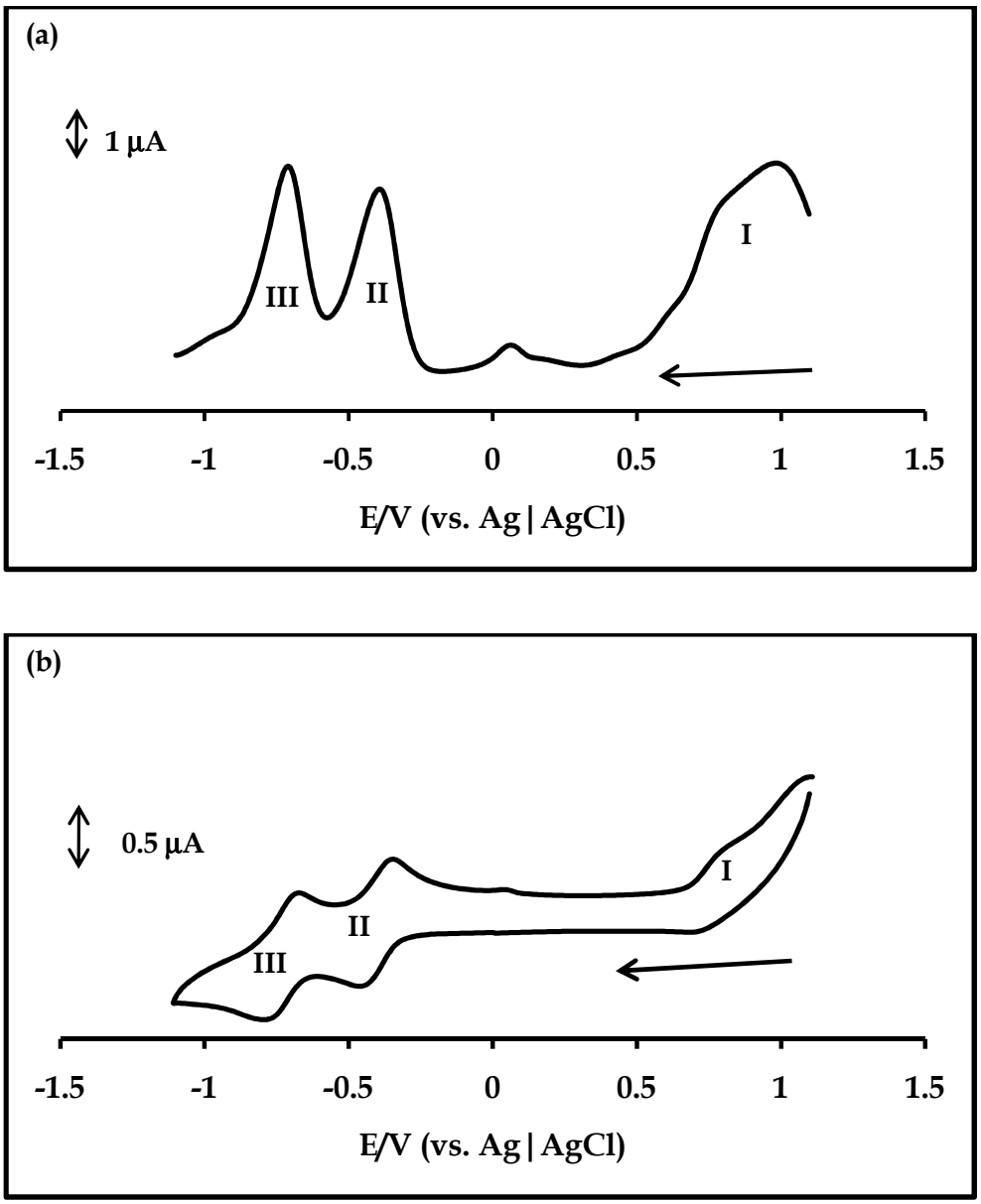

Figure 5.2: Square wave (a) and cyclic (b) voltammograms for complex 25 in DMF containing 0.1 M $TBABF_4$. Scan rate = 100 mV/s.

Pyridine groups seemingly make reduction more difficult hence more negative $E_{1/2}$ values for $Ti^{IV}Pc^{-2}/Ti^{III}Pc^{-2}$ and $Ti^{III}Pc^{-2}/Ti^{III}Pc^{-3}$ compared to the phenyl groups in

Table 5.1; oxidation is easier because of the electron donating nature of N hence observed in Table 5.1. The non peripherally substituted TiPc complexes {**24,** β-OTiPc(SPh)$_4$} are more difficult to reduce than the peripherally substituted complexes {**25**, β-OTiPc(SPh)$_4$}; this is as a result of the increased electron cloud around the phthalocyanine complex caused by the electron donating substituents on the non-peripheral position closest to the Pc ring compared to substituents on the peripheral position.

Table 5.1: List of redox potentials of TiPc complexes studied in this work in dimethly formamide (DMF) using tetrabutyl ammonium tetrafluoroborate (TBABF$_4$) half-wave potential (E$_{1/2}$) as V vs. Ag|AgCl.

MPc	**III**	**II**	**I**
	$Ti^{III}Pc^{-2}$/ $Ti^{III}Pc^{-3}$	**$Ti^{IV}Pc^{-2}$/ $Ti^{III}Pc^{-2}$**	**$Ti^{IV}Pc^{-2}$/ $Ti^{IV}Pc^{-1}$**
24	-0.85	-0.46	0.78
25	-0.74	-0.40	0.75
α-OTiPc(SPh)$_4$ [70]	-0.46	-0.07	No oxidation
β-OTiPc(SPh)$_4$ [70]	-0.37	-0.07	No oxidation

In order to further determine the nature of the redox processes for all the new complexes in this work, spectroelectrochemistry was performed on an optically transparent thin layer electrochemical (OTTLE) cell. The β (peripheral, **25**) and their corresponding α (non-periphera, **24**) substituted complexes showed similar behaviour, thus only one set of spectral changes for each set of complexes is discussed. Fig 5.3 (a) shows the spectral changes for complex **24** at potentials more

negative of processes **II** for **24** and **25** (-0.46 or -0.40V vs Ag|AgCl) in DMF containing $TBABF_4$. The first spectrum shows aggregation at the concentrations used for the OTTLE cell. On reduction, the spectral changes that were observed include a shift of the Q band from 716 to 691 nm, accompanied with disaggregation of the TiPc complex (**24**) with an increase in the intensity of the Q band, a change of colour of the solution in the OTTLE cell from green to a blue occurred, Fig. 5.3(a). The isosbestic points were not too defined, due to aggregation and also due to the possibility of exchange of axial ligands (with the electrolyte) on reduction. The spectral changes observed in Fig. 5.3(a) are typically associated to central metal redox processes [13], as judged by the shift in Q band without a drastic decrease in intensity. The n value calculated for both complexes **24** and **25** was approximately ~1 using Equation 5.1:

$$Q = nFCV \qquad (5.1)$$

where n is the number of electrons involved; *F*, Faraday's constant; *C*, solution concentration and *V*, volume of the solution.

It was deduced from the above discussion that, process **II** is the reduction $Ti^{IV}Pc^{-2}$ to $Ti^{III}Pc^{-2}$. Further reduction at more negative potentials of process **III** (-0.85 or -0.74 V vs Ag|AgCl, for **24** or **25**, respectively) was undertaken. A decrease in the intensity (without shifting in position) of the Q band and the appearance of new peaks between 500 and 600 nm together with a clear isosbestic points at 649 and 448 nm were noticed, Fig 5.3(b). Typically, these changes are associated with ring reduction processes [222], associated with reduction of $Ti^{III}Pc^{-2}$ to $Ti^{III}Pc^{-3}$ as observed in

literature [70, 72]. The regeneration (to 78 %) of the initial species was achieved, confirming the reversibility of the couples and ~ 1 electron was transfered using Equation 5.1. Application of the potentials more positive of process **I**, resulted in spectral changes shown in Fig. 5.3(c) consisting of a decrease in the Q band with no new peaks being formed indicative of the degradation of the complex confirming irreversibility of the oxidation processes. However the oxidation peaks are attributed to the Pc ring and the substituents, since no oxidation is expected on the central metal. Process **I** is assigned to ring oxidation, where the assignment is $Ti^{IV}Pc^{-2}/Ti^{IV}Pc^{-1}$, Fig. 5.3(c), Table 5.1.

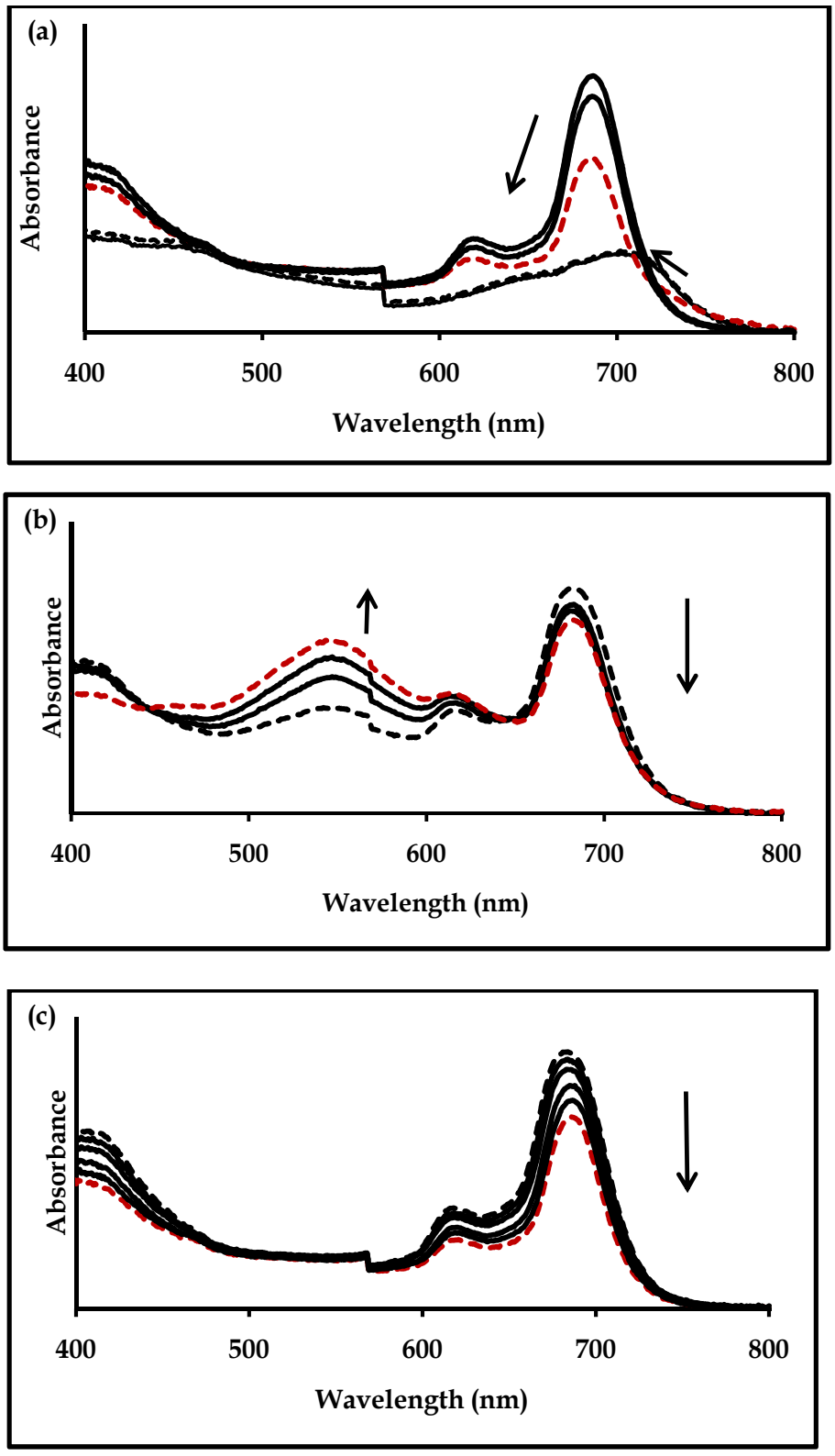

Figure 5.3: Observed UV/Vis spectral changes for complex 24 at potentials (a) -0.5 V (process II), (b) -0.9 V (process III) and (c) 0.8 V (process I), in DMF with 0.1 M $TBABF_4$.

Based on the electrochemical observations described above, for both TiPc complexes (**24** and **25**), the assignments for processes **I – III** are as follows:

$Ti^{IV}Pc^{-2} \rightarrow Ti^{IV}Pc^{-1} + e^-$ (Process **I**)

$Ti^{IV}Pc^{-2} + e^- \rightarrow Ti^{III}Pc^{-2}$ (Process **II**)

$Ti^{III}Pc^{-2} + e^- \rightarrow Ti^{III}Pc^{-3}$ (Process **III**)

5.2. Vanadium phthalocyanines

Similar to titanium complexes, the electrochemistry of vanadium complexes has not received a lot of attention. There have been few reports [67, 115, 116] and this work further explores their electrochemistry. Fig. 5.4(a) and (b) show the CV and SWV for complexes **27** (representative of both **26** and **27**). There are two main reduction processes labelled **II** and **III** and one oxidation process (**I**). The broadness in process **II** is attributed to aggregation. The couples were observed at half-wave ($E_{1/2}$) potentials of -0.24, -0.58 and 0.99V (for **27**) and at -0.36, -0.82 V and 1.11 vs Ag|AgCl (for **26**), Table 5.2, for processes **II**, **III** and **I**, respectively. Process **III** was reversible {ΔE ~ 81 mV (**26**), and 93 mV (**27**)} and **II** quasi reversible {ΔE 127 mV (**26**) to 185 mV (**27**)}. The split nature of couple **II** is related to aggregation [221] tendencies of the Pc. For all the redox processes for the VPc complexes (**26** and **27**), plots of peak currents (i_p) versus the square root of scan rate ($v^{1/2}$) were linear signifying that the processes were diffusion controlled. Again the non-peripherally (**26**) substituted complex is more difficult to reduce than peripherally (**27**) substituted derivatives.

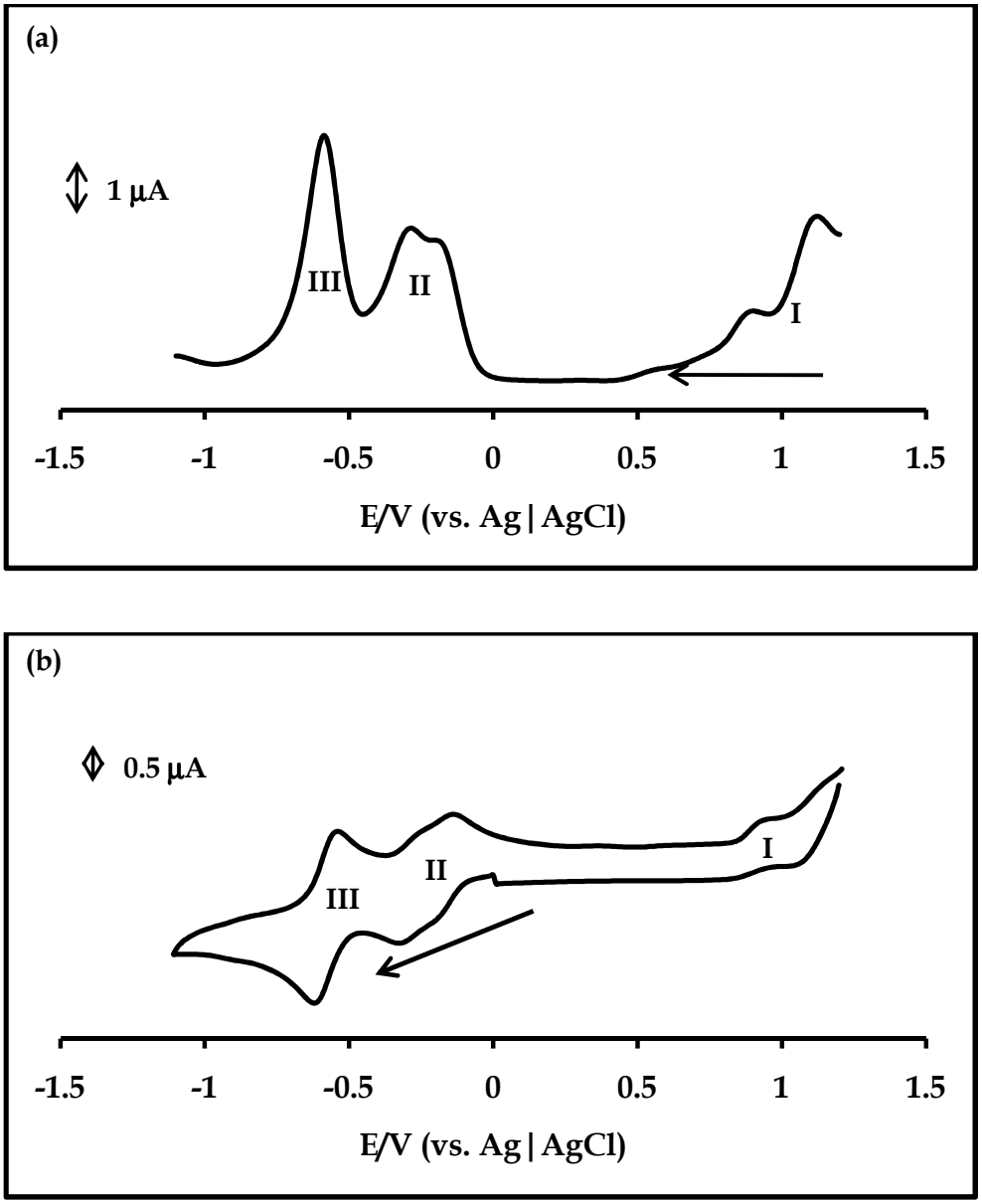

Figure 5.4: Square wave (a) and cyclic (b) voltammograms for complex 27 in DMF containing 0.1 M $TBABF_4$. Scan rate = 100 mV/s.

Table 5.2: List of redox potentials of VPc complexes studied in this work in dimethly formamide (DMF) using tetrabutyl ammonium tetrafluoroborate ($TBABF_4$) half-wave potential ($E_{1/2}$) as V vs. Ag|AgCl.

MPc	**III**	**II**	**I**
	$V^{IV}Pc^{-3}$/ $V^{IV}Pc^{-4}$	**$V^{IV}Pc^{-2}$/ $V^{IV}Pc^{-3}$**	**$V^{IV}Pc^{-2}$/ $V^{IV}Pc^{-1}$**
26	-0.82	-0.36	1.11
27	-0.58	-0.24	0.99

In the same way as TiPc complexes, spectroelectrochemical experiments were performed for the further investigation of the redox processes observed for OVPc complexes **26** and **27**. Fig. 5.5 shows the observed spectral changes for complex **27** (representing both **26** and **27**) at potentials more negative of process **II** (-0.36 V vs Ag|AgCl), Fig. 5.5(a). The spectral changes consist of a gradual decrease of the Q band, an emergence of news peak between 500 and 600 nm and a clear isosbetic point at 660 nm. The green colour of the solution changes to blue in the OTTLE cell. These spectral changes were very similar to those observed before for $OVPC(SC_6H_{13})_8$ and other VPc derivatives [67, 115], and these were attributed to ring reduction. Similarly in this work, the observed spectral changes for process **II** can be attributed to ring reduction: $V^{IV}Pc^{-2}$ to $V^{IV}Pc^{-3}$. Further reduction at potentials of process **III** (-0.82 V vs Ag|AgCl), Fig. 5.5(b), resulted in a further decrease in the intensity of the Q band and the appearance of new absorptions between 500 and 600 nm. This process shows further reduction to give $V^{IV}Pc^{-3}$ to $V^{IV}Pc^{-4}$. Oxidation is expected only on the ring for VPc complexes, hence process **I** is assigned to the formation of $V^{IV}Pc^{-1}$.

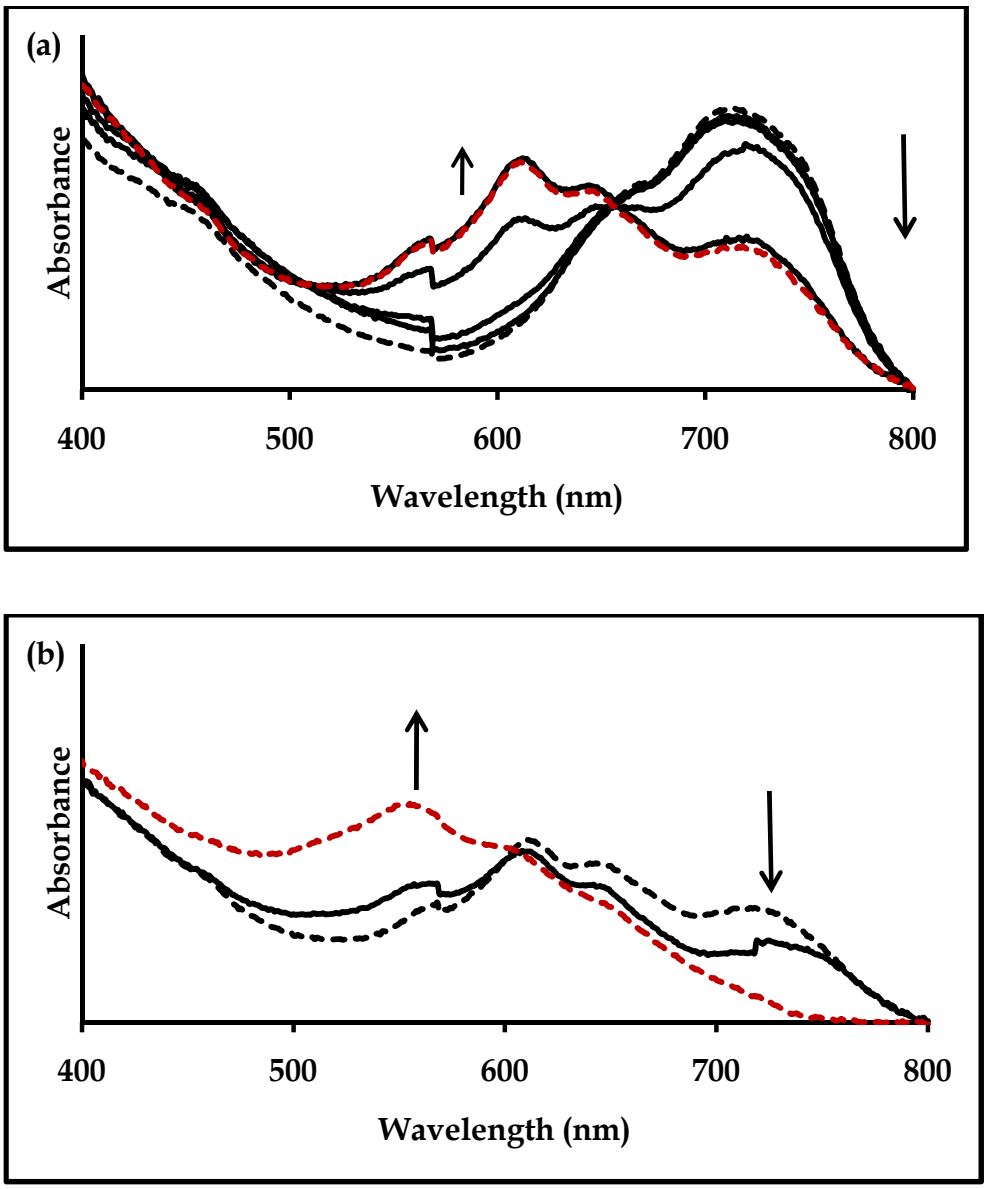

Figure 5.5: Observed UV/Vis spectral changes for complex 26 at potentials (a) -0.4 V (process II), (b) -0.9 V (process III) in DMF with 0.1 M $TBABF_4$.

Based on the electrochemical observations described above, for (**26** and **27**), the assignments for processes **I – III** for both complexes are as follows:

$V^{IV}Pc^{-2} \rightarrow V^{IV}Pc^{-1} + e^-$ (Process **I**)

$V^{IV}Pc^{-2} + e^- \rightarrow V^{IV}Pc^{-3}$ (Process **II**)

$V^{IV}Pc^{-3} + e^- \rightarrow V^{IV}Pc^{-4}$ (Process **III**)

5.3. Tantalum phthalocyanines

Tantalum phthalocyanines are rare and their scarcity stems from the difficulty in synthesising them due to the large tantalum metal which does not fit perfectly into the cavity of a Pc ring. Cyclic voltammogram experiments were performed in de-aerated DMF (for complex **28**) and DCM (for complexes **29a** and **29b**) with $TBABF_4$ as the supporting electrolyte. The oxidation of these complexes is expected to occur at the ring and this was confirmed by spectroelectrochemistry as discussed below. For unsubstituted TaPc complex no oxidation peaks were observed [65] due to the fact that Ta^V has a high oxidation state, which makes ring oxidation more difficult. The electro-rich alkylthio and mercaptopyridine substituents in this work resulted in the ease of oxidation of the ring, since these substituents enhance electron density on the ring thus making it easy for oxidation to occur. Hence oxidation peaks are observed, Table 5.3.

The CV of TaPc complex (**28**) is shown in Fig. 5.6 Reduction processes labelled **III** and **IV** at half-wave ($E_{1/2}$) potentials of -0.57 and -0.99 V vs Ag|AgCl, respectively were observed, Table 5.3. The numbering is designed for comparison with other TaPc derivatives in Table 5.3. The ΔE values of 84 and 90 mV for couples **III** and **IV** suggests reversibility. Process **I** is irreversible and is observed at 0.86 V.

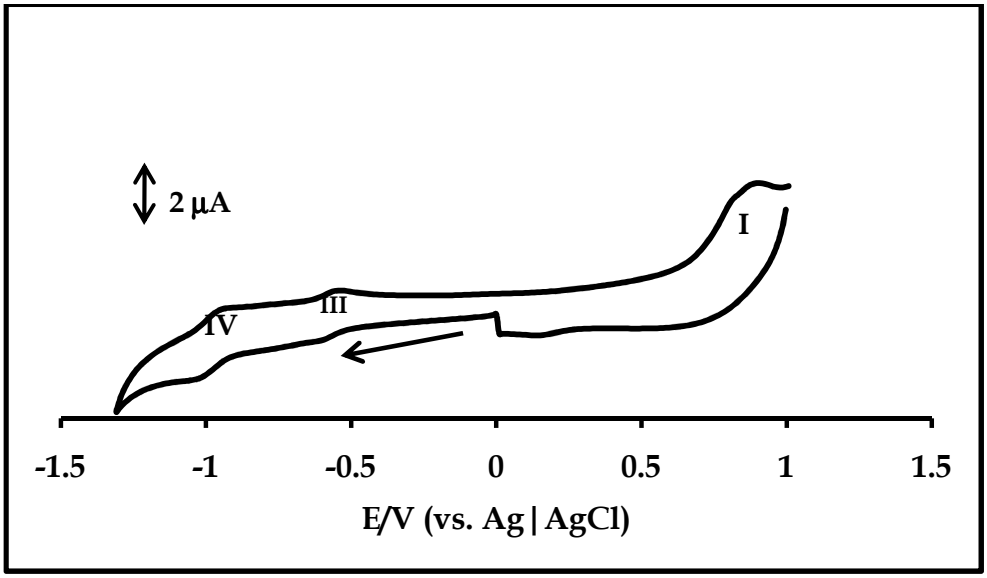

Figure 5.6: Cyclic voltammogram for complex 28 in DMF containing 0.1 M $TBABF_4$. Scan rate = 100 mV/s.

The cyclic [CV(a)] and square wave [SWV (b)] voltammetries for complexes **29a** and **29b** are shown in Figs. 5.7 and 5.8, respectively. These were performed in de-aerated DCM with $TBABF_4$ as the supporting electrolyte. The cyclic and square wave voltammograms of complex **29a**, Fig 5.7(a) and (b), show two reduction processes labelled **III** and **IV** at half-wave ($E_{1/2}$) potentials of -0.74 and -1.13 V vs Ag|AgCl, respectively, Table 5.3. The ratio of anodic to cathodic current (I_{pa}/I_{pc}) was near unity for the two couples. The cathodic and anodic peak separations (ΔE) of 70 mV (similar to that of the ferrocene standard) for couples, **III** and **IV**, suggests reversibility due to fast electron transfer process. For both the reduction couples, the plots of peak currents (i_p) versus the square root of scan rate ($v^{1/2}$) were linear suggesting that the processes were diffusion controlled.

Table 5.3: List of redox potentials of TaPc complexes studied in this work in DMF or DCM using tetrabutyl ammonium tetrafluoroborate ($TBABF_4$) half-wave potential ($E_{1/2}$) as V vs. Ag|AgCl.

MPc	**V**	**IV**	**III**	**II/I**
	$Ta^{IV}Pc^{-2}$/ $Ta^{IV}Pc^{-4}$	**$Ta^{IV}Pc^{-2}$/ $Ta^{IV}Pc^{-3}$**	**$Ta^{V}Pc^{-2}$/ $Ta^{IV}Pc^{-2}$**	**Ring oxidations**
28 (DMF)	-	-0.99	-0.57	0.86
29a (DCM)	-	-1.13	-0.74	0.37, 0.99
29b (DCM)	-1.48	-1.02	-0.67	0.47, 0.59, 0.99
TaPc (DMF)	-0.98	-0.43	-0.31	-

[a] from ref [65]

The oxidation of **29a** consists of irreversible processes with sharp peaks due to adsorption processes**,** Fig 5.7. Process **II** has a broad pre-peak followed by a sharp peak typical of adsorption [112, 221]. It is known [112] that the adsorption of a product of the electrode reaction results in the formation of a sharp peak preceded by a more regular peak, the latter being due to the diffusion of the electroactive species from solution to the electrode. On return scan, a sharp peak appeared for process **II**, Fig. 5.7(b). Smaller mainly irreversible oxidation peaks are observed at larger oxidation potentials (processes **I**).

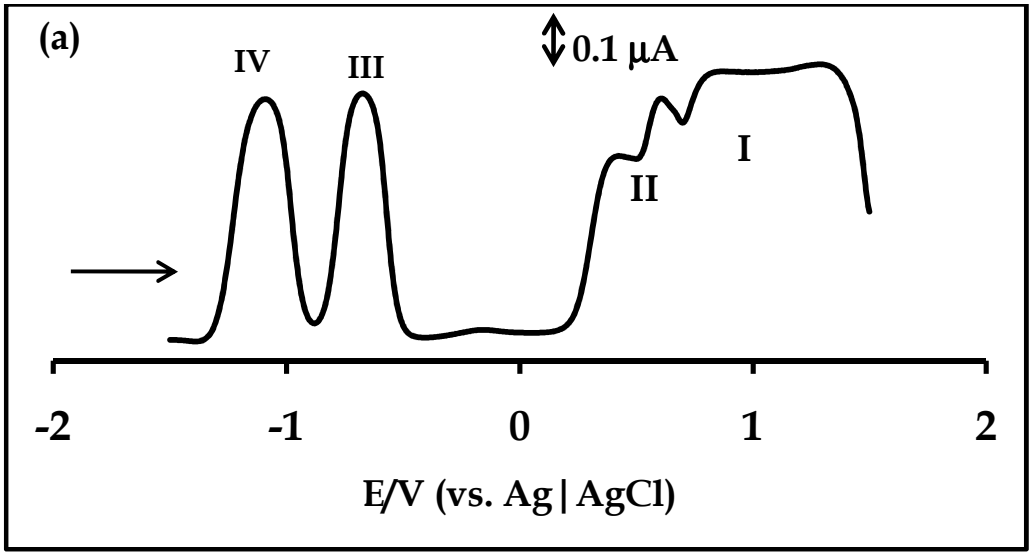
(a)
0.1 µA
IV
III
II
I
-2
-1
0
1
2
E/V (vs. Ag | AgCl)

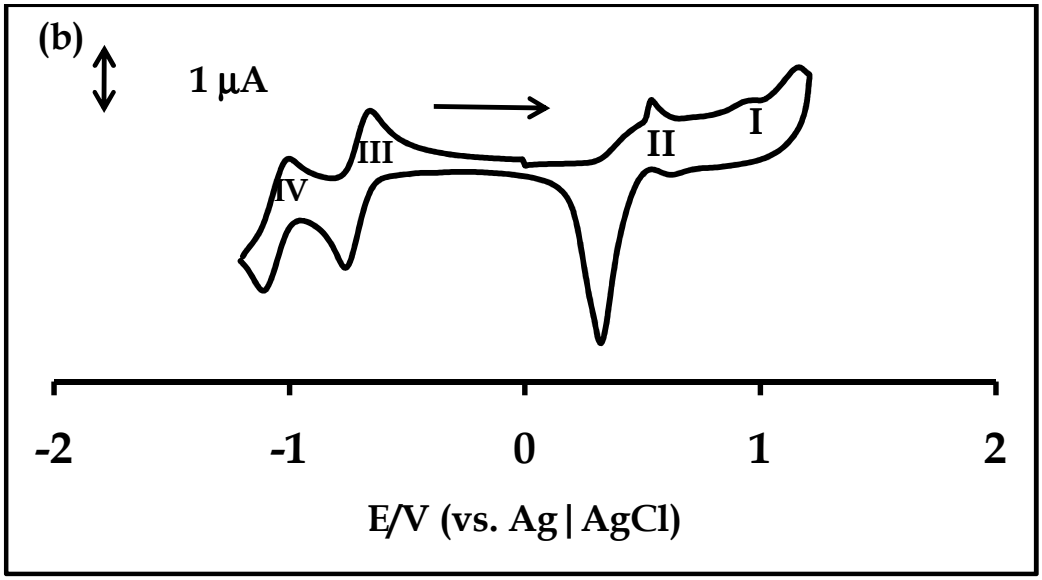
(b)
1 µA
III
IV
II
I
-2
-1
0
1
2
E/V (vs. Ag | AgCl)

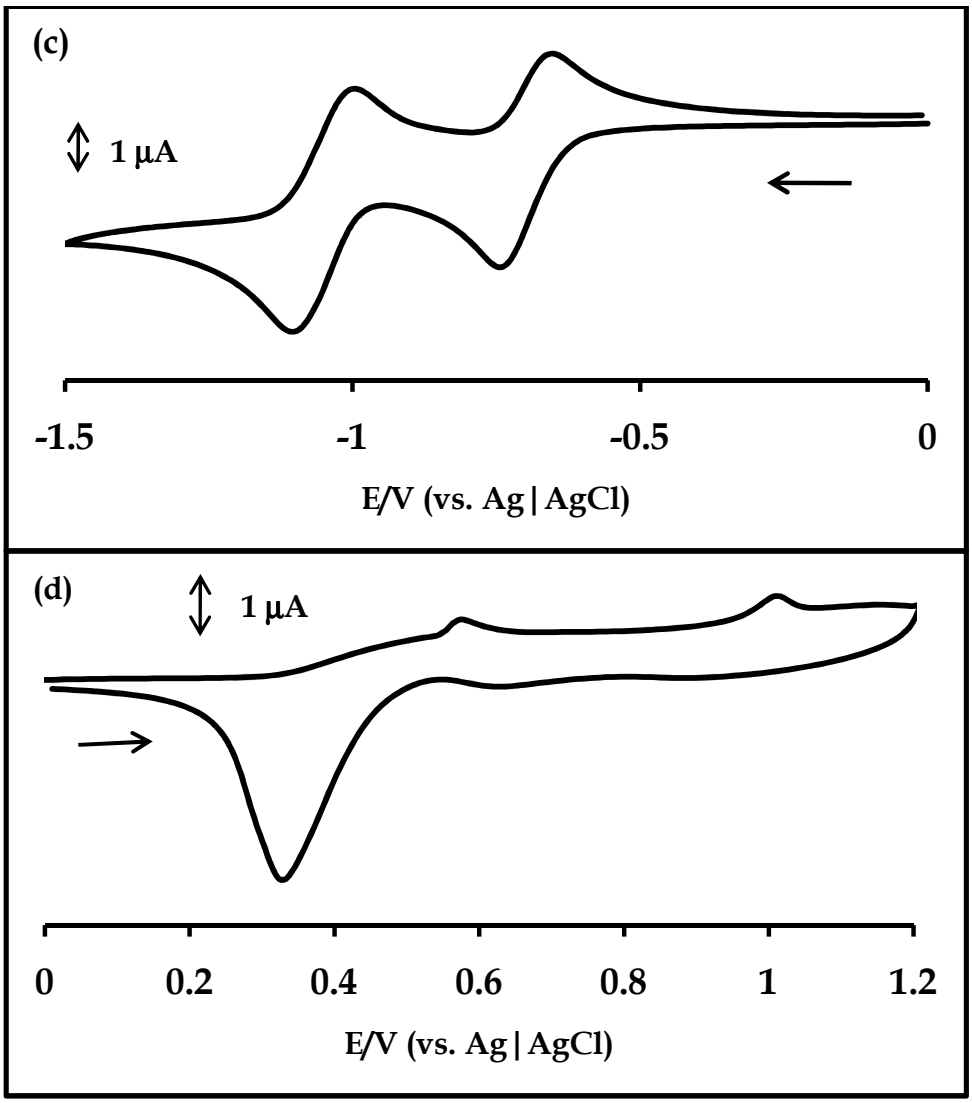

Figure 5.7: Square wave (a), cyclic (b) voltammograms for complex 29a in DCM containing 0.1 M $TBABF_4$, (c) cyclic voltammgrams observed when recording from 0V to negative or (d) positive potentials. Scan rate = 100 mV/s.

There was no change in the shape oxidation processes when the potential was scanned from 0 V to negative or positive potentials, Fig. 5.7(c) or (d).

Three reduction processes labelled **III, IV** and **V** were observed at $E_{1/2}$ of -0.67, -1.02 and -1.48 V vs Ag|AgCl, respectively, for complex **29b**, Fig. 5.8, Table 5.3. The anodic and cathodic peak separations (ΔE) for couples **III** was 60 mV, suggesting

reversibility. The reduction currents for **III** and **IV** are larger than for **V**, suggesting the possibility of different number of electrons transferred. However chronocoulometric analysis did not show significant differences in the number of electrons involved. The lower currents for **V** could be a result of the fact that this couple is at high negative potentials and hence near the limits of the electrode/electrolyte system, which may affect this peak. The effects of the limits of the system are clearer on the SWV.

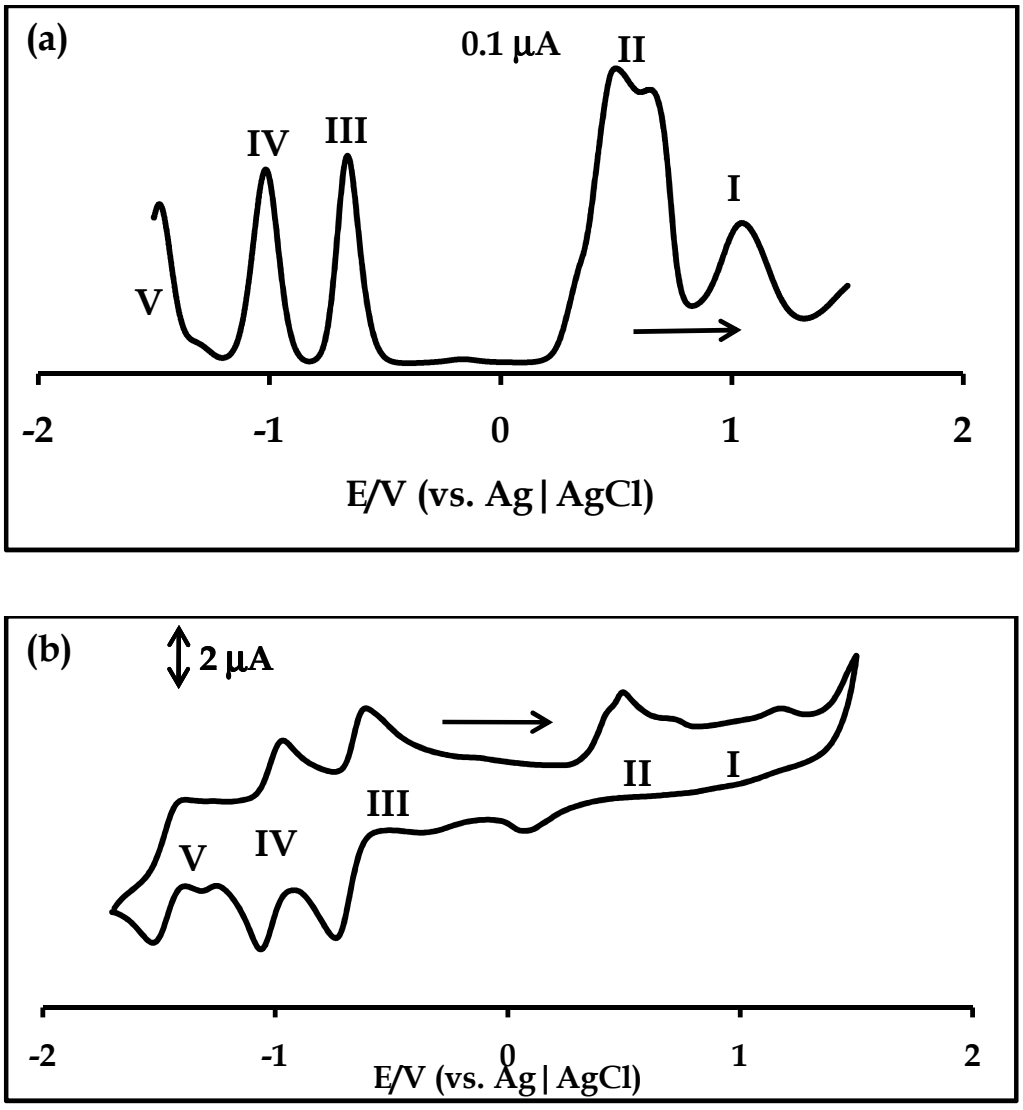

Figure 5.8: Square wave (a) and cyclic (b) voltammograms for complex 29b in DCM containing 0.1 M $TBABF_4$. Scan rate = 100 mV/s.

Comparing the reduction potentials of **29b** with those of **29a**, Table 5.3, shows that it is easier to reduce hence **29b** since an extra process **V** is observed. The ease of reduction of **29b** is accompanied by difficult oxidation compared to **29a** (in terms process **II**), possibly due to the differences in chain length.

Spectroelectrochemical experiments were performed for further investigation of the redox processes observed for complex **28**. The changes are shown Fig. 5.9, where on applying potentials more negative than potentials of couple **III** (-0.57 V vs Ag|AgCl), a shift of the split Q band from 667 and 701 nm to 601 and 664 nm was observed. The combination of aggregation and loss of symmetry may have resulted in broadening of the spectra in Fig. 5.9(a). Isosbestic points were rather diffuse, possibly due to axial ligand exchange and aggregation as discussed above for complex **24**. Typically, the changes in Fig. 5.9(a) are due to redox processes occurring at the central metal [13], since there is no drastic decrease in intensity of the Q band. Therefore, process **III** is attributed to the reduction $Ta^{V}Pc^{-2}$ to $Ta^{IV}Pc^{-2}$. Further reduction at potentials of process **IV** (-0.99 V vs Ag|AgCl), Fig. 5.9(b), resulted in a decrease in the intensity of the Q band and the appearance of new peaks at ~ 560 nm. The appearance of new bands between 500 and 600 nm is typical of ring reduction processes [222], i.e. $Ta^{IV}Pc^{-2}$ is reduced to $Ta^{IV}Pc^{-3}$. Oxidation is expected only on the ring for Ta(IV)Pc complexes, hence process **I** is assigned to the formation of $Ta^{IV}Pc^{-1}$.

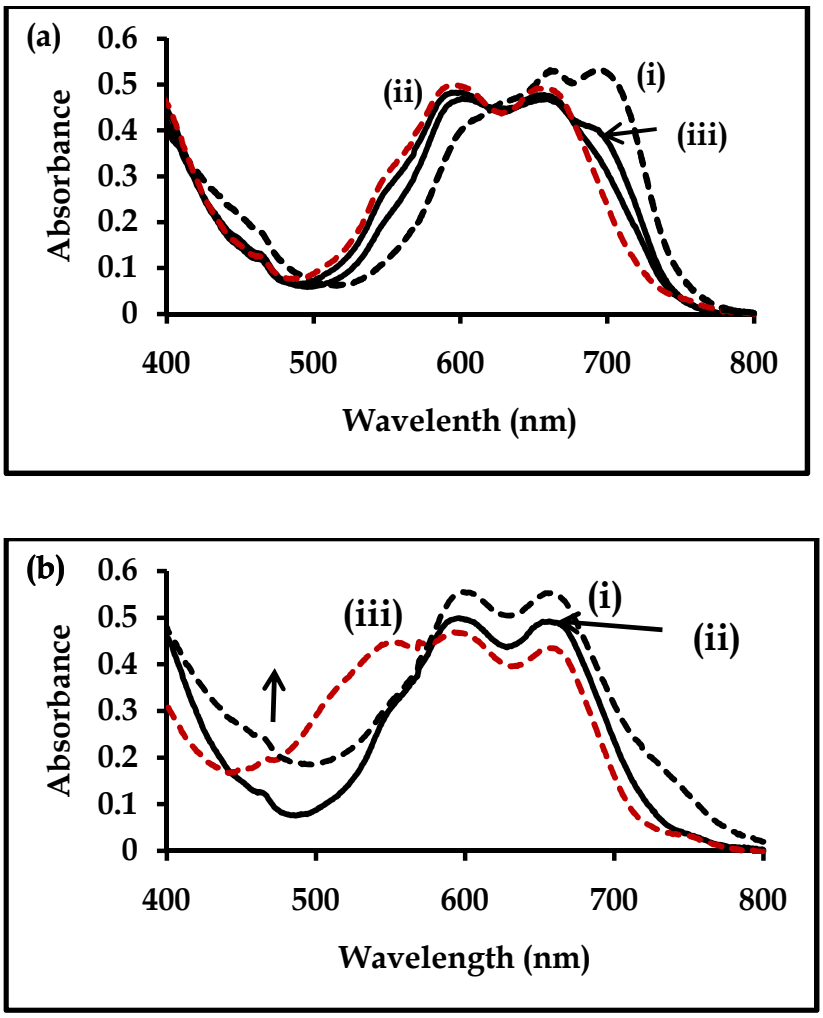

Figure 5.9: Observed UV/Vis spectral changes for complex 28 at potentials (a) -0.6 V (process III) and (b) -1.0 V (process IV) in DCM with 0.1 M $TBABF_4$. (i) starting, (ii) intermediate and (iii) final spectra

Fig 5.10 (a) shows the observed spectral changes for complex **29a** at potentials more negative of process **III** (-0.74 V vs Ag|AgCl) in DCM containing $TBABF_4$ as a supporting electrolyte. Upon reduction, the spectral changes observed include a shift of the Q band from 808 to 770 nm, with a slight decrease in the intensity of the Q band. There was also an emergence of new peaks at ~ 450 nm and a slight change of colour of the solution in the OTTLE cell from purple to blue. Diffuse isosbestic points were observed suggesting the presence of more than one species in solution. The

lack of clear isosbestic points could be a result of change of axial ligands during the reduction process. In related Ta porphyrin derivatives, axial ligand exchange reactions readily occur in slightly acid media [223]. The spectral changes observed in Fig. 5.10(a) consist of a shift in the Q band to shorter wavelengths, without the drastic decrease in intensity. These spectral changes are typical of redox processes occurring at the central metal [13], whereby the Q band shifts without a drastic decrease in intensity. The n value calculated for reduction of **29a** at potentials of process **III** processes was approximately ~1 using Equation 5.1.

From the discussion above, process **III** can be associated with the reduction $Ta^{V}Pc^{-2}$ to $Ta^{IV}Pc^{-2}$. Further reduction at potentials more negative of process **IV** (-1.2 V vs Ag|AgCl), Fig. 5.10(b), resulted in a decrease in the intensity (without shifting in position) of the Q band and the appearance of new peaks between 500 and 650 nm together with diffuse isosbestic points near 665 and 490 nm. These changes are typical of ring reduction processes [222], i.e. $Ta^{IV}Pc^{-2}$ is reduced to $Ta^{IV}Pc^{-3}$. The regeneration (to ~ 72 %) of the initial species was achieved, confirming the reversibility of the couples. Application of the potentials more positive of process **II**, resulted in spectral changes shown in Fig. 5.10(c) consisting of a decrease in the Q band with no new peaks forms indicative of the degradation of the complex confirming irreversibility of the oxidation processes. However the oxidation peaks are attributed to the Pc ring and the substituents, since no oxidation is expected on the central metal.

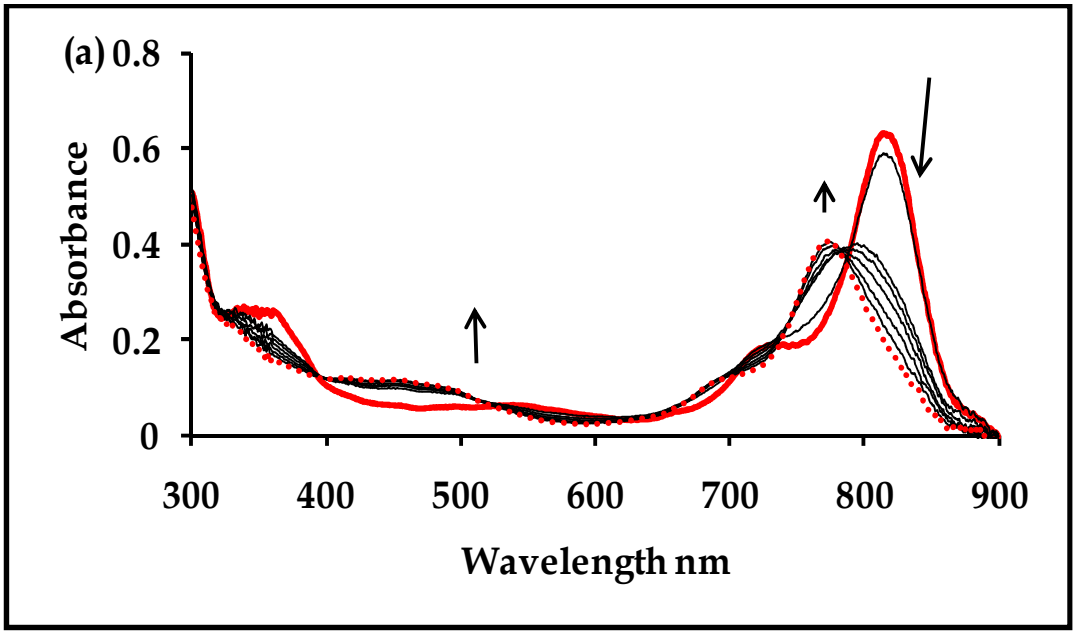
(a)
0.8
0.6
0.4
0.2
0
Absorbance
300
400
500
600
700
800
900
Wavelength nm

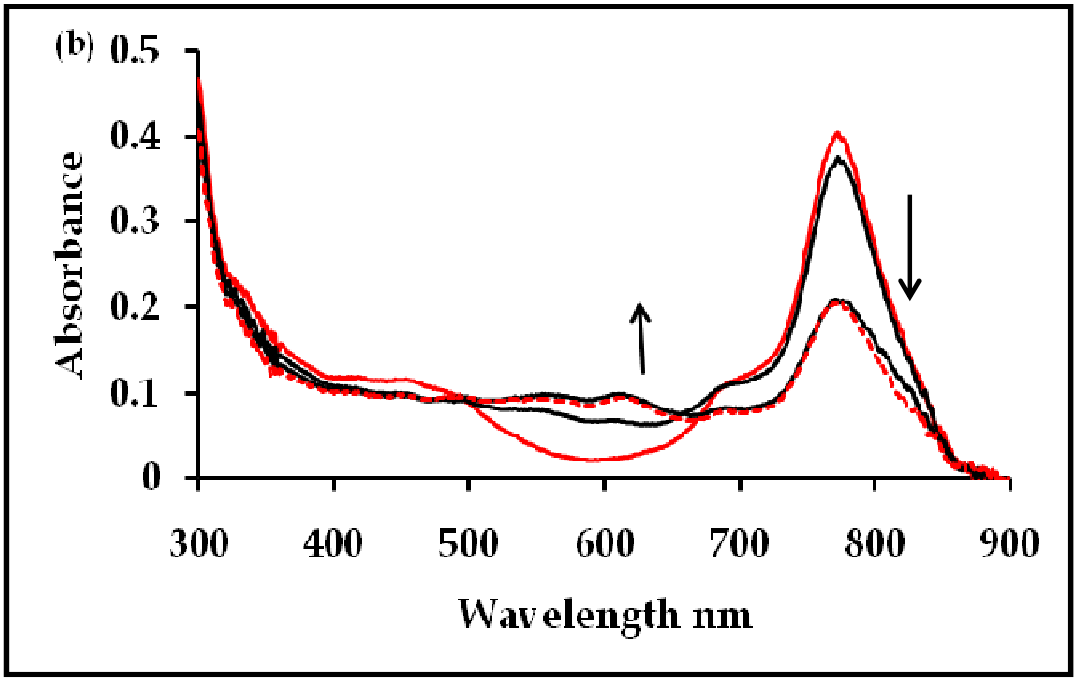
(b)
0.5
0.4
0.3
0.2
0.1
0
Absorbance
300
400
500
600
700
800
900
Wavelength nm

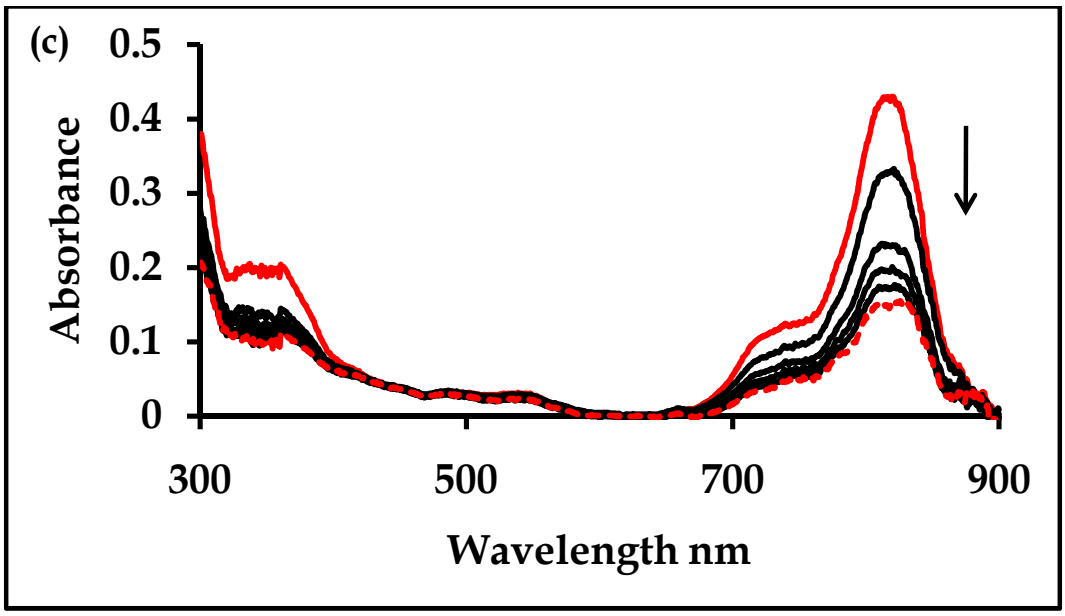

Figure 5.10: Observed UV/Vis spectral changes for complex 29a at potentials (a) -0.8 V (process III), (b) -1.2 V (process IV) and (c) 1.1 V (process II), in DCM with 0.1 M TBABF$_4$. Solid red line; before and dotted red line; after application of the appropriate potential. The last scan in (a) is the same as the first scan in (b).

Similarly, spectroelectrochemical experiments were performed for the further investigation of the redox processes observed for complex **29b**. Fig 5.11 (a) shows the observed spectral changes for complex **29b**, at potentials more negative of process **III** (-0.67 V vs Ag|AgCl). The changes consisted of a shift of the Q band from 814 to 765 nm, with an increase in the intensity, the emergence of new peaks at ~ 460 nm and a change of colour of the solution in the OTTLE cell from purple to blue were observed. Again isosbestic points were diffuse, due to possible axial ligation as discussed above for **29a**. The observed changes are typical of redox processes occurring at the central metal [13] as discussed for **29a**. Therefore, process **III** can be attributed to the reduction $Ta^{V}Pc^{-2}$ to $Ta^{IV}Pc^{-2}$. Further reduction at potentials of process **IV** (-1.01 V vs Ag|AgCl), Fig. 5.11(b), resulted in a decrease in the intensity

of the Q band and the appearance of new absorptions in the 600 nm region, together with clear isosbectic points at 670 nm. These spectral changes are typical of ring reduction processed [222], i.e. $Ta^{IV}Pc^{-2}$ is reduced to $Ta^{IV}Pc^{-3}$. Again, the regeneration of the initial species of ~ 69 % was achieved, confirming some reversibility of the couples. Process **IV** is attributed to further ring reduction.

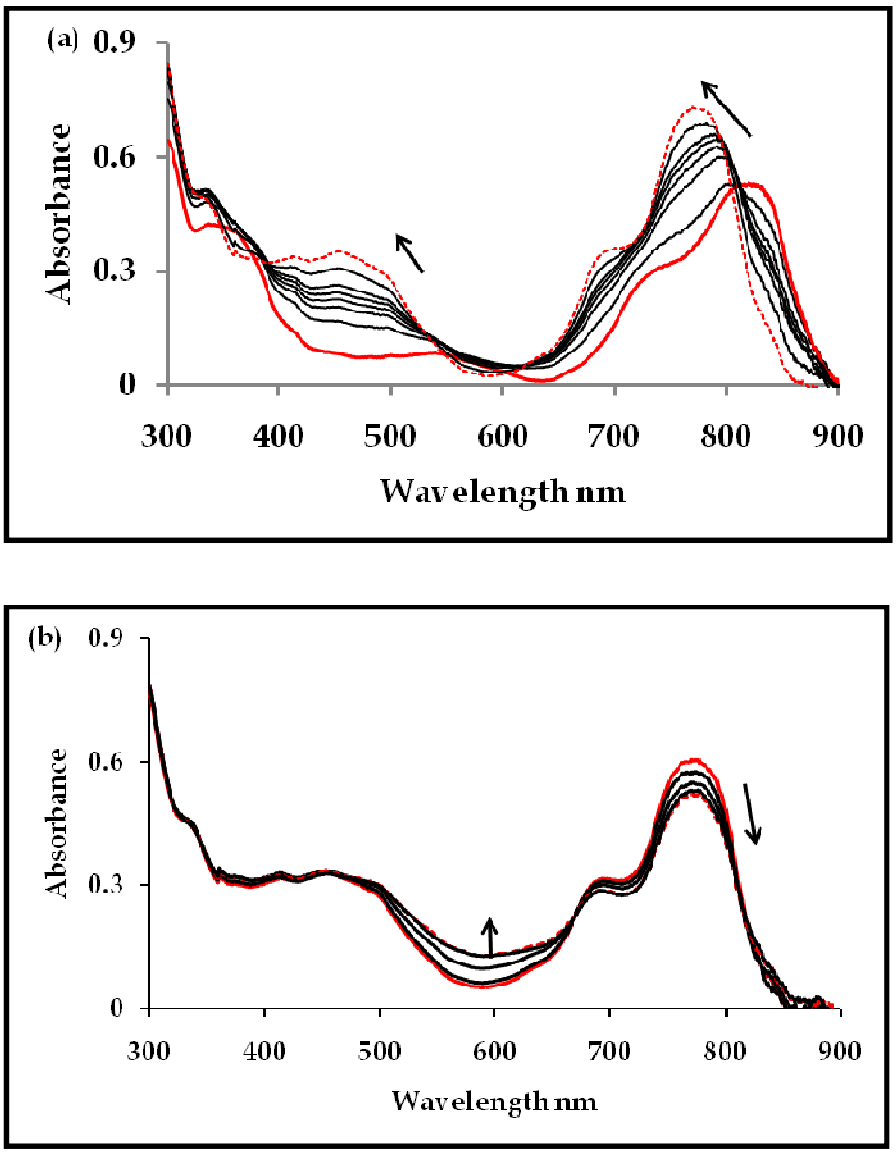

Figure 5.11: Observed UV/Vis spectral changes for complex 29b at potentials (a) -0.7 V (process III) and (b) -1.1 V (process IV) in DCM with 0.1 M $TBABF_4$. Solid red line; before and dotted red line; after application of the appropriate potential. The last scan in (a) is the same as the first scan in (b).

Based on the electrochemical observations described above, for TaPc complexes the assignments for processes **I – III** for complex **28** are as follows:

$Ta^{V}Pc^{-2} \rightarrow Ta^{V}Pc^{-1} + e^{-}$ (Process **I**)

$Ta^{V}Pc^{-2} + e^{-} \rightarrow Ta^{IV}Pc^{-2}$ (Process **III**)

$Ta^{IV}Pc^{-2} + e^{-} \rightarrow Ta^{IV}Pc^{-3}$ (Process **IV**)

Oxidation is expected to occur only on the ring for these complexes. The assignments for processes **I – IV** for complex **29a** are as follows:

$Ta^{V}Pc^{-1} \rightarrow Ta^{V}Pc^{0} + e^{-}$ (Process **I**)

$Ta^{V}Pc^{-2} \rightarrow Ta^{V}Pc^{-1} + e^{-}$ (Process **II**)

$Ta^{V}Pc^{-2} + e^{-} \rightarrow Ta^{IV}Pc^{-2}$ (Process **III**)

$Ta^{IV}Pc^{-2} + e^{-} \rightarrow Ta^{IV}Pc^{-3}$ (Process **IV**)

Similarly, processes for complex **29b** are assigned as follows:

$Ta^{V}Pc^{-2} \rightarrow Ta^{V}Pc^{-0} + e^{-}$ (Process **I**)

$Ta^{V}Pc^{-2} \rightarrow Ta^{V}Pc^{-1} + e^{-}$ (Process **II**)

$Ta^{V}Pc^{-2} + e^{-} \rightarrow Ta^{IV}Pc^{-2}$ (Process **III**)

$Ta^{IV}Pc^{-2} + e^{-} \rightarrow Ta^{IV}Pc^{-3}$ (Process **IV**)

$Ta^{IV}Pc^{-2} + e^{-} \rightarrow Ta^{IV}Pc^{-4}$ (Process **V**)

5.4. Conclusions

The reduction couples for all the complexes were reversible to quasi-reversible and oxidation processes are irreversible. The vanadium complexes (**26** and

27) did not show any metal based processes. Spectroelectrochemistry confirmed metal reduction processes for the TiPc (**24** and **25**) and TaPc (**28**, **29a** and **29b**) complexes, with the rest of the redox processes being centered on the phthalocyanine ring.

Chapter 6: Electrocatalytic properties

In this chapter the electrocatalytic activity of NiTAPc, TiPc, VPc and TaPc complexes toward the oxidation or detection of BPA and PNP (the latter, only for NiTAPc) is discussed. These experiments were done on Au electrode because they display insignificant background currents, are sensitive and show good reproducibility. The size of the AuNPs used in this section was ~ 10 nm.

6.1. Electrode modification and surface coverage

6.1.1. Electropolymerisation of NiTAPc

Even though NiTAPc is a known complex, it was chosen in order to compare it with the new complexes for the detection of BPA. The modification of the working Au electrode was achieved via electropolymerisation of NiTAPc in DMF by repetitive cycling at a constant scan rate of 0.1 Vs^{-1} to form *poly*-NiTAPc. The electropolymerisation of tetraamino substituted Pcs such as MnTAPc on glassy carbon electrodes is now well known [224]. The formation of self assembled monolayers (SAMs) of CoTAPc, CuTAPc and FeTAPc on Au and Ag has been reported [225]. The formation of SAM is not expected to be significant during the time used for electropolymerisation because it takes hours for significant coverage for SAMs. The Au oxide and stripping peaks were not observed under the conditions (organic media) of the electropolymerisation process in this work.

6.1.1.1. Cyclic voltammetry

Fig. 6.1 shows a series of CVs (20 scans) during electropolymerisation of Ni(II)TAPc. The number of scans was increased to 30 scans, but as has been observed before [148], the polymer film tends to lose conductivity with an increasing number

of scans. The main aim was to form O-Ni-O oxo bridges for the catalytic oxidation of BPA. The formation of O-Ni-O oxo bridges was based on the optimum number of scans of 20. It is well known that repetitive cyclic voltammetry scanning of amino substituted MPc complexes results in polymer formation of the MPc onto the electrode surface [223 - 227]. This is as a result of the formation of radicals on oxidizing the amino substituents [226], whereby the formed radicals attack the vulnerable amino groups on the phenyl rings of neighbouring molecules thus forming a polymer [226]. The CV evolution shown in Fig. 6.1 is similar to that reported in literature [226]. A general increase in currents together with the formation of new peaks was observed. The polymer formed on the electrode was clearly noticeable on the surface of the electrode as a dark green surface. *Poly*-NiTAPc will be used to represent the Ni(II)TAPc polymer on Au electrode surface. A slight shift on the positive potentials with increase in scan number was observed. This is indicative of an increase in electrical resistance of the polymer film and thus over-potential is needed to overcome resistance [228].

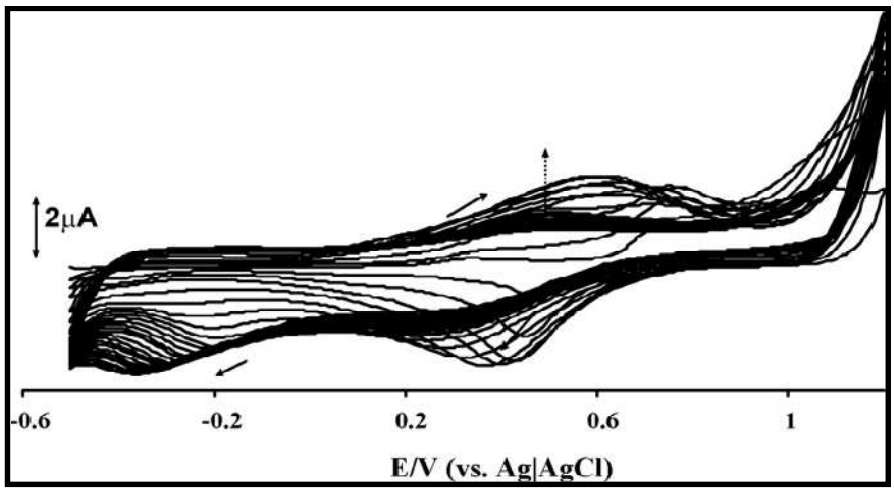

Figure 6.1: Repetitive cyclic voltammogram of 1 x 10^{-3} mol L^{-1} NiTAPc in DMF containing 0.1 mol L^{-1} $TBABF_4$ at the gold electrode. Scan rate = 100 mVs^{-1}.

Following the electropolymerisation of Ni(II)TAPc, transformation of the *poly*-NiTAPc into 'O-Ni-O oxo bridges' was done by cycling repetitively in 0.1 mol L^{-1} solution of NaOH between -0.2 and 1.2 V. Fig. 6.2 shows the formation and increase of both the anodic and cathodic peaks between -0.2 and +0.5 V. These peaks are documented as Ni^{III}/Ni^{II} redox process and are similar to literature [146, 229]. The insert in Fig. 6.2 shows a cyclic voltammogram of the transformed polymer in pH 12 phosphate buffer, which is the pH employed for the detection of BPA. There is only a small shift to more positive potential values in pH 12 compared to 0.1 mol L^{-1} NaOH. The cyclic voltammetry peaks between -0.2 and +0.5 V can be explained by the formation of 'O-Ni-O oxo bridges' in alkaline aqueous solutions and are indicative of transformation of the *poly*-NiTAPc into O-Ni-O oxo bridges [228 - 231].

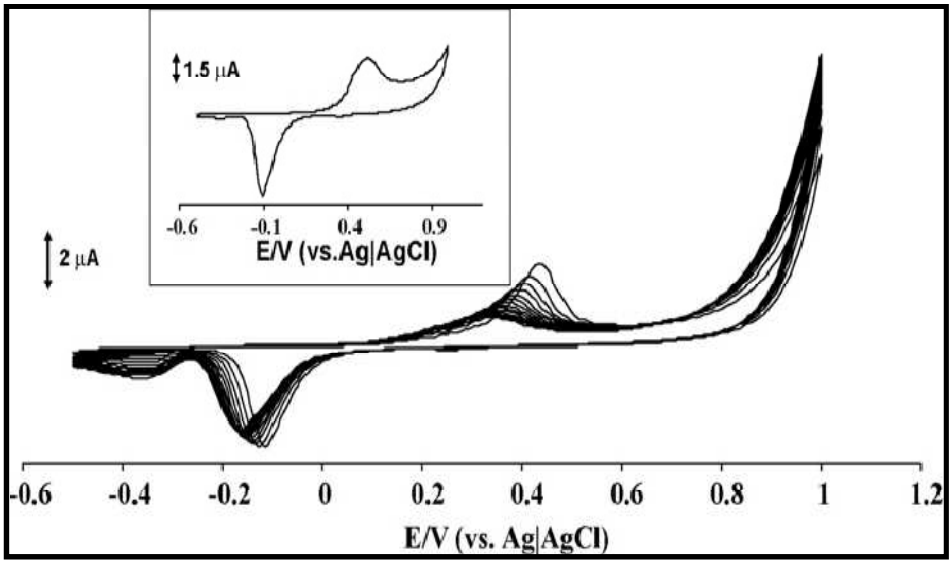

Figure 6.2: Repetitive cyclic voltammograms of *poly*-NiTAPc in 0.1 mol L^{-1} NaOH. Insert is the polymer in buffer. Scan rate 100 mVs^{-1}.

The modified electrode will now be represented as *poly*-Ni(OH)TAPc–Au. Although the mechanism of transformation is not fully known, it has been suggested [231, 232]

that the transformation is initiated by the electrooxidation of the OH^- in the electrolyte solution to the hydroxyl radical ($OH^{\cdot}$). The high current observed between 0.7 – 1.2 V has been attributed to the electrooxidation of the OH^- in the electrolyte solution to the hydroxyl radial ($OH^{\cdot}$) [233]. The $OH^{\cdot}$ radicals assist with the insertion of the oxygen atom (O) between the NiPcs. With increase in scanning, more $OH^{\cdot}$ radicals are generated thus leading to the interlinking of the Ni atoms to form 'O-Ni-O oxo bridges'. There are no peaks due to Au alone at the pH employed.

The thickness of the films is governed by the number of scans during polymerisation. The more the number of scans, the thicker the film. Ideally a thicker film should give better catalytic behaviour than a thinner film. This is expected because of the availability of more catalytic sites. However, it has been shown before that the accessibility to the redox centres within the electropolymerised films is limited to the external layers [223]. Fig. 6.3 shows the cyclic voltammograms of Au electrode (insert), (i) *poly*-30-Ni(OH)NiTAPc, (ii) *poly*-50-Ni(OH)NiTAPc, (iii) *poly*-70-Ni(OH)NiTAPc, (iv) *poly*-90-Ni(OH)NiTAPc in 1 x 10^{-3} mol L^{-1} $K_3[Fe(CN)_6]$ containing 0.1 mol L^{-1} KCl where the number represents the number of scans. The bare electrode in Fig. 6.3 (insert) shows a redox couple at half-wave potential, ($E_{1/2}$) of 65 mV and an anodic to cathodic peak separation (ΔE) of 60 mV. Figs. 6.3 (i) – (iv) show reversible cyclic voltammograms with $E_{1/2}$ values decreasing with increase in polymer thickness from $E_{1/2}$ = 135 mV for *poly*-30-Ni(OH)NiTAPc, 130 mV for *poly*-50-Ni(OH)NiTAPc, 120 mV for *poly*-70-Ni(OH)NiTAPc and 115 mV for *poly*-90-Ni(OH)NiTAPc. The decrease in ΔE values was also observed with polymer thickness (with the exception of *poly*-90-Ni(OH)NiTAPc) as follows: 120 mV for *poly*-

30-Ni(OH)NiTAPc, 80 mV for *poly*-50-Ni(OH)NiTAPc, 60 mV for *poly*-70-Ni(OH)NiTAPc and 70 mV for *poly*-90-Ni(OH)NiTAPc. This order suggests improved kinetics with increase in polymer thickness.

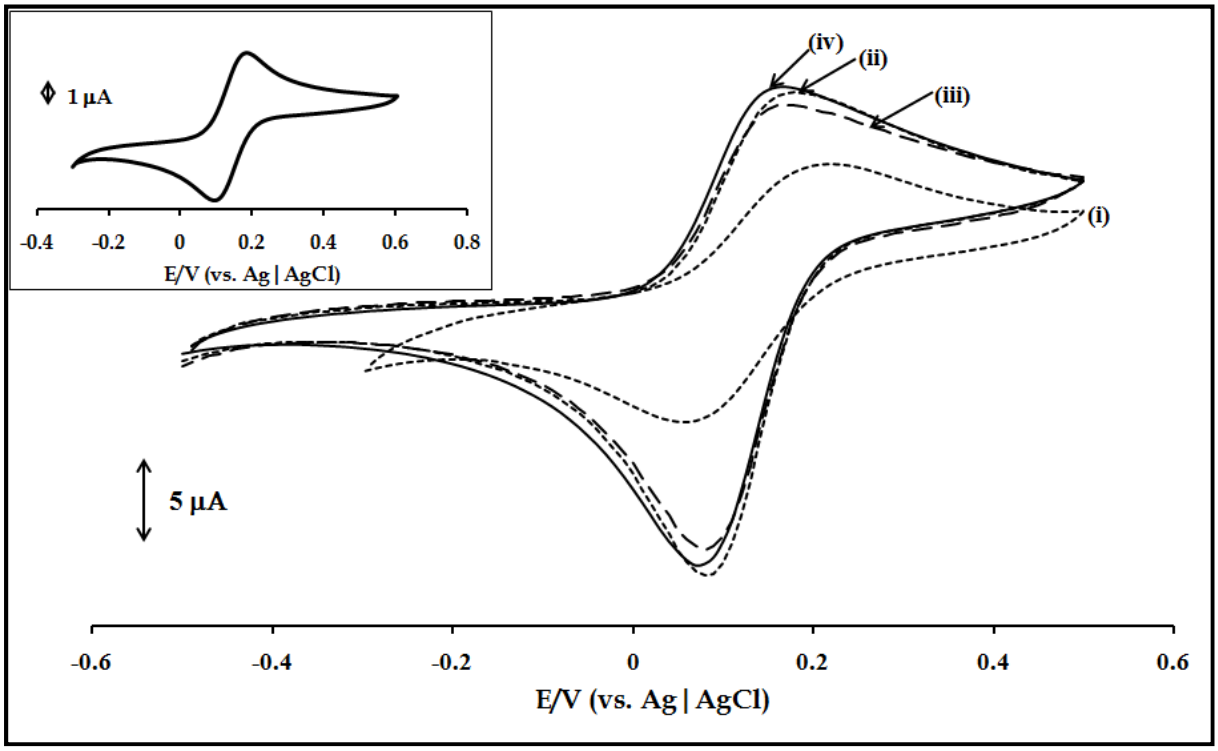

Figure 6.3: Cyclic voltammograms of (i) *poly*-30-Ni(OH)NiTAPc, (ii) *poly*-50-Ni(OH)NiTAPc, (iii) *poly*-70-Ni(OH)NiTAPc, (iv) *poly*-90-Ni(OH)NiTAPc in 1 x 10^{-3} mol L^{-1} $K_3[Fe(CN)_6]$ containing 0.1 mol L^{-1} KCl, insert is Au bare electrode.

The surface coverages were calculated for the NiTAPc polymers and adsorbed complexes by first determining the effective area of the Au electrode using the $[Fe(CN)_6]^{3-/4-}$ redox system and applying the Randles–Sevcik {Eq. (1.19, now 6.1)} for a reversible process [128]

$$I_{pa} = (2.69 \times 10^5) n^{3/2} D^{1/2} v^{1/2} A C_o \qquad (6.1)$$

where D and C_o are the diffusion coefficient and bulk concentration of the redox probe (1 mM $K_3[Fe(CN)_6]$), respectively. n is the number of electrons transferred (n = 1), v is the scan rate and A is the effective surface area. From the D value for $K_3[Fe(CN)_6]$ = 7.6×10^{-6} cm^2 s^{-1} [127], the surface roughness of the electrode was found to be 1.36 (ratio of I_{pa} experimental/I_{pa} theoretical) corresponding to a real electrode area of 0.0274 cm^2 (roughness factor × theoretical surface area, =0.0201 cm^2).

The surface coverages ($\Gamma_{polyNiTAPc}$) of polymer modified electrodes were estimated by integrating the charge under the reduction peak in Fig. 6.2 (inset), using equation (6.2).

$$\Gamma_{polyMTAPc} = \frac{Q}{nFA} \qquad (6.2)$$

where Q (C) is the charge under the metal oxidation peak, n (=1) is the number of electrons, A is the effective area of the electrode (calculated from equation 1) and F is Faraday's constant (95485 C mol^{-1}). Using the effective area of the electrodes, the calculated surface coverage values for the various polymers are listed in Table 6.1. The determined values range from 1.11 x 10^{-10} to 5.46 x 10^{-10} mol cm^{-2} for different *poly*-NiTAPc modified Au electrode. These values are in the range for monolayer coverage in MPc complexes [234], suggesting multilayer coverage except for 1.11 x 10^{-10} mol cm^{-2} obtained for poly-90-Ni(OH)TAPc-Au.

Table 6.1: EIS parameters and surface coverage values for *poly*-NiTAPc films, and Recovery values for detection of BPA and PNP in pH 12 buffer.

Electrode	Surface coverage (Γ) mol cm^{-2} (MPc)	ΔE vs. Ag|AgCl (mV)	R_{CT} (x 10^{-3} Ω)	R_S (kΩ)	C_{dl} (μF)
***poly*-30-Ni(OH)NiTAPc-Au**	1.79 x 10^{-10}	120	9.3	0.19	0.373
***poly*-50-Ni(OH)NiTAPc-Au**	2.20 x 10^{-10}	80	5.7	0.19	0.532
***poly*-70-Ni(OH)NiTAPc-Au**	5.46 x 10^{-10}	60	4.3	0.18	0.822
***poly*-90-Ni(OH)NiTAPc-Au**	1.11 x 10^{-10}	70	4.5	0.15	0.816

6.1.1.2. Electrochemical impedance spectroscopy

Electrochemical impedance spectroscopy (EIS) was employed for further characterization of the modified electrodes. The Nyquist plot (-Z″ vs Z′) was fitted and analyzed using the Randles equivalent circuit (Fig. 6.4 insert) which takes into consideration the diffusion and kinetic control parameters [235 - 237]. The Randles equivalent circuit used for fitting impedance data consisted of the solution or electrolyte resistance (R_S) connected in series to the parallel combination of the capacitance and charge-transfer resistance (R_{CT}) in series with Warburg impedance (Z_W).

Fig. 6.4 shows the Nyquist plots for (i) *poly*-30-Ni(OH)NiTAPc, (ii) *poly*-50-Ni(OH)NiTAPc, (iii) *poly*-70-Ni(OH)NiTAPc and (iv) *poly*-90-Ni(OH)NiTAPc modified Au electrodes recorded in 1 x 10^{-3} mol L^{-1} $[Fe(CN)_6]^{3-/4-}$ in 0.1 mol L^{-1} KCl.

The Nyquist plots of all the modified electrodes [Fig. 6.4 (i) – (iv)] resemble a semi-circle pattern (due to barrier to the interfacial electron-transfer) followed by a straight line in the low frequency region (the Warburg line).

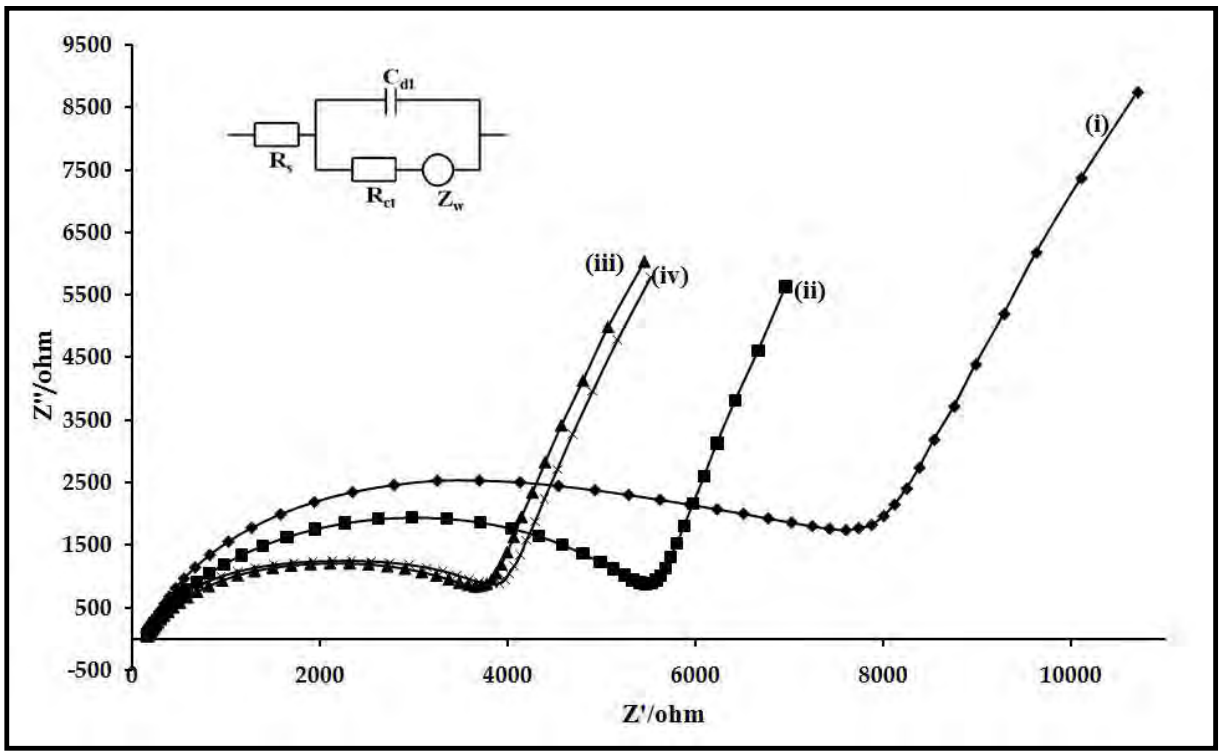

Figure 6.4: Nyquist plots of electrodes of this work recorded in 1 x 10^{-3} mol L^{-1} $[Fe(CN)_6]^{3-/4-}$ in 0.1 mol L^{-1} KCl: (i) *poly*-30-Ni(OH)NiTAPc, (ii) *poly*-50-Ni(OH)NiTAPc, (iii) *poly*-70-Ni(OH)NiTAPc, (iv) *poly*-90-Ni(OH)NiTAPc modified Au electrodes. The insert shows the Randles equivalent circuit of the electrodes.

The charge transfer resistance (R_{CT}), Table 6.1, decreases with film thickness, except for *poly*-70-Ni(OH)NiTAPc and *poly*-90-Ni(OH)NiTAPc, whose values are almost the same. The behaviour of *poly*-70-Ni(OH)NiTAPc and *poly*-90-Ni(OH)NiTAPc implies that the increase in film thickness in this case does not necessarily mean less charge transfer resistance or better catalytic activity as reported before [232]. The general

decrease in R_{CT} values with film thickness could be attributed to the catalytic nature of the surface confined polymer films as has been observed before [238, 239]. This behaviour may be interpreted as the result of decreased electrical resistance to mass transport through the film. The decrease in R_{CT} values confirm the cyclic voltammetry results which showed improvement in ferrocene peak separation with film thickness. The R_s values (Table 6.1) between the different polymers on Au electrodes were not significantly different (0.15 – 0.19 kΩ). The polymers on the electrode surfaces are not expected to change the solution resistance significantly, hence this was expected. The C_{dl} values were different, with *poly*-70-Ni(OH)NiTAPc showing the highest value of 0.82 μF, the differences show the different conducting abilities of the films.

6.1.2. Adsorbed TaPc complexes

The cyclic voltammograms of all the complexes used in this work were obtained in pH 7.4 and 12 phosphate buffer but BPA was mainly determined at pH 12. The bare or modified electrodes were scanned between -1.2 V and 1.0 V vs. Ag|AgCl for the drop-dry modified electrodes. Gracia *et al*. [240] have reported the use of adsorbed AuNPs onto Au disk electrode where they observed no gold oxidation for AuNPs below 0.6 V on indium tin oxide coated glass (ITO). Similarly, AuNPs do not show any gold oxidation on Au disk electrodes [241, 242] below 0.6 V. The oxidation peak of AuNPs has been reported at 1.28 V (versus saturated calomel electrode) and the reduction peak at 0.81 V [240].

Fig. 6.5 (a) shows the cyclic voltammogram of the Au disk electrode and the AuNPs adsorbed on gold disk. The gold oxide peak is observed at 0.99 V and its subsequent reduction at 0.36 V at pH 7.4. In the presence of AuNPs, the peaks decreased in intensity, suggesting passivation of bulk gold by AuNPs. Fig. 6.5(b) shows a cyclic voltammogram of gold electrodes with AuNPs adsorbed onto the electrode surface in pH 12 phosphate buffer. The gold oxide peak was slightly shifted compared to observations in pH 7.4, the peak was at 1.1 V and the reduction peak was at 0.43 V. Fig 6.5 (c) shows a cyclic voltammogram of bare electrode in 0.1M KOH. The well defined reversible peaks on Fig. 6.5(c) illustrate the 'crystallinity' of gold and the absence of oxidizable particles or contaminants [128], hence the observed voltammograms in Fig. 6.5(a) are not due to contaminants on the gold disk electrode.

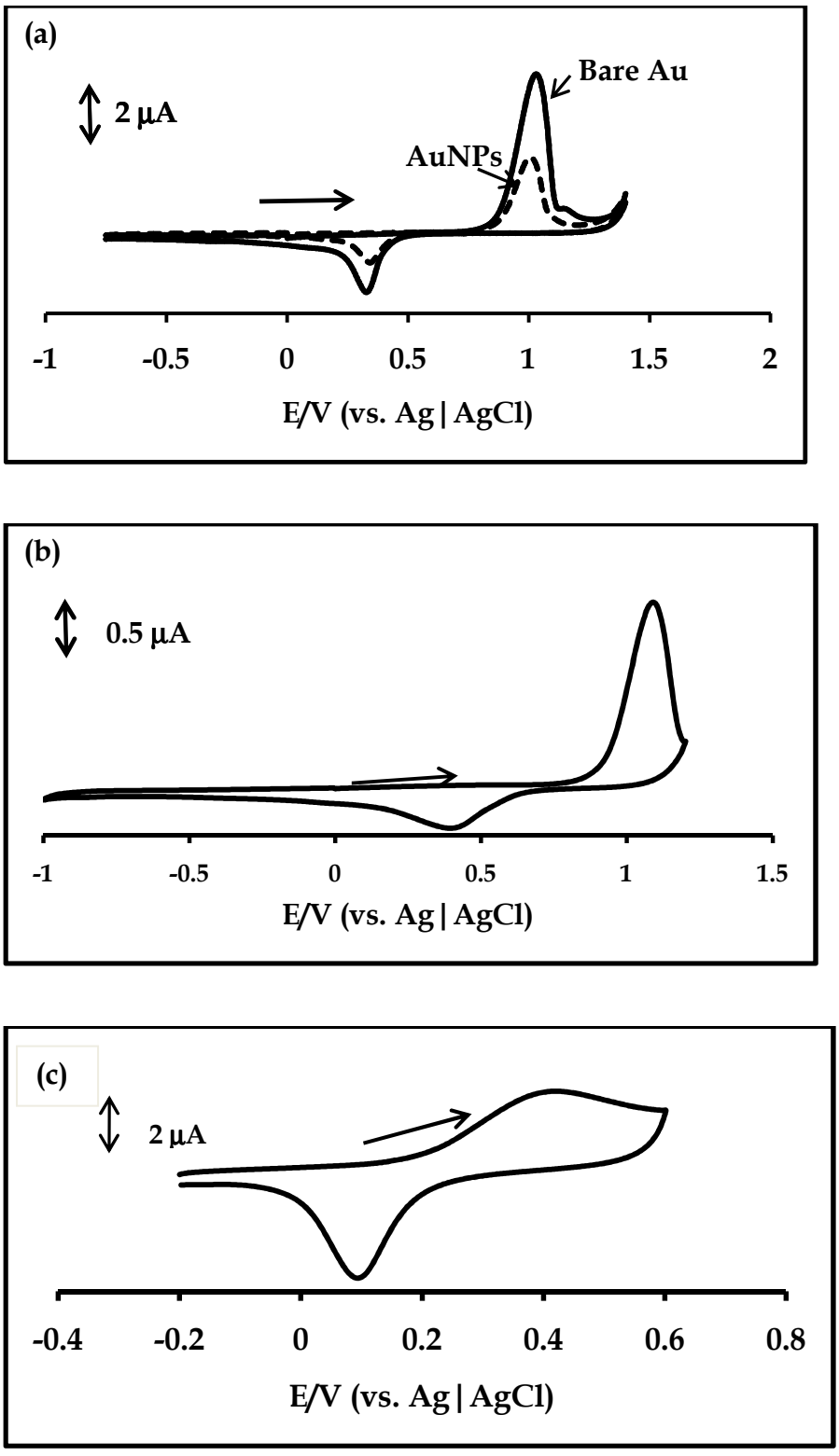

Figure 6.5: Cyclic voltammogram of (a) bare gold disk electrode and AuNP on gold disk electrode, in pH 7.4 phosphate buffer, (b) cyclic voltammogram of AuNPs in pH 12 phosphate buffer and (c) bare gold electrodes in 0.1M KOH

6.1.2.1. Complex 28 and AuNPs conjugates

Fig. 6.6 shows cyclic voltammogram of adsorbed complex **28** on Au disk in pH 12 phosphate buffer. The broad peak at ~ 0.5 V on the Au electrode confirms the presence of **28** even though the peak is broad.

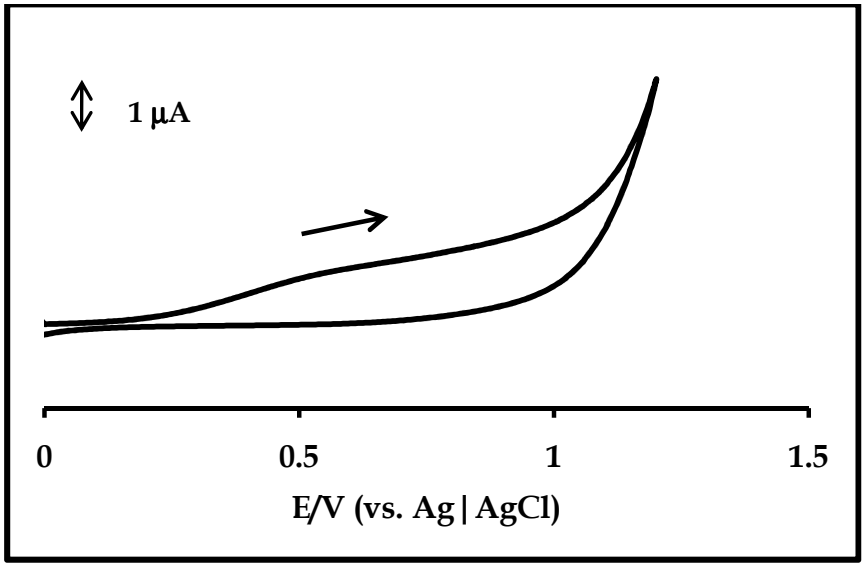

Figure 6.6: Cyclic voltammograms of adsorbed complex 28 in pH 12 phosphate buffer. Scan rate 100 mVs^{-1}.

The surface coverage values of complex **28** and **28**-AuNPs on Au electrode disk were determined using the methods discussed earlier (following Eqs. 6.1 and 6.2). The surface coverage values were 1.54 x 10^{-10} and 5.25 x 10^{-10} mol cm^{-2} for **28** and **28**-AuNPs, respectively, Table 6.2. These values were higher than monolayer value of 1 x 10^{-10} mol cm^{-2} for Pcs. A noticeable increase on the surface coverage of **28**-AuNPs was observed indicating that there was conjugation between complex **28** and AuNPs.

Table 6.2: Table 1: EIS parameters for poly-Ni(OH)NiTAPc and selected TaPc and their AuNPs conjugates; and BPA detection potentials.

Electrode	**R_{CT} (x 10^{-3} Ω)**	**ΔE vs. Ag|AgCl (mV)**	***n***	**Surface coverage (Γ, mol cm^{-2})**
AuNPs	20.9	233	0.90	2.87 x 10^{-10}
29a	0.72	75	0.80	1.98 x 10^{-10}
29a-AuNPs	2.25	93	0.85	4.51 x 10^{-10}
29b	1.84	125	0.79	2.47 x 10^{-10}
29b-AuNPs	2.81	80	0.82	9.94 x 10^{-10}
28	-	-	-	1.54 x 10^{-10}
28-AuNPs	-	-	-	5.25 x 10^{-10}

6.1.2.2. Complexes 29a and 29b and their AuNPs conjugates

Fig. 6.7 shows cyclic voltammogram of adsorbed complexes **29a** and **29a-**AuNPs on Au disk.

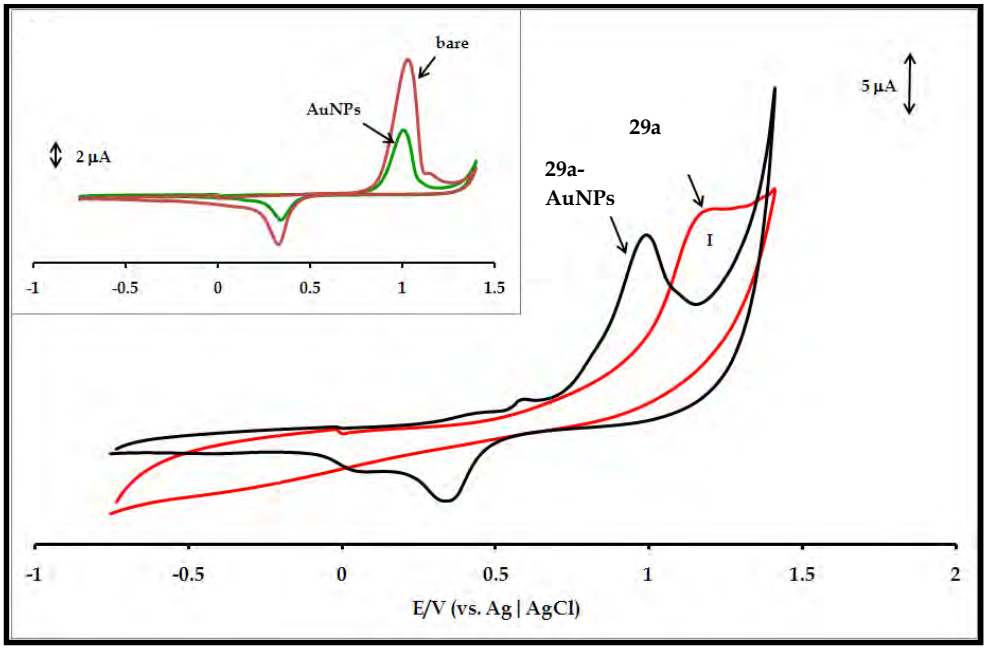

Figure 6.7: Cyclic voltammogram of complexes 29a, 29a-AuNPs and AuNPs. Insert = bare gold disk electrode and AuNPs on gold disk electrode in pH 7.4 phosphate buffer.

The Au oxidation and reduction peaks were observed at 0.92 V and 0.35 V for adsorbed **29a-**AuNPs, Fig. 6.7. The peaks near 0.5 V are due to complex **29a**, see Fig. 5.7, (for **29a** alone in solution). These peaks are not evident on adsorbed complex **29a**. Also for adsorbed **29a** without AuNPs, the Au oxidation peak is shifted to more positive potentials and there is no clear gold oxide reduction peak near 0.35 V. It is also possible that the adsorbed **29a** (without the AuNPs) passivates the Au disk electrode and the peak near 1.2 V is due to ring processes of complex **29a**. The behaviour shown in Fig. 6.7 was also observed for complex **29b** and **29b-**AuNPs.

Fig. 6.8 shows the cyclic voltammograms of (a) (i) **29a**, (ii) **29b**; (b) (iii) **29a-**AuNPs, (iv) **29b-**AuNPs and (v) AuNPs in 1 x 10^{-3} mol L^{-1} $K_3[Fe(CN)_6]$ containing 0.1 mol L^{-1} KCl. The cyclic voltammograms shown in Fig. 6.8 (ii) – (vi), for the modified electrodes have $E_{1/2}$ values that range from 121 to 157 mV. The ΔE values were 233

mV for AuNPs, 75 mV for complex **29a**, 93 mV for **29a-**AuNPs, 125 mV for complex **29b**, and 80 mV for **29b-**AuNPs. For bare Au electrode, ΔE = 60 mV (Fig. 6.3 insert). The largest ΔE value was obtained for AuNPs on gold (ΔE = 233 mV), showing slow electrode kinetics followed by the **29b** modified electrode, Table 6.2.

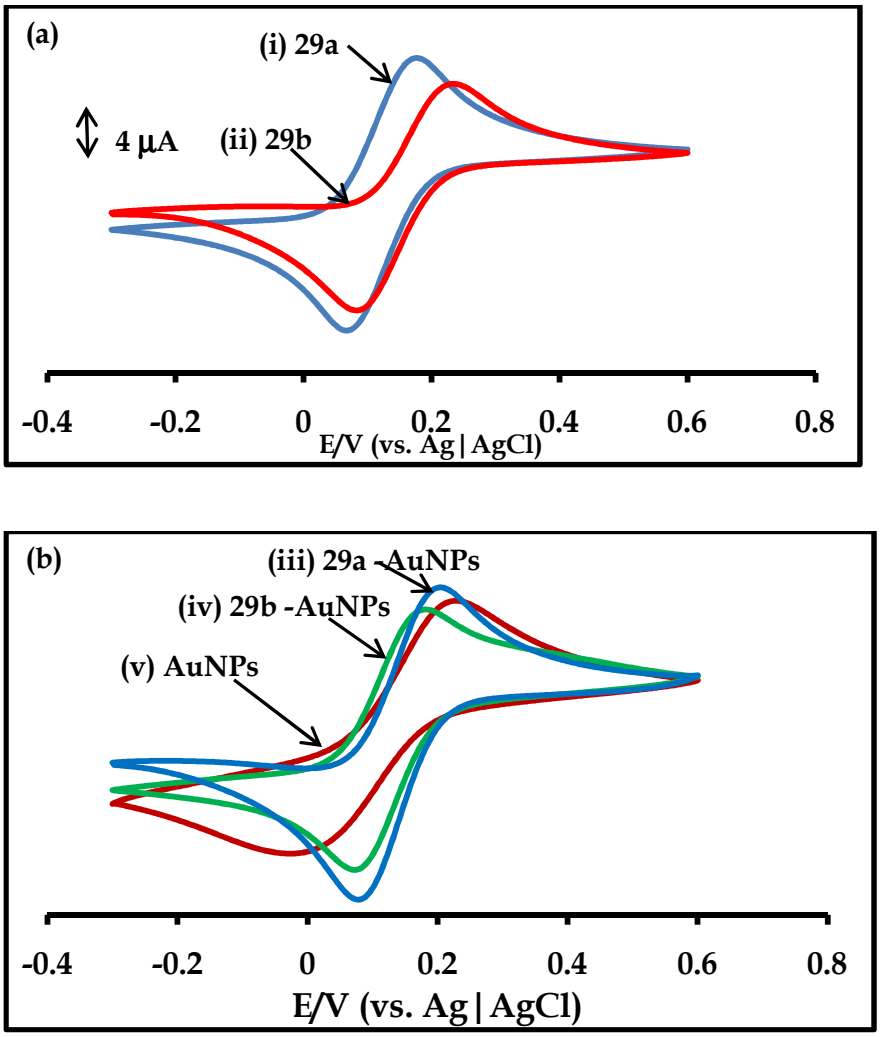

Figure 6.8: Cyclic voltammograms of (a) (i) 29a, (ii) 29b; (b)(iii) 29a-AuNPs, (iv) 29b-AuNPs, (v) AuNPs in 1 x 10^{-3} L^{-1} $K_3[Fe(CN)_6]$ containing 0.1 mol L_{-1} KCl.

For **29b** (containing longer chain than **29a**), slower electrode kinetics were observed when adsorbed onto Au electrode compared to **29a**, but improved in the presence of

AuNPs. It is possible that the long alkyl chain in **29b** affects its ability to absorb onto the electrode compared to **29a**. The surface coverage values were determined as described above and using Eqs. 6.1 and 6.2. The surface coverage values for TaPc complexes and their conjugates ranged from 1.98 x 10^{-10} to 9.94 x 10^{-10} mol cm^{-2}, Table 6.2. An increase in the surface coverage values after conjugation with AuNPs is observed (Table 6.2) thus confirming the success of conjugation. These values are larger than 1 x 10^{-10} mol cm^{-2} suggesting that the films were more than monolayer surfaces.

Shown in Fig. 6.9 are Nyquist plots for selected MPcs and AuNPs, **29a, 29a-**AuNPs, **29b** and **29b-**AuNPs modified Au disk electrodes. The Nyquist plots of all the modified electrodes resemble the characteristic semi-circle pattern (as a result of barrier to the interfacial electron-transfer) followed by a straight line in the low frequency region (the Warburg line) [129].

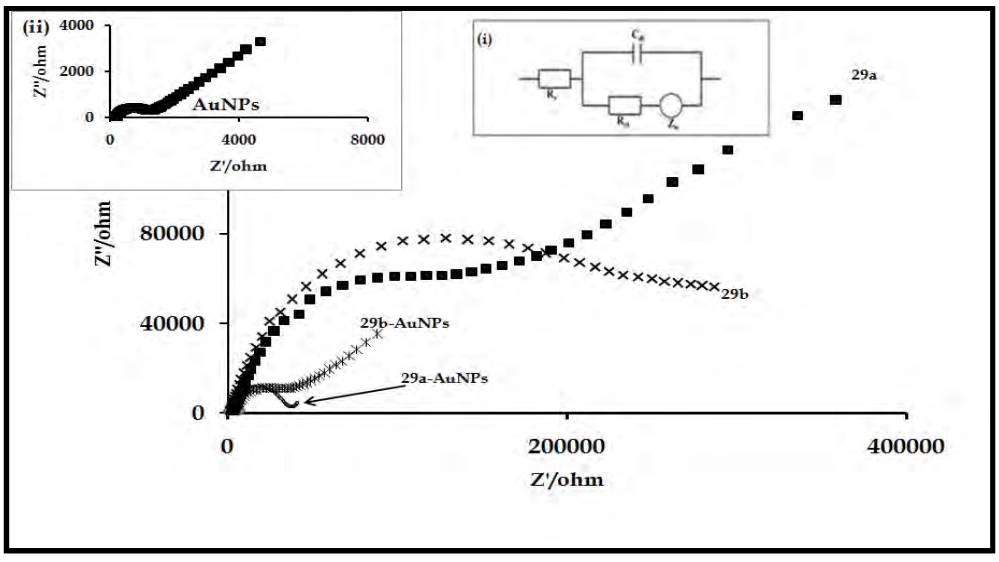

Figure 6.9: Nyquist plots for bare and AuNPs, 29a, 29a-AuNPs, 29b, and 29b-AuNPs modified Au electrodes; in 1 x 10^{-3} mol L^{-1} $[Fe(CN)_6]^{3-/4-}$ in 0.1 mol L-1M KCl.

The R_{CT} values for AuNPs for complexes **29a** and **29b** are 0.72 and 1.84 kΩ, respectively, Table 6.2. The values increased for the **29a-**AuNPs **a**nd **29b-**AuNPs**,** showing more resistance and decreased electrode kinetics. Complex **29a** shows lower R_{CT} compared to **29b**, confirming cyclic voltammetry (CV) studies which showed **29a** to have better electrode kinetics than **29b**. The *n* values were less than 1 suggesting that the electrodes are not ideal capacitors.

6.1.2.3. 28-SWCNT conjugates

These studies were only done for complexes **28** and **29a** as they showed the best catalytic activity for BPA detection. Fig. 6.10(a) shows the cyclic voltammogram of **28**-SWCNT in pH 12 phosphate. A broad peak starting at ~ 0.4 was observed and can be attributed to the oxidation of complex **28**.

To probe whether the **29a** (or **28**)-SWCNT formed a 'film' on the gold electrode surface, the inhibition of faradaic processes associated with the bare gold were studied, Fig. 6.10(b) in 1 x 10^{-3} mol L^{-1} $K_3[Fe(CN)_6]$ containing 0.1 mol L^{-1} KCl. The inset to Fig. 6.10(b) shows the cyclic voltammograms of bare gold electrode (solid line) and SWCNT (dashed line) also in 1 x 10^{-3} mol L^{-1} $K_3[Fe(CN)_6]$ containing 0.1 mol L^{-1} KCl. There is a larger increase in ΔE value on SWCNT and **29a**-SWCNT with a much distorted shape, showing slow electrode kinetics on these electrodes.

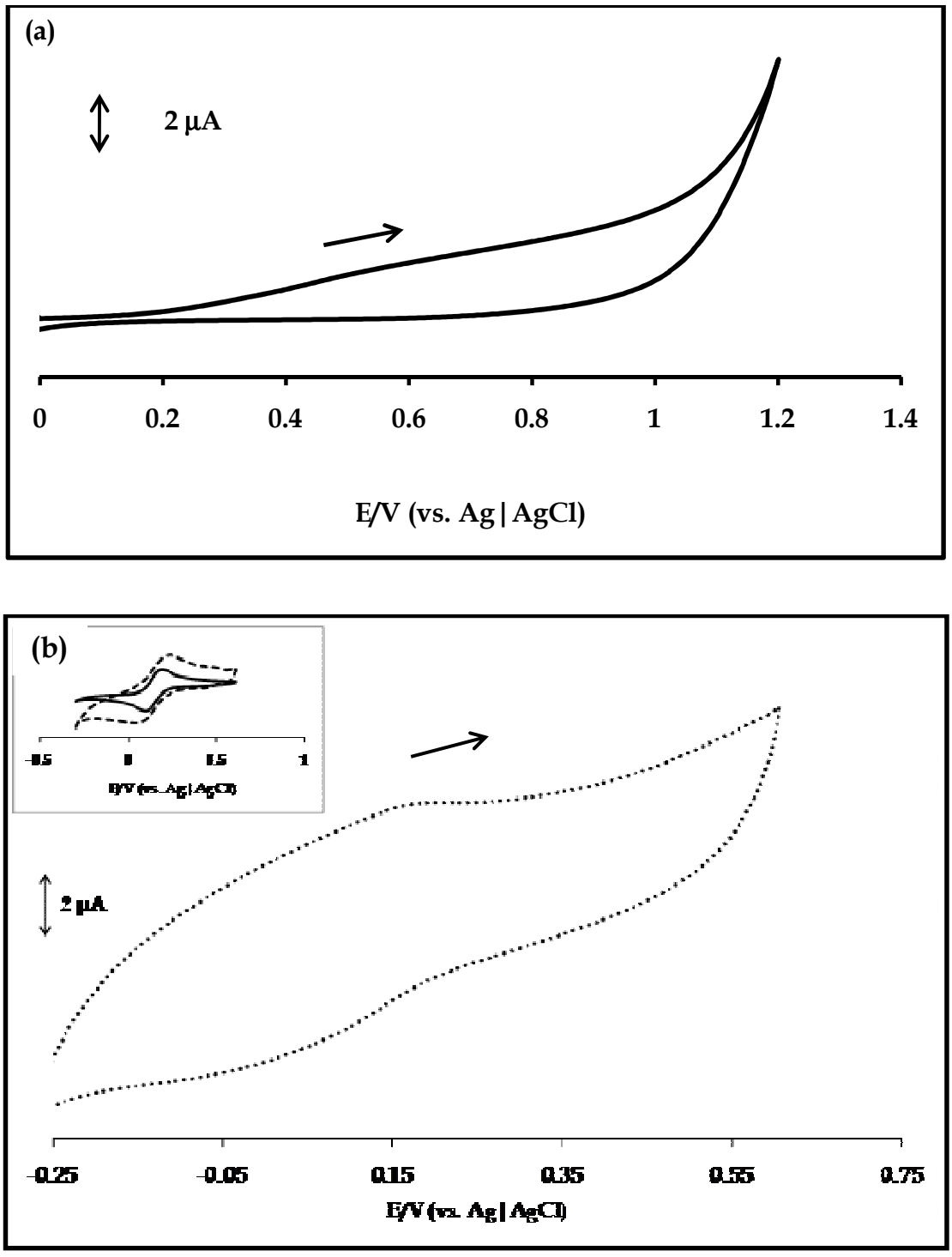

Figure 6.10: Cyclic voltammograms of adsorbed (a) 28-SWCNT in pH 12 phosphate buffer and (b) adsorbed 29a-SWCNT in 1 x 10^{-3} mol L^{-1} $K_3[Fe(CN)_6]$ containing 0.1 mol L^{-1} KCl. Insert bare Au bulk electrode (solid line), and SWCNT (dashed line) in 1 x 10^{-3} mol L^{-1} $K_3[Fe(CN)_6]$ containing 0.1 mol L^{-1} KCl. Scan rate = 50 mVs^{-1}.

Surface coverage values were determined using Eqs. 6.1 and 6.2 and by integrating the peak under ~ 0.4 V peak to get charge (Q). Table 6.3 summerises the surface coverage values for SWCNTs and TaPc-SWCNTs modified electrodes. An increase in the surface coverage of TaPc-SWCNTs is seen and the coverages were more than a typical monolayer value. The surface coverage value for SWCNTs alone, Table 6.3, was slightly lower than that of AuNPs.

Table 6.3: Surface coverage values for selected TaPc complexes and their SWCNTs conjugates; and BPA detection potentials.

Electrode	**Surface coverage (Γ, mol cm^{-2})**
SWCNTs	1.88 x 10^{-10}
28	1.54 x 10^{-10}
28-SWCNTs	3.39 x 10^{-10}
29a	1.98 x 10^{-10}
29a-SWCNT	2.55 x 10^{-10}

6.1.3. TiPc and VPc-AuNPs conjugates

Fig. 6.11 shows cyclic voltammogram of adsorbed complexes **24** and **24-**AuNPs, **25**-AuNPs and **26**, **27**, **27**-AuNPs on Au disk. The gold oxidation and reduction peaks for the titanium complexes and their AuNPs conjugates {Fig. 6.11(a)} were seen at ~ 0.43 V and -0.14 V, respectively. In both the presence and absence of AuNPs, for both complexes **24** and **25**, Fig. 6.11(a), two couples, although not too pronounced for complex **24**, at – 0.75 V and -1.02 V were observed. In

comparison to solution electrochemistry, the peaks at ~ -0.75 V can be attributed to $Ti^{IV}Pc^{-2}/Ti^{III}Pc^{-2}$. No reduction processes were observed for adsorbed VPc complexes and their AuNPs conjugates, Fig 6.11(b).

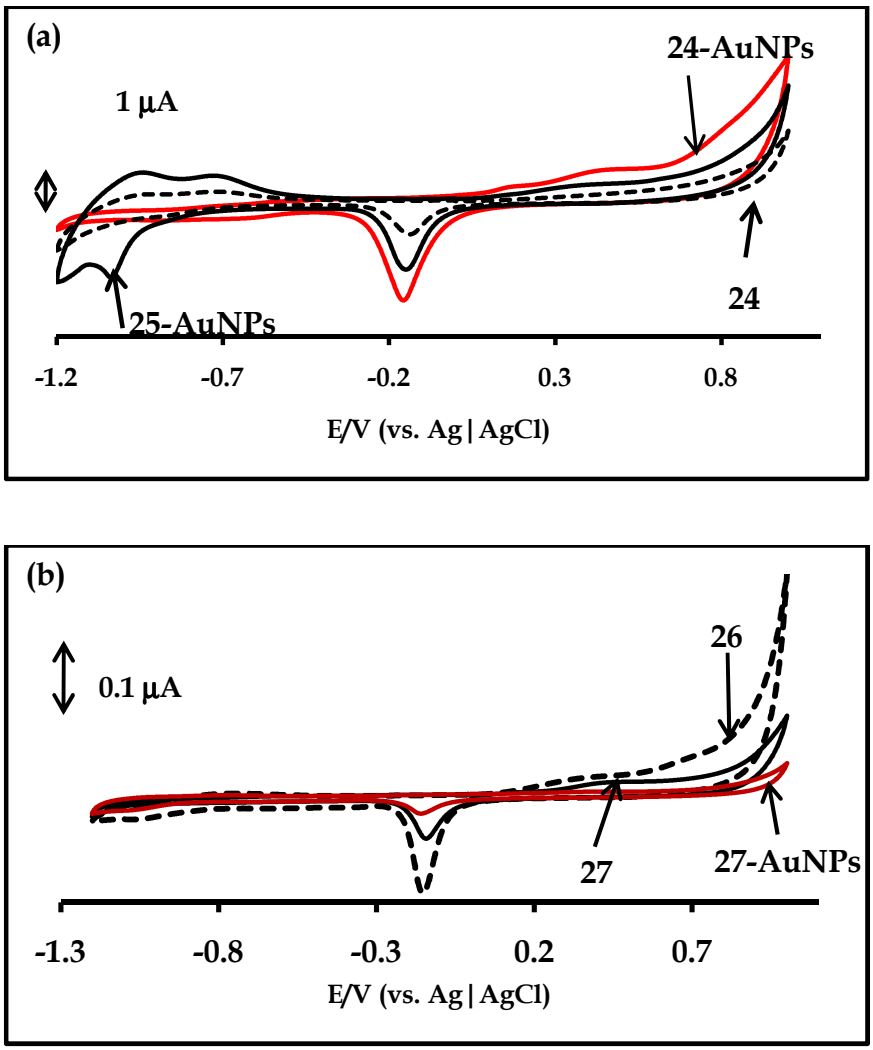

Figure 6.11: Cyclic voltammograms of (a) complexes 24, 24-AuNPs and 25-AuNPs and (b) complexes 26, 27 and 27-AuNPs.

The surface coverage values for TiPc and VPc modified electrodes listed in Table 6.4 were determined following methods described earlier and Eqs. 6.1 and 6.2. A significant increase in the surface coverage on introducing AuNPs was observed and

the values showed multilayer coverage as they were more than the expected for monolayer coverage.

Table 6.4: Surface coverage values for selected TiPc and VPc complexes and their AuNPs conjugates; and BPA detection potentials.

Electrode	**Surface coverage (Γ, mol cm^{-2})**
AuNPs	2.87 x 10^{-10}
24	2.29 x 10^{-10}
24-AuNPs	3.54 x 10^{-10}
25	3.31 x 10^{-10}
25-AuNPs	6.63 x 10^{-10}
26	1.87 x 10^{-10}
26-AuNPs	3.40 x 10^{-10}
27	2.46 x 10^{-10}
27-AuNPs	6.25 x 10^{-10}

6.2. Electrocatalysis of BPA

6.2.1. NiTAPc polymers

Fig. 6.12(a) shows the cyclic voltammograms of 2 x 10^{-3} mol L^{-1} BPA in pH 12 phosphate buffer (which was prepared from Na_2HPO_4 and NaOH) on *poly*-n-Ni(OH)NiTAPc (containing O-Ni-O bridges, where n is the number of polymerization scans).

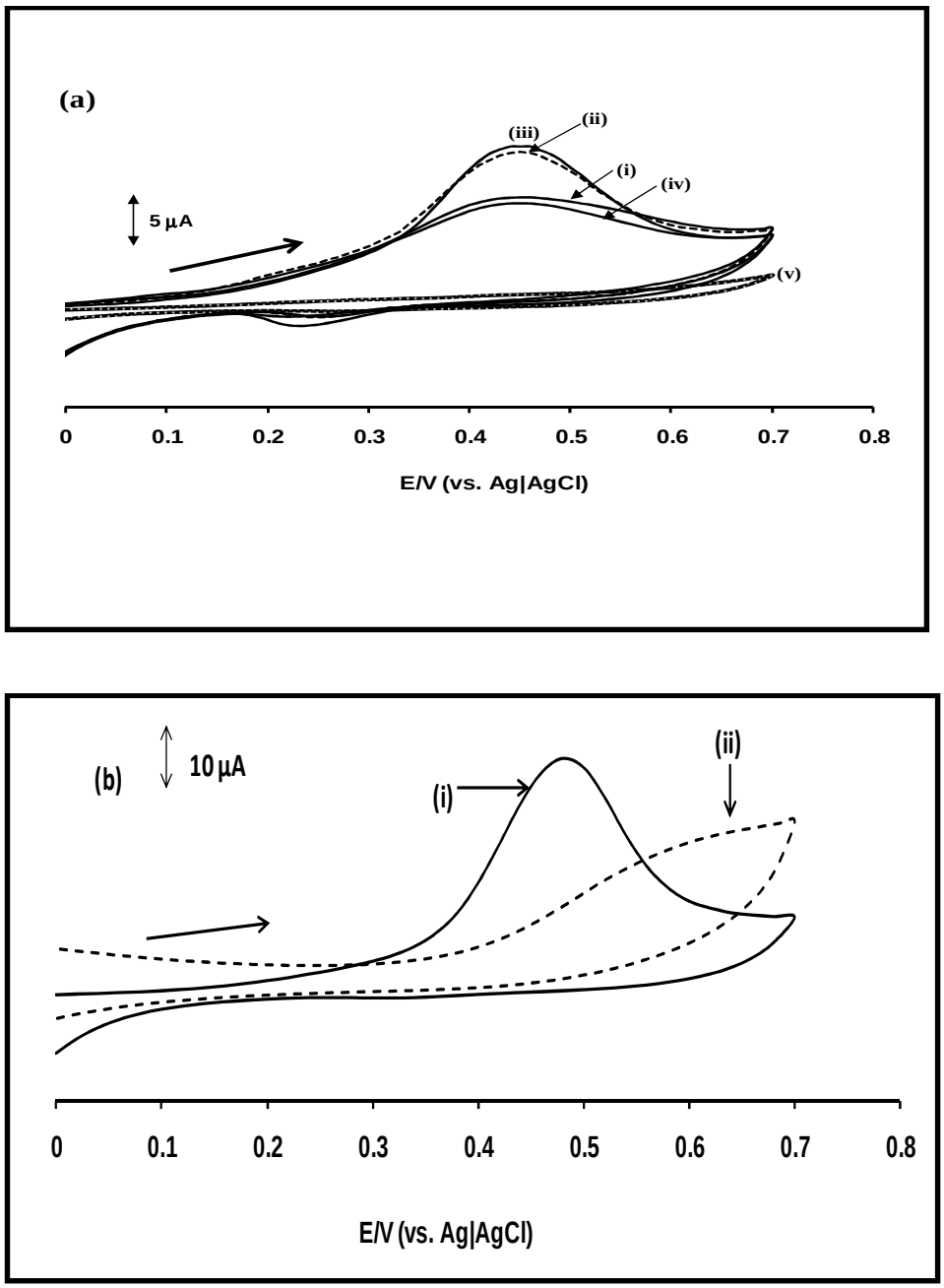

Figure 6.12: Cyclic voltammograms in 2 x 10^{-3} mol L^{-1} BPA in pH 12 phosphate buffer: (a) (i) *poly*-30-Ni(OH)NiTAPc, (ii) *poly*-50-Ni(OH)NiTAPc, (iii) *poly*-70-Ni(OH)NiTAPc, (iv) *poly*-90-Ni(OH)NiTAPc, (iv) bare gold electrode; (b) of *poly*-Ni(OH)TAPc (i) and *poly*-NiTAPc (ii) modified electrodes. Scan rate: 100 mV s^{-1}.

As shown in Fig 6.12(a), the modified electrodes showed peaks for BPA oxidation, indicating that the NiPc species catalyses the oxidation. While there were no BPA peaks on bare Au electrode, the peak for the oxidation of BPA was observed at 0.45 V (vs. Ag|AgCl), Table 6.5, which is 0.41 V vs. saturated calomel electrode

(SCE) (using a -0.045 V correction factor [221]). This value is slightly less positive than the value of 0.45 V vs. SCE obtained on CoPc-carbon paste electrode (CPE) [137]. However, since no oxidation peak for BPA is observed on bare Au electrode in the current work, the detection of this species is more convenient compared to its detection on CPE. The return peak near 0.28 V in Fig. 6.12(a) is attributed to the reduction of the oxidation products of BPA. It is expected that a thicker film should be the most sensitive (due to the availability of more catalytic sites). However, this was not the case in this study. It has also been shown before that catalysis by polymerized films is only limited to external layers [233]. *Poly*-70-Ni(OH)NiTAPc was the most sensitive in terms of current towards the oxidation of BPA of all the polymers. This could be explained by the fact that the R_{CT} value of *poly*-70-Ni(OH)NiTAPc showed less resistance, making the polymer more catalytic. Table 6.5 also shows that the largest surface coverage was by *poly*-70-Ni(OH)NiTAPc of all NiTAPc derivatives.

Table 6.5: BPA oxidation parameters by different electrode surfaces at pH 12 unless otherwise stated.

Electrode	Ep (V) vs. Ag|AgCl (BPA oxidation)	Surface coverage (Γ, mol cm-2)
***poly*-NiTAPc**	0.64	-
***poly*-30-Ni(OH)NiTAPc-Au**	0.45	1.79×10^{-10}
***poly*-50-Ni(OH)NiTAPc-Au**	0.45	2.20×10^{-10}
***poly*-70-Ni(OH)NiTAPc-Au**	0.45	5.46×10^{-10}
***poly*-90-Ni(OH)NiTAPc-Au**	0.45	1.11×10^{-10}
AuNPs	0.45 (0.51, pH 7.4)	2.87×10^{-10}
SWCNT	0.20	1.88×10^{-10}
TaPc complexes		
28	0 .22	1.54×10^{-10}
28-AuNPs	0.38	5.25×10^{-10}
28-SWCNT	0.16	3.39×10^{-10}
29a	0.19 (0.41, pH 7.4)	1.98×10^{-10}
29a-AuNPs	0.41 (0.51, pH 7.4)	4.51×10^{-10}
29a-SWCNT	0.19	2.55×10^{-10}
29b	0.26	2.47×10^{-10}
29b-AuNPs	0.41	9.94×10^{-10}
TiPc complexes		
24	0.21	2.29×10^{-10}
24-AuNPs	0.38	3.45×10^{-10}
25	0.14	3.31×10^{-10}
25-AuNPs	0.36	6.63×10^{-10}
VPc complexes		
26	0.20	1.87×10^{-10}
26-AuNPs	0.34	3.40×10^{-10}
27	0.21	2.46×10^{-10}
27-AuNPs	0.35	6.25×10^{-10}

Fig. 6.12(b) demonstrates that *poly*-Ni(OH)TAPc modified electrode (i) shows good catalytic activity to bisphenol A compared to *poly*-NiTAPc modified electrode (ii) without 'O-Ni-O' bridges. This is judged by the fact that *poly*-Ni(OH)TAPc displays less positive potential for bisphenol A detection (0.45 V vs. Ag|AgCl) compared to *poly*-NiTAPc which detected bisphenol A at ~0.62 V vs. Ag|AgCl, Fig. 6.12 (b). Also, a higher peak current in the detection of bisphenol A was obtained on the *poly*-Ni(OH)TAPc (i) relative to *poly*-NiTAPc (ii), Fig. 6.12(b). Furthermore, a sharper and better defined bisphenol A detection peak was displayed by the *poly*-Ni(OH)TAPc (i) relative to *poly*-NiTAPc (ii), Fig. 6.12(b). Compared to the rest of the electrodes in Table 6.5, the oxidation of BPA is less favoured on *poly*-NiTAPc since it shows the most positive potential.

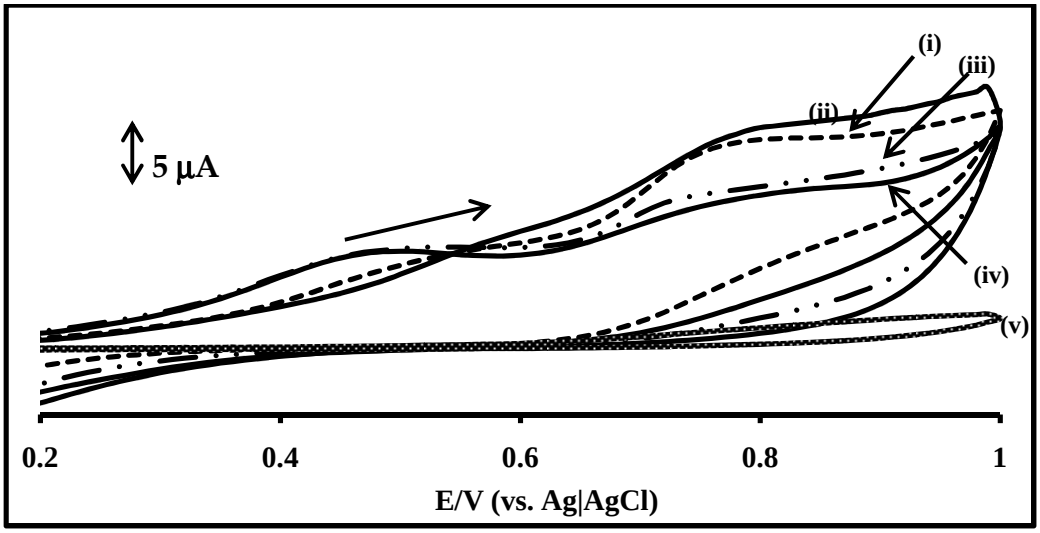

Figure 6.13: Cyclic voltammograms of 2mM PNP in pH 12 phosphate buffer: (i) *poly*-30-Ni(OH)TAPc, (ii) *poly*-50-Ni(OH)TAPc, (iii) *poly*-70-Ni(OH)TAPc, (iv) *poly*-90-Ni(OH)TAPc and (v) bare gold electrode.

Fig. 6.13 shows the cyclic voltammograms of 2 x 10^{-3} mol L^{-1} *p*-nitrophenol (PNP in pH 12 phosphate buffer on *poly*-Ni(OH)TAPc (containing O-Ni-O bridges) for comparison purposes with BPA. There was a significant potential shift (peak at ~0.76

V) for the catalytic oxidation of PNP compared to BPA (peak at 0.45 V). The peak observed at ~0.5 V for PNP catalysis by *poly*-30-Ni(OH)TAPc and *poly*-90-Ni(OH)TAPc is most likely due to Ni^{III}/Ni^{II} in comparison with Fig. 6.2. *Poly*-30-Ni(OH)TAPc and *poly*-50-Ni(OH)TAPc were the most sensitive towards the oxidation of PNP, Fig. 6.13 in terms of current, while, as stated above, *poly*-70-Ni(OH)TAPc was the most sensitive for BPA. There was a decrease in current after *poly*-70-Ni(OH)TAPc for BPA and after *poly*-50-Ni(OH)TAPc for PNP.

The mechanism for the oxidation of BPA is expected to be similar to that proposed for its oxidation on CoPc-CPE [137], **Scheme 6.1**, but catalysed by $Ni^{III}Pc/Ni^{II}Pc$ instead of the corresponding CoPc couple. Catalysis was carried out in basic media where BPA deprotonates (step 1). The catalytic oxidation occurs at potentials where Ni^{III} exits for *poly*-Ni(OH)TAPc, hence it catalyses oxidation of BPA to form radicals (step 3) which subsequently dimerises to form polymers as indicated in steps (4 – 5). For *poly*-NiTAPc, only ring based processes will be involved since, without transformation to Ni-O-Ni bridges, NiPc complexes do not show the Ni^{III}/Ni^{II} couple.

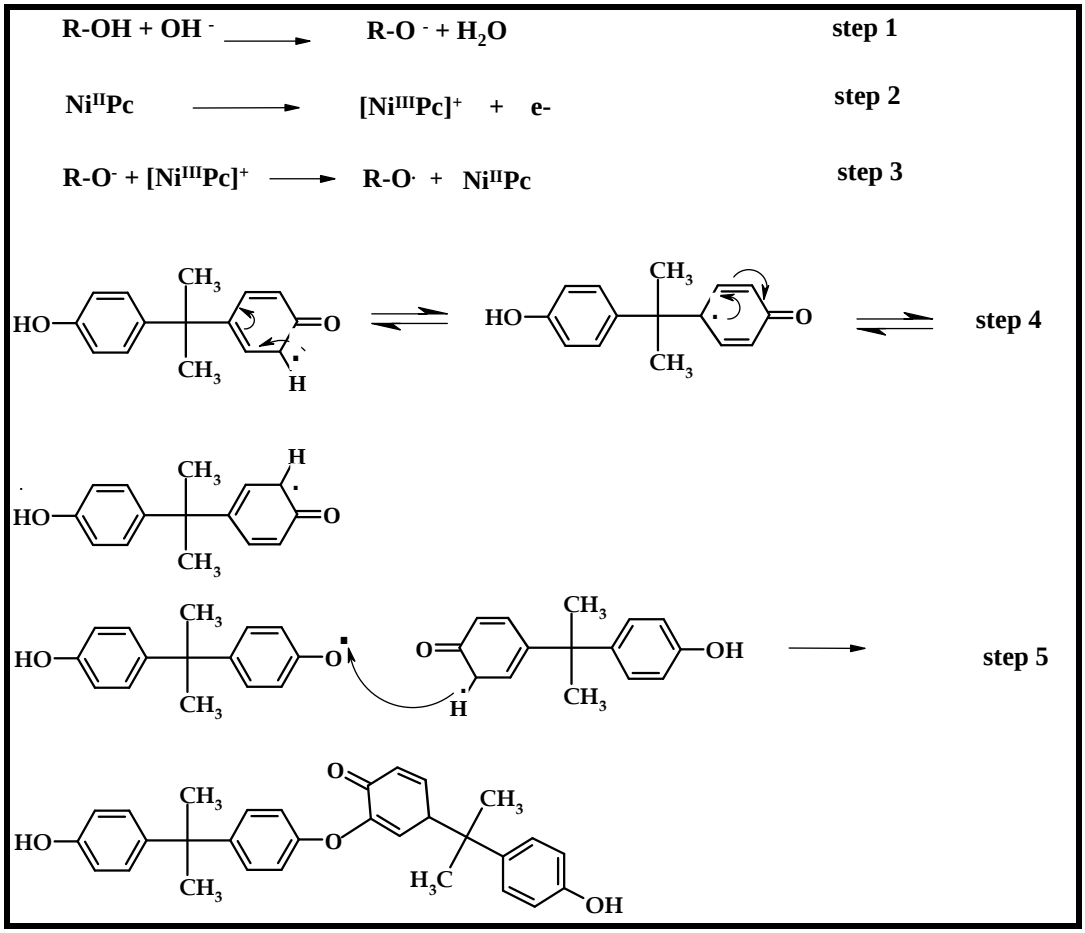

Scheme 6.1: Proposed reaction mechanism for the electrooxidation of BPA, where R (in steps 1 and 3) represents the rest of the BPA molecule.

6.2.2. AuNPs conjugates

6.2.2.1. Octasubstituted TaPc complexes (29a and 29b)

In order to improve the electrocatalytic oxidation of BPA, octasubstituted TaPc complexes (**29a** and **29b**) were employed together with their AuNPs conjugates and will later be compared to tetrasubstituted TiPc and TaPc complexes. The catalytic nature of the modified electrodes is shown in Fig. 6.14. The bare electrode showed no sensitivity towards BPA detection. The Au oxide formation and its stripping are not expected at the potential range shown in Fig. 6.14, thus all the peaks are due to BPA.

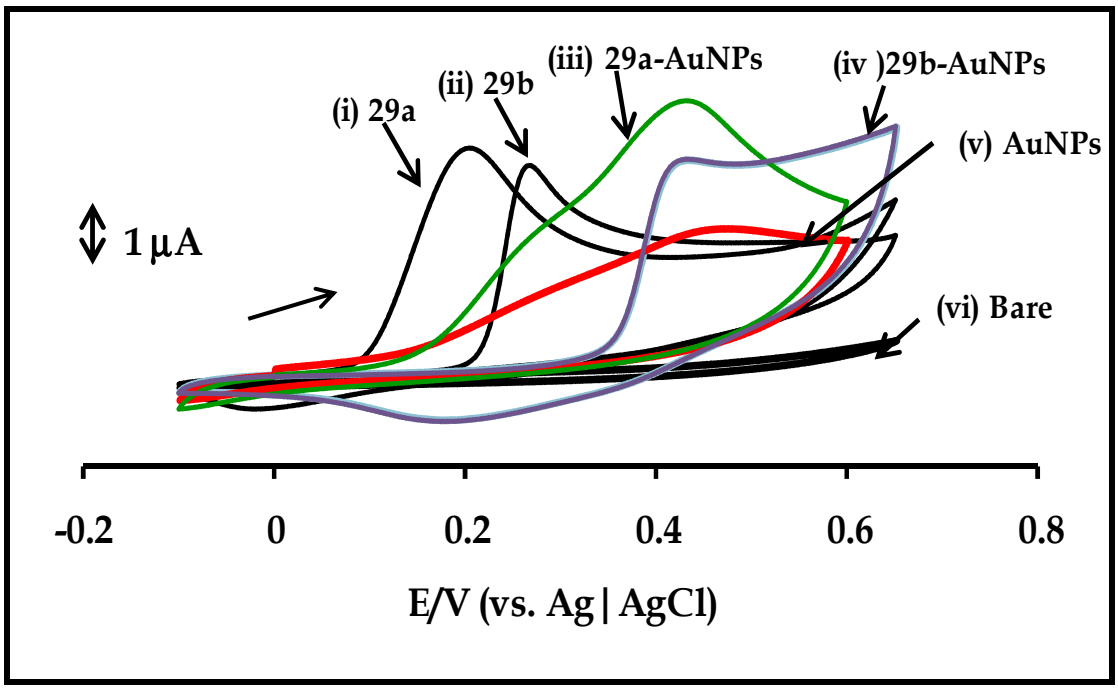

Figure 6.14: Cyclic voltammograms recorded in 7 x 10^{-3} mol L^{-1} BPA in pH 12 phosphate buffer: (i) 29a, (ii) 29b, (iii) 29a-AuNPs, (iv) 29b-AuNPs, (v) AuNPs and (vi) bare gold electrode, at scan rate of 100 mVs^{-1}.

This means that **29a** and **29b** are able to catalyse the oxidation of BPA with high current responses and peaks at 0.19 and 0.26 V, respectively, Table 6.5 at pH 12, were obtained, whereas peaks were not observed for bare. Catalytic behaviour is characterised by an increase in currents and improvement in the potential (that shifts to less positive values during oxidation). For **29a** and **29b**, the potential for BPA detection is lower than obtained on NiTAPc containing 'O-Ni-O' oxo bridges (*poly*-n-Ni(OH)TAPc), CoPc-CPE [137] and MWNTs-CoPc [138] with BPA oxidations peaks at 0.45 V, 0.41 V and 0.58 V, respectively.

Complexes **29a** and **29b** catalysed BPA oxidation at less positive potentials compared to their AuNPs conjugates and AuNPs alone, Table 6.5. The established trend based on shifting of catalytic peak potentials to less positive values is as follows: **29a > 29b**

> **29b-**AuNPs = **29a-**AuNPs > AuNPs**.** The MPc-AuNPs conjugates showed enhanced sensitivity (in terms of current and potential) towards BPA compared to AuNPs alone. This indicates the involvement of TaPc complexes in catalysis. Nanoparticles are quite different from their bulk materials [154]. Their electronic, optical, and catalytic properties originate from their quantum dimensions. AuNPs function as "electron antennae"; they tunnel electrons between the electrodes and analyte [243, 244]. Given the fact that the 'bulk' Au electrode was not sensitive towards the oxidation of BPA, it was interesting to see that Au in its nanosize could catalyse the oxidation of BPA. This thus confirms that indeed AuNPs have extra-ordinary catalytic properties. In terms of surface coverage, **29b**-AuNPs and **29a-**AuNPs gave large values compared to **29a** or **29b** alone, Table 6.5, hence it would be expected that they would give the largest current enhancement, however Fig. 6.14 does not show much difference in BPA currents on the electrodes, suggesting that it is only the top layer which is involved in catalysis as reported before for MPc polymers [233].

The biological effects of BPA are quite detrimental hence the interest in investigating the catalytic nature of these electrodes at pH 7.4 (physiological pH for mammals). Complex **29a** exhibited the best results at pH 12, in terms of shifting the potential to less positive values, Table 6.5. It was therefore chosen together with its conjugate (**29a-**AuNPs) and AuNPs for detection at pH 7.4 phosphate buffer. Fig. 6.15 shows the cyclic voltammograms of BPA in pH 7.4 phosphate buffer, on complex **29a**, (ii) **29a-**AuNPs, (iii) AuNPs and (iv) bare electrode.

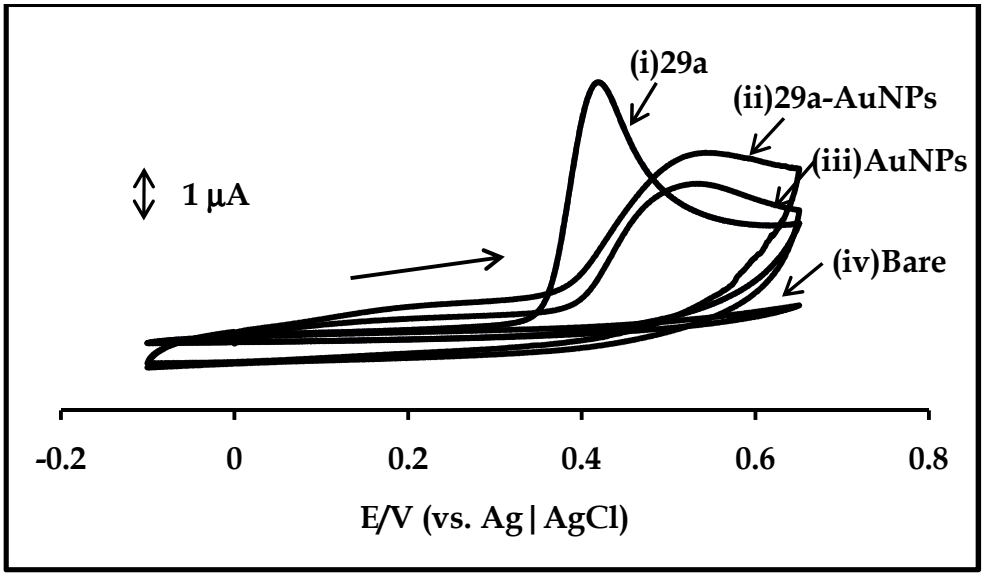

Figure 6.15: Cyclic voltammograms recorded in 7 x 10^{-3} mol L^{-1} BPA in pH 7.4 phosphate buffer: (i) 29a, (ii) 29a-AuNPs, (iii) AuNPs and (iv) bare gold electrode, at scan rate 100mVs^{-1}.

The potentials were however more positive compared to electrocatalytic oxidation at pH 12, Table 6.5. Complex **29a** was more sensitive, as shown by enhanced peak currents and lower potential, compared to **29a-**AuNPs and AuNPs. The sharp rise in current for **29a** and **29b** for both pH 7.4 and 12, confirms good catalytic activity.

6.2.2.2. Tetrasubstituted complexes

The electrocatalytic investigation of BPA was carried on using the tetrasubstituted newly synthesised TiPc, VPc and TaPc complexes and their AuNPs conjugates. Figs. 6.16 and 6.17 show the CVs for the electrocatalytic oxidation of BPA in basic media, pH 12 phosphate buffer. The Au oxide formation and its stripping are not expected at the potential range shown in these figure, thus all the peaks are due to BPA oxidation. The bare electrode, Fig. 6.17(iv), showed no detection of BPA, as already stated.

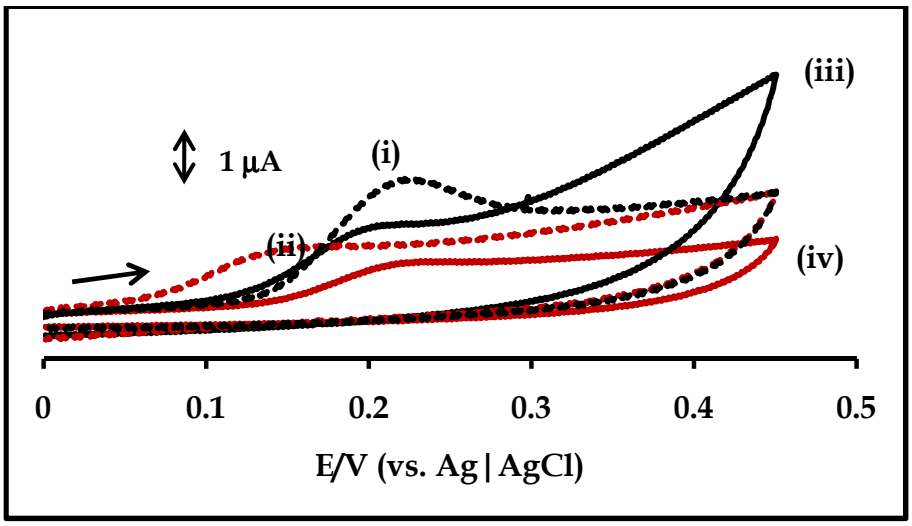

Figure 6.16: Cyclic voltammograms recorded in 7 x 10^{-3} mol L^{-1} BPA in pH 12 phosphate buffer: (i) 28, (ii) 25, (iii) 26 and (iv) 27 at scan rate 100mVs^{-1}.

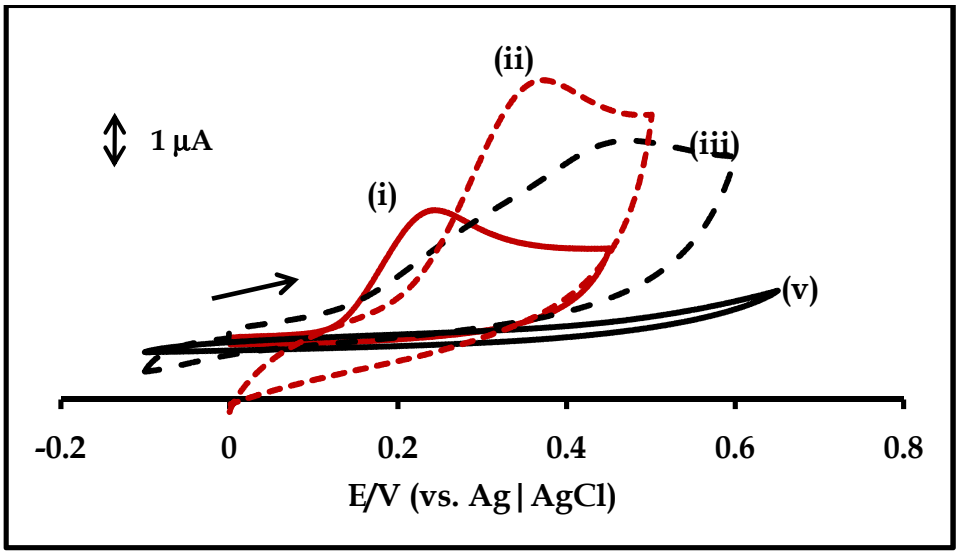

Figure 6.17: Cyclic voltammograms recorded in 7 x 10^{-3} mol L^{-1} BPA in pH 12 phosphate buffer: (i) 28, (ii) 28-AuNPs, (iii) AuNPs, (iv) bare gold electrode, at scan rate 100mVs^{-1}.

The TiPc complexes (**24** and **25**) showed good catalytic oxidation with in terms of potentials with complex **25** having the lowest oxidation potential of 0.14 V, Fig. 6.16 and Table 6.5. VPc complexes (**26** and **27**) oxidised BPA at 0.20 and 0.21 V, repectively and the TaPc complex (**28**) oxidation potential was at 0.22. However complex **28** showed the best catalysis in terms of current as shown in Fig. 6.16(i)

compared to complexes **25**, **26** and **27**. The TiPc, VPc and TaPc complexes were not very sensitive in the abscence of AuNPs (Figs. 6.17) in terms of current. However, TaPc (**28**) gave larger currents relative to TiPc and VPc complexes, Fig. 6.16. On conjugating complex **28** to AuNPs, Fig 6.17, there was a drastic increase in current signifying importance of AuNPs in enhancing sensitivity. The same increase in current was observed for complex **25**, **26** and **27**. On comparing different MPcs in this work, they were all more or less in the same potential range for BPA oxidation with TiPc complex (**24**) showing the best catalysis in terms of potentials, Table 6.5. In all cases, there was a large increase in oxidation potential for MPc-AuNPs, showing resistance to oxidation in the presence of AuNPs, Table 6.5. All the detection potentials were again improved compared to NiTAPc containing 'O-Ni-O' bridges.

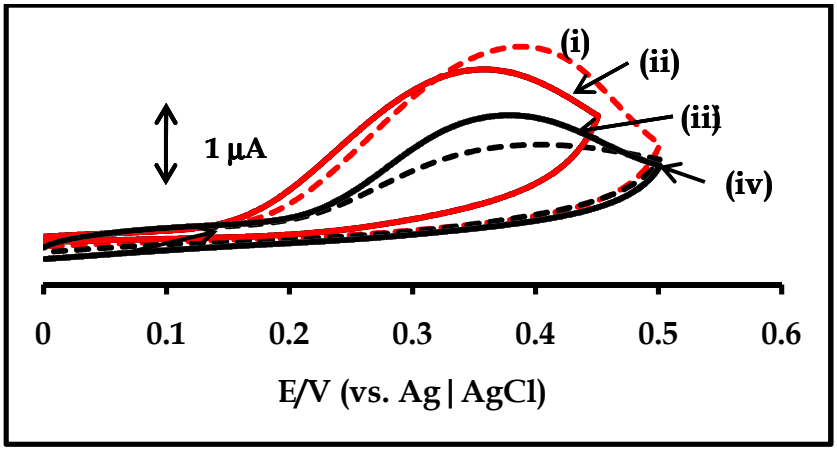

Figure 6.18: Cyclic voltammograms recorded in 7 x 10^{-3} mol L^{-1} BPA in pH 12 phosphate buffer: (i) 28-AuNPs, (ii) 27-AuNPs, (iii) 25-AuNP, and (iv) 24-AuNPs, at scan rate 100mVs^{-1}.

Comparing the MPc-AuNPs electrodes, Fig. 6.18, **28**-AuNPs showed large currents compared to the rest of the tetra substituted complexes. TiPc-AuNPs conjugates (**24**-AuNPs and **25**-AuNPs) showed the least currents.

6.2.3. TaPc - SWCNT conjugates

TaPc complexes (**28** and **29a**) were chosen as representatives of tetra- and octasubstituted complexes studied in this work. Complex **28** was chosen because it showed good catalytic activity towards BPA oxidation (Fig. 6.16) in terms of current compared to the rest of the tetrasubstituted complexes and **29a** due to lower potential value compared to **29b**, Table 6.5. Fig. 6.19 which compares cyclic voltammetric responses of (i) **29a**-SWCNT, (ii) **28**-SWCNT and (iii) SWCNT towards the oxidation of BPA. The oxidation potential for the three species were more or less the same although the oxidation potential by **28**-SWCNT was slightly less at 0.16 V. In terms of sensitity, **29a**-SWCNT was by far the most sensitive toward BPA thus making it a better catalyst. It was interesting to note that the SWCNT alone improved BPA oxidation significantly Fig 6.19 {insert (iii)}, compared to bare electrode which shows no BPA peak.

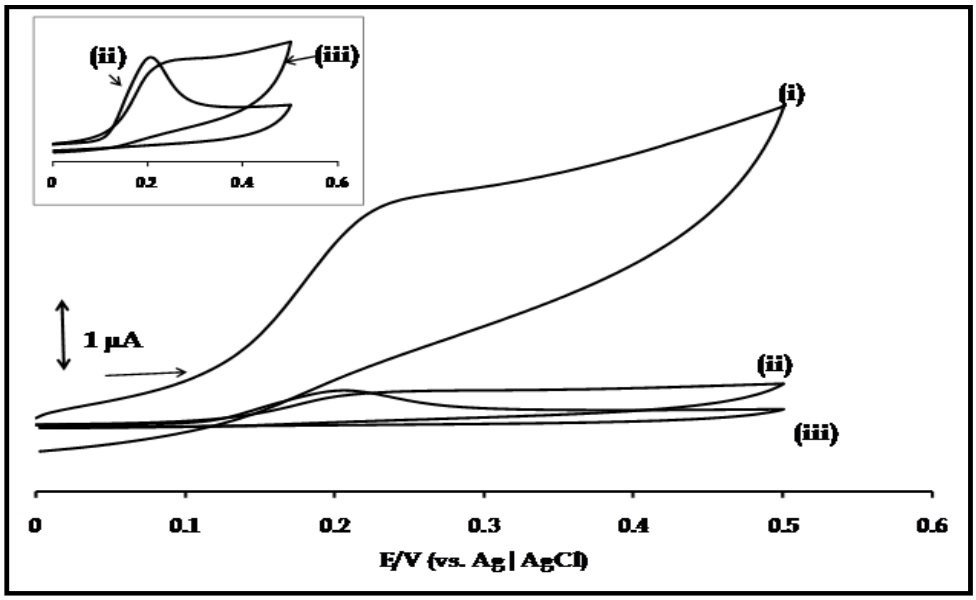

Figure 6.19: Cyclic voltammograms recorded in 7 x 10^{-3} mol L^{-1} BPA in pH 12 phosphate buffer: (i) 29a-SWCNT, (ii) 28-SWCNT and (iii) SWCNT. Insert: (ii) 28-SWCNT and (iii) SWCNT, at scan rate 100mVs^{-1}.

6.2.4. Mechanism

The mechanism (in basic media) for the oxidation of BPA is expected to be similar to that proposed for its oxidation on CoPc-CPE [137] and shown **Scheme 6.1**, but ring based catalysis. Catalysis was carried out in basic media where BPA deprotonates (step 1). The broad peaks due to ring oxidation observed in Figs. 6.6, 6.7, 6.10 and 6.11 are in the range for the oxidation of BPA, hence the oxidation was catalysed by the complexes (step 3), following their oxidation in step 2. The BPA oxidation subsequently dimerize to form polymers as indicated in steps (step 4).

Scheme 6.2: Proposed reaction mechanism for the electrooxidation of BPA, where R (in steps 1, 3 and 4) represents the rest of the BPA molecule and M represents the different metals Ta^{V}, Ti^{IV} or V^{IV}.

6.2.5. Electrode stability

Phenolic type compounds are known for fouling electrode surfaces. This is due to the fact that when they are oxidized, phenol polymerization and hydroquinone formation take place [142, 143] and thus block the electrode surface.

6.2.5.1. NiTAPc polymers

Passivation is indicated by a decrease in current with scan number. Fig. 6.20 shows a decrease in current responses of BPA and PNP cyclic voltammetry scan number on poly-n-Ni(OH)TAPc. There is a decrease in current after the first scan followed by stabilization of the current. The electrodes could be partially regenerated by rinsing in pH 7.4 buffer, with percentage recovery values that ranged from 16 to 72 % for BPA and 65 to 91 % for PNP, Table 6.6.

Table 6.6: Percentage recovery values for the detection of BPA and PNP by *poly*-n-Ni(OH)NiTAPc on a Au electrode.

Electrode	**% Recovery for BPA**	**% Recovery for PNP**
***Poly*-30-Ni(OH)NiTAPc-Au**	16	76
***Poly*-50-Ni(OH)NiTAPc-Au**	25	91
***Poly*-70-Ni(OH)NiTAPc-Au**	61	91
***Poly*-90-Ni(OH)NiTAPc-Au**	72	65

It was also observed that percentage recovery values increased with increase in polymer thickness, Table 6.6 for BPA. These studies showed that it was easier to regenerate surfaces with PNP oxidation products than those of BPA.

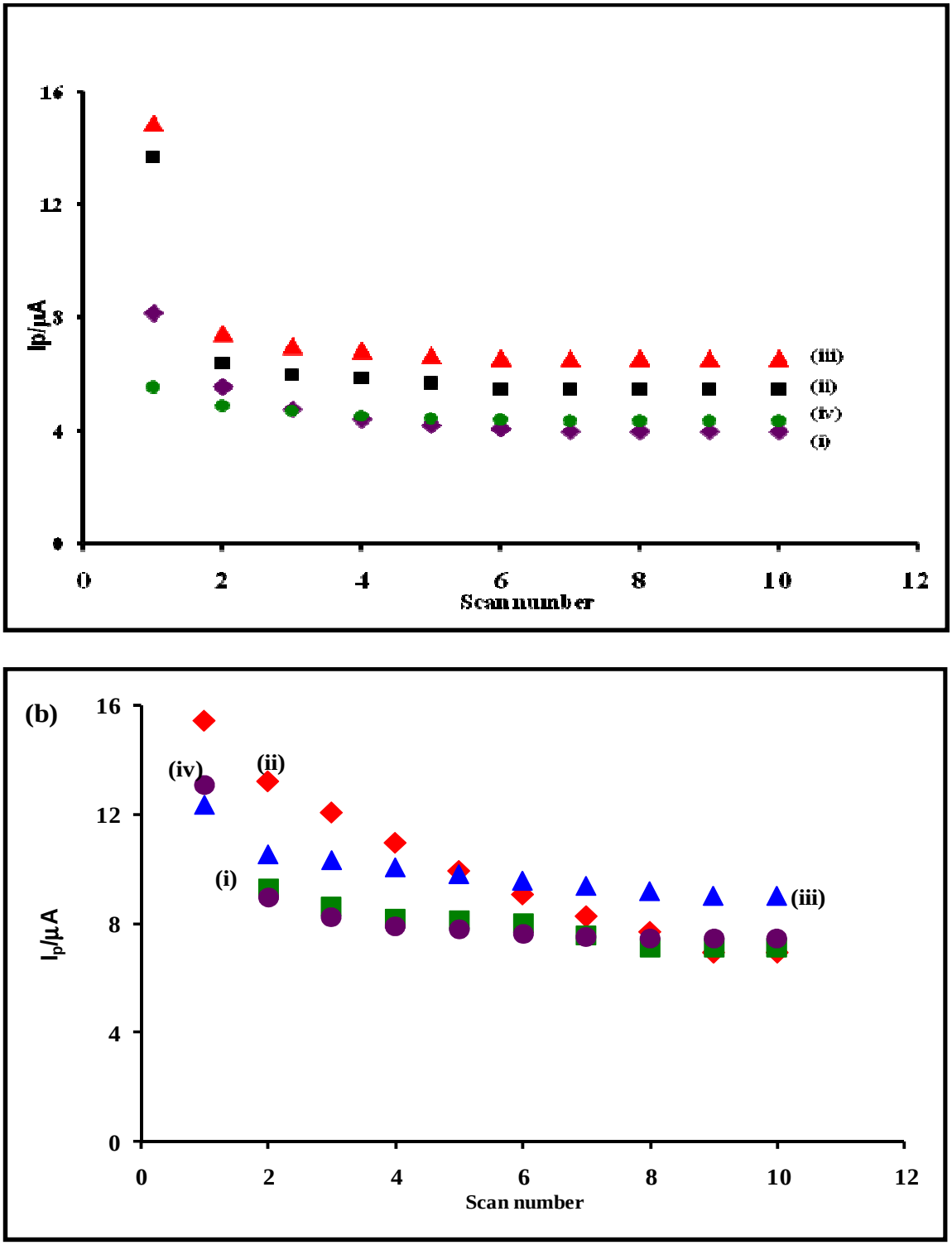

Figure 6.20: The variation of peak currents with scan number for the voltammetric responses of 2 x 10^{-3} mol L^{-1} (a) BPA and (b) PNP at (i) *poly*-30-Ni(OH)NiTAPc, (ii) *poly*-50-Ni(OH)NiTAPc, (iii) *poly*-70-Ni(OH)NiTAPc, (iv) *poly*-90-Ni(OH)NiTAPc modified gold electrode, scan rate 100 mVs^{-1}.

6.2.5.2. AuNPs TaPc conjugates

As stated above, passivation is indicated by a drastic decrease in current, shown Fig. 6.21 (a) where (i) shows the first BPA electrooxidation scan and (ii) shows passivation after the 8th scan for complexe **29a**. The electrodes could be partially regenerated by rinsing in a fairly concentrated solution of NaOH, shown in Fig. 6.21 (b), where (i) is the first scan and (ii) the cyclic voltammogram of BPA after rinsing in NaOH.

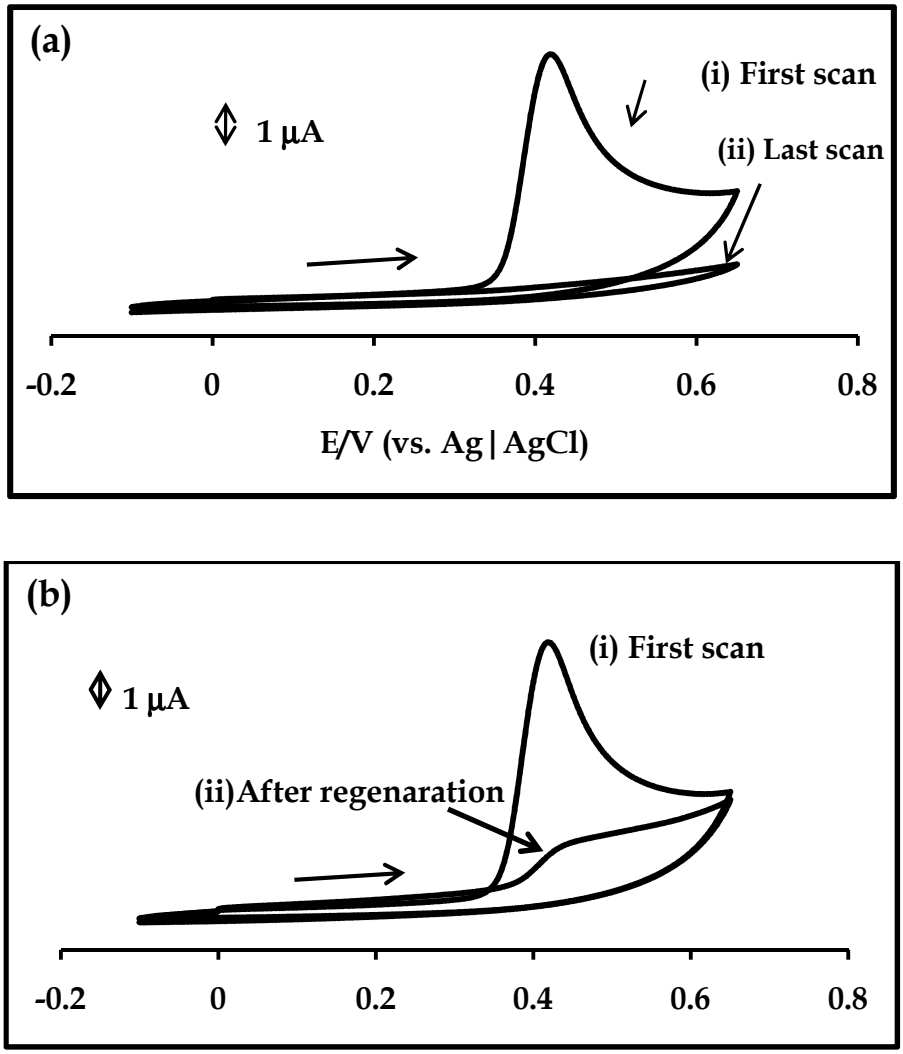

Figure 6.21: (a) Cyclic voltammograms recorded in 7 x 10^{-3} mol L^{-1} BPA in pH phosphate buffer (on 29a) showing (i) the first and the (ii) last 8th scan (b) voltammograms recorded in 7 x 10^{-3} mol L^{-1} BPA in pH 7 phosphate buffer showing (i) the first scan and (ii) the effects of regeneration. Scan rate: 100 mVs^{-1}.

As shown in Fig. 6.22(a), there was a drop in I_p with increase in scan number, indicating passivation, on both **28**-AuNPs and **28**. In the presence of AuNPs, however, the drop in current was gradual, implying that the presence of AuNPs reduces passivation. The electrodes could be partially regenerated by rinsing in a rather concentrated solution of NaOH (2.0 M) as shown in Fig. 6.22(b) which is illustrative of recovery, where (i) is the first scan and (ii) is the cyclic voltammogram of BPA after rinsing in NaOH for complex **28**. The recovery was roughly 22 %.

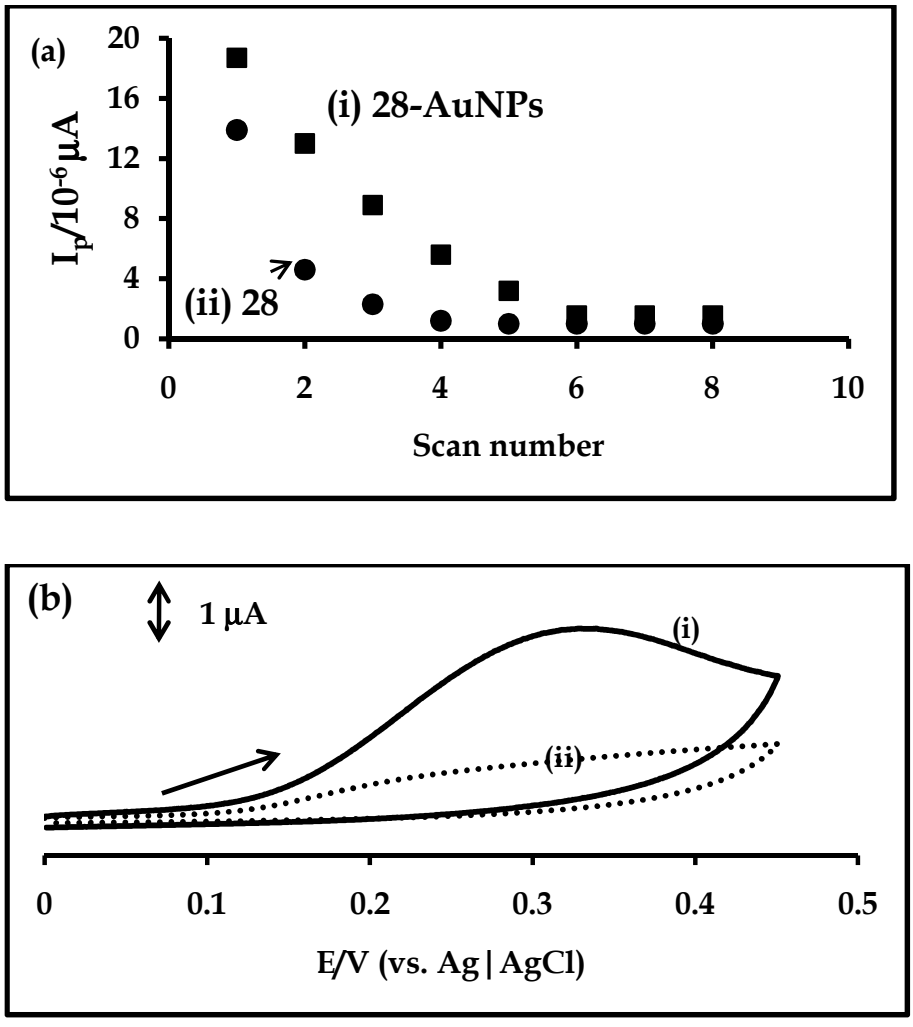

Figure 6.22: Variation of peak current with scan number for the voltammetric responses in 7 x 10^{-3} mol L^{-1} BPA in pH 12 phosphate buffer for (a) (i) 28-AuNP and (ii) 28, and (b) are the (i) first scan and (ii) the scan following re-use and rinsing in concentrated NaOH (2.0 M), respectively.

6.2.5.3. TaPc SWCNT conjugates

Fig. 6.23(a) showed virtually no passivation on **29a**-SWCNTs as opposed to **28**-AuNPs, Fig. 6.22(a). This reiterates the fact mentioned earlier that less fouling is experienced in the presence of SWCNTs. Furthermore, recovery by rinsing in concentrated NaOH solution was almost up to ~ 98 % {Fig. 6.23(b)}, again proving that SWCNT are remarkable in preventing passivation.

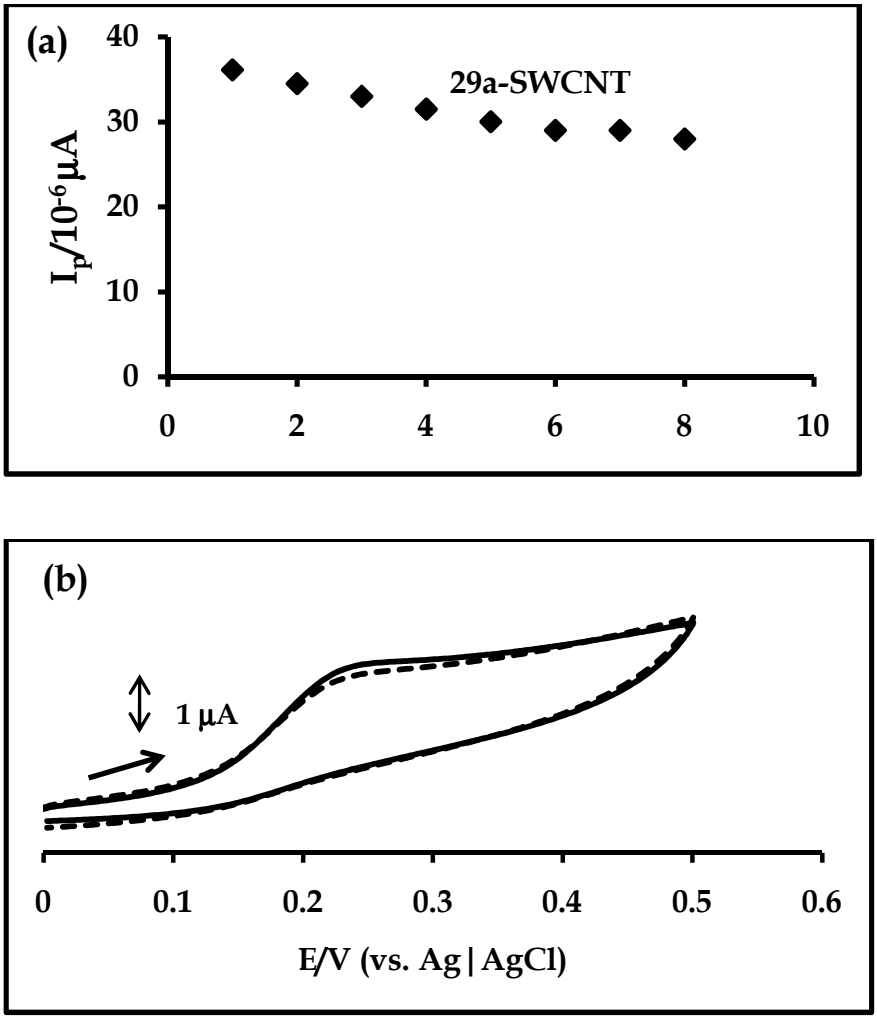

Figure 6.23: Variation of peak current with scan number for the voltammetric responses in 7 x 10^{-3} mol L^{-1} BPA in pH 12 phosphate buffer for (a) (i) 29a-SWCNTS and (b) are the cyclic voltammograms recorded in 7 x 10^{-3} mol L^{-1} BPA for the re-use 29-SWCNT, the first scan (solid line) and the scan following re-use (dotted line) and rinsing in concentrated NaOH, respectively.

6.2.6. Sensivity and limit of detection (LOD) values

The limit of detection (LOD) was obtained, according to literature [233], by first recording the chronoamperometry of the modified electrode in pH 12 buffer. The LoD was then calculated by multiplying the standard deviation of the chronoamperometry current by three and then dividing the result by the gradient of the calibration curve. The MPc complexes that showed the best activty towards BPA (TaPc derivatines) were selected for LOD values and are summerised in Table 6.7.

Table 6.7: Selectivity and limits of detection for the detection of BPA on TaPc complexes and NiTAPc

Electrode modifier	**Sensitivity (**μA mmol^{-1} L^{1} cm^{-2})	**LOD** (mol L^{-1})
***Poly*-70-Ni(OH)TAPc**	6.56 x 10 $^{-6}$	3.68 x 10^{-9}
28	3.21 x 10^{-5}	1.02 x 10^{-10}
28-AuNP	3.30 x 10^{-5}	1.87 x 10^{-10}
28-SWCNT	3.47 x 10^{-4}	1.90 x 10^{-10}
29a	4.20 x 10^{-5}	4.78 x 10^{-10}
29b	1.84 x 10^{-5}	2.76 x 10^{-10}
29a-AuNP	4.29 x 10^{-5}	2.03 x 10^{-10}
29a-SWCNT	2.12 x 10^{-4}	1.16 x 10^{-10}

A linear variation of the electrocatalytic currents plateaus (steady-state currents) with BPA concentrations in the range of 7×10^{-4} to 3×10^{-2} mol L^{-1} for Au *poly*-70-Ni(OH)NiTAPc is shown in Fig. 6.24. The calculated sensitivity (obtained from the slope of the linear plot) was 6.56 × 10^{-6} A mol^{-1} L^{1}.

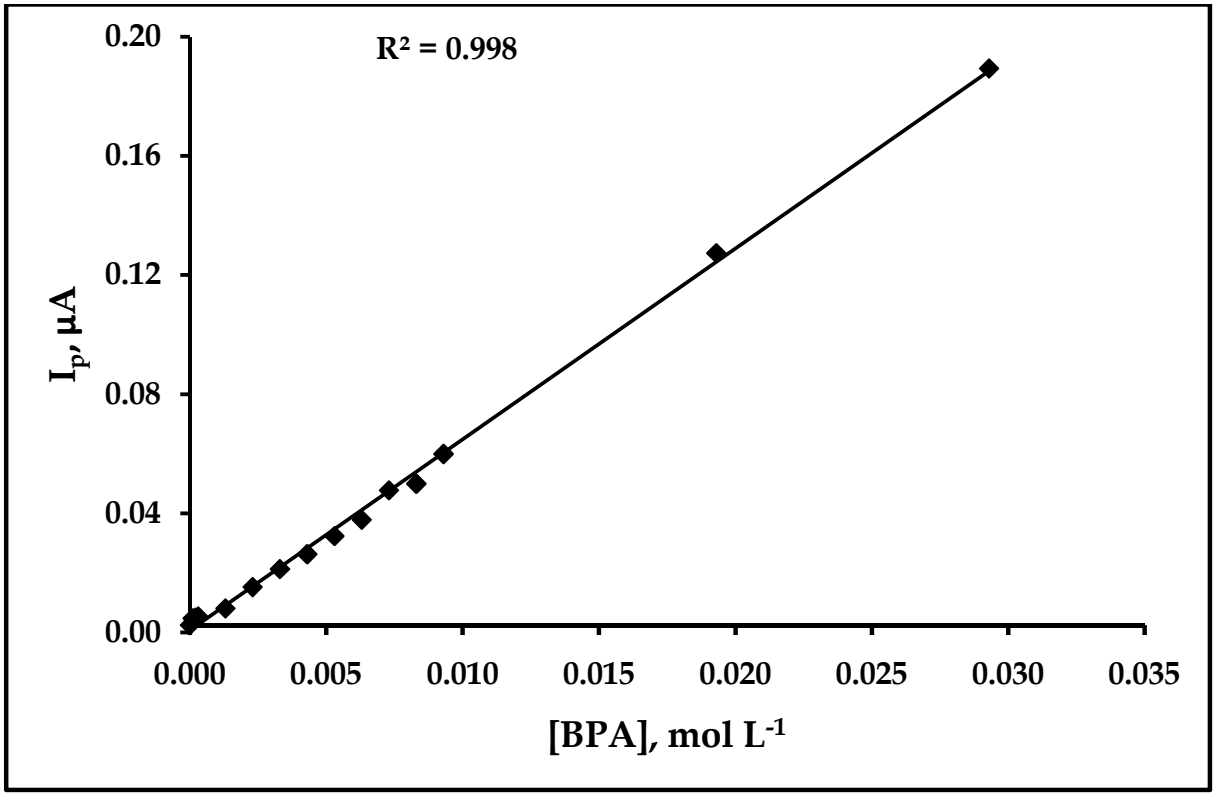

Figure 6.24: Calibration curves for BPA detection by *poly*-70-Ni(OH)NiTAPc (pH = 12).

The LoD of Au *poly*-70-Ni(OH)NiTAPc for BPA (3σ criteria, based on signal to noise ratio, from chronoamperometry as explained above) was 3.68 x 10^{-9} mol L^{-1}, Table 6.7. This value is better than that reported for CoPc-CPE (LoD = 1.0 x 10^{-8} mol L^{-1}) [137] and carbon electrode which had been modified with a multi-walled carbon nanotubes-gold nanoparticles hybrid film [138]. Thus the *poly*-Ni(OH)NiTAPc on gold shows improved sensitivity for BPA. Fig. 6.25 (i) shows chronoamperograms of pH 12 phosphate buffer followed by the addition of BPA solution of concentration 1 x 10^{-8} mol L^{-1}. The observed increase in current illutratrates the sensitity of the *poly*-70-Ni(OH)NiTAPc electrode toward BPA at that concentration.

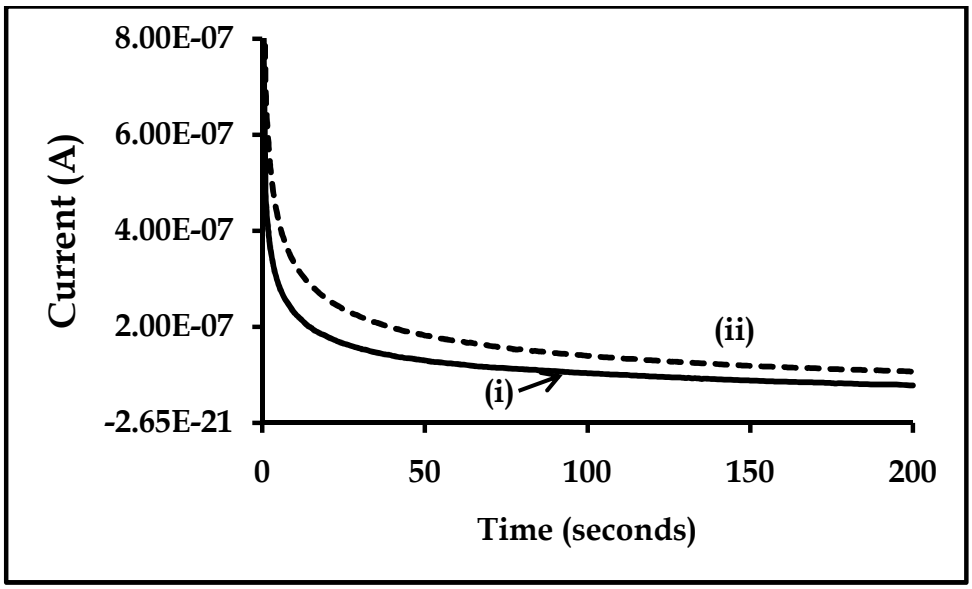

Figure 6.25: Chronoamperograms of (i) pH 12 phosphate buffer and (ii) BPA solution of concentration 1.08 x 10^{-8} mol L^{-1}.

Fig. 6.26 shows the linear variation of the cyclic voltammetry currents with BPA concentrations in the range of 1 to 8 mM for **29a** and **29b**.

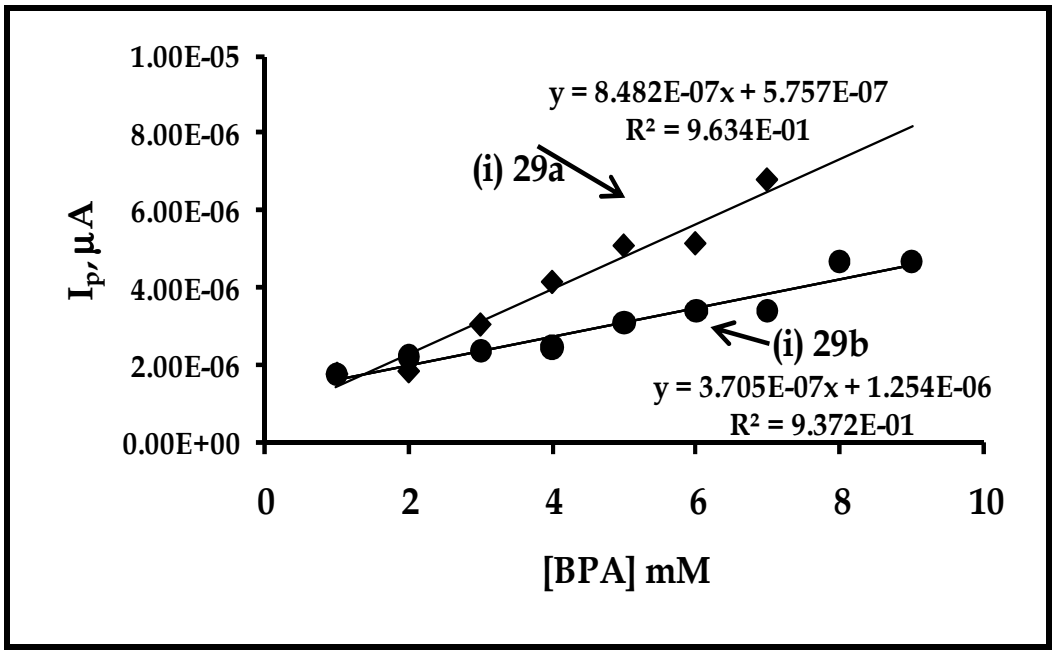

Figure 6.26: Calibration curves for BPA detection (i) 29a and (ii) 29b in pH 12 phospahte buffer.

The LoD of **29a** and **29b** for BPA (3σ criteria, based on signal to noise ratio) was 4.78 x 10^{-10} and 2.76 x 10^{-10} mol L^{-1}, Table 6.7. These values are improved compared to *poly*-70-Ni(OH)NiTAPc which had an LOD of 3.68 x 10^{-9} mol L^{-1}.

The limits of detection (LoD) for complexes **28, 28-**AuNP, **28-**SWCNT, and **29a-**SWCNT in pH 12 buffer are listed in Table 6.7 and they ranged from 1.02 x 10^{-10} to 1.90 x 10^{-10} mol L^{-1}, Table 6.7. Quiet noticeable are the LOD values for **28**-SWCNT and **29a**-SWCNT which were improved compared to all the complexes.

The sensitivity values for selected TaPc, TaPc-AuNPs and TaPc-SWCNTs conjugates are listed in Table 6.7. The presence of AuNPs increased the sensivity and the conjugation with SWCNTs significantly improved sensivity, for example sensivity for **28**-AuNPs increased from 3.30 x 10^{-5} to 3.47 x 10^{-4} for **28**-SWCNTs.

6.2.7. Real samples

BPA concentrations were calculated in the two types of plastics that were obtained from a local food store for practical analysis using *poly*-70-Ni(OH)TAPc which was the most sensitive towards the oxidation of BPA amongst the poly-n-Ni(OH)NiTAPc. This was performed to determine the possible potential of the modified gold electrodes in the detection of BPA in real sample applications. A standard addition method was employed, where it was discovered that the microwave oven plastic had more BPA concentration (2.55 μM) than the soft drink bottle which had a BPA concentration of 0.585 μM. Values in the μM range were obtained for similar samples [137]. For analysis using complex **28** BPA

concentrations in the plastic was found to be 1.89 μM. No BPA was detected on the feeding bottle.

6.3. Conclusions

The electrooxidation of BPA in pH 12 buffer by different *poly*-NiTAPc of different thicknesses was investigated. It was also demonstrated that thicker films do not necessarily give better catalysis. *Poly*-70-Ni(OH)NiTAPc was the most sensitive for the electrocatalysis of BPA. The stability of the electrodes increased with polymer thickness. The *poly*-70-Ni(OH)TAPc modified electrode (which showed the largest sensitivity) could reliably detect bisphenol A in a concentration range of 7×10^{-4} to 3×10^{-2} mol L^{-1} . The electrocatalytic oxidation of BPA was improved on TiPc, VPc and TaPc complexes modified electrodes and their AuNPs or SWCNT conjugates in terms of potential, compared to *poly*-n-Ni(OH)TAPc. The presence of AuNPs increases sensitivity and interestingly AuNPs alone showed BPA detection which was not obtained on the bare Au electrode. Passivation was inevitable; however, in the presence of AuNPs the process of passivation was gradual. Regeneration of the electrode surface was achieved partially by rinsing the passivated electrode in a solution of concentrated NaOH. The modified electrodes showed improved sensitivity towards BPA catalytic oxidation compared to what has been previously studied and NiTAPc. **28**- and **29a-**SWCNT showed very high activity towards BPA analysis with minimal fouling, hence improved recovery.

7. General conclusions

TiPc, VPc and TaPc derivatives substituted with mercapto-pyridine or alkylthio on the α and β positions were successfully synthesized. Their photochemical, photophysical parameters and electrochemical properties in the absence and presence of AuNPs and SWCNTs (for selected TaPc complexes) were studied. The Q band of the complexes shift to the red with the change in the central metal as follows: Ta > V > Ti. The reduction couples for all the complexes were reversible to quasi-reversible and oxidation processes are irreversible. Spectroelectrochemistry confirmed one metal reduction, with the rest of the redox processes being centered on the phthalocyanine ring, except the VPc complexes, where all processes are ring based.

Photocatalytic oxidation of cyclohexene was carried out successfully on the TiPc and TaPc complexes due to the singlet oxygen production that was improved significantly by the presence of AuNPs. The improved singlet oxygen quantum yield was attributed to the good triplet quantum yields. The percentage conversion of cyclohexene was improved by the presence of gold nanoparticles. Percentage selectivity values were generally improved when compared to literature values, but photobleaching occurred with increased time during photolysis. The percentage yields were improved significantly compared to literature values.

The electrooxidation of BPA in pH 12 buffer by different *poly*-NiTAPc of different thicknesses was investigated. It was also demonstrated that thicker films do not necessarily give better catalysis. *Poly*-70-Ni(OH)NiTAPc was the most sensitive for

the electrocatalysis of BPA. The stability of the electrodes increased with polymer thickness. The electrocatalytic oxidation of BPA was even more improved by TiPc, VPc and TaPc complexes and their AuNPs or SWCNT conjugates. The presence of AuNPs increases sensitivity significantly and interestingly AuNPs alone showed BPA detection which was not obtained on the bare Au electrode. Passivation was inevitable; however, in the presence of AuNPs the process of passivation was gradual. Regeneration of the electrode surface was achieved partially by rinsing in a solution of concentrated NaOH. The modified electrodes showed improved sensitivity towards BPA catalytic oxidation compared to what has been previously studied **28-** and **29a-**SWCNT showed very high activity towards BPA analysis with minimal fouling, hence improved recovery.

8. References:

1. R. Bonnett, *Chemical aspects of photodynamic therapy*, Gordon and Breach Science Publishers, Germany, 2000.
2. A. Von Braun, J. Tscheniac, *Ber. Deut. Chem. Ges*., 40 (1907) 2709.
3. H. de Diesbach, E. von de Weid, *Helv. Chim. Acta*, 10 (1927) 886.
4. G. T. Byrne, R. P. Linstead, A. R. Lowe, *J. Chem. Soc*., (1934) 1017.
5. R. P. Linstead, A. R. Lowe, *J. Chem. Soc*., (1934) 1022.
6. C. E. Dent, R. P. Linstead, *J. Chem. Soc*., (1934) 1027.
7. J. A. Elvidge, R. P. Linstead, *J. Chem. Soc*., (1955) 3526.
8. J. M. Robertson, *J. Chem. Soc*., (1935) 615.
9. J. M. Robertson, *J. Chem. Soc*., (1936) 1195.
10. J. M. Robertson, I. Woodward, *J. Chem. Soc*., (1937) 3536.
11. G. P. Moss, *Eur. J. Biochem*., 178 (1988) 277.
12. C. C. Leznoff, A. B. P. Lever (eds)., *Phthalocyanines: Properties and Applications*, VCH Publishers, Inc., Weinheim: New York, Vol 2 (1993).
13. M. J. Stillman, T. Nyokong, In *Phthalocyanines: Properties and Applications*, C. C. Leznoff, A.B.P. Lever (eds), VCH publishers, New York, Vol. 1 (1989) .
14. K. Shweiger, A. Kienast, B. Latte, H. Z. Homborg, *Anorg. Allg. Chem*., 623 (1997) 973.
15. W. Hiller, J. Strähle, W. Kobel, M. Z. Hanack, *Krystallogra*., 159 (1982) 173.
16. R. F. Ziolo, C. H. Griffiths, J. M. Troup, *Dalton Trans* (1980) 2300.
17. V. Goedken, G. Dessy, C. Ercolana, V. Fares, L. Gastaldi, *Inorg. Chem*., 24 (1985) 991.

18. M. K. Engel, *Single-Crystal Structures of Phthalocyanine Complexes and Related Macrocycles in The Porphyrin Handbook: Phthalocyanines: Structural Characterisazation*,. K. M. Kadish, K. M. Smith, R. Guilard (eds), Academic Press, Carlifonia USA, Vol 20 (2003).
19. N. Sehlotho, T. Nyokong, *J. Mol. Catal. A: Chem*., 219 (2004) 201.
20. P. Tau, T. Nyokong, *J. Mol. Catal. A: Chem*., 52 (2007) 3641.
21. R. A Sheldon, *J. Mol. Catal*., 20 (1983) 1.
22. D. Wöhrle, J. Gitzel, G. Krawczyk, E. Tsuchida, H. Ohno, T. Nishisaka, *J. Macromol.Sci. Chem: A*, 25 (1998). 1227.
23. D. Wöhrle, D. Meissner, *Adv. Mater*., **3** (1991) 129.
24. M. Hanack, M. Lang, *Adv. Mater*., 6 (1994) 819.
25. M. Hanack, M. Lang, *Chemtracts*, 8 (1995) 131.
26. H. Schultz, H. Lehman, M. Rein, M. Hanack, *Structure and Bonding 74*, Springer-Verlag, Heidelberg, (1992).
27. U. Drechsler, M. Hanack, in *Comprehensive Supramolecular Chemistry*, J. L. Atwood, J. E. D. Davies, D. D. McNicol (eds.), F. Vögtle, Pergamon: Oxford, 9 (1996).
28. M. Hanack, H. Heckmann, R. Polley, in Methoden *de Organischen Chemie (Houben-Weyl),* Thieme Verglag (ed): Stuttgart, Vol 4 (1997).
29. J. F. van der Pol, E. Neelman, J. W. Zwikker, R. J. M. Nolte, W. Drenth, J. Aerts, R. Visser, S. J. Picken, *Liq. Cryst*., 61 (1989) 557.
30. J. Simon, C. Sirlin, *Pure Appl. Chem*., 61 (1989) 1625.

31. M. K. Engel, P. Bassoul, L. ossio, H. Lehmann, M. Hanack, J. Simon, *Liq. Cryst*., 15 (1993) 709.
32. G. G. Roberts, M. C. Petty, S. Barker, M. T. Fowler, N. J. Thomas, *Thin Solid Films,* 132 (1985) 113.
33. M. J. Cook, A. J. Dunn, F. M. Daniel, R. C. O. Hart, R. M. Richardson, S. J. Rose, *Thin Solid Films*, 159 (1988) 469.
34. S. Palacin, P. Lesieur, I. Stefanelli, A. Barraud, *Thin Solid Films*, 159 (1988) 83.
35. M. Burghard, M. Schmelzer, S. Roth, P. Haisch, M. Hanack, *Langmuir*, 10 (1994) 4265.
36. S. Takano, T. Enokida, A Kambata, *Chem. Lett*., (1984) 2037.
37. S. Zhou, X. Jin, W. Hu, Y. Liu, S. Liu, *Solid State Commun*. 112 (1999) 269.
38. D. M. Pai, B. E. Springett, *Rev. Mod. Phys.,* 65 (1993) 163.
39. J. E. Kuder, *Imaging Sci*., 32 (1988) 51.
40. S. Kobayashi, K. Iwasaki, H. Sasaki, S. Oh-Hara, M. Nishizawa, M. Katayose, *Jpn. J. Appl. Phy*., 30 (1991) 114.
41. R. Ao, L. Kümmert, D. Haarer, *Adv. Mater*., 5 (1995) 495.
42. A. B. P. Lever, M. R. Hempstead, C. C. Lezznoff, W. Liu, M. Melnik, W. A. Nevin, P. Seymour, *Pure Appl. Chem*., 58 (1986) 1467.
43. B. Simic-Glavaski in *Phthalocyanines: Properties and Applications*, eds. A. B. P. Lever, C. C. Leznoff, VCH, New York, Vol 3 (1993)3.
44. J. Simon, J. J. Andre, *Mol. Semicond.,* Springer, Berlin, (1995).
45. J. Simon, T. Toupance *in Comprehensive Supremolecular Chemistry,* Reinhoudt (ed), Supramolecular Technology, Pergamon, London, (1996).

46. D. Dini, M. Hanack, The porphyrin handbook: *Physical Properties of phthalocyanine-based materials*, K.M. Kadish, K.M. Smith, R. Guilard(eds), Academic press, USA Vol 17, (2003).
47. N. S. Nalwa, J. S. Shirk, *in Phthalocyanines: Properties and Applications*, A. B. P. Lever, C. C. Leznoff (eds), Vol 4, (1996).
48. M. K. Casstevens, M. Samoc, J. Pfleger, P. N. Prasad, *J. Chem. Phy*., 92 (1990) 2019.
49. R. Bonnett, *Chem. Soc. Rev*., 95 (1995) 19.
50. S. B. Brown, T. G. Truscott, *Chem. Ber.,* 29 (1993) 955.
51. D. Wöhre, M. Shopova, S. Müller, A. D. Milev, V. N. Mantareva, K. K. Krastev, *J. Photochem. Photobiol. B*., 21 (1993) 955.
52. P. A. Barrett, C. E. Dent, R. P. Linstead, *J. Chem. Soc.,* (1936) 1719.
53. R. P. Linstead, *J. Chem. Soc*., (1934) 1016.
54. P. J. Brach, S. J. Grammatica, O. A. Ossanna, L. Weinberger, *J. Heterocyclic. Chem*., 7 (1970) 1430.
55. J. A. Elvidge, R. P. Linstead, *J. Chem. Soc*., 3536 (1955).
56. A. Tomoda, S. Saito, S. Ogawa, S. Shiraishi, *Chem. Lett*., (1980) 1277.
57. A. Tomoda, S. Saito, S. Shiraishi, *Chem. Lett*., (1983) 313.
58. M. Hanack, H. Heckmann, R. Polley, *in Modern der Organischem Chemie* (Houben – Weyl), 4th Ed.; Thieme Verlag: Stuttgart, Vol E9d (1997).
59. M. Sommerauer, C. Rager, M. Hanack, *J. Am. Chem. Soc*., 118 (1996) 10085.
60. D. Wohrle, G. Kossmehl, G. Maneck, *Macromol.,* 154 (1972).

61. S. Foley, G. Jones, R. Luizzi, D.J. McGarvey, M.H. Perry, T.G. Truscott, *J. Chem. Soc., Perkin Trans*. 2 (1997) 1725.
62. G. Torres, A.T. Torres *J. Porphyrins Phthalocyanines*, 1 (1997) 221.
63. E. V. Kudrik, E. M. Bauer, C. Ercolani, A. Chiesi-Villa, C. Rizzoli, A. Gaberkorn, P. A. Stuzhin, *Mendeleev. Commun.,* (2001) 45.
64. P. M Burnham, M.J Cook, L.A Gerrard, M.J Heeney, D.L Hughes, *J. Chem Soc. :Chem. Commun.,*(2003) 2064.
65. P. Tau, T. Nyokong, J. *Porphyrins Phthalocyanines,* 10 (2006) 69.
66. P. Tau, T. Nyokong, *Inorg. Chim. Acta.,* 360 (2007) 2615.
67. G. Mbambisa, T. Nyokong, *Polyhedron* 27 (2008) 2799.
68. Burkingham, M. R. Evans, C. M. Ellis, R. J. Jackson, A. C. Assignee Minnesota Mining Company, U. S. Patent 5168031 (1992).
69. Y. Arslanoglu, E. Hamuryudan, *Dyes Pigments.,* 68 (2006) 1.
70. T. Tau, T. Nyokong, *Dalton Trans*., (2006) 4482.
71. Y. Arslanoglu, A. M. Servim, E. Hamuryudan, A. Gul, *Dyes Pigments* 68 (2006) 119.
72. G. Mbambisa, T. Tau, E. Antunes, T. Nyokong, *Polyhedron,* 26 (2007) 5355.
73. M. Gouterman, *In The Porphyrins,* (Ed. D. Dolphin), *Part A*. Physical Chemistry, Academic Press, New York, (1978).
74. A. J. McHugh, M. Gouterman, C. Weiss, *Theoret. Chim. Acta,* 24 (1987), 246.
75. A. M. Schaffer, M. Gouterman, E. R. Davidson, *Theoret. Chim. Acta,* 30 (1973), 9.

76. N. A. Kuznetsova, N. S. Gretsova, V.M. Derkacheva, O.L. Kaliya, E.A. Luk'yanets, *J. Porphyrins Phthalocyanines*. 7**,** (2003) 147.

77. N. Kobayashi, H. Ogata, N. Nonaka, E. A. Lu'yanets, *Chem. Eur. J.,* 34 (2003) 5123.

78. N. Kobayashi, N. Sasaki, Y. Higashi, T. Osa, *J. Inorg. Chem.,* 34 (1995) 1636.

79. T. Muto, T. Temmo, M. Kimura, K. Hanabusa, H. Shirai, *J. Org. Chem.*, 66 (2001) 6109.

80. J. Obirai, T. Nyokong, *Electrochim. Acta*, 50 (2005) 3296.

81. A. Gilbert and J. Baggott, *Essentials of Molecular Photochemistry*, library of congress, USA, (1995).

82. P. Kubát, J. Mosinger, *J. Photochem. Photobiol. A: Chem.*, 96 (1996) 93.

83. M. Durmuş, T. Nyokong, *Polyhedron,* 26 (2007) 3323.

84. M. Durmuş, T. Nyokong, *Tetrahedron,* 63 (2007), 1385.

85. A. Harriman, G. Porter, M.-C. Richoux, *J. Chem. Soc., Faraday Trans.*, 76 (1980) 1618.

86. J. McVie, R. S. Sinclair, T. G. Truscott, *J. Chem. Soc. Faraday Trans.*, 74 (1978) 1870.

87. P. B. Merkel, D. R. Kearns, *J. Am. Chem. Soc.*, 97 (1989) 833.

88. A. Ogunsipe, T. Nyokong, *J. Photochem. Photobiol. A: Chem.*, 173 (2005) 211.

89. M. Ritchie, *Chemical Kinetics in Homogeneous Systems*, Oliver and Boyd, London, 1966.

90. M. Idowu, T. Nyokong, *J. Photochem. Photobiol A: Chem*, 188 (2007) 200.

91. W. Chidawanyika, A. Ogunsipe, T. Nyokong, *New J. Chem.*, 31 (2007) 377.

92. G. Schnurpfeil, A. Sobbi, W. Spiller, H. Kliesch, D. Wöhrle, *J. Porphyrins Phthalocyanines*, 1 (1997) 159.

93. M. D. Maree, N. Kuznetsova, T. Nyokong, *J. Photochem. Photobiol. A; Chem.*, 140 (2001) 117.

94. S. Maree, T. Nyokong, *J. Porphyrin Phthalocyanines,* 5 (2001) 5782.

95. J. D. Spikes, *Photochem. Photobiol*., 55 (1992) 797.

96. D. Dini, M. Calvete, S. Vargin, M. Hanack, A. Eriksson, C. Lopes, *J. Porphyrin and Phthalocyanines*, 10 (2006) 1165.

97. T. Dumas, W. Bulani, *Oxidation of Petrochemicals: Chemistry and Technology*, Applied Science Publishers, London, (1974).

98. J. McMurry, *Organic Chemistry*, Library of Congress Catalaging, USA, 5th edition, (2000).

99. B. Meunier, A. Sorokin, *Acc. Res.,* 30 (1997) 470.

100. A. Sorokin, S. De Suzzoni-Dezard, D. Poullain, J-P. Noël, B. Meunier, *J. Am. Chem. Soc.*, 118 (1996) 7418.

101. A. Hadasch, A. Sorokin, A. Rabion, L. Fraisse, B. Meunier, *Bull. Soc. Chim., Fr.*, 134 (1997) 1025.

102. D. Wöhrle, O. Suvorova, R. Gerdes, O. Bartels, L. Lapok, N. Baziakina, S. Makarov, A. Slodek, *J. Porphyrins Phthalocyanines*, 8 (2004) 1020.

103. G. Schneider, D. Wöhrle, W. Spiller, J. Stark, G. Schulz-Ekloff, *Photochem. Photobiol.*, 60 (1994) 333.

104. R. Gerdes, O. Bartels, G. Schneider, D. Wöhrle, G. Schulz-Ekloff, *Intern. J. Photoenergy*, 1 (1999) 41.

105. A. Maldotti, A. Molinari, R. Madelli, *Chem. Rev.,* 102 (2002) 3811.

106. T. Shiragami, J. Matsumoto, H. Inoue, M. Yasuda, J. *Photochem. Photobiol. C: Photochem. Rev*., 6 (2005) 227.

107. G. Centri, F. Cavan, F. Trifiro, S*elective Oxidation by Heterogeneous Catalysts*, Kuwer Academic Plenum Publishers, New York, 1st edition, (2001).

108. X. Xue, Y. Xu, *J. Mol. Catal. A: Chem.,* 276 (2007) 80.

109. M. L'Her, A. Pondaven *in The Porphyrin Handbook*, K.M Kadish, K.M Smith, R. Guilard (eds) , Academic Press, California, Vol 16 (2003) 117.

110. D. W. Clack, N. S. Hush, *J. Am. Chem. Soc*., 87 (1965) 4238.

111. A. B. P. Lever, *Adv. Inorg. Radiochem*., 7 (1965) 28.

112. P. T. Kissinger, W. R. Heineman, *Laboratory Techniques in Electroanalytical Chemistry*, Marcel Dekker, Inc., 2nd editon, (1996), 84.

113. T. Tau, T. Nyokong, *Electrochim. Acta.,* 52 (2007) 3641.

114. N. Nombona, T. Tau, N. Sehlotho, T. Nyokong, *Electrochim. Acta.,* 53 (2008) 3139.

115. Z. Jiang, Z Ou, N. Chen, J. Wang, J. Huang, J. Shao, K.M Kadish, *J. Porphyrins Phthalocyanines*, 9 (2005) 352.

116. H. Handa, A. Suzuki, S. Shoji, K. Kasuga, K. Sogabe, *Inorg. Chim. Acta*, 230 (1995) 41.

117. J. O'M Bockris, A. K. Reddy, M. De Gamboa-Aldeco, *Modern Electrochemistry*, Vol 2A, Plenum Publishers, (2000).

118. D. R. Crow, *Principles and Applications of Electrochemistry*, Blackie Academics and Professional, 4th edition, (1994).

119. J. Hagen, *Industrial Catalysis: A Practical Approach*, Wiley-VCH, 2nd ed, Weinheim, (2006).

120. K-C. Cheung, W-L. Wong, D-L Ma, T-S Lai, K-Y. Wong, *Coord. Chem. Rev.*, 251 (2007) 2367.

121. M. C. Granger, J.S Xu, J.W Strojek, *Anal. Chim. Acta*, 397 (1997) 145.

122. X. Xing, D. A Scherson, *Anal. Chem*., 60 (1988)1723.

123. J. Zagal, *Coord. Chem. Rev*, 119 (1992) 89.

124. P. Vasuvedan, N. Phougat, A. K. Shuklat, *Appl. Organomet. Chem*., (1996) 951.

125. S. Mho, B. Ortiz, S.-M. Park, *J. Electrochem. Soc*., 142 (1995) 1436.

126. J. Obirai, T. Nyokong, *Electrochim. Acta*, 49 (2004) 349.

127. J. J. Gooding, V. G. Praig, E. A. H. Hall, *Anal. Chem*., 70 (1998) 2396.

128. A. J. Bard, L. R. Faulkner (Eds), *Electrochemical Methods: Fundamentals and Application*, Wiley, New York (1980).

129. E. Barsoukov, J. R. Mcdonald, *Impedance Spectroscopy Theory, Experiment, and Applications*, John Wiley & Sons Inc, 2nd edtion (2005).

130. B. E. Conway, J. Bockris, R. E. White, *Mordern Aspects of Electrochemistry*, Kluwer Academic/Plenum Publishers, New York, Vol 32, (1999).

131. C. A. Staples, B. P. Dome, G. M. Klecka, S. T. Oblock, L. R. Harris, *Chemosphere,* 36 (1998) 2149.

132. E. Burridge, *Euro. Chem. News*, 17 (2003) 14.

133. F. S. Vom Saal, C. Hughes, *Environ. Health Perspect*., 113 (2005) 926.

134. V. W. Welshons, K. A. Thayer, B. M. Judy, J. A. Taylor, E. M. Curran, F. S. Vom Saal, *Envirion. Health Perspect*., 111 (2003) 994.

135.R. Pulgar, M. F. Olea-Serrano, A. Novillo-Fertrell, A. Rivas, P. Pazos, V. Pedraza, J. M. Navajas, N. Olea, *Environ. Health Perspect*., 108 (2000) 21.

136.A. Gonzalez-Casado, N. Navas, M. Del-Olmo, J. L. Vilchez, *J. Chromatogr. Sci*., 36 (1998) 565.

137.H. -S. Yin, Y.-L. Zhou, S.-Y. Ai, J. *Electroanal. Chem*., 626 (2009) 80.

138.H. -S. Yin, Y. Zhou, S.-Y. Ai, L. Cui, L. Zhu, A, *Anal. Chim. Acta,* 659 (2010) 144.

139.D. Mita, A. Attanasio, F. Arduini, N. Diano, V. Grano, U. Bencivega, S. Ossi, A. Amine, D. Moscone, *Biosens. Bioelectron*., 23 (2007) 60.

140.S. Andreescu, O. Sadik, *Anal. Chim. Acta.,* 479 (2003) 143.

141.M. Murugananthan, S. Yoshihara, T. Rakuma, T. Shirakashi, *J. Harzard. Mater*., 154 (2008) 213.

142.B. Agboola, T. Nyokong, *Electrochim. Acta*, 52 (2007) 5039.

143.B. O. Agboola, K. I. Ozoemena, T. Nyokong, *Electrochim. Acta*, 51 (2006) 6470.

144.A. Alif, P. Boule, *J. Photochem. Photobiol.A: Chem* , 59 (1991) 357.

145.N. Takahashi, T. Nakai, Y. Satoh, Y. Katoh, *Water Res*., 28 (1996) 345.

146.Z. Wu, Y. Cong, M. Zhou, T. Tan, *J. Chem. Eng.,* 106 (2005) 83.

147.V. C. Dall'orto, C. Dalowicz, J. Hurst, A. L. Balbo, I. Rezzano, *Electroanal*., 10 (1998) 127.

148.J. Obirai, F. Bedioui, T. Nyokong, *Electroanal. Chem*., 576 (2005) 323.

149.H. Sakurai, M. Haruta, *Appl. Catal. A,* 127(1995) 93.

150.M. C. Daniel, D. Astruc, *Chem. Rev*., 104 (2004) 293.

151.J. Zhou, J. Ralston, R. Sedev, D. A. Beattie, *J. Colloid and Interface Sci.,* 331 (2009) 251.

152.N. N. Greenwood, A. Earnshow, *Chemistry of elements*, Elservier Science, Oxford, (1997).

153.M. Greenwood, L. M. Liz-Marza, *Mat. Today*, 2 (2004) 26.

154.A. P. Alivisatos, *Science,* 271 (1996) 933.

155.M. M. Maye, Y. Lou, C. J. Zhong, *Langmuir,* 16 (2000) 7520.

156.C. F. Bohrem, D. R. Huffman, *Absorption and Scattering of light by Small Particles,* Wiley, New York (1983).

157.P. Mulvaney, *Langmuir*, 12 (1996) 788.

158.C. Burda, X. Chen, R. Narayanan, M. A. El-Sayed, *Chem. Rev*., 105 (2005) 1025.

159.S. Link, C. Burda, Z. L. Wang, M. A. El-Sayed*, J. Chem. Phys*., 111 (1999) 1255.

160.P. K. Jain, X. Huang, I. H. El-Sayed, M. A. El-Sayed, *Acc. Chem. Res*., 41 (2008) 1578.

161.E. Hutter, J, H. Fendler, *Adv. Mater*., 16 (2004) 1685.

162.R. W. Murray, *Chem. Rev.,* 108 (2008) 2688.

163.L. D. Bozano, B. W. Kean, M. Beinhoff, K. R. Carter, P. M. Rice, J. C. Scott, *Adv. Funct. Mater*., 15 (2005) 1933.

164.J. Ouyang, C.-W. Chu, D. Sieves, Y. Yang, *Appl. Phys. Lett.,* 86 (2005) 123507.

165.D. I. Gittins, D. Betthell, D. J. Schiffrin, R. J. Nichols, *Nature*, 408 (2000) 67.

166.L. M. Liz-Marzan, *Mat. Today*, 2 (2004) 26.

167.B. V. Enustun, J. Turkevich, *J. Am. Chem. Soc*., 85 (1963) 3317.

168.J. Kimling, M. Maier, B. Okenve, V. Kotaidis, H. Ballot, A Plech, *J. Phys. Chem. B.,* 110 (2006) 15700.

169.M. Brust, M. Walker, D. Bethell, D. J. Schiffrin, R. Whyman, *J. Chem. Soc. Chem. Commun*., 7 (1994) 801.

170.A. C. Templeton, W. P. Wuelfing, R. W. Murray, *Acc. Chem. Res*., 33 (2000) 27.

171.D. C. Hone, P. I. Walker, R. Evans-Gowing, S. FitzGerald, A. Beeby, I. Chambrier, M. J. Cook, D. A. Russell, *Langmuir,* 18 (2002) 2985.

172.M. Pal, V. Ganesan, *Langmuir*, 25 (2009) 13234.

173.S. Iijima, T. Ichihashi, *Nature*, 363 (1993) 603.

174.D. S. Bethune, C. H. Klang, M. S. de Vries, G. Gorman, R. Savoy, J. Vazquez, et al., *Nature*, 363 (1993) 605.

175.A. Oberlin, M. Endo, T. Koyama*, J. Cryst. Growth*, 32 (1976) 335.

176.C. Ehli, S. Campidelli, F. G. Brunetti, M. Prato, D. M. Guldi, J. *Porphyrins Phthalocyanines*, 11 (2007) 442.

177.P. J. F. Harris, *Carbon Nanotubes and Related Structures: New Materials for the Twenty-First Centuaty*, Cambridge University Press:Cambridge, UK (2001).

178.M. Inagaki, K. Kaneto, T. Nishizawa, *Carbon,* 42 (2004) 1401.

179.N. Nakashima, *Int. J. Nanoscien*., 4 (2005) 119.

180.Y. Zhang, T. Ichihashi, E. LAndree, F. Nihey, S. Iijima, *Science,* 285 (1999) 1719.

181.M. S. Gudiksen, L. J. Lauhon, J. Wang, D. C. Smith, C. M. Lieber, *Nature,* 415 (2002) 617.

182.J. J. Davis, K. S. Coleman, B. R. Azamian, C. B. Bagshaw, M. L. H. Green, *Chem. Eur. J*., 9 (2003) 3733.

183.G. L. Hornyak, J. Dutta, H. F. Tibbals, A. K. Rao, *in Introduction to Nanoscience,* CRC Press, Taylor and Francis Group, Boca Raton (2008)

184.B. K. Price, J. M. Tour, *J. Am. Chem. Soc.,* 128 (2006) 12899.

185.H. Murakami, T. Nomura, N. Nakashima, Chem. *Phys. Lett.,* 465 (2008) 73.

186.R. J. Chen, Y. G. Zhan, D. W. Wang, H. J. Dai, *J. Am. Chem. Soc.*, 123 (2001) 3838.

187.A. Ma, J. Lu, S. Yang, K. M. Ng, J. *Cluster Science,* 17 (2006) 599.

188.D. A. Geraldo, A. T. Chamunorwa, J. Limson, T.Nyokong, *Electrochim. Acta*, 53 (2008) 8051.

189.J. F. Silva, S. Grieau, C. Richard, J. H. Zagal, F. Bedioui, *Electrochem. Commun.* 9 (2007) 1629.

190.C. B. Murray, C. R. Kagan, M. G. Bawendi, *An. Rev. Mat. Sci.,* 30 (2000) 545.

191.J. L. West, N. Halas, *Current Opinion in Biotechnology,* 11(2000) 215.

192.G. Binnig, C. F. Quate, Ch. Gerber, *Phys. Rev. Lett.,* 56 (1986) 930.

193.http://www.physics.uwo.ca/~smittler/Silvia%20Mittler%20OMCVD.htm

194.S. Sapra, D. D. Sarma, *Pramana*, 65 (2005) 565.

195.B. N. Achar, P. K. Jayasree, Syn. Met., 104 (1999) 101.

196.N. Sehlotho, M. Durmus, V. Ahsen, T. Nyokong, *Inorg. Chem. Com.*, 11 (2008) 479.

197.N. Saydan, M. Durmus, M. G. Dizge, H. Yaman, A. G. Gurek, E. Antunes, V. Ahsen, T. Nyokong, *J. Porphyrins Phthalocyanines,* in press.

198.P. M. Burnham, M.J. Cook, L. A. Gerrard, M. J. Heeney, D.L. Hughes, *Chem. Commun*. (2003) 2064.

199.J. Morita, H. Nakatsiju, T. Misaki, Y. Tanabe, *Green. Chem.,* 10 (2005) 711.

200. A. Kotiaoho, R. Lahtinen, A. Efimov, H-K. Metsberg, E. Sariola, H. Lehtivuori, N. V. Tkachenko, H. Lemmetyinen, *J. Phys. Chem. C.* 114 (2010) 162.

201. J. Liu, A. G. Rinzla, H. Dai, J. H. Hafner, R. K. Bradley, P. J. Boul, A. Lu, T. Iverson, K. Shelimov, C. B. Huffman, F. Rodriguez-Macias, T. Y-Seon Shon, R. Lee, D. T. Cobert, R. E. Smalley, *Science*, 280 (1998) 1253.

202. A. B. Anderson, T. L. Gorden, M. E. Kenney, *J. Am. Chem. Soc*. 107 (1985) 192.

203. K. Konami, M. Hatano, A. Tajiri., *Chem. Phy. Lett.,* 166 (1990) 605.

204. F. Fukuda, T. Shiguro, N. Kobayashi. *Tetrahed.Lett*, 46 (2005) 2907.

205. T. M. Keller, T. R. Price, J. R. Griffith, *Synthesis*, 74 (1980) 613.

206. A. W. Snow, J. R. Griffith, *Macromol.,* 17 (1984) 1614.

207. W. Chidawanyika, T. Nyokong, *J. Photochem. Photobiol. A*: Chem. 206 (2009) 169.

208. A. Ogunsipe, M. Durmuş D. Atilla, A. G. Gürek, V. Ahsen, T. Nyokong, *Syn. Met.,* 158 (2008) 839.

209. A. Ogunsipe, D. Maree, T. Nyokong, *J. Mol. Struct*., 650 (2003) 131.

210. J. A. Creighton, D. G. Eadon, *J. Chem. Soc. Faraday Trans*., 87 (1991) 3881.

211. B. D. Chithrani, A. A. Ghazani, W .C. W. Chan, *Nanoletters*, 6 (2006), 662.

212. S. Perun, J. Tatchen, C.M. Marian, *Chem. Phys. Chem*., 9 (2008) 282.

213. S. Maree, T. Nyokong, *J. Porphyrins Phthalocyanines*, 5 (2001) 782.

214. Y. Zhang, K. Aslan, M. J. R. Previte, C. D. Geddes, *J. Fluoresc.*, 17 (2007) 345 - 49.

215. N. d'Alessandro, L. Tonucci, A. Morvillo, L.K. Dragani, M. Di Deo, M. Bressan, *J. Organomet. Chem.,* 690 (2005) 213.

216.R. Słota, G. Dyrda, *Inorg. Chem*., 42 (2003) 5743.

217.C. S. Foote, J. W. Peters, *J. Am. Soc.,* 93 (1971) 3795.

218.P. R. Ogilby, C. S. Foote, *J. Am. Soc.,* 103 (1981) 1219.

219.B. M. Monroe, *J. Phys. Chem*., 82 (1978) 15.

220.P. D. Bartlett, A. P. Schaap, *J. Am. Soc.,* 92 (1970) 3223.

221.A. B. P. Lever, E. R. Milaeva, G. Speier, In Leznoff CC, Lever ABP (Eds),. *Phthalocyanines: Properties and Applications*, New York: VCH Publishers; Vol 3 (1993).

222.T. Nyokong T. in J. Jiang J (Ed), *Functional Phthalocyanine Molecular Materials*, Springer, New York, (2010), 94.

223.D. Y. Dawson, H. Brand, J. Arnold, *J. Am. Chem. Soc*., 116 (1994) 9797.

224.J. Obirai and T. Nyokong, *Electrochim. Acta,* 49 (2004) 1417.

225.A. Sivanesan, J. S. Abraham, *Langmuir*, 24 (2008) 2186.

226.Y. -H. Tse, P. Janda, H. Lam, W. J. Pietro, A. B. P. Lever, *J. Porph. Phthal*., 1 (1997) 3.

227.K. L. Brown, J. Shaw, M. Ambrose, H. A. Mattola, *Microchem. J.,* 72 (2002) 285.

228.A. Goux, F. Bedioui, L. Robbiola, M. Pontie, *Electroanalysis*, 15 (2003) 969.

229.T. F. Otero, E. D. Larreta-Azelain, *Polymer*, 29 (1988) 1522.

230.M. S. Ureta-Zanartu, A. Alarcon, C. Berrios, G. I. Cardenas-Jiron, J. Zagal, C. Guitierrez, *J. Electroanal. Chem*. 580 (2005) 94.

231.T. R. I. Cataldi, D. Centonze, G. Ricciardi, *Electroanalysis*, 7 (1995) 312.

232.T. R. I. Cataldi, E. Desimoni, G. Ricciardi, L. Francesco, *Electroanalysis.,* 7 (1995) 435.

233.S. Trevin, F. Bedioui, M. G. Gomez Villegas, C. Bied-Charreton, *J. Mater. Chem.* 7 (1997) 923.

234.Z. Li, M. Lieberman, *Supramol. Sci*., 5 (1998) 485.

235.P. Westbroek, G. Priniotakis, P. Kiekens, *Analytical Electrochemistry in Textiles*, Woodhead Publishing Limited and CRC Press LLC, Cambridge, England, (2005).

236.P. S. Kumar, *Langmuir,* 23 (2007) 1548.

237.L. Yang, Y. Li, *Biosens. Bioelectron*., 20 (2005) 1407.

238.I. A. Akinbulu, T. Nyokong, *Electrochim. Acta*., 55 (2009) 37.

239.S. Khene, D. A. Geraldo, C. A. Togo, J. Limson, T. Nyokong, Electrochim. Acta. 54 (2008) 183.

240.T. García, E. Casero, M. Revenga-Parra, J. Martín-Benito, F. Pariente, L. Vázquez, E. Lorenzo*, Biosens and Bioelect.,* 24 (2008**)** 184.

241.L. Wang, W. Mao, D. Ni, J. Di, Y. Wu, Y. Tu, *Electrochem. Comm*., 10 (2008) 673.

242.G. K. Ahirwal, C.K. Mitra, *Sensors,* 9 (2009) 881.

243.K. R. Brown, A. P. Fox, M. J. Nathan*, J. Am. Chem. Soc*.,118 (1996**)** 1154.

244.Y. Z. Xian, H. T. Wang, Y. Y. Zhou, D. M. Pan, F. Liu, L.T. Jin, *Electrochem. Commun*., 6 (2004) 1270.